University of Southampton

SYNTHESIS AND STUDIES ON TRANSITION METAL AND GROUP 15 COMPLEXES INCORPORATING ACYCLIC AND MACROCYCLIC CHALCOGENOETHER LIGANDS

by Andrew James Barton

A Thesis Submitted for the Degree of Doctor of Philosophy

Department of Chemistry

October 2000

UNIVERSITY OF SOUTHAMPTON

ABSTRACT

FACULTY OF SCIENCE

CHEMISTRY

Doctor of Philosophy

SYNTHESIS AND STUDIES ON TRANSITION METAL AND GROUP 15 COMPLEXES INCORPORATING ACYCLIC AND MACROCYCLIC CHALCOGENOETHER LIGANDS

by Andrew James Barton

A series of transition metal complexes and main group complexes incorporating thio-, seleno- and telluro-ether ligands are described.

The syntheses of the first series of Group 6 carbonyl telluroether complexes $[M(CO)_4(L\text{-}L)]$ (M = Cr, Mo or W, L-L = $MeTe(CH_2)_3TeMe$, $PhTe(CH_2)_3TePh$ or $o\text{-}C_6H_4(TeMe)_2$) are described along with some dithioether (L-L = $MeS(CH_2)_2SMe$, $MeS(CH_2)_3SMe$) and diselenoether (L-L = $MeSe(CH_2)_2SeMe$, $MeSe(CH_2)_3SeMe$ or $o\text{-}C_6H_4(SeMe)_2$) analogues. Characterisation of the complexes has been achieved using multinuclear NMR (^1H, $^{13}C\{^1H\}$, $^{77}Se\{^1H\}$, $^{125}Te\{^1H\}$ and ^{95}Mo) and IR spectroscopies, FAB mass spectrometry and elemental analysis. The crystal structure of $[Cr(CO)_4\{MeSe(CH_2)_2SeMe\}]$ has been determined and reveals a *cis* disubstituted distorted octahedral geometry. Trends in the bonding in complexes of these Group 16 ligands are discussed.

The syntheses and characterisation of a series of Group 6 derivatives *fac*-$[M(CO)_3L^3]$ (M = Mo or W, $L^3 = MeC(CH_2SMe)_3$, $MeC(CH_2SeMe)_3$ or $MeC(CH_2TeMe)_3$), prepared from $[M(CO)_3(MeCN)_3]$, have been investigated. IR, ^1H, $^{13}C\{^1H\}$, $^{77}Se\{^1H\}$, $^{125}Te\{^1H\}$ and ^{95}Mo NMR spectroscopies have been used to characterise the complexes. The complexes are prone to decomposition in solution into the tetracarbonyls, and attempts to isolate $[Cr(CO)_3L^3]$ have been unsuccessful. The complexes *cis*-$[Cr(CO)_4\{\eta^2\text{-}MeC(CH_2SMe)_3\}]$ and *cis*-$[Mo(CO)_4\{\eta^2\text{-}MeC(CH_2SeMe)_3\}]$ have been similarly characterised.

The complexes *trans*-$[OsCl_2(L\text{-}L)_2]$ (L-L = $o\text{-}C_6H_4(TeMe)_2$, $RTe(CH_2)_3TeR$ (R = Ph or Me)) have been prepared from *trans*-$[OsCl_2(dmso)_4]$ and the ditelluroethers in ethanol. The reaction of $[OsCl_2(PPh_3)_3]$ with the ditelluroethers or $MeS(CH_2)_2SMe$ or $MeSe(CH_2)_2SeMe$ in ethanol in the presence of NH_4PF_6 gave *trans*-$[OsCl(PPh_3)(L\text{-}L)_2]PF_6$. The complexes have been characterised by analysis, IR, UV-Vis and multinuclear NMR spectroscopy. The crystal structures of *trans*-$[OsCl_2\{PhTe(CH_2)_3TePh\}_2]$ and $[OsCl_2(dmso)_2\{MeSe(CH_2)_3SeMe\}]$ are reported. The reaction of $[OsCl_2(dmso)_4]$ with the distibine $Ph_2Sb(CH_2)_3SbPh_2$ affords *trans*-$[OsCl_2\{Ph_2Sb(CH_2)_3SbPh_2\}_2]$ which has also been characterised by crystallography.

A series of new antimony(III) and bismuth(III) complexes incorporating acyclic and macrocyclic Group 16 ligands has been synthesised. Single crystal X-ray diffraction studies on several of these complexes has revealed a varied array of unusual structural motifs. The structure of $[Bi_2I_6\{MeC(CH_2SeMe)_3\}]$ shows discrete dimeric units whereas $[BiCl_3([8]aneSe_2)]$, $[BiBr_3([16]aneSe_4)]$, $[SbBr_3\{MeC(CH_2SeMe)_3\}]$, $[SbCl_3\{MeC(CH_2SMe)_3\}]$ and $[SbI_3\{MeC(CH_2SMe)_3]$ give rise to infinite one-dimensional structures. Furthermore, infinite two-dimensional arrays are obtained from the single crystal X-ray diffraction studies of $[BiCl_3\{MeC(CH_2SeMe)_3\}]$ and $[(SbBr_3)_2([16]aneSe_4)]$. Bismuth(III) complexes with Group 16 donor ligands are rare and the antimony(III) species constitute the first examples of seleno- and telluro-ether complexes of antimony(III).

Acknowledgements

I would like to acknowledge Dr Gillian Reid and Prof. Bill Levason for all their support, advice, enthusiasm and time they have willingly given during the past three years at Southampton. I am also grateful to Prof. B. Levason for the guidance given whilst writing up this thesis and for his help, along with that of Simon Orchard, in obtaining NMR spectra and microanalyses. Dr John Langley has been helpful throughout in the realms of mass spectrometry. Acknowledgements must also go to Dr G. Reid, Dr A.R.J. Genge and Mr B. Patel for X-ray crystallographic data collection. The EPSRC must also be acknowledged for funding of this project.

There are many people who have graced the 7th floor in the old building and the 2nd floor in the new synthetic building over the past three years who have induced many a smile within the laboratory and over the occasional pint or few. Thanks guys! I have to acknowledge the stars of the Levason/Reid Research Group, past and present, Simon Pope, Julie Connolly and Tony Genge, veterans of the group, who helped me considerably in the early stages and up until their departures for challenges elsewhere. Plus the usual suspects of lab. 2005, Bhavesh Patel, Nick Hill, Simon Orchard and Mike Popham, who have made the bad times easier to forget and the good times more difficult to remember. Cheers to you all!

Ginny has to have the biggest thank you. She has given me encouragement on countless occasions throughout the three years of my Ph.D. All members of my family have supported me in many ways and I wish to thank them all, I could not have done it alone.

"If I have seen further it is by standing on the shoulders of Giants".

Sir Isaac Newton, 1676.

CONTENTS

LIST OF TABLES

LIST OF FIGURES

ABBREVIATIONS

Substituent Groups

Me	Methyl
Et	Ethyl
Ph	Phenyl
^{n}Bu	n-Butyl
^{t}Bu	tertiary-Butyl
R	Alkyl or aryl

Solvents

DMF	Dimethylformamide
EtOH	Ethanol
MeOH	Methanol
thf	Tetrahydrofuran
Et_2O	Diethyl Ether
MeCN	Acetonitrile
dmso	Dimethylsulphoxide
Me_2CO	Acetone

Techniques

UV/Vis	Ultra Violet/Visible Spectroscopy
IR	Infrared
NMR	Nuclear Magnetic Resonance
ES^+	Electrospray Mass Spectrometry
FAB	Fast Atom Bombardment
APCI	Atmospheric Pressure Chemical Ionisation

Spectroscopy

sh	shoulder
s	strong

m	medium
w	weak
br	broad
Hz	Hertz
δ	Chemical Shift (in parts per million, p.p.m)
J	Coupling Constant
m	Multiplet
s	Singlet
d	Doublet

Miscellaneous

acac	Acetylacetone
3-NOBA	3-Nitrobenzyl-alcohol
Rongalite	Sodium formaldehyde sulfoxylate
S.C.E	Saturated Calomol Electrode
tht	tetrahydrothiophene
nbd	norbornadiene. Bicyclo[2.2.1]hepta-2,5-diene
TMPA	N,N,N',N'-Tetramethyl-1,3-propanediamine
mmol	millimoles
HOMO	Highest Occupied Molecular Orbital
LUMO	Lowest Unoccupied Molecular Orbital
En	1,2-diaminoethane

Nomenclature

A standard form of nomenclature has been used in this thesis to describe the nomenclature of macrocyclic compounds

$R_wR'_x[N]aneA_yB_z$

Where R = substituent on donor atom, R' = substituent on ring atoms, N = number of atoms in ring, A and B = donor atom type, *w,x,y,z* = integers, denoting the numbers of each.

[8]aneSe_2	=	1,5-diselenacyclooctane
[9]aneS_3	=	1,4,7-trithiacyclononane
[12]aneS_4	=	1,4,7,10-tetrathiacyclododecane
[12]aneSe_4	=	1,3,7,9-tetraselenacyclododecane
[14]aneS_4	=	1,4,8,11-tetrathiacyclododecane
[14]aneSe_4	=	1,4,8,11-tetraselenacyclotetradecane
[15]aneS_5	=	1,4,7,10,13-pentathiacyclopentadecane
[16]aneSe_4	=	1,5,9,13-tetraselenacyclohexadecane
[18]aneS_6	=	1,4,7,10,13,16-hexathiacyclooctadecane
[18]aneSe_6	=	1,3,7,9,13,15-hexaselenacylooctadecane
[24]aneSe_6	=	1,5,9,13,17,21-hexaselenacyclotetracosane
[24]aneS_8	=	1,4,7,10,13,16,19,22-octathiacyclotetracosane

For Ginny, Alexander,

and all my Family.

CHAPTER 1

Introduction

1.1 INTRODUCTION

The coordination chemistry of Group 16 donor ligands has generated interest within the research group at Southampton for some time. The complexation chemistry of thioether and selenoether ligands with low valent organometallic species has been well established whereas that of telluroethers is less well defined. The vast majority of compounds involving thio- and seleno-ether coordination incorporate d-block elements. However, there are relatively few examples of complexes involving p-block elements with these ligands. This thesis describes the complexation of thio-, seleno- and telluro-ether ligands with a range of low valent transition metal centres, including Group 6 carbonyls and the platinum group metals. Also, the chemistry of acyclic and macrocyclic Group 16 ligands with heavier p-block elements including antimony(III) and bismuth(III) will be discussed.

1.2 Metal-Ligand Bonding

1.2.1 M-S/Se/Te Bonding

The general electronic configuration of the Group 16 elements is ns^2,np^4, nd^0. Hence in the case of dialkylated species such as thioethers, selenoethers and telluroethers there are two of these valence electrons involved in bonding interactions with the alkyl groups, leaving four electrons in non-bonding orbitals on the heteroatom.

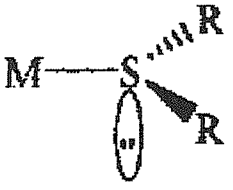

Figure 1.1 – Sp^3 hybridised sulfur showing approximate tetrahedral geometry.[1]

In a review of thioether complexes of transition metals Murray and Hartley describe the orbitals on the Group 16 elements as varying from sp^3 hybridised on oxygen, to an s and three p orbitals on tellurium, with sulfur and selenium lying somewhere between these two extremes.[1] In the case of thioethers they consider sulfur to be sp^3 hybridised resulting in two lone pairs. One or both of these may be involved in a coordinate bond to an electron acceptor (Lewis acid) (in a way similar to the Dewar-Chatt model for phosphines, which have a single lone pair of electrons, binding to metal centres which involves P→M σ-donation and M→P π-back-donation).[2] However, for chalcogenoethers, if only one lone pair is involved in bonding then the other may either remain non-bonding resulting in stereoelectronic repulsion, or take part in π donation by rehybridisation to sp^2 followed by π donation of the lone pair from a p orbital to the electron acceptor.

Although π donation might be anticipated with early transition metals having empty suitable symmetry d orbitals to act as acceptors, there is very little evidence to support such bonding.

As well as filled valence orbitals, all Group 16 elements have empty nd orbitals providing the possibility for π back-donation from metal to ligand. Whenever there are orbitals of correct symmetry available for bonding there is a possibility of such bonding occurring. The importance of this π back-donation is ill-defined but should decrease down the group. However, the back donation is certainly much less than exists in phosphine, arsine and stibine complexes.

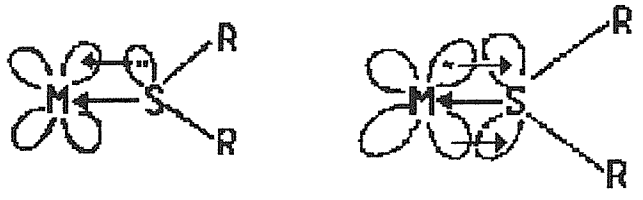

Figure 1.2 – Metal-thioether bonding assuming sp^3 hybridisation at S taken from ref. 3

In summary, Figure 1.2 illustrates, using thioethers as the example, that if one lone pair of electrons of R_2S is involved in σ-bonding to the metal centre, the

second lone pair is then capable of π-donation to the metal. In addition, the S-donor has empty d-orbitals that may be of the correct symmetry and energy to act as π-acceptor orbitals.

Orpen and Connelly have suggested on the basis of structural evidence that back-donation into a P-X σ* orbital (X = substituent on P) is involved in M-P π-bonding.[4] For thioethers, as with Group 15 ligands, suitably oriented S-C σ* orbitals are considered to be the most likely acceptors of π backbonding.[5] In a review of structurally characterised examples of late transition metal complexes of [9]aneS_3 Blower *et al.* argue that they observe increasing S-C bond lengths consistent with π backbonding into these σ* orbitals. In the most extreme example, $[Re([9]aneS_3)_2]^{2+}$, it was suggested that this effect was strong enough to break the S-C bonds, releasing ethene, forming $[Re([9]aneS_3)(SCH_2CH_2SCH_2CH_2S)]^+$. It is also important to include that this argument carries for Se-C σ* and Te-C σ* too. However, it remains unclear whether this theory can be extended to other systems.

With no strong π back-donation, modest σ donor abilities and any stereoelectronic effects arising from the non-bonding pair of electrons, Group 16 ethers are considered rather poor ligands relative to Group 15 ligands.

Since donor orbital size increases and electronegativity decreases down the group, metal-ligand σ bond strengths have been shown to follow the order M-S > M-Se > M-Te. However, providing the match in orbital overlap and energy remains good, increasing σ-donation would be expected as the group is descended. In low valent or zero-valent metals the orbital size and energy of the expanded d-orbitals is likely to be a better match for the larger element in Group 16 i.e. tellurium. Hence, based on molecular orbital calculations and ligand exchange experiments on the $[(C_5H_5)Fe(CO)_2]^+$ species, Hoffmann and co-workers argued that M-E bond strengths increase down Group 16 in the order M-Te >> M-Se > M-S.[6]

1.2.2 M-CO Bonding

The CO ligand is able to form adducts with low valent metals. In molecular orbital terms, CO has a carbon-centred lone pair (HOMO) and degenerate π^* levels (LUMOs). Ligands capable of accepting an appreciable amount of π-electron density, from the metal atoms into empty π or π^* orbitals of their own are referred to as π-acceptor or π-acid ligands.[7] Of these, carbon monoxide is the most important and the most extensively studied. The way in which CO engages in bonding to a metal atom may be stated as follows:

1. Overlap of a filled carbon σ orbital with a σ-type orbital on the metal atom as in Figure 1.3. Electron flow C to M in such a dative overlap would lead to an unacceptable concentration of electron density on the metal atom. The metal therefore attempts to reduce this charge by pushing electrons back to the ligand. This of course is possible only if the ligand has suitable acceptor orbitals.

2. A second dative overlap of a filled $d\pi$ or hybrid $dp\pi$ metal orbital with the empty, $p\pi$ orbital on carbon monoxide, which can act as an acceptor of electron density (Figure 1.3 b).

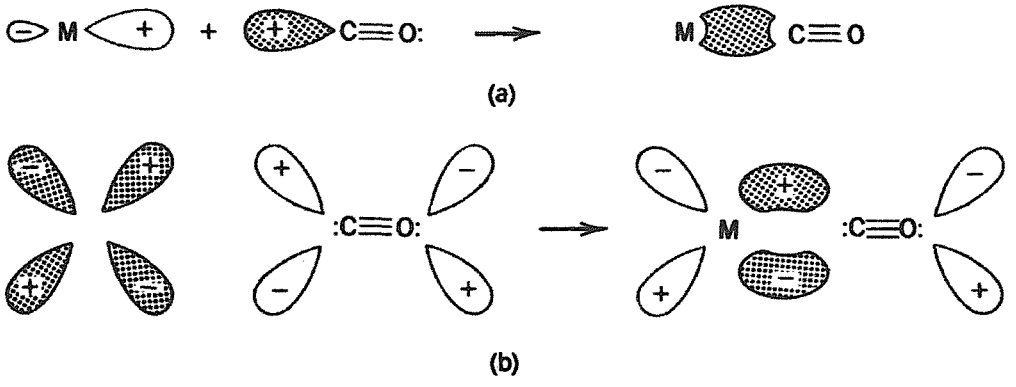

Figure 1.3 – (a) The formation of the metal ← carbon σ bond using an unshared pair of electrons on the C atom. (b) The formation of the metal → carbon π bond. The other orbitals on the CO are omitted for clarity.

This bonding mechanism is synergic, since the drift of metal electrons, referred to as back-bonding, into CO orbitals, will tend to make the CO as a whole negative, hence to increase its basicity *via* the σ orbital of carbon; at the same time the drift of electrons to the metal in the σ bond tends to make the CO positive, thus enhancing the acceptor strength of the π orbitals. Thus up to a point the effects of σ-bond formation strengthen the π bonding, and vice versa i.e. synergic bonding.

1.3 Ligand Synthesis

1.3.1 Synthesis of Dithio- and Diselenoether Ligands

The acyclic dithioether ligands described in this thesis were prepared by reaction of a dithiol, $HS(CH_2)_nSH$, with sodium ethoxide and subsequent addition of an alkyl halide.[8]

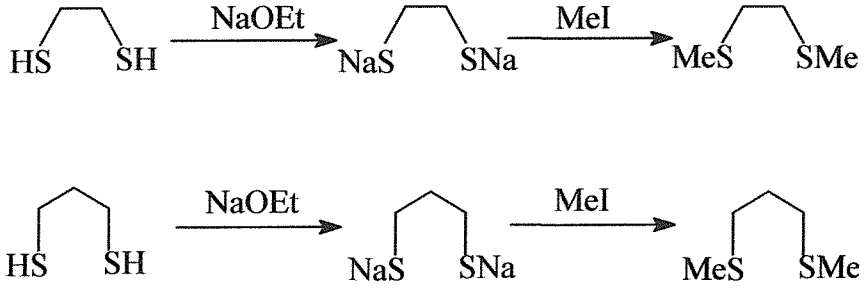

Figure 1.4 – Reaction scheme for the synthesis of $MeS(CH_2)_nSMe$ (n = 2, 3)

The preparation of open chain selenoethers was undertaken using methodology developed by Levason and co-workers.[9] Hence, the bidentate selenoethers were prepared by reaction of MeLi and Se_8 in THF, which generates MeSeLi, and subsequent *in-situ* reaction with the dichloroalkanes afforded the products in high yield (Figure 1.5).[10]

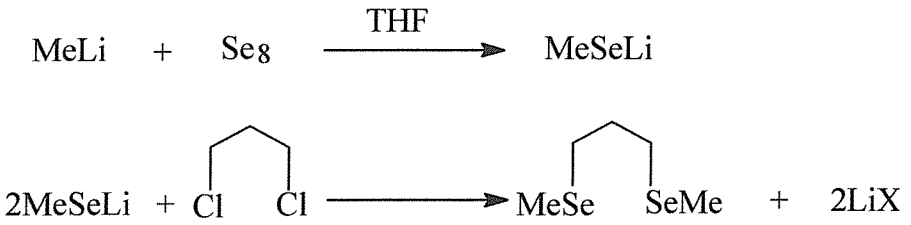

Figure 1.5 – Reaction scheme for the synthesis of $MeSe(CH_2)_3MeSe$

Preparation of the ligand o-$C_6H_4(SMe)_2$ entails the formation of o-$C_6H_4(SMe)Cl$ as a precursor. The addition of o-dichlorobenzene to NaSMe, prepared from Na/NH_3 reduction of Me_2S_2 in THF, followed by *in vacuo* fractionation affords this precursor. The ligand is obtained in high yield from lithiation of this prescursor by ^nBuLi, followed by addition of Me_2S_2 and fractionation *in vacuo* (Figure 1.6).

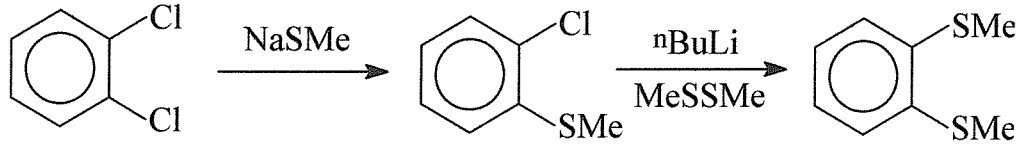

Figure 1.6 – Reaction scheme for the synthesis of o-$C_6H_4(SMe)_2$[8]

The synthesis of the selenoether equivalent, o-$C_6H_4(SeMe)_2$, is generated following the reaction scheme shown in Figure 1.7.[11] The poly-o-phenylenediselenide, o-$\{SeC_6H_4Se\}_n$, obtained from o-$C_6H_4Br_2$ and Na_2Se_2 in DMF, is cleaved by 'Rongalite' ($HOCH_2SO_2Na.2H_2O$) to the anion o-$C_6H_4Se_2^{2-}$ and this is alkylated with MeI.

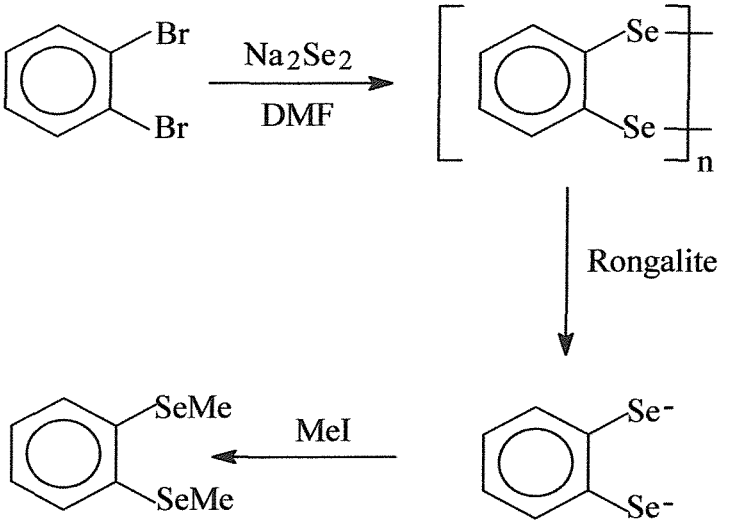

Figure 1.7 – Reaction scheme for the synthesis of o-$C_6H_4(SeMe)_2$

1.3.2 Synthesis of Ditelluroethers

RTeLi and $X(CH_2)_3X$ (X = Cl or Br) at room temperature gave R_2Te_2 and olefin as major products as detected by ^{125}Te NMR spectra of the products, but addition of the 1,3-dihalopropane to frozen RTeLi gave high yields of $RTe(CH_2)_3TeR$ (R = Ph, 85%; R = Me, 73 %).[12] Once isolated the ligands are quite stable under nitrogen.[13,14]

1.3.3 Synthesis of Tripod Ligands

The tripodal selenoether $MeC(CH_2SeMe)_3$ was obtained straightforwardly from reaction of $MeC(CH_2Br)_3$ and $MeSe^-$ as shown in Figure 1.8. This is an example of the route into the synthesis of Group 16 trichalcogenoethers. This reaction path can be altered accordingly to create the thio- and telluro-ether analogues.[9,12] An excess of MeE^- is required to avoid incomplete substitution of bromine.

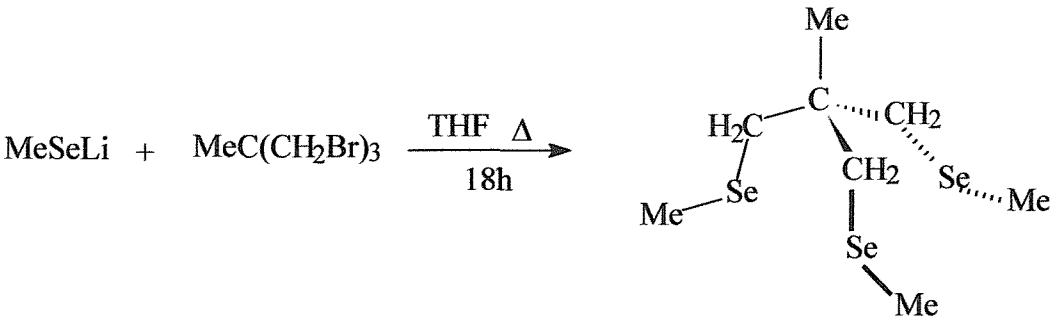

Figure 1.8 – Reaction scheme for the synthesis of $MeC(CH_2SeMe)_3$

1.4 Multidentate Ligand Chemistry

1.4.1 Chelate Effect[15]

The term chelate effect refers to the enhanced stability of a complex system containing chelate rings as compared to the stability of a system that is as similar as possible but contains monodentate ligands. Consider the following equilibrium stability constants:

$M^{2+}(aq) + 6NH_3(aq) = [M(NH_3)_6]^{2+}(aq)$ $\log \beta = 8.61$

$M^{2+}(aq) + 3en(aq) = [M(en)_3]^{2+}(aq)$ $\log \beta = 18.28$

The system $[M(en)_3]^{2+}$ in which three chelate rings are formed is nearly 10^{10} times more stable than that in which no such ring is formed. Although the effect is not always so pronounced, such a chelate effect is a very general one.

To understand this effect, we must invoke the thermodynamic relationships:

$$\Delta G^\circ = -RT \ln \beta$$

$$\Delta G^\circ = \Delta H^\circ - T\Delta S^\circ$$

Thus, as the stability constant, β, increases, ΔG° becomes more negative. A more negative ΔG° can result from making ΔH° more negative or from making ΔS° more positive. It is the entropy term that usually makes the decisive contribution since the chelate effect is observed when ΔH° is either positive or

negative, but only when $\Delta S°$ is positive. The main cause of the large, positive entropy change is the net increase in the number of unbound molecules. Thus, although six NH_3 ligands replace six H_2O molecules, giving no net change in the number of independent molecules, it takes only 3 en molecules to displace 6 H_2O molecules.

Another more pictorial way to look at the problem is to visualise a chelate ligand with one end attached to the metal ion.[16] The other end is held in close proximity, and the probability of it, too, becoming attached to the metal atom is greater than if this other end were instead another independent molecule, which would have access to a much larger volume of the solution.

The latter view provides an explanation for the decreasing magnitude of the chelate effect with increasing ring size. When the ring that must be formed becomes sufficiently large (seven membered or more), it becomes more probable that the other end of the chelate molecule will contact another metal ion than that it will come around to the first one and complete the ring.

1.5 Pyramidal Inversion

Pyramidal inversion had been suggested as early as 1924[17] and confirmed experimentally for nitrogen atoms some years later.[18,19] Abel and co-workers first investigated the pyramidal inversion process at sulfur donors in metal complexes in 1966.[20] Extensive ^1H NMR studies undertaken on the Pt(II) complex $[PtCl_2\{MeS(CH_2)_2SMe\}]$ showed that the inversion process could be monitored by NMR spectroscopy.[21] In general, the inversion process consists of two energetically equivalent configurations (A and C) which interconvert *via* a planar transition state (B) (Figure 1.9).[22]

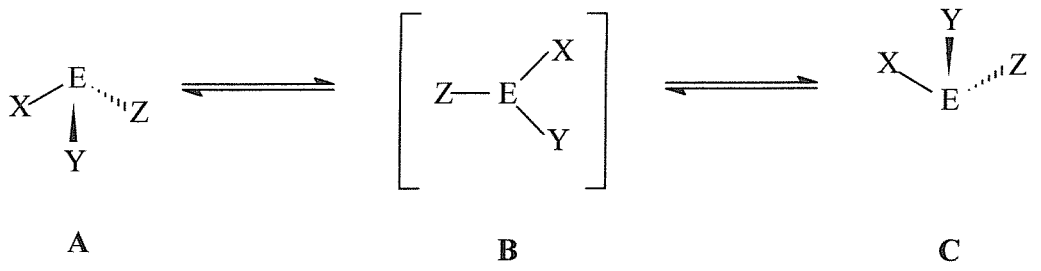

A B C

Figure 1.9 – Proposed inversion mechanism

1.6 Macrocyclic Chemistry[15]

Macrocycles are usually defined as cyclic molecules composed of nine or more atoms, at least three of which are heteroatoms.[23] The properties of a macrocyclic ligand are determined by a number of factors including the size of the macrocyclic cavity (ring-size), the number and type of donor atom (e.g. O, N, S, Se, P) and the degree of unsaturation and/or substitution of the ring. Many systems have been studied to date although crown ethers and azacrowns, containing hard oxygen and nitrogen donors respectively, and thioethers, which incorporate soft sulfur donors, dominate studies. Numerous mixed donor macrocyclic systems containing these heteroatoms have also been reported.

1.6.1 The Macrocyclic Effect.

One of the reasons for the development of macrocyclic chemistry is due to the inherent stability of metal complexes of macrocyclic ligands.[24]

In addition to those benefits imparted by the chelate effect, the macrocyclic effects bestows further stability upon closure of a ring system around a metal ion.[23,25] The chelate effect, in which a complex coordinated by mulitdentate ligands with n donor atoms is more stable than one with n monodentate ligands, can be attributed to formation of the former being entropically more favourable than the latter, However, the origins of the macrocyclic effect are not so clearly defined. Usually, the effect is a mixture of both enthalpic and entropic factors which result in the preferential binding of a closed ring system rather than an open chain analogue to a metal ion. In

summary, the main features to note are those of kinetic and thermodynamic stability.

Kinetic Stability:

The uptake of a macrocycle or an open chain analogue by a metal ion is expressed as follows

$$M + L \underset{k_d}{\overset{k_f}{\rightleftharpoons}} ML$$

The k_f and k_d terms refer to the second order formation constant and first order dissociation constant respectively. The stability constant K, defined as the ratio of k_f / h_d, is a reflection of the stability of the complex. This is almost always larger for a macrocyclic complex *versus* an acyclic analogue, an indication of the enhanced stability of the former. The reasoning of this phenomenon may be explained as follows.

Although, the rates of formation k_f are usually lower for macrocyclic complexes *versus* acyclic systems; it is the substantially higher dissociation values of k_d for acyclic systems compared with those observed for macrocyclic systems, which result in larger values for K for the latter. This reflects the view that the stepwise removal of a cyclic ligand from the coordination sphere of a metal tends to be more difficult than for an acyclic analogue. The coordinated macrocycle may require significant rearrangement and distortion of bond lengths and angles (probably resulting in a high energy activation transition state) before dissociation can occur. However, dissociation for the acyclic analogue occurs at a terminal donor most probably *via* an "unzipping" mechanism as shown in Figure 1.10.

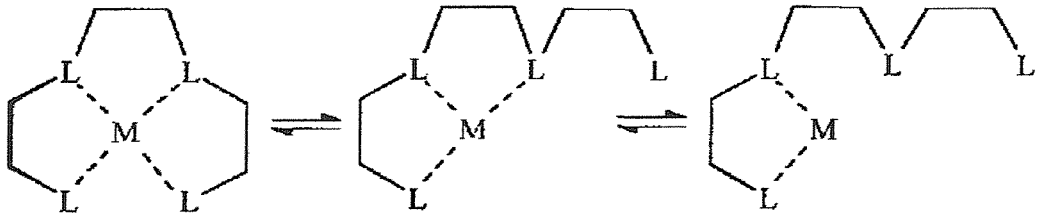

Figure 1.10 – Possible Dissociation Mechanism for acyclic ligands

Thermodynamic Stability:

In considering the thermodynamics of the uptake of a macrocycle at the expense of a open chain analogue it is convenient to discuss the concept using the Gibbs Free Energy equation $\Delta G = \Delta H - T\Delta S$. In the following example, ΔG for the reaction at 298 K is –33.67 kJ mol^{-1}.[26] This arises from the enthalpic ΔH, and the entropic $T\Delta S$ term.

trans-$[NiL(H_2O)_2]^{2+}$ + $[14]aneN_4$ ⇌ *trans*-$[Ni([14]N_4)(H_2O)_2]^{2+}$ + L

(L = $H_2N(CH_2)_2NH(CH_2)_3NH(CH_2)_2NH_2$)

The Enthalpic Contribution

The variability of the enthalpy term reflects a number of influences. An important concern is any difference in the nature of bonds between metal ion and the respective ligands, together with the match or otherwise of the macrocyclic cavity for the metal ion. The different solvation energies of the open chain ligand and macrocycle may play an important role in determining the overall enthalpic contribution. For example, in the above reaction ΔH = -20.5kJ mol^{-1}. It has been argued that solvation occurs more readily for the open chain analogue than the macrocyclic ligand, which is more rigid and compact in its uncoordinated form.[26] Consequently, macrocyclic coordination leads to a favourable term in the above reaction. Care must be taken in using this

argument, since the enthalpy of solvation of the open chain analogue upon dissociation, will depend on the ability of the solvent to form an interaction with the ligand donor atom and the ligand functionalities.

The Entropic Contribution

The value of the entropic term $T\Delta S$ in the above reaction is 13.2 kJ mol^{-1}. This can be attributed to a higher entropy for the open chain analogue in its free form *versus* that entropy for the free macrocycle in its uncoordinated form. This, in part, is due to the open chain analogue exhibiting a greater number of rotational and vibrational degrees of freedom in the free form than in the coordinated form. For the macrocycle which is compact and rigid in its free form, coordination to a metal ion only leads to a small reduction in the number of internal degrees of freedom. Therefore, there is a net gain in entropy upon release of the acyclic ligand into solution.

1.6.2 Synthesis of Macrocyclic Selenoethers

A considerable amount of effort and time was devoted to the synthesis of macrocyclic selenoether ligands prior to studies into new coordination chemistry of these ligands. The following section summarises the methodology employed during the non-trivial reaction procedures required in the synthesis of selenoether macrocycles.

The synthesis of $NCSe(CH_2)_3SeCN$ (Figure 1.11) was accomplished by the reaction of slightly greater than two molar equivalents of KSeCN with one molar equivalent of $Br(CH_2)_3Br$ in dry DMF.[27]

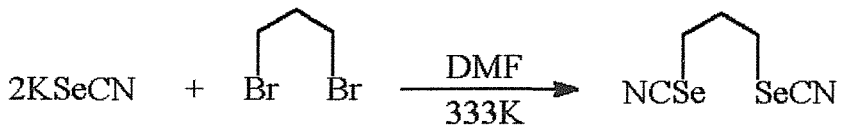

Figure 1.11 – Reaction scheme for the formation of $NCSe(CH_2)_3SeCN$[27]

The reaction to produce the three ring systems (Figure 1.12) was performed at low temperatures, initially at 195 K increasing to 223 K *via* an Me_2CO/solid CO_2 slush bath. Addition of $NCSe(CH_2)_3SeCN$ and sodium produces a two electron reduction at the site of each selenium atom, to produce a solution of $NaSe(CH_2)_3SeNa$ and NaCN. A slight excess of $Br(CH_2)_3Br$ in THF is added dropwise over 5 h. This gradually produces a precipitate of NaBr.

The synthesis of macrocycles is reliant upon certain conditions to promote cyclisation over the statistically preferred polymerisation. In the above synthesis, the important points to consider are whether cyclisation is promoted by the sodium ions acting as templates, or ring closure proceeds *via* a high dilution mechanism, or finally whether the reaction proceeds by a combination of both factors. Since the total volume of the reaction after the completion of the dihaloalkane addition in dry THF is no more than 500 cm^3 (reduced by *ca.* 200 cm^3 by slow evaporation of the ammonia), it is more likely that the mechanism of cyclisation will be due to the first effect. Additionally, the low temperature might also be expected to inhibit the polymer formation by slowing the reaction kinetics and act to limit the solubility of the precursors.

The rate of addition of dihaloalkane is also an important consideration. At high rates of addition, the selectivity for cyclisation *versus* polymerisation should be less than for lower rates of addition of dihaloalkane.

The mixture containing the cyclic selenoethers was purified by column chromatography on silica with an eluting mixture of 1:19 ethyl acetate:hexane. The first ligand to be eluted from the column is [8]aneSe_2 ($R_f = 0.6$). The second is [16]aneSe_4 ($R_f = 0.3$) and the third product is [24]aneSe_6 ($R_f = 0.1$). Figure 1.12 illustrates the reaction scheme.

Further to the examples discussed above there are other macrocyclic selenium containing ligands described in literature. Pinto and co-workers generated the [12]aneSe_4 and [18]aneSe_6 macrocycles by the reaction of sodium propane-1,3-bis(selenolate) with dibromomethane in liquid ammonia.[27] The analogous reaction of sodium ethane-1,2-bis(selenoate) with 1,3-dibromopropane afforded [14]aneSe_4.

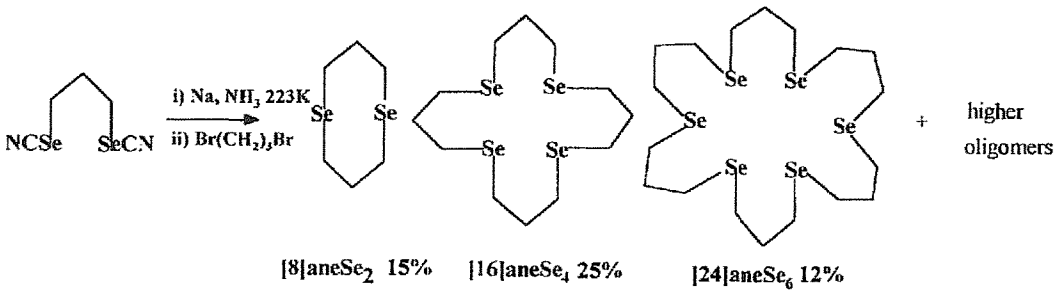

Figure 1.12 – Reaction scheme for the synthesis of [8]aneSe$_2$, [16]aneSe$_4$ and [24]aneSe$_6$[27]

1.7 The Elements of Group 15

Group 15 constitutes the third column of the p-block of the periodic table and comprises the elements nitrogen, phosphorus, arsenic, antimony and bismuth and they are often referred to as pnictogens. Despite being in the same group, however, the properties of the elements vary to a considerable degree as the group is descended. Thus, whereas nitrogen and phosphorus are typical non-metals, arsenic and antimony are more usually described as metalloids and bismuth has many properties associated with metallic behaviour. Nitrogen, which has the obvious distinction of being gaseous under normal conditions, is not included, as there is little resemblance between the characteristics it displays and the other Group 15 elements except for the stoichiometries of some simple ionic compounds (e.g. NH_3, PH_3, NCl_3, $BiCl_3$). Table 1.1 shows a selection of physical properties of Group 15 elements.

Table 1.1 – Physical Properties of the Group 15 elements.[28]

Element	Electronic Configuration	Melting Point (° C)	Electronegativity (Allred-Rochow)	Covalent radius[a] (Å)
P	$[Ne]3s^2 3p^3$	44.1	2.06	1.1
As	$[Ar]3d^{10} 4s^2 4p^3$	813	2.2	1.21
Sb	$[Kr]4d^{10} 5s^2 5p^3$	630.5	1.82	1.41
Bi	$[Xe]4f^{14} 5d^{10} 6s^2 6p^3$	271.3	1.67	1.52

a. For trivalent state.

The common oxidation states for arsenic, antimony and bismuth are +3 (III) and +5 (V) with the +3 oxidation state being the most common. The reluctance of the heavier p-block elements to achieve the group oxidation state (in this case +5) is a general feature in the chemistry of the p-block elements and is usually referred to as the 'inert pair effect', with the clear implication that there is an inert pair of electrons (the s pair) which are not easily involved in bonding. The large fourth and fifth ionization energies for bismuth provide some support for this assertion. In the case of arsenic and antimony other parameters play a role with a regard to stability of the +3 oxidation state apart from relativistic effects. In fact this energetic stabilization of the s pair is only part of the picture and in some ways the term 'inert pair effect' is a misnomer. Also important is the fact that bonds get weaker as the group is descended such that for the heavier elements the energetic cost of involving the s pair is not compensated by the formation of two extra but rather weak bonds.[29,30] Antimony(V) and bismuth (V) compounds are not considered in this work.

The Group 15 compounds in the +3 oxidation state can act as Lewis bases and this is well documented and is exemplified by the ability of triorganyl derivatives, for example EPh_3, to act as ligands to transition metals. In contrast to the very large number of metal phosphine complexes, far fewer such complexes are known for the heavier elements, with the number of well

characterised examples dropping dramatically as the group is descended. This observation illustrates a more general point relating to the decrease in basicity as the group is descended. A good explanation is that the increasingly poor hybridisation of the valence s and p orbitals resulting from their increasingly disparate radial extensions results in the bonding occurring primarily through p orbitals, with the lone pair residing in an orbital of largely s character. Since s orbitals have poorer directional properties compared with s-p type hybrids, it is partly for this reason that bonds become progressively weaker as the group is descended (in addition to the general trend towards weaker bonds for larger atoms) thereby accounting for the reduced basicity.

Perhaps less well appreciated is the Lewis acidity of the elements in the +3 oxidation state, since the presence of one pair of electrons generally leads to the expectation of Lewis basic behaviour, as discussed above. Whatever basicity such compounds may exhibit, a considerable degree of Lewis acidity is also evident especially where the Group 15 element is bonded to significantly more electronegative atoms or groups. Thus, antimony and bismuth trihalides, SbX_3 and BiX_3, for example, are sufficiently Lewis acidic to exhibit quite an extensive coordination chemistry with ligands such as phosphines (PR_3), phosphine oxides (OPR_3), ethers (OR_2), and halide ions (X^-).[31-33] The origin of this Lewis acidity together can be rationalised on the basis of a bonding model in which Sb-X or Bi-X σ^* orbitals are the primary acceptor orbitals through which the ligands bond. Hence, the conventional description which employs vacant d orbitals is dismissed as the d-orbitals in question are too high in energy to play any significant role in conferring Lewis acidity upon the heavy p-block elements.[34] The E-X σ^* bonding model relies upon X being more electronegative than E. The bonding σ orbital will be polarised towards X, since this is the lower energy atomic orbital, whereas the antibonding σ^* orbital will be polarised more towards the less electronegative element E (Figure 1.13). If this σ^* orbital is sufficiently low in energy, it can act as an acceptor orbital on E through which a Lewis base, B, can bond. Furthermore, as the B-E interaction becomes stronger

(and the L-E bond shorter) the population of the σ* orbital increases, which will lead to a lengthening and weakening of the E-X bond.

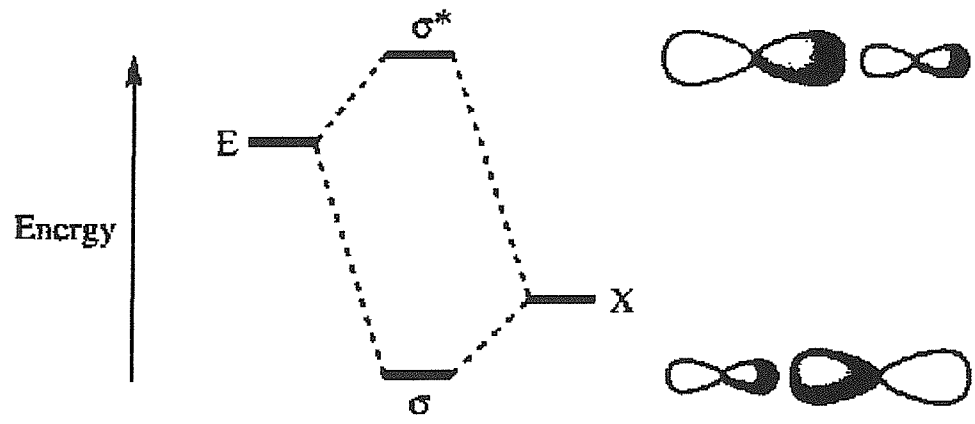

Figure 1.13 – A two-orbital interaction diagram for an E-X bond (E = Group 15 element; X = halogen)

There are two variables to account for when considering the nature of E-X interactions. The effect of changing the halide for a set of compounds can be seen by looking at the examples of $[BiPhX_2(thf)]$ (X = Cl, Br or I) (Figure 1.14).

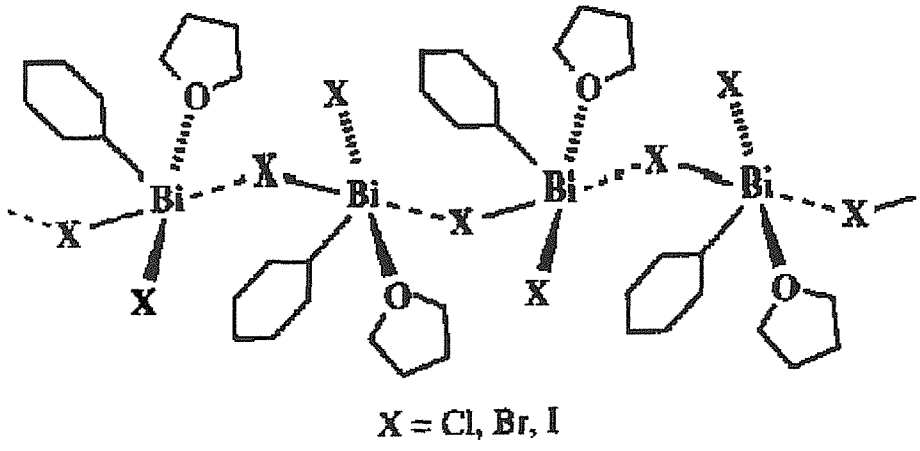

Figure 1.14 – View of the structure of $[BiPhX_2(thf)]$[35,36]

On going from chloride to iodide, the difference between the primary and secondary Bi-X bond lengths (Δ) decreases (for the two *trans* related halides, the shorter bond is defined 'primary' and the longer bond is defined 'secondary').[38] This feature of primary and secondary E-X bonds becoming more equal in length

on progressing to the heavier halides is, in fact, quite general.[37] Furthermore, it is observed when comparing a range of structures, for given E and X, that primary and secondary E-X bond distances are correlated such that as the secondary distance gets shorter the primary distance gets longer.[38]

The above example focuses on the effect on primary and secondary bond distances of changing the halide for a given Group 15 element E. The isomorphous triiodide structures EI_3 (E = As, Sb or Bi) illustrate the effect of changing the Group 15 element. In AsI_3, the arsenic atom is displaced towards three mutually *cis* iodines, giving three shorter As-I bonds, and three *trans* bonds, which are longer (Δ = 0.876 Å), whereas in BiI_3, the bismuth is in a regular octahedral environment with all six Bi-I distances equal (Δ = 0 Å). In SbI_3 the situation is intermediate with Δ = 0.45 Å.

Thus, overall there are two important trends. First, there is a tendency for secondary bonding to be more pronounced for the heavier halides, and, second, secondary bonding is also seen to be more significant for the heavier Group 15 elements; in the case of bismuth triiodide, the distinction between primary and secondary bonding has been lost.

In considering why heavier element E complexes should show more pronounced secondary bonding, two factors become important. First, on descending the group, the electronegativity of E will decrease, which will be reflected in a raising of the energy of the valence E orbital. This will result in a greater difference between the energies of the atomic orbitals of E and X leading to poorer overlap and a corresponding lower energy σ^* orbital, and higher energy σ orbital. Second, the increasing size of the heavier element E means larger and more diffuse orbitals, which will also result in poorer overlap, with, importantly, the same consequences for the energies of the σ orbital and σ^* orbital. The lower the energy of the σ^* orbital, the more available for bonding this orbital becomes, resulting in a corresponding increase in the likely extent of secondary bonding interactions.

In accounting for the effect of changing X for a given E(III) atom, both the acceptor properties of E(III) and the donor capability of X must be considered. The heavier halides are better electron donors and thus have a greater tendency toward bridging. In addition, as halide orbitals become larger and more diffuse down Group 17, overlap with the E(III) orbitals is reduced and thus the σ* is lowered in energy. Crucial however, is the raising in energy of the halide atomic orbitals relative to those of the E(III) atom. This reduces the energy separation of E and X, raising the σ* orbital energy (thus decreasing its availability for interaction with a Lewis base) and reducing the polarisation of this orbital toward the E atom. Overall, the availability of the σ* orbital is tempered by the reduced E-X orbital energy separation.

As indicated by Carmalt and Norman, the E-X σ* bonding models is not without ambiguity. Indeed, a recent computational study upon secondary interactions in heavy main group elements proposed an alternative, van der Waals type mechanism.[39] Further work is necessary to establish a rigorous theoretical understanding and ultimately a qualitatively scale of secondary bonding. However, the current E-X σ* model is qualitatively successful in accounting for E(III) Lewis acidity, secondary bonding interactions and E-X bond distances, and is a useful tool in rationalising the solid state structures obtained in this and previous studies.

1.8 Transition Metal Complexes

The transition elements may be defined as those as elements (and in any of their commonly occurring oxidation states) have partly filled d or f shells. The large number of transition elements is subdivided into three main groups: (i) the main transition elements or d-block elements, (ii) the lanthanide elements and (iii) the actinide elements. The work discussed within this thesis concerns only the d-block elements which have partially filled d shells only.

Substituted Group 6 carbonyls (chromium, molybdenum and tungsten) have been studied in great detail with a wide variety of ligand types, and are thus

very suitable systems in which to explore the properties of new ligands.[40] The chemistry of ditelluroether ligands with low valent metal and organometallic species remains a largely unexplored area of chemistry (*c.f.* complexes with Group 8-11 metals).[41-43] Hence, there is an opportunity to study these new complexes in parallel with thio- and seleno-ether analogues, which have already received considerable attention.

Likewise, the chemistry of tridentate telluroether and selenoether ligands with a variety of metal centres including both homoleptic and halocomplexes with Pd(II), Pt(II), Rh(III) and Ir(III), Ru(II) and Rh(I) complexes, and homoleptic Cu(I) and Ag(I) have been explored and once again Group 6 carbonyl complexes have received very little attention. An aim of this work was to redress this imbalance.

Whilst a wide range of bidentate and polydentate phosphine and arsine complexes of Os(II), Os(III) and Os(IV) are readily made obtaining complexes with Group 16 donors (S, Se or Te) has proved considerably more difficult. New synthetic routes are needed to access the chemistry of Os(II) with dithio- and diseleno-ether ligands and there is also the added interest of extending the list of ditelluroether complexes with platinum group metals (platinum, palladium, iridium, ruthenium and rhodium) to osmium.

1.9 Characterisation Techniques

The complexes formed in this study were all characterised using a combination of techniques. Microanalyses were collected for all solids isolated. Multinuclear NMR spectroscopy (^{1}H, $^{13}C\{^{1}H\}$, $^{77}Se\{^{1}H\}$, $^{125}Te\{^{1}H\}$, $^{31}P\{^{1}H\}$ and ^{95}Mo) has been used extensively to characterise many of the compounds described in this research. The other means of characterisation were infrared (IR) spectroscopy, mass spectrometry and single crystal X-ray diffraction. The following is a brief overview of these techniques.

1.9.1 Multinuclear NMR Spectroscopy

Multinuclear NMR spectroscopy (^{1}H, $^{13}C\{^{1}H\}$, $^{31}P\{^{1}H\}$, $^{77}Se\{^{1}H\}$, $^{125}Te\{^{1}H\}$ and ^{95}Mo) have been used routinely to characterise the compounds described in this thesis and to probe the interaction of the ligand with the metal centres.

^{77}Se NMR Spectroscopy[44]

Selenium has six naturally occuring isotopes. The ^{77}Se nucleus has a spin of I = ½, a natural abundance of 7.6 % and a receptivity relative to ^{1}H of 5.3 x 10^{-4} making it suitable for study by NMR spectroscopy. It has been studied extensively and a comprehensive range of δ (^{77}Se) values has been established for both ligands (phosphine selenides, diselenides, selenoethers etc) and metal complexes alike. Shifts are typically referenced to neat Me_2Se which is assigned δ 0.[45] When an M-Se σ bond is formed on coordination the Se centre is usually deshielded and the resulting shift is usually to high frequency, consistent with a shift of electron density away from the Se donor to the metal centre. The size of shifts are also dependent, in the case of bidentate selenoether, upon the size of the chelate ring. For example, the coordination shifts for five membered rings are always larger than for six membered chelate analogues.[41]

^{125}Te NMR spectroscopy[46]

Tellurium has seven naturally occurring isotopes of which it is ^{125}Te, with spin I = ½, natural abundance 7.0 % and a relative receptivity to ^{1}H of 2.21 x 10^{-3} which is used in NMR spectroscopic studies. Detracting from this is the negative magnetogyric ratio (γ = -8.453 x 10^{7} rad T^{-1} s^{-1}) which may lead to signal diminuation *via* the Nuclear Overhauser Effect (NOE). For most nuclei this ratio is positive and has the effect of enhancing the signal by an amount defined by:

$$NOE_{max} = 1 + [\chi_S / 2\chi_I]$$

χ_I = magnetogyric ratio of observed species

χ_s = magnetogyric ratio of irradiated species

When the negative magnetogyric ratio is placed in this equation a negative effect is observed, i.e. signal diminuation. Resonances for ^{125}Te are referenced to the resonance of neat Me_2Te. The same high frequency shifts discussed for other nuclei are observed with electron-rich substituents. With coordination, a high frequency shift is observed as the tellurium nucleus is deshielded.

^{95}Mo NMR Spectroscopy

Molybdenum has two NMR active nuclei, ^{95}Mo and ^{97}Mo, both of which are quadrupolar with spin I = 5/2. ^{95}Mo has a natural abundance of 15.72 % with a low relatively receptivity of 5.07 x 10^{-4} but its small quadrupole moment (0.015 x 10^{-28} m^2) makes it the easier of the two nuclei to study. [^{97}Mo has a larger quadrupole moment (0.15 x 10^{-28} m^2) and natural abundance of 9.46 %]. Extensive research on Mo-carbonyl complexes has been undertaken using ^{95}Mo NMR spectroscopy.

1.9.2 Mass Spectrometry

Mass spectrometry is useful because it can provide information about the relative molecular mass of a compound. Once this is known it can be compared with that calculated for the expected products based on the relative atomic masses of the constituent elements and the composition of the molecule. Mass spectrometry provides a basis for separating the different ions of the molecule of interest due to their mass-to-charge ratio (*m/z*) and this can be achieved in a number of ways. The ionisation methods encountered for complexes and ligands during work for this thesis are described below.

Fast Atom Bombardment

There are occasions when heating a sample and bombarding it with accelerated electrons (as in electron impact ionisation) provides too much energy and the molecules are not just ionised but also start to break up into smaller

fragments. This is especially true for molecules containing relatively weak bonds or easily fragmented groups such as organometallic compounds; in these cases the technique of fast atom bombardment (FAB) is often preferred. In this method the compound of interest is dissolved in a suitable non-volatile 'matrix' material before being bombarded by charged atoms or argon or xenon. This method results in a higher chance of observing the parent or molecular ion with less fragmentation; however, it may also give rise to peaks due to the matrix material.

Electrospray

In the most general sense, electrospray is a method of generating a very fine liquid aerosol through electrostatic charging, rather than the more familiar gas methods. In electrospray, the plume of droplets is generated by electrically charging a volume of liquid to a (very) high voltage. The liquid becomes unstable as it is forced to hold more and more charge. Soon the liquid reaches a critical point, at which it can hold no more electrical charge and it blows apart into a cloud of tiny, although still highly charged "daughter" droplets. These tiny droplets (<10 μm in diameter) then fly about searching for a potential surface opposite in charge to their own to land on, the counter-electrode. Electrospray ionisation is the process of generating a gas phase ion from an otherwise neutral chemical species. It is called "soft" since the molecule being ionised does not fall apart or break-up during the process.

1.9.3 Infra-red Spectroscopy

Infra-red spectroscopy was used extensively in this work to provide evidence for the identity of the products and the presence of carbonyl ligands. For Chapter 2 and Chapter 3, describing the Group 6 carbonyl complexes, IR spectroscopy provided a useful way of monitoring the progress of the reactions and determining the geometry about the metal centre (from group theory). The bismuth(III) and antimony chloride complexes were found to show several features assigned as ν(E-Cl) in the range 230 – 300 cm^{-1}.

1.10 Aims of the Study

The aim of this research study was to synthesise and characterise a variety of metal complexes with bidentate, tridentate and macrocyclic ligands incorporating thioether, selenoether and telluroether donor atoms. The complexes have been characterised by a wide range of spectroscopic methods including, in several cases, single crystal X-ray diffraction. Comparisons have been made between different ligand donors, metal ions and between acyclic and macrocyclic ligand systems. The aims for each chapter are outlined below.

Chapter 2: To prepare and characterise a series of bidentate Group 16 ligand derivatives of M(0) carbonyls (M = Cr, Mo or W) and to probe the coordinating abilities of ditelluroether ligands *versus* the established trends for thio- and seleno-ether ligands in these species.

Chapter 3: To generate the first examples of $[M(CO)_3\{MeC(CH_2EMe)_3\}]$ (M = Mo or W; E = Se or Te).

Chapter 4: To extend the previous studies of ditelluroethers with platinum group metals Pt or Pd,[47-49] Ir,[47,49] Ru or Rh,[48] to osmium; and to draw comparisons with sulfur and selenium analogues.

Chapters 5 and 6: To synthesise and structurally characterise a range of new antimony(III) and bismuth(III) halide complexes with tridentate and macrocyclic Group 16 ligands. The main emphasis of this piece of work is to investigate structural motifs obtained under the reaction conditions used.

1.11 REFERENCES

1. S.G. Murray and F.R. Hartley, *Chem. Rev.*, 1981, **81**, 365.
2. C.A. McAuliffe and W. Levason, '*Phosphine, Arsine and Stibine Complexes of Transition Elements*,' Elsevier, Amsterdam, 1979.
3. A.J.Blake and M. Schroder, *Adv. Inorg. Chem.*, 1990, **35**, 1.
4. A.G. Orpen and N.G. Connelly, *J. Chem. Soc., Chem. Commun.*, 1985, 1310.
5. G.D. Mullen, M.J. Went, S. Wocadlo, A.K. Powell and P.J. Blower, *Angew. Chem. Int. Ed. Engl.*, 1997, **36**, 1205.
6. H. Schumann, A.A. Arif, A.L. Rheingold, C. Janiak, R. Hoffmann and N. Kuhn, *Inorg. Chem.*, 1991, **30**, 1618.
7. '*Organometallics 1: Complexes with Transition Metal-Carbon σ-Bonds*,' M. Bochmann, Oxford University Press, Oxford, 1994.
8. F.R. Hartley, S.G. Murray, W. Levason, H.E. Soutter and C.A. McAuliffe, *Inorg. Chim. Acta*, 1979, **35**, 265.
9. D.J. Gulliver, E.G. Hope, W. Levason, S.G. Murray and G.L. Marshall, *J. Chem. Soc., Dalton Trans.*, 1985, 1265.
10. D.J. Gulliver, E.G. Hope, W. Levason, S.G. Murray, D.M. Potter and G.L. Marshall, *J. Chem. Soc., Perkin Trans. II*, 1984, 429.
11. E.G. Hope, T. Kemmit and W. Levason., *J. Chem. Soc., Perkin Trans. II*, 1987, 487.
12. E.G. Hope, T. Kemmitt and W. Levason, *Organometallics*, 1987, **6**, 206.
13. T.Kemmitt and W. Levason, *Organometallics*, 1989, **8**, 1303.
14. E.G. Hope, T. Kemmitt and W. Levason, *Organometallics*, 1988, **7**, 78.
15. J.J.R.F. da Silva, *J. Chem. Educ.*, 1983, **60**, 390.
16. D.R. Rosseinsky, *J. Chem. Soc., Dalton Trans.*, 1979, 732.
17. J. Meisenheimer, C. Angerman, O. Finn and E. Vieweg, *Chem. Ber.*, 1924, **57**, 1745.
18. E.F. Barker, *Phys. Rev.*, 1929, **33**, 684.
19. D.M. Dennisson and J.D. Hardy, *Phys. Rev.*, 1932, **39**, 938.

20. E.W. Abel, R.P. Bush, F.J. Hopton and C.R. Jenkins, *J. Chem. Soc., Chem. Commun.*, 1966, 58.

21. E.W. Abel, S.K. Bhargava and K.G. Orrell, *Prog. Inorg. Chem.*, 1984, **32**, 1.

22. E.W. Abel, M. Booth and K.G. Orrell, *J. Chem. Soc., Dalton Trans.*, 1980, 1582.

23. '*The Chemistry of Macrocyclic Ligand Complexes*,' L.F. Lindoy, Cambridge University Press, Cambridge, 1989.

24. C.W.G. Ansell, M.K. Cooper, K.P. Dancey, P.A. Duckworth, K. Henrick, M. McPartlin and P.A. Tasker, *J. Chem. Soc., Chem. Commun.*, 1985, 439.

25. '*Coordination Chemistry of Macrocyclic Compounds*,' G.A. Melson, Plenum, New York, 1979.

26. D.K. Cabbiness, *J. Am. Chem. Soc.*, 1969, **91**, 6540.

27. R.J. Batchelor, F.W.B. Einstein, I.D. Gu, B.D. Johnston and B.M. Pinto, *J. Am. Chem. Soc.*, 1989, **111**, 6582.

28. '*Advanced Inorganic Chemistry*,' F.A. Cotton and G. Wilkinson, 5th Edition, Wiley, New York, 383.

29. N.C. Norman, '*Periodicity and the s- and p-Block Elements*,' Oxford University Press, Oxford, 1997.

30. J. Barrett, '*Understanding Inorganic Chemistry*,' Ellis Horwood, Chichester, Sussex, 1991.

31. C.J. Carmalt, W. Clegg, M.R.J. Elsegood and N.C. Norman, *Inorg. Chem.*, 1996, **35**, 3709.

32. C.J. Carmalt, A.H. Cowley, A. Decken and N.C. Norman, *J. Organomet. Chem.*, 1995, **496**, 59.

33. N.C. Norman and N.L. Pickett, *Coord. Chem. Rev.*, 1995, **145**, 27.

34. A.E. Reed and P.V.R. Schleyer, *J. Am. Chem. Soc.*, 1990, **112**, 1434.

35. W. Clegg, R.J. Errington, G.A. Fisher, *J. Chem. Soc., Dalton Trans.*, 1992, 1967.

36. W.Clegg, R.J. Errington, G.A. Fisher, *J. Chem. Soc., Dalton Trans.*, 1993, 637.
37. N.C. Norman, *Phosphorus Sulfur*, 1994, **87**, 167.
38. N.W. Alcock, *Adv. Inorg. Chem. Radiochem.*, 1972, **15**, 1.
39. P. Pykko, *Chem. Rev.*, 1997, **97**, 597.
40. '*Comprehensive Organometallic Chemistry I and II*,' E.W. Abel, F.G.A. Stone and G. Wilkinson (Eds), Pergammon, Oxford, 1982, 1995.
41. E.G. Hope and W. Levason, *Coord. Chem. Rev.*, 1993, **122**, 103.
42. T. Kemmitt, W. Levason and M. Webster, *Inorg. Chem.*, 1989, **28**, 692.
43. T. Kemmitt and W. Levason, *Inorg. Chem.*, 1990, **29**, 731.
44. '*Multinuclear NMR*,' Ed. J. Mason, Plenum, New York, 1987.
45. D.W. Anderson, E.A.V. Ebsworth, G.D. Meikle and D.W.H. Rankin, *Mol. Phys.*, 1973, **25**, 381.
46. '*NMR and the Periodic Table*,' R.K. Harris and B.E. Mann (Eds), Academic Press, London, 1978.
47. T. Kemmitt, W. Levason and M. Webster, *Inorg Chem.*, 1989, **28**, 262.
48. T. Kemmitt and W. Levason, *Inorg. Chem.*, 1990, **29**, 731.
49. W. Levason, S.D. Orchard, G. Reid and V. Tolhurst, *J. Chem. Soc., Dalton Trans.*, 1999, 2071.

CHAPTER 2

Group 6 Carbonyl Complexes of Thio-, Seleno- and Telluro-ether Ligands

2.1 INTRODUCTION

The aim of the work in this chapter was to investigate the coordination chemistry of three ditelluroether ligands (Figure 2.1) with Group 6 carbonyls. The M(0) carbonyl compounds were of the form $[M(CO)_4(L)]$, (M = Cr, Mo or W). The study was carried out in parallel with studies of thio- and seleno-analogues, to place the trends within Group 16 in context.

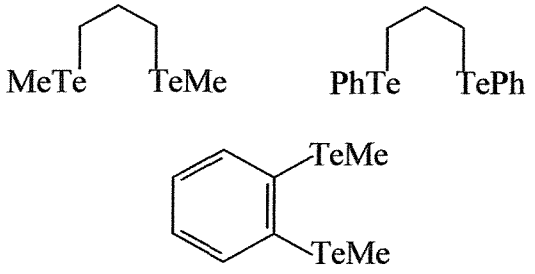

Figure 2.1 – The bidentate telluroether ligands

The coordination chemistry of the Group 6 metal carbonyl complexes has been investigated using multinuclear (^1H, $^{13}C\{^1H\}$, $^{77}Se\{^1H\}$, $^{125}Te\{^1H\}$ and ^{95}Mo) NMR and IR spectroscopies, FAB mass spectrometry and in one case, single crystal X-ray diffraction.

2.1.1 Group 6 Metal Carbonyl Chemistry

Substituted Group 6 carbonyls have been studied in great detail with a wide variety of ligand types,[1] and are thus very suitable systems in which to explore the properties of new ligands. The continued growth in interest of the chemistry of Group 6 metal carbonyls is a consequence of many factors, including the readily availability of $[M(CO)_6]$ (M = Cr, Mo, W), but in particular because of the remarkable variety of chemistry displayed. A number of investigations were carried out during the 1960's concerning Group 6 tetracarbonyls in reactions with Lewis acids.[2-12] Many of the investigations gave illustrations of reactions of $[M(CO)_4(L\text{-}L)]$ (M = Cr, Mo or W; L-L = bidentate

ligand) where the result was the exclusive replacement of one bidentate ligand for another, leaving the carbonyl groups around the metal intact.[2-5,7]

2.1.2 Ditelluroether Ligand Complexes

In the 10 years since a range of chelating ditelluroether ligands was reported,[13-15] thorough investigations of their coordination chemistry with a variety of metals in medium oxidation states have been carried out, including: palladium(II), platinum(II),[16-18] platinum(IV),[19] iridium(III),[16,17,20] rhodium(III), ruthenium(II)[18] and cobalt(III) halides,[21] homoleptic copper(I) and silver(I) systems,[22,23] and tin(IV) halides.[24] In contrast, their chemistry with low valent metal and organometallic species remains largely unexplored. However, complexes with manganese and rhenium carbonyl halides have been reported recently by our research group.[25]

2.1.3 Thio- and Seleno-ether Complexes of Cr, Mo and W

The coordination chemistry of Group 6 carbonyl complexes with acyclic Group 16 ligands is well established.[1,26] Derivatives of sulfur ligands predominate, with fewer examples of selenium complexes. Examples of monosubstituted thioether complexes include $[Cr(CO)_5(SR_2)]$ (R = C_2H_5, CH_3, C_2H_3 and $(CH_3)(CH_2Cl)$),[27] $[Cr(CO)_5(SBu_2)]$,[28,29] $[M(CO)_5(SR^1R^2)]$ (M = Cr, Mo, W; R^1 = C_2H_5, R^2 = C_2H_5, CH_2Ph),[30-32] $[Mo(CO)_5(SR_2)]$ (R = Me, Ph),[30] $[M(CO)_5\{MeS(CH_2S)_nMe\}]$ (M = Cr, W; n = 2, 3),[33] $[Mo(CO)_5L]$ (L = S^tBu_2, tht),[28,29] $[W(CO)_5\{S(CH_2CH)Ph\}]$,[34] $[W(CO)_5(^tBuSCH_2S^tBu)]$[35] and$[W(CO)_5(C_4H_6S)]$.[36]

In contrast to ditelluroethers the corresponding dithioether and diselenoether complexes have received considerable attention.[33,37-53] The variety of complexes studied include $[M(CO)_4\{RS(CH_2)_2SR\}]$ (M = Cr, Mo, W; R = Me, Et, ^{t}Bu),[40,42,50] $[Cr(CO)_4\{^tBuSCH{=}CHS^tBu\}]$,[55] $[Cr(CO)_4\{L\text{-}L\}]$ (L-L = $PhCH_2S(CH_2)_2SCH_2Ph$, $MeS(CH_2)_2SMe$, $^tBuS(CH_2)_2S^tBu$),[6,11,53,56] and $[M(CO)_5\{RS(CH_2)_2SR\}]$ (M = Cr, Mo; R = Et, ^{t}Bu).[40,54]

The primary aim of this chapter was to undertake a systematic study on carbonyl derivatives of Cr(0), Mo(0) and W(0) with a series of ditelluroethers. During the time of the research a range of known and new complexes involving dithioether and diselenoether ligands have been prepared for comparison purposes since we required vibrational data recorded under the same conditions for all the complexes, and literature multinuclear NMR data are very limited. The sulfur and selenium containing ligands are shown in Figure 2.2. The characterisation of ditelluroether complexes with Group 6 carbonyls is of interest in its own right, but it also offers an opportunity to compare ligand properties of dithioethers, diselenoethers and ditelluroethers. For this purpose we used ν(CO) stretching vibrations and the relative magnitude of the ^{77}Se- and ^{125}Te NMR shifts. In principle, the δ(CO) shifts in the $^{13}C\{^{1}H\}$ NMR spectra and for the tungsten complexes the $^{1}J(^{13}C\text{-}^{183}W)$ coupling constants on the CO_{trans}L-L resonances, should also provide useful information.

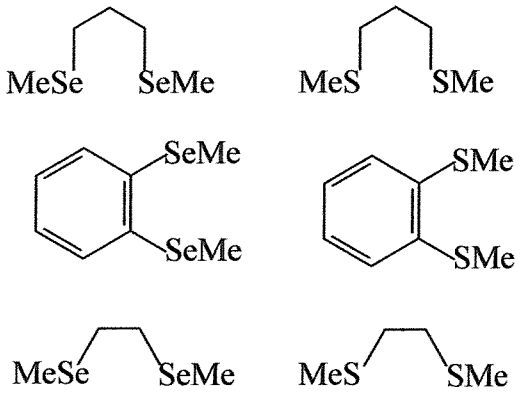

Figure 2.2 – The bidentate thio- and seleno-ether ligands

2.2 RESULTS AND DISCUSSION

2.2.1 Group 6 Metal Carbonyl Complexes

The ligands $MeTe(CH_2)_3TeMe$, $PhTe(CH_2)_3TePh$ and o-$C_6H_4(TeMe)_2$ were synthesised using the literature procedures.[13,14] The synthesis of the complexes with the three ditelluroethers and a range of dithioether and diselenoether analogues were straightforward, utilising reaction of the ligand with $[Cr(CO)_4(nbd)]$, $[Mo(CO)_4(nbd)]$ or $[W(CO)_4(TMPA)]$. The molybdenum and tungsten tetracarbonyl starting reagents were prepared by established methods,[12,57] whilst $[Cr(CO)_4(nbd)]$ was prepared by an amalgamation between two published methods.[12,58] It was the preparation of $[Cr(CO)_4\{MeSe(CH_2)_2SeMe\}]$ by Abel that prompted the use of $[M(CO)_4(nbd)]$ (M = Cr or Mo) as a useful starting material for the preparation of coordinated chalcogen complexes.[45] Abel found that only traces of $[M(CO)_4\{MeSe(CH_2)_2SeMe\}]$ were obtained by the direct reaction of the requisite metal hexacarbonyl; but the displacement of the bidentate diene ligand from $[Cr(CO)_4(nbd)]$ gave a 65 % yield of the desired product.

$$[Mo(CO)_4(nbd)] + L\text{-}L \xrightarrow[\text{room temp., 16 h}]{\text{toluene, } N_2} [Mo(CO)_4(L\text{-}L)]$$

$$[Cr(CO)_4(nbd)] + L\text{-}L \xrightarrow[50^\circ\text{ C, 16 h}]{\text{toluene, } N_2} [Cr(CO)_4(L\text{-}L)]$$

$$[W(CO)_4(tmpa)] + L\text{-}L \xrightarrow[70^\circ\text{ C, 16 h}]{\text{toluene, } N_2} [W(CO)_4(L\text{-}L)]$$

Figure 2.3 – Syntheses of the Group 6 Metal carbonyl complexes

Where M = Mo, the ligand was added to a dry degassed toluene solution of $[Mo(CO)_4(nbd)]$ and the reaction monitored by IR solution spectroscopy. On formation of $[Mo(CO)_4(L\text{-}L)]$ IR spectroscopic studies showed the absence of

bands associated with the starting material and subsequent work-up with $CHCl_3$ and *n*-pentane afforded the products as yellow solids.

The same methodology was applied to the synthesis of $[Cr(CO)_4(L\text{-}L)]$ and, in this case, the reaction was undertaken successfully at 50 °C. Subsequent work-up afforded the products as yellow or orange solids.

The methodology used to successfully synthesise $[W(CO)_4(L\text{-}L)]$ employs the reaction of $[W(CO)_4(tmpa)]$ with the ligand at elevated temperatures in a solution of toluene for a period of about 16 hours. Subsequent work-up afforded the products as orange and yellow solids.

The complexes are air-stable in the solid state and reasonably so in solution when pure. They were insoluble in hydrocarbons, but very soluble in chlorocarbon solvents.

FAB mass spectrometric data for each complex showed peaks corresponding to $[M(CO)_4(L\text{-}L)]^+$ the parent ion, and often fragments corresponding to sequential carbonyl loss. The FAB mass spectrum data (Figure 2.4) are shown for $[Cr(CO)_4\{MeSe(CH_2)_3SeMe\}]$, in which the loss of CO from $[M(CO)_4(L\text{-}L)]^+$ was observed. The data show good agreement with the calculated isotope distributions. These data, together with microanalyses confirmed the formulation of the new complexes as $[M(CO)_4(L\text{-}L)]$.

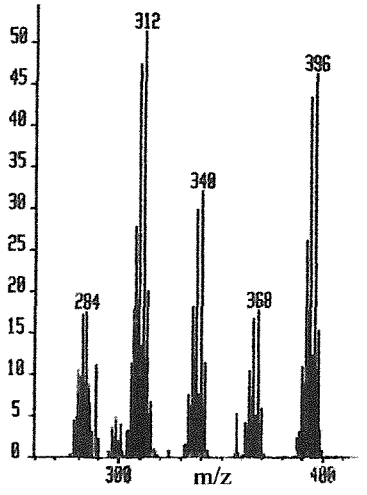

Figure 2.4 – FAB mass spectrum of $[Cr(CO)_4\{MeSe(CH_2)_3SeMe\}]$

The use of solution IR spectroscopy was fundamental to the characterisation of these complexes. As mentioned, IR spectroscopic studies allowed the character of these complexes to be followed throughout the reaction. During the synthesis of $[M(CO)_4(L\text{-}L)]$, the three CO stretches associated with the Group 6 metal tetracarbonyl precursor (Figure 2.5) disappeared and, on formation of the subsequent *cis*-tetracarbonyl $[M(CO)_4(L\text{-}L)]$ three new strong CO bands were observed. Group theory for a *trans* isomer predicts one IR active mode (E_u) and for a *cis* isomer, four stretches ($2A_1 + B_1 + B_2$). The observation of only three bands in the majority of cases is due to the failure to resolve the A_1 and B_1 modes at *ca*, 1900cm^{-1}. A similar effect has been noted in some dithioether complexes.[46] Table 2.1 gives the solution IR data for the complexes. A typical IR spectrum is shown in Figure 2.6. Consideration of ν(CO) shows that for a given metal, the frequencies, especially that of the A_1 mode of the CO's *trans*$_{L\text{-}L}$, fall with donor from S to Se and then there is a rather greater fall to Te. On the conventional M-CO bonding model, this reflects greater electron density on the metal centre resulting in greater π-back-bonding to the CO's and hence a weakening of the C-O bond. The most obvious way of increasing the metal electron density is increased σ-donation from the Group 16 donors. As Group 16 is descended, the electronegativity of the donor atoms fall, and providing the match in orbital overlap and energy remains good, increasing σ-donation would be expected. In metals in positive oxidation states, especially as the formal charge rises, the contraction of the metal d-orbitals has been suggested to lead to mismatch in orbital size and energy at tellurium,[15] but in the expanded d-orbitals of zero-valent metals as in the present case this is unlikely to be a problem. It should also be noted that the frequency for stretching modes of the carbonyl group are generally higher for molybdenum complexes with the chromium tetracarbonyl complexes having the lowest stretching frequencies of the series. Therefore, the frequency of tungsten carbonyl stretching modes are generally between those of the molybendum and chromium for a given ligand

This trend can be attributed to the greater electronegativity of the chromium compared to that of molybdenum.

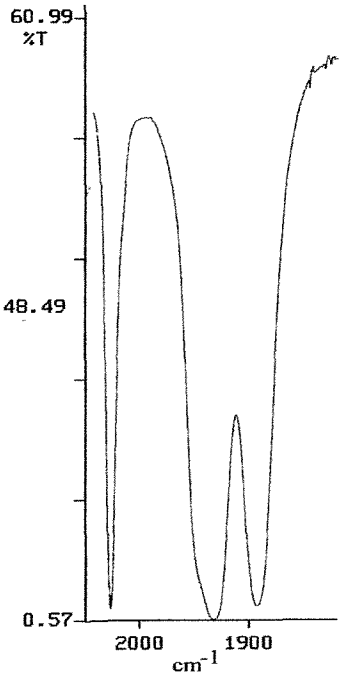

Figure 2.5 – ν(CO) region of IR spectrum of [Cr(CO)$_4$(nbd)]

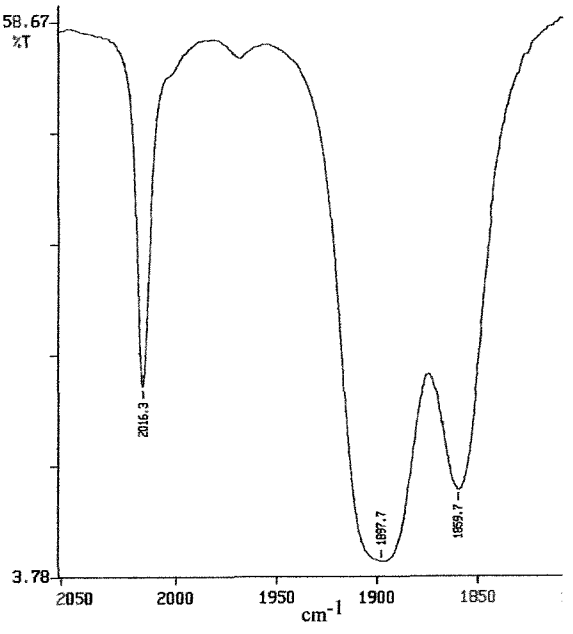

Figure 2.6 – ν(CO) region of IR spectrum of [Cr(CO)$_4${MeS(CH$_2$)$_2$SMe}]

Table 2.1 – IR spectroscopic data (CO region)

Complex	υ(CO)/cm$^{-1,a}$			
$[Cr(CO)_4\{MeTe(CH_2)_3TeMe\}]$	2000(m)	1887(s, br)		1858(s)
$[Mo(CO)_4\{MeTe(CH_2)_3TeMe\}]$	2015(m)	1908(s, br)		1862(s)
$[W(CO)_4\{MeTe(CH_2)_3TeMe\}]$	2010(m)	1894(s, br)		1859(s)
$[Cr(CO)_4\{PhTe(CH_2)_3TePh\}]$	2003(m)	1903(sh)	1891(s, br)	1870(s)
$[Mo(CO)_4\{PhTe(CH_2)_3TePh\}]$	2018(m)	1907(s, br)		1875(s)
$[W(CO)_4\{PhTe(CH_2)_3TePh\}]$	2013(m)	1895(s, br)		1869(s)
$[Cr(CO)_4\{o\text{-}C_6H_4(TeMe)_2\}]$	2005(m)	1902(s, br)		1873(s)
$[Mo(CO)_4\{o\text{-}C_6H_4(TeMe)_2\}]$	2020(m)	1920(sh)	1911(s)	1880(s)
$[W(CO)_4\{o\text{-}C_6H_4(TeMe)_2\}]$	2015(m)	1900(s, br)		1875(s)
$[Cr(CO)_4\{MeS(CH_2)_2SMe\}]$	2016(s)	1898(s, br)		1860(s)
$[Mo(CO)_4\{MeS(CH_2)_2SMe\}]$	2024(s)	1910(s, br)		1863(s)
$[W(CO)_4\{MeS(CH_2)_2SMe\}]$	2019(m)	1897(s, br)		1859(s)
$[Mo(CO)_4\{o\text{-}C_6H_4(SMe)_2\}]$	2028(m)	1917(s, br)		1870(s)
$[Cr(CO)_4\{MeS(CH_2)_3SMe\}]$	2015(s)	1900(s)	1890(sh)	1854(s)
$[Mo(CO)_4\{MeS(CH_2)_3SMe\}]$	2023(s)	1910(s, br)	1895(sh)	1856(s)
$[W(CO)_4\{MeS(CH_2)_3SMe\}]$	2018(m)	1897(s)	1890(sh)	1852(s)
$[Cr(CO)_4\{MeSe(CH_2)_2SeMe\}]$	2011(s)	1900(sh)	1889(s)	1860(s)
$[Mo(CO)_4\{MeSe(CH_2)_2SeMe\}]$	2021(m)	1909(s, br)		1862(s)
$[W(CO)_4\{MeSe(CH_2)_2SeMe\}]$	2016(m)	1895(s, br)		1858(s)
$[Cr(CO)_4\{MeSe(CH_2)_3SeMe\}]$	2009(m)	1894(s, br)		1852(s)
$[Mo(CO)_4\{MeSe(CH_2)_3SeMe\}]$	2020(m)	1908(s)	1895(sh)	1855(s)
$[W(CO)_4\{MeSe(CH_2)_3SeMe\}]$	2015(m)	1896(s)	1885(sh)	1850(s)
$[Cr(CO)_4\{o\text{-}C_6H_4(SeMe)_2\}]$	2015(s)	1902(s, br)		1866(s)
$[Mo(CO)_4\{o\text{-}C_6H_4(SeMe)_2\}]$	2025(m)	1914(s, br)		1870(m)
$[W(CO)_4\{o\text{-}C_6H_4(SeMe)_2\}]$	2019(m)	1901(s, br)		1866(s)

a. Spectra measured in CH_2Cl_2 solution

2.2.2 NMR Spectroscopic Studies

Multinuclear (^{1}H, $^{13}C\{^{1}H\}$, $^{77}Se\{^{1}H\}$, $^{125}Te\{^{1}H\}$ and ^{95}Mo) NMR spectroscopic studies were undertaken to give an insight into the character of these species in solution. The good solubility of Group 6 metal carbonyl complexes with bidentate ligands is one of the main reasons for systems of this type being employed in inversion studies at coordinated chalcogens. Examples include the complexes $[Cr(CO)_4(L\text{-}L)]$, (L-L = $MeSeCH_2CMe_2CH_2SeMe$,[38] $^{i}PrSeCH_2CH_2SePr^{i}$[39] and $PhCH_2SCH_2CH_2SCH_2Ph$[59]).

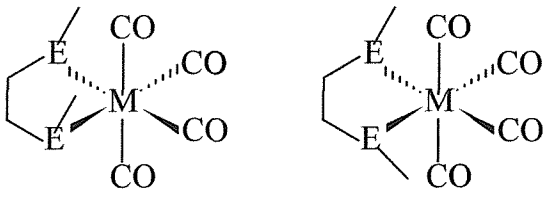

Figure 2.7 – The isomeric forms of *cis*-$[M(CO)_4(L\text{-}L)]$

For a $[M(CO)_4(ditelluroether)]$ complex two stereoisomers (invertomers) are expected: *meso* and *DL* (Figure 2.7), which interconvert by pyramidal inversion at tellurium. When inversion is slow on the NMR timescale, the two invertomers are readily distinguished in the ^{1}H-NMR spectra. Previous studies[60] have established that for dithioether and diselenoether complexes, the energy barriers to inversion are dependent on the following factors. They are sensitive to the nature of the inverting chalcogen with the barrier to inversion in the order Se > S; and the ligand backbone also has the potential to influence energies via π-conjugation effects, ring strain and ring size leading to the ordering $-(CH_2)_2- > -(CH_2)_3- > o\text{-}C_6H_4$. The Group 6 metal also affects inversion barriers in the order W > Cr > Mo. The only quantitative data on ditelluroethers is from $[PtMe_3I(ditelluroether)]$ complexes,[19] which revealed that inversion was a higher energy process in these complexes than in diselenoether analogues.

The following section outlines the ^{1}H, $^{13}C\{^{1}H\}$, $^{77}Se\{^{1}H\}$, $^{125}Te\{^{1}H\}$ and ^{95}Mo NMR spectroscopic data recorded for all the Group VI metal species in this work.

^{1}H NMR Spectroscopic Studies

The ^{1}H NMR spectra of the new complexes were recorded at 300 K. Coordination of the ligand to the metal centre is supported by the change of chemical shift with respect to the free ligand. All the ditelluroether complexes show resonances for both invertomers. This is illustrated in Figure 2.9. This is consistent with relatively high inversion barriers. The ^{1}H NMR data show that all the dithioether complexes are inverting rapidly on the NMR timescale at ambient temperatures, consistent with previous detailed studies.[33,44] Thus, for $[Mo(CO)_4\{MeS(CH_2)_2SMe\}]$ (Figure 2.8) one sharp, singlet is observed at *ca.* δ 3ppm corresponding to the equivalent methyl groups, and similarly there is a singlet observed for the CH_2 protons and there is no distinguishing between *DL* and *meso* invertomers for the dithioether complexes. The behaviour of the diselenoether complexes is more complicated. Thus, the NMR spectra of $[M(CO)_4\{MeSe(CH_2)_2SeMe\}]$ (M = Cr or W) at 300 K show sharp resonances attributable to the *meso* and *DL* forms, whereas $[M(CO)_4\{MeSe(CH_2)_3SeMe\}]$ (M = Cr or Mo) and $[Mo(CO)_4\{\underline{o}\text{-}C_6H_4(SeMe)_2\}]$ exhibit much simpler averaged spectra due to rapid inversion. The other four complexes, $[Mo(CO)_4\{MeSe(CH_2)_2SeMe\}]$, $[W(CO)_4\{MeSe(CH_2)_3SeMe\}]$ and $[M(CO)_4\{\underline{o}\text{-}C_6H_4(SeMe)_2\}]$, (M = Cr or W) show broadened resonances typical of systems near to coalescence. These results conform with expected trends in inversion barriers[60] outlined earlier.

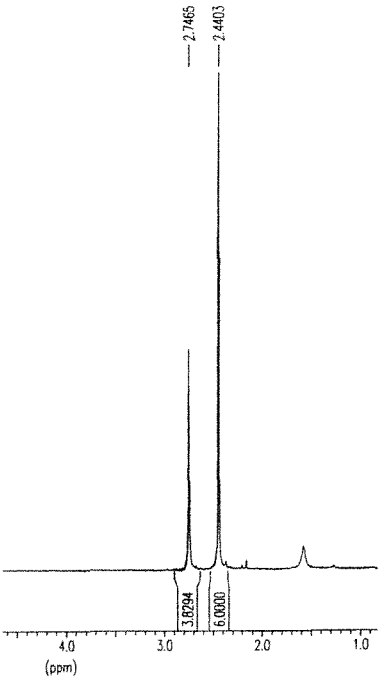

Figure 2.8 – ^{1}H NMR spectrum of [Mo(CO)$_4${MeS(CH$_2$)$_2$SMe}]

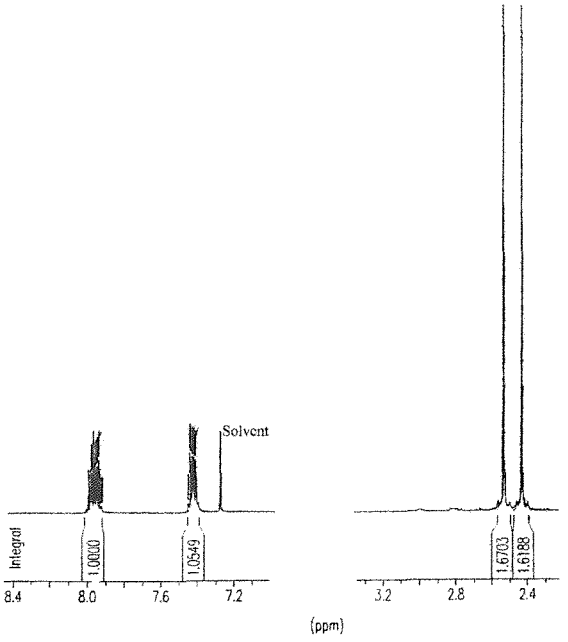

Figure 2.9 – ^{1}H NMR spectrum of [Mo(CO)$_4${o-C$_6$H$_4$(TeMe)$_2$}] showing resonances for *meso* and *DL* invertomers (approx. 1:1 ratio)

Table 2.2 – ^{1}H NMR spectroscopic data

Complex	δ $^1H^a$
$[Cr(CO)_4\{MeTe(CH_2)_3TeMe\}]$	1.70(m)(CH_2), 2.12, 2.18(Me), 2.68(m)(CH_2Te)
$[Mo(CO)_4\{MeTe(CH_2)_3TeMe\}]$	1.93(m)(CH_2), 2.16, 2.21(Me), 2.68(m)(CH_2Te)
$[W(CO)_4\{MeTe(CH_2)_3TeMe\}]$	1.90(m)(CH_2), 2.23, 2.28(Me), 2.73(m)(CH_2Te)
$[Cr(CO)_4\{PhTe(CH_2)_3TePh\}]$	1.71(m)(CH_2), 2.83(m), 3.0(m)(CH_2Te), 7.3-7.8(m)(Ph)
$[Mo(CO)_4\{PhTe(CH_2)_3TePh\}]$	1.9(m)(CH_2), 2.85(m), 2.95(m)(CH_2Te), 7.3-7.8(m)(Ph)
$[W(CO)_4\{PhTe(CH_2)_3TePh\}]$	1.9(m)(CH_2), 2.9(m), 3.1(m)(CH_2Te), 7.4-7.8(m)(Ph)
$[Cr(CO)_4\{o\text{-}C_6H_4(TeMe)_2\}]$	2.31, 2.41(Me), 7.4(m), 7.8(m)(C_6H_4)
$[Mo(CO)_4\{o\text{-}C_6H_4(TeMe)_2\}]$	2.33, 2.42(Me), 7.4(m), 7.4(m)(C_6H_4)
$[W(CO)_4\{o\text{-}C_6H_4(TeMe)_2\}]$	2.43, 2.53(Me), 7.4(m), 7.8(m)(C_6H_4)
$[Cr(CO)_4\{MeS(CH_2)_2SMe\}]$	2.35(Me), 2.65(CH_2)
$[Mo(CO)_4\{MeS(CH_2)_2SMe\}]$	2.44(Me), 2.74(CH_2)
$[W(CO)_4\{MeS(CH_2)_2SMe\}]$	2.62(Me), 2.78(CH_2)
$[Mo(CO)_4\{o\text{-}C_6H_4(SMe)_2\}]$	2.83(Me), 7.4(m), 7.8(m)(C_6H_4)
$[Cr(CO)_4\{MeS(CH_2)_3SMe\}]$	2.14(m)(CH_2), 2.41(Me), 2.78(m)(CH_2S)
$[Mo(CO)_4\{MeS(CH_2)_3SMe\}]$	2.20(m)(CH_2), 2.49(Me), 2.88(m)(CH_2S)
$[W(CO)_4\{MeS(CH_2)_3SMe\}]$	2.32(m)(CH_2), 2.67(Me), 3.02(m)(CH_2S)
$[Cr(CO)_4\{MeSe(CH_2)_2SeMe\}]$	2.14, 2.23(Me), 3.1, 3.3(CH_2)
$[Mo(CO)_4\{MeSe(CH_2)_2SeMe\}]$	2,2(v.br,Me), 3.0(v.br,CH_2)
$[W(CO)_4\{MeSe(CH_2)_2SeMe\}]$	2.37, 2.55(Me), 3.3, 3.35(CH_2)
$[Cr(CO)_4\{MeSe(CH_2)_3SeMe\}]$	2.18(CH_2), 2.30(Me), 2.8(br,CH_2Se)
$[Mo(CO)_4\{MeSe(CH_2)_3SeMe\}]$	2.25(CH_2), 2.37(Me), 2.8(br,CH_2Se)
$[W(CO)_4\{MeSe(CH_2)_3SeMe\}]$	2.39(CH_2), 2.53(Me), 3.0(br,CH_2Se)
$[Cr(CO)_4\{o\text{-}C_6H_4(SeMe)_2\}]$	2.60(br,Me), 7.4(m), 7.8(m)(C_6H_4)
$[Mo(CO)_4\{o\text{-}C_6H_4(SeMe)_2\}]$	2.66(Me), 7.4(m), 7.9(m)(C_6H_4)
$[W(CO)_4\{o\text{-}C_6H_4(SeMe)_2\}]$	2.43, 2.53(Me), 7.4(m), 7.9(m)(C_6H_4)

a. In $CDCl_3$, all resonances are singlets unless otherwise indicated.

$^{13}C\{^1H\}$ NMR Spectroscopic Studies

Data obtained from $^{13}C\{^1H\}$ NMR spectroscopy are shown in Table 2.3 and Table 2.4. The $^{13}C\{^1H\}$ NMR spectra for these derivatives were recorded at 300 K. Their appearance depends upon whether the complex is undergoing fast inversion or not, this time on the energy of the ^{13}C NMR time scale. If fast inversion is occurring then only two δ(CO) resonances are expected due to the CO groups mutually *trans* and those $trans_{L\text{-}L}$. However, if inversion is slow, five δ(CO) resonances are expected by symmetry, two due to CO $trans_{L\text{-}L}$ in the *meso* and *DL* invertomers respectively, one due to the mutually *trans* CO in the *DL* form, and two due to the CO $trans_{CO}$ in the *meso* form, which are distinguished by being *syn* or *anti* to the R-groups on the ligands. In practice (Table 2.3 and Table 2.4) whilst five resonances are seen in some cases, e.g. $[Cr(CO)_4\{MeTe(CH_2)_3TeMe\}]$, in others, e.g. $[Cr(CO)_4\{o\text{-}C_6H_4(TeMe)_2\}]$, only four are seen, which is due to accidental coincidence of the δ(CO) $trans_{L\text{-}L}$ in the two invertomers.

For the range of selenium and sulfur ligand analogues the $^{13}C\{^1H\}$ NMR data show that all the dithioether complexes are inverting rapidly on the ^{13}C NMR time scale, resulting in only two δ(CO) resonances, consistent with the previously mentioned detailed studies.[33,44] The behaviour of the diselenoether complexes is more complicated. Thus, the NMR spectra of $[M(CO)_4\{MeSe(CH_2)_3SeMe\}]$ and $[M(CO)_4\{o\text{-}C_6H_4(SeMe)_2\}]$ (M = Cr, Mo or W) at 300K exhibit simple averaged spectra due to rapid inversion, whereas $[W(CO)_4\{MeSe(CH_2)_2SeMe\}]$ shows five resonances and $[M(CO)_4\{MeSe(CH_2)_2SeMe\}]$ (M = Cr or Mo) exhibit four resonances attributable to the *meso* and *DL* forms.

Table 2.3 – $^{13}C\{^1H\}$ NMR spectroscopic data for ditelluroether complexes

Complex	$\delta^{13}C\{^1H\}$[a]
$[Cr(CO)_4\{MeTe(CH_2)_3TeMe\}]$	228.1, 227.9, 224.0, 223.2, 221.5(CO), 25.8, 25.6(CH_2), 6.3, 5.9(CH_2Te), -10.5, -12.5(Me)
$[Mo(CO)_4\{MeTe(CH_2)_3TeMe\}]$	215.7, 211.5, 211.0, 209.3(CO), 27.2(CH_2), 7.6, 6.5(CH_2Te), -10.4, -11.4(Me)
$[W(CO)_4\{MeTe(CH_2)_3TeMe\}]$	206.2(170), 204.8(-), 203.9(-), 201.9(120)(CO)[b], 28.1, 27.8(CH_2), 8.7, 7.6(CH_2Te), -8.0, -9.5(Me)
$[Cr(CO)_4\{PhTe(CH_2)_3TePh\}]$	227.7, 227.3, 224.4, 222.0, 220.5(CO), 137-129(Ph), 27.0, 26.3(CH_2), 11.8, 11.6(CH_2Te)
$[Mo(CO)_4\{PhTe(CH_2)_3TePh\}]$	215.6, 211.2, 210.8, 208.6(CO), 137-130(Ph), 28.0, 27.4(CH_2), 13.3, 12.8(sh)(CH_2Te)
$[W(CO)_4\{PhTe(CH_2)_3TePh\}]$	205.5(-), 205.3(160), 205.0(-), 203.5(125), 203.4(-), 137-129(Ph), 28.9, 27.9(CH_2), 13.9, 13.5(CH_2Te)
$[Cr(CO)_4\{o\text{-}C_6H_4(TeMe)_2\}]$	230.7, 221.6, 220.9, 220.5(CO), 139-126(C_6H_4), -4.0, -4.6(Me)
$[Mo(CO)_4\{o\text{-}C_6H_4(TeMe)_2\}]$	218.3, 208.8, 208.6, 208.4(CO), 139-123(C_6H_4), -3.5, -3.8(Me)
$[W(CO)_4\{o\text{-}C_6H_4(TeMe)_2\}]$	208.7(-), 208.6(-), 201.6, 201.1(-), 200.5(-)(CO), 139-123(C_6H_4), -1.5, -1.7(Me)

a. In CH_2Cl_2-10 % $CDCl_3$ containing $Cr(acac)_3$.

b. Values in parentheses are $^1J(^{183}W\text{-}^{13}C)$/Hz, (-) indicates couplings unclear or satellites not observed.

Table 2.4 – $^{13}C\{^1H\}$ NMR spectroscopic data for dithio- and diselenoether complexes

Complex	$\delta\ ^{13}C\{^1H\}$[a]
$[Cr(CO)_4\{MeS(CH_2)_2SMe\}]$	227.1, 216.3(CO), 35.4(CH_2), 24.6(Me)
$[Mo(CO)_4\{MeS(CH_2)_2SMe\}]$	217.5, 206.5(CO), 35.2(CH_2), 25.3(Me)
$[W(CO)_4\{MeS(CH_2)_2SMe\}]$	207.9(164), 201.4(135)(CO)[b], 36.5(CH_2), 26.8(Me)
$[Mo(CO)_4\{o\text{-}C_6H_4(SMe)_2\}]$	217.6, 205.8(CO), 138-130(C_6H_4), 32.6(Me)
$[Cr(CO)_4\{MeS(CH_2)_3SMe\}]$	225.8, 217.0(CO), 38.6(CH_2S), 25.5(Me), 24.5(CH_2)
$[Mo(CO)_4\{MeS(CH_2)_3SMe\}]$	217.0, 207.1(CO), 39.7(CH_2S), 26.5(Me), 25.0(CH_2)
$[W(CO)_4\{MeS(CH_2)_3SMe\}]$	207.6(156), 202.7(126)(CO), 39.9(CH_2S), 28.0(Me), 24.9(CH_2)
$[Cr(CO)_4\{MeSe(CH_2)_2SeMe\}]$	229.0, 219.2, 217.8, 216.7(CO), 28.5, 28.0(CH_2), 14.5, 13.5(Me)
$[Mo(CO)_4\{MeSe(CH_2)_2SeMe\}]$	217.9, 207.9, 207.4, 207.0(CO), 31.1, 26.9(CH_2), 14.9(sh), 14.2(Me)
$[W(CO)_4\{MeSe(CH_2)_2SeMe\}]$	208.3(sh), 208.2(156), 203.2(-), 202.1(-), 200.8(-)(CO), 29.4, 28.0(CH_2), 16.8, 15.6(Me)
$[Cr(CO)_4\{MeSe(CH_2)_3SeMe\}]$	227.0, 219.0(CO), 29.1(CH_2Se), 25.5(CH_2), 14.3(Me)
$[Mo(CO)_4\{MeSe(CH_2)_3SeMe\}]$	216.8, 208.3(CO), 20.5(CH_2Se), 26.3(CH_2), 15.5(Me)
$[W(CO)_4\{MeSe(CH_2)_3SeMe\}]$	206(v.br), 219.0(v.br)(CO), 20.0(CH_2Se), 26.0(CH_2), 16.4(Me)
$[Cr(CO)_4\{o\text{-}C_6H_4(SeMe)_2\}]$	227.8, 211.6(CO), 134-126(C_6H_4), 24.8(Me)
$[Mo(CO)_4\{o\text{-}C_6H_4(SeMe)_2\}]$	218.0, 206.7(CO), 135-130(C_6H_4), 22.9(Me)
$[W(CO)_4\{o\text{-}C_6H_4(SeMe)_2\}]$	208.4(165), 201(v.br)(-), 135-130(C_6H_4), 24.8(Me)

a. In CH_2Cl_2-10 % $CDCl_3$ containing $Cr(acac)_3$.

b. Values in parentheses are $^1J(^{183}W\text{-}^{13}C)$/Hz, (-) indicates coupling unclear or satellites not observed.

$^{125}Te\{^1H\}$ and $^{77}Se\{^1H\}$ NMR Spectroscopic Studies

The $^{125}Te\{^1H\}$ NMR data on the complexes are given in Table 2.5. As mentioned previously provided, pyramidal inversion is slow enough on the NMR timescale, both forms, *DL* and *meso*, will be seen in the NMR spectra. It is important to note that NMR timescales differ for each nucleus considered. All ditelluroether complexes show two resonances. Likewise, apart from $[Mo(CO)_4\{o\text{-}C_6H_4(SeMe)_2\}]$ and $[M(CO)_4\{MeSe(CH_2)_3SeMe\}]$ (M = Cr or Mo), which show single averaged signals (fast inversion), the selenium containing complexes each show two resonances. $^{77}Se\{^1H\}$ NMR data for the diselenoethers are given in Table 2.5.

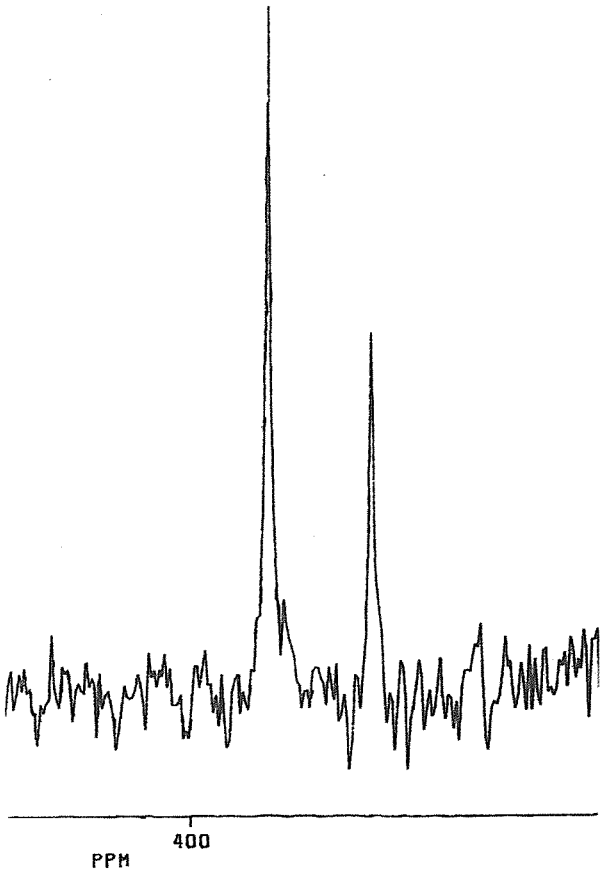

Figure 2.10 - $^{125}Te\{^1H\}$ NMR spectrum for $[W(CO)_4\{PhTe(CH_2)_3TePh\}]$

Table 2.5 – $^{77}Se\{^1H\}$ and $^{125}Te\{^1H\}$ NMR Spectroscopic Data

Complex	δ $^{77}Se\{^1H\}$ or $^{125}Te(^1H\}^a$		Δ^b
$[Cr(CO)_4\{MeTe(CH_2)_3TeMe\}]$	259	253	152
$[Mo(CO)_4\{MeTe(CH_2)_3TeMe\}]$	169.5	162	61
$[W(CO)_4\{MeTe(CH_2)_3TeMe\}]$	94	93	-10
$[Cr(CO)_4\{PhTe(CH_2)_3TePh\}]$	550	548	83
$[Mo(CO)_4\{PhTe(CH_2)_3TePh\}]$	477	476	10
$[W(CO)_4\{PhTe(CH_2)_3TePh\}]$	396	390	-73
$[Cr(CO)_4\{o\text{-}C_6H_4(TeMe)_2\}]$	864	856	488
$[Mo(CO)_4\{o\text{-}C_6H_4(TeMe)_2\}]$	725	723.5	382
$[W(CO)_4\{o\text{-}C_6H_4(TeMe)_2\}]$	664	657	289
$[Cr(CO)_4\{MeSe(CH_2)_2SeMe\}]$	289	286	141.5
$[Mo(CO)_4\{MeSe(CH_2)_2SeMe\}]$	213	206	88.5
$[W(CO)_4\{MeSe(CH_2)_2SeMe\}]$	183	179	60
$[Cr(CO)_4\{MeSe(CH_2)_3SeMe\}]$	387	384	183.5
$[Mo(CO)_4\{MeSe(CH_2)_3SeMe\}]$	331		129
$[W(CO)_4\{MeSe(CH_2)_3SeMe\}]$	306	303	103
$[Cr(CO)_4\{o\text{-}C_6H_4(SeMe)_2\}]$	98		24
$[Mo(CO)_4\{o\text{-}C_6H_4(SeMe)_2\}]$	64		-10
$[W(CO)_4\{o\text{-}C_6H_4(SeMe)_2\}]$	37	24[c]	-43

a. In CH_2Cl_2-10 % $CDCl_3$ relative to neat external Me_2Se or Me_2Te.

b. Average $\delta_{complex} - \delta_{free\ ligand}$.

c. No resonance observed at 300 K, presumably due to inversion broadening, data obtained at 230 K.

In all cases, coordination to the $M(CO)_4$ fragment produces characteristic frequency shifts, the magnitude of the coordination shifts (Δ) reflecting the chelate ring size present, those in 5-membered rings being markedly greater than those in 6-membered ones.[16] For a particular ligand, the largest high-frequency shift is observed in the chromium complex, a smaller shift occurs for the molybdenum analogue, and the smallest for the tungsten. In the cases of $[W(CO)_4\{RTe(CH_2)_3TeR\}]$ (R = Me or Ph), the δ(Te) resonances are to low frequency of that of the free ligand.

The relative population of *meso* and *DL* invertomers also varies with the metal and ligand combination. For o-$C_6H_4(TeMe)_2$ complexes of Cr and Mo in CH_2Cl_2 solution, the two invertomers have similar abundances, but the tungsten complex the *meso*:*DL* ratio is *ca.* 10:7. In the complexes of $MeTe(CH_2)_3TeMe$, the invertomers are of approximately equal abundance for all three metals, but in complexes of $PhTe(CH_2)_3TePh$, the *DL* invertomer predominates (>70 %), possibly indicating destabilising interactions between the Ph groups and the axial carbonyl group in the *meso* form.

As stated above the shifts are very sensitive to the ring size and the metal present. However, if we compare the data on complexes of the same metal with isostructural ligands, we see similar trends, with larger coordination shifts in the tellurium spectra as usually observed.[15] In many organoselenium and organotellurium systems the relative magnitude of the heteroatom chemical shifts (δ(Te)/δ(Se)) are *ca.* 1.8,[15,61] and this ratio is also found in several series of seleno- and telluro-ether complexes with platinum metal halides.[16] However, in the present carbonyl systems for a fixed metal and ligand type the ratios are significantly greater, (see Table 2.6), which indicates that the tellurium centre is deshielded to an unexpected degree and is consistent with greater Te $\rightarrow$ M σ-donation. The $^{77}Se\{^1H\}$ NMR spectrum of $[W(CO)_4\{MeSe(CH_2)_3SeMe\}]$ was not observed at room temperature, and the data obtained at 230 K were used (see Table 2.5). Since $^{77}Se\{^1H\}$ NMR shifts often vary with temperature the

comparison is subject to larger errors than in the other cases, but nonetheless exhibits the expected trend.

Table 2.6. – Relative magnitude of chemical shifts ratio (δ(Te)/δ(Se))

	Cr	Mo	W
o-$C_6H_4(EMe)_2$	2.25	2.2	2.2
$MeE(CH_2)_3EMe$	2.6	2.6	3

^{95}Mo NMR Spectroscopic Studies

$[Mo(CO)_4\{MeTe(CH_2)_3TeMe\}]$ exhibits two ^{95}Mo resonances consistent with the presence of both invertomers, whilst for $[Mo(CO)_4\{PhTe(CH_2)_3TePh\}]$ there is a high frequency shoulder on the major ^{95}Mo resonance. However, the ^{95}Mo NMR spectra of the seven complexes (Table 2.7), each contain only a single resonance. The δ(Mo) shifts sequentially to high frequency with donor in the order Te < Se < S and with chelate ring size in the order 5 < 6. For seven of the complexes, the ^{95}Mo NMR spectra do not distinguish the invertomers, indicating either that inversion is fast on the molybdenum NMR time scale or that the individual resonances are not resolved in the line-width. Since the lines are relatively sharp (≤ 300 Hz), the former seems much more likely. This behaviour is in marked contrast to $[Mn(CO)_3X(ditelluroether)]$, $[PtX_2(ditelluroether)]$ or $[PtMe_3X(ditelluroether)]$ (X = halide), where the ^{55}Mn or ^{195}Pt NMR spectra show well-separated resonances for the individual invertomers.[16,17,19,25] On cooling the samples, the lines broaden rapidly, possibly due to the ^{95}Mo quadrupole (^{95}Mo, I = 5/2) and low-temperature spectra were not obtained, an effect previously observed for dithioether complexes.[44] The interpretation of metal nuclei NMR chemical shifts is usually based upon the Ramsey equation,[62] which in its simplest form separates the overall shielding parameter σ into diamagnetic (σ_d) and paramagnetic (σ_p) components, hence $\sigma = \sigma_d + \sigma_p$

For heavy nuclei such as ^{95}Mo, the paramagnetic term is the dominant factor influencing changes in nuclear shielding. Deshielding results from small values of ΔE (the average excitation energy – essentially the weighted mean ligand field strength) and with a reduced d-electron delocalisation. The shielding of the Mo nuclei with, Te > Se > S, could thus be due to increasing ligand field splitting as Group 16 is descended, and/or better delocalisation (π-acceptance) in the same order. Theoretical studies by Schumann and Hoffmann[63] concluded that π effects were negligible in Group 16 donor ligands, and thus, the trends in the molybdenum NMR data are most likely due to increased σ-donation in the order S→Se→Te.

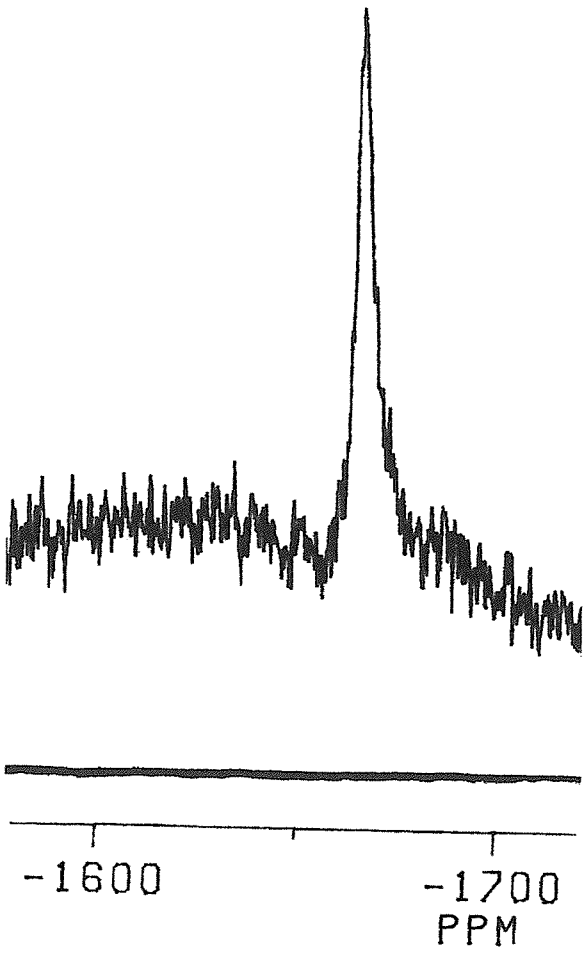

Figure 2.11 – ^{95}Mo NMR spectrum of $[Mo(CO)_4\{o\text{-}C_6H_4(TeMe)_2\}]$ in CH_2Cl_2

Table 2.7 – ^{95}Mo NMR spectroscopic data

Complex	$\delta\ ^{95}Mo^{a\ b}$	
$[Mo(CO)_4\{MeTe(CH_2)_3TeMe\}]$	-1597(200)	-1621(200)
$[Mo(CO)_4\{PhTe(CH_2)_3TePh\}]$	-1580(sh)	-1594(300)
$[Mo(CO)_4\{o\text{-}C_6H_4(TeMe)_2\}]$	-1667(140)	
$[Mo(CO)_4\{MeSe(CH_2)_2SeMe\}]$	-1432(160)	
$[Mo(CO)_4\{MeSe(CH_2)_3SeMe\}]$	-1437(200)	
$[Mo(CO)_4\{o\text{-}C_6H_4(SeMe)_2\}]$	-1340(200)	
$[Mo(CO)_4\{MeS(CH_2)_3SMe\}]$	-1372(85)	
$[Mo(CO)_4\{o\text{-}C_6H_4(SMe)_2\}]$	-1375(260)	
$[Mo(CO)_4\{MeS(CH_2)_3SMe\}]$	-1294(50)	

a. Relative to external aqueous Na_2MoO_4 ($W_{1/2}$ in parentheses Hz).

b. Spectra recorded in CH_2Cl_2-10 % $CDCl_3$

2.2.3 X-Ray Crystallography

In order to confirm the stereochemistry at the metal centres and to establish bond length and bond angle distributions, single crystal structure analysis was undertaken on $[Cr(CO)_4\{MeSe(CH_2)_2SeMe\}]$. Crystals were obtained from vapour diffusion of *n*-pentane into a solution of the complex in CH_2Cl_2.

Crystal Structure of $[Cr(CO)_4\{MeSe(CH_2)_2SeMe\}]$

The complex exists as discrete molecules. The structure reveals the expected *cis* disubstituted distorted octahedron about the central chromium atom, with Se-Cr-Se 86.59(5) °, the C-Cr-Se angles slightly greater than 90 ° and the C-Cr-C less than 90 °. Other substituted carbonylchromium complexes have shown similar deviations away from the octahedral ideal.[41,64-68] The ligand adopts the *DL* conformation with Cr-Se 2.517(1), 2.520(2) Å, and Cr-$C_{cis\text{-}Se}$ 1.891(8), 1.892(7) and Cr-$C_{trans\text{-}Se}$ 1.832(7), 1.8314(8) Å. The structural data

may be compared with those in $[Cr(CO)_4\{DL\text{-}EtS(CH_2)_2SEt\}]$ where Cr-S = 2.418(1), Cr-$C_{cis\text{-}S}$ = 1.887(3), and Cr-$C_{trans\text{-}S}$ = 1.831(3) Å.[41] The differences in the Cr-chalcogen bond length reflects the larger size of Se. The Cr-C distances are not significantly different (for $[Cr(CO)_4\{MeSe(CH_2)_2SeMe\}]$ Cr-$C_{cis\text{-}Se}$ = 1.891(8) and Cr-$C_{trans\text{-}Se}$ = 1.832(7)). Unfortunately, we have been unable to grow good quality crystals of a chromium telluroether complex to complete the comparisons. In the structure of $[Cr(CO)_4\{MeSe(CH_2)_2SeMe\}]$, the two Cr-$C_{trans\text{-}Se}$ bonds (1.832(7) and 1.834(8) Å) are significantly shorter than the two Cr-$C_{trans\text{-}C}$ bonds (1.891(8) and 1.892(7) Å). The bond order of Cr-C increases when *trans* to selenium as a result of the increased electron density on the metal centre creating more π back bonding on the carbonyl group.

In the structure of $[Cr(CO)_4\{MeSe(CH_2)_2SeMe\}]$ there is some evidence of strain in the five-membered chelate ring. Thus the angle at the chromium atom (85.59 °) is less than the ideal 90 ° and the angles at the bridging carbon atoms (113.2 °) are greater than normal tetrahedral values.

The two *trans*-C-O bonds (1.172(8) and 1.159(8) Å) can be considered not significantly different than the two *cis*-C-O bonds (1.149(8) and 1.154(8) Å). The carbonyl groups are coordinated in the usual linear fashion, the Cr-C-O angles being 176.1(7) and 173.9(6) ° for the *cis* carbonyl groups, and 172.2(6) and 175.5(6) ° for the *trans* carbonyl groups. The C(2)-Cr(1)-C(1) bond angle is 175.5(6) ° indicating that the axial carbonyl groups are bent in the direction away from the $MeSe(CH_2)_2SeMe$ ligand. The five-membered chelate ring has the expected puckered conformation, with the atoms C(6) and C(7) above and below the plane defined by the atoms Se(1), Cr, Se(2).

Table 2.8 – Crystallographic data for $[Cr(CO)_4\{MeSe(CH_2)_2SeMe\}]$

Formula	$C_8H_{10}CrO_4Se_2$
Formula Weight	380.08
Colour, morphology	yellow, block
Crystal Dimensions/mm	0.50 x 0.27 x 0.20
Crystal System	triclinic
Space Group	P1
a / Å	8.069(5)
b / Å	11.314(8)
c / Å	7.909(4)
α/ °	91.41(6)
β/ °	115.74(4)
γ/ °	69.43(5)
V / Å^3	601.8(8)
Z	2
F(000)	364
D_{calc}/ g cm^{-3}	2.097
μ(Mo-K_α)/ cm^{-1}	69.89
Unique observed reflections	2125
Observed reflections with $[I_o > 2\sigma(I_o)]$	1698
No. of parameters	136
Goodness of fit	2.91
R[a]	0.038
Rw[b]	0.037

a. $R = \Sigma (|F_{obs}|_i - |F_{calc}|_i)^2 / \Sigma |F_{obs}|_i$

b. $R_w = \sqrt{[\Sigma w_i(|F_{obs}|_i - |F_{calc}|_i)^2 / \Sigma w_i |F_{obs}|_i^2]}$

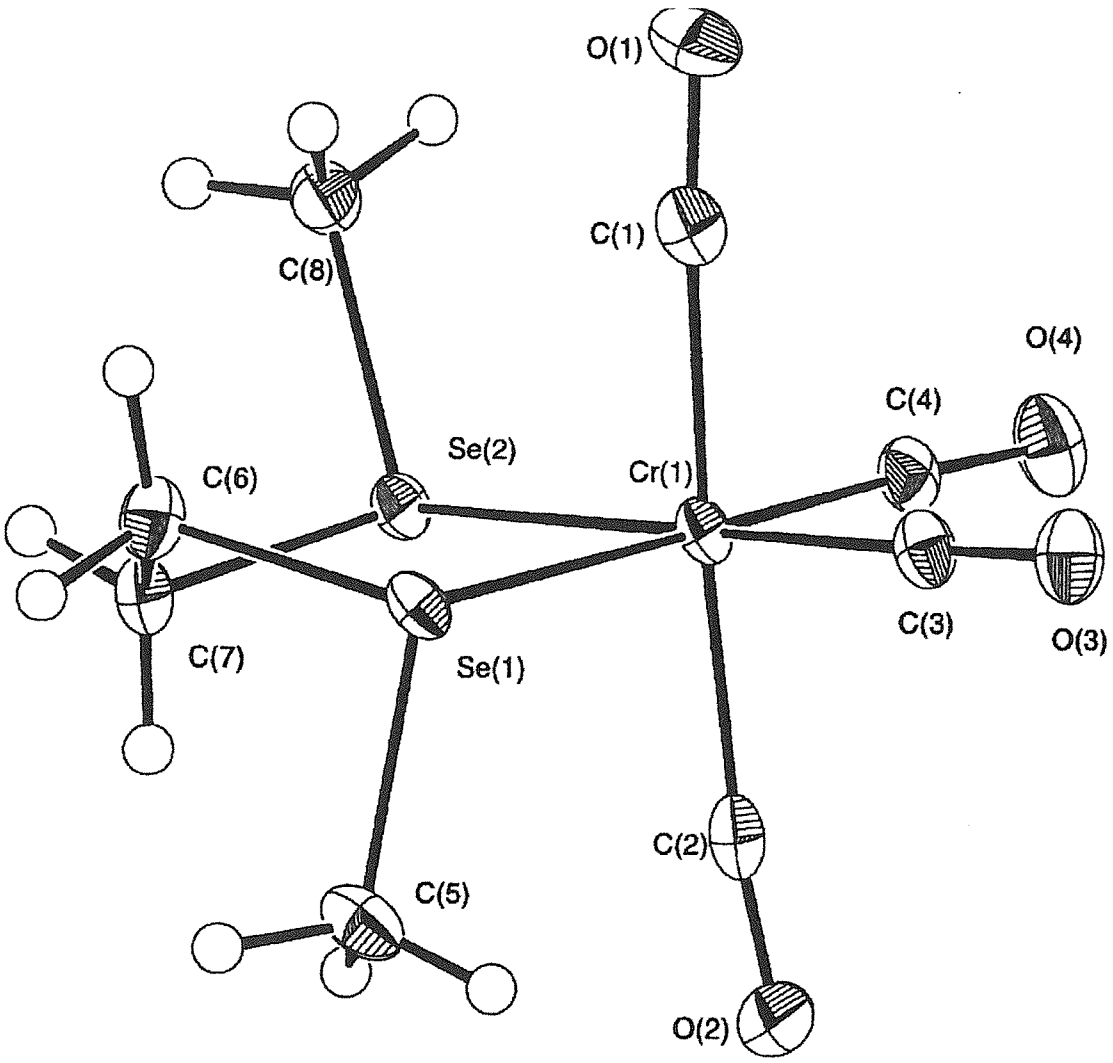

Figure 2.12 – View of $[Cr(CO)_4\{MeSe(CH_2)_2SeMe\}]$ with numbering scheme adopted. Ellipsoids are shown at 40% probability.

Table 2.9 – Selected bond lengths (Å) for $[Cr(CO)_4\{MeSe(CH_2)_2SeMe\}]$

Cr(1)	C(1)	1.891(8)
Cr(1)	C(2)	1.892(7)
Cr(1)	C(3)	1.833(7)
Cr(1)	C(4)	1.834(8)
Se(1)	Cr(1)	2.517(1)
Se(2)	Cr(1)	2.521(2)
Se(1)	C(5)	1.946(7)
Se(1)	C(6)	1.956(7)
Se(2)	C(7)	1.955(7)
Se(2)	C(8)	1.948(7)
O(1)	C(1)	1.149(8)
O(2)	C(2)	1.154(8)
O(3)	C(3)	1.159(8)
O(4)	C(4)	1.172(8)
C(6)	C(7)	1.52(1)

Table 2.10 – Selected bond angles (degrees) for $[Cr(CO)_4\{MeSe(CH_2)_2SeMe\}]$

Cr(1)	Se(1)	C(5)	107.2(2)	Se(2)	Cr(1)	C(4)	92.4(2)
Cr(1)	Se(1)	C(6)	102.5(2)	C(1)	Cr(1)	C(2)	175.9(3)
C(5)	Se(1)	C(6)	97.1(3)	C(1)	Cr(1)	C(3)	88.5(3)
Cr(1)	Se(2)	C(7)	103.5(2)	C(1)	Cr(1)	C(4)	89.6(3)
Cr(1)	Se(2)	C(8)	108.4(2)	C(2)	Cr(1)	C(3)	87.6(3)
C(7)	Se(2)	C(8)	97.0(3)	C(2)	Cr(1)	C(4)	88.9(3)
Se(1)	Cr(1)	Se(2)	86.59(5)	C(3)	Cr(1)	C(4)	87.9(3)
Se(1)	Cr(1)	C(1)	90.2(2)	Cr(1)	C(1)	O(1)	176.1(7)
Se(1)	Cr(1)	C(2)	91.3(2)	Cr(1)	C(2)	O(2)	173.9(6)
Se(1)	Cr(1)	C(3)	93.2(2)	Cr(1)	C(3)	O(3)	177.2(6)
Se(1)	Cr(1)	C(4)	178.9(2)	Cr(1)	C(4)	O(4)	175.5(6)
Se(2)	Cr(1)	C(1)	91.6(2)	Se(2)	C(7)	C(6)	113.3(5)
Se(2)	Cr(1)	C(2)	92.3(2)	Se(1)	C(6)	C(7)	113.1(5)
Se(2)	Cr(1)	C(3)	179.7(2)				

2.3 CONCLUSIONS

The complexes $[M(CO)_4(L\text{-}L)]$ (M = Cr, Mo or W; L-L = various dithioether, diselenoether or ditelluroether ligands) have been prepared as yellow or orange solids in moderate to good yield. The compounds were characterised using IR and multinuclear (^1H, $^{13}C\{^1H\}$, $^{77}Se\{^1H\}$, $^{125}Te\{^1H\}$ and ^{95}Mo) NMR spectroscopies, FAB mass spectrometry and microanalyses.

All the ditelluroether complexes show resonances for both *meso* and *DL* invertomers in the ^1H NMR consistent with relatively high inversion barriers. Whereas, all the dithioether complexes are inverting rapidly on the ^1H NMR time scale.

X-ray crystallograpic analyses of $[Cr(CO)_4\{MeSe(CH_2)_2SeMe\}]$ revealed the expected *cis* disubstituted distorted octahedron about the central chromium with the ligand adopting the *DL* conformation.

The ^{95}Mo NMR data also support the conclusion that the telluroethers are the best σ-donors in the series of ligands. The spectroscopic data clearly support the proposal of Schumann and Hoffmann[63] that telluroethers are the best donors among Group 16 ligands towards low valent metal centres. The findings from this research compare well with results from work carried out by a colleague on the manganese and rhenium systems $[M(CO)_3X(L\text{-}L)]$ where L-L are the same Group 16 bidentates employed in the Cr, Mo and W work. When considering IR spectra the most significant trend is with changes in the Group 16 donor atom. The CO bonds weaken in the order S → Se → Te. Therefore, supporting the proposal that the results are general for low valent carbonyl systems where mismatch of the Te orbitals with the expanded metal orbitals is less likely to be significant.

2.4 EXPERIMENTAL

2.4.1 Ligand and Complex Synthesis

All preparations were performed under a dinitrogen atmosphere using standard Schlenk techniques. The $[M(CO)_6]$ were obtained from Aldrich and converted into $[Cr(CO)_4(nbd)]$, $[Mo(CO)_4(nbd)]$ and $[W(CO)_4\{Me_2N(CH_2)_3NMe_2\}]$ by minor modifications of literature routes.[12,57] The ligands were synthesised following the literature procedures.[13,14,69-71]

a). Synthesis of $[Cr(CO)_4\{MeTe(CH_2)_3TeMe\}]$

$[Cr(CO)_4(nbd)]$ (0.12 g, 0.47 mmol) was dissolved in degassed toluene ($15cm^3$) and the ligand (0.15 g, 0.47 mmol) added *via* a syringe. The reaction mixture was stirred at 50 °C overnight and the solution IR spectrum monitored until the reaction had reached completion. Toluene was removed *in vacuo*. The residue was dissolved in $CHCl_3$ ($5cm^3$), filtered and cold *n*-pentane added to yield a bright yellow powder. This was filtered off, washed with *n*-pentane and vacuum dried (yield 0.15 g, 76 %). Required for $[C_9H_{12}CrO_4Te_2]$: C = 21.9, H = 2.4 %; found: C = 21.7, H = 2.2 %. FAB mass spectrum (3-NOBA matrix): found *m/z* = 492, 464, 436, 408, 380; calculated for $[^{52}Cr(CO)_4[Me^{130}Te(CH_2)_3{}^{130}TeMe\}]^+$ *m/z* = 496, $[Cr(CO)_3\{MeTe(CH_2)_3TeMe\}]^+$ *m/z* = 468, $[Cr(CO)_2\{MeTe(CH_2)_3TeMe\}]^+$ *m/z* = 440, $[Cr(CO)\{MeTe(CH_2)_3TeMe\}]^+$ *m/z* = 412, $[Cr\{MeTe(CH_2)_3TeMe\}]^+$ *m/z* = 384.

b). Synthesis of $[Cr(CO)_4\{o\text{-}C_6H_4(TeMe)_2\}]$

Method as for a) above, but using $[Cr(CO)_4(nbd)]$ (0.12 g, 0.47 mmol) and o-$C_6H_4(TeMe)_2$ (0.17 g, 0.47 mmol) to give an orange/yellow precipitate (yield 0.13 g, 52 %). Required for $[C_{12}H_{10}CrO_4Te_2]$: C = 27.4, H = 1.9 %; found: C = 27.8, H = 2.0 %. FAB mass spectrum (3-NOBA matrix): found *m/z* = 526, 440; calculated for $[^{52}Cr(CO)_4\{o\text{-}C_6H_4(^{130}TeMe)_2\}]^+$ *m/z* = 530, $[Cr(CO)\{o\text{-}C_6H_4(TeMe)_2\}]^+$ *m/z* = 446.

c). Synthesis of [Cr(CO)$_4${PhTe(CH$_2$)$_3$TePh}]

Method as for a) above but using [Cr(CO)$_4$(nbd)] (0.12 g, 0.47 mmol) and PhTe(CH$_2$)$_3$TePh (0.21 g, 0.47 mmol) to give a yellow precipitate (yield 0.21 g, 73 %). Required for [$C_{19}H_{16}CrO_4Te_2$]: C = 37.1, H = 2.6 %; found C = 36.5, H = 2.7 %. FAB mass spectrum (3-NOBA matrix): found *m/z* = 616, 560; calculated for [^{52}Cr(CO)$_4${Ph^{130}Te(CH$_2$)$_3$^{130}TePh}]$^+$ *m/z* = 620, [Cr(CO)$_2${PhTe(CH$_2$)$_3$TePh}]$^+$ *m/z* = 564.

d). Synthesis of [Cr(CO)$_4${MeS(CH$_2$)$_2$SMe}]

Method as for a) above but using [Cr(CO)$_4$(nbd)] (0.12 g, 0.47 mmol) and MeS(CH$_2$)$_2$SMe (0.06 g, 0.47 mmol) to give a yellow precipitate (yield 0.08 g, 57 %). Required for [$C_8H_{10}CrO_4S_2$]: C = 33.6, H = 3.5 %; found C = 33.7, H = 3.5 %. FAB mass spectrum (3-NOBA matrix): found 286, 258, 230, 202; calculated for [^{52}Cr(CO)$_4${Me^{32}S(CH$_2$)$_2$^{32}SMe}]$^+$ *m/z* = 286, [Cr(CO)$_3${MeS(CH$_2$)$_2$SMe}]$^+$ *m/z* = 258, [Cr(CO)$_2${MeS(CH$_2$)$_2$SMe}]$^+$ *m/z* = 230, [Cr(CO){MeS(CH$_2$)$_2$SMe}]$^+$ *m/z* = 202.

e). Synthesis of [Cr(CO)$_4${MeS(CH$_2$)$_3$SMe}]

Method as for a) above but using [Cr(CO)$_4$(nbd)] (0.12 g, 0.47 mmol) and MeS(CH$_2$)$_3$SMe (0.064 g, 0.47 mmol) to give a yellow precipitate (yield 0.08 g, 56 %). Required for [$C_9H_{12}CrO_4S_2$]: C = 36.0, H = 4.0 %; found C = 35.4, H = 3.9 %. FAB mass spectrum (3-NOBA matrix): found 300, 272, 244, 216; calculated for [^{52}Cr(CO)$_4${Me^{32}S(CH$_2$)$_3$^{32}SMe}]$^+$ *m/z* = 300, [Cr(CO)$_3${MeS(CH$_2$)$_3$SMe}]$^+$ *m/z* = 272, [Cr(CO)$_2${MeS(CH$_2$)$_3$SMe}]$^+$ *m/z* = 244, [Cr(CO){MeS(CH$_2$)$_3$SMe}]$^+$ *m/z* = 216.

f). Synthesis of [Cr(CO)$_4${MeSe(CH$_2$)$_2$SeMe}]

Method as for a) above but using [Cr(CO)$_4$(nbd)] (0.12 g, 0.47 mmol) and MeSe(CH$_2$)$_2$SeMe (0.1 g, 0.47 mmol) to give a bright yellow precipitate (yield 0.09 g, 50 %). Required for [$C_8H_{10}CrO_4Se_2$]: C = 25.3, H = 2.6 %; found C = 25.2, H = 2.7 %. FAB mass spectrum (3-NOBA matrix): found 382, 354, 326;

calculated for $[^{52}Cr(CO)_4\{Me^{80}Se(CH_2)_2{}^{80}SeMe\}]^+$ *m/z* = 380, $[Cr(CO)_3\{MeSe(CH_2)_2SeMe\}]^+$ *m/z* = 352, $[Cr(CO)_2\{MeSe(CH_2)_2SeMe\}]^+$ *m/z* = 324.

g). Synthesis of $[Cr(CO)_4\{MeSe(CH_2)_3SeMe\}]$

Method as for a) above but using $[Cr(CO)_4(nbd)]$ (0.12 g, 0.47 mmol) and $MeSe(CH_2)_3SeMe$ (0.1 g, 0.47 mmol) to give a bright yellow precipitate (yield 0.13 g, 69 %). Required for $[C_9H_{12}CrO_4Se_2]$: C = 27.4, H = 3.1 %; found C = 27.2, H = 2.7 %. FAB mass spectrum (3-NOBA matrix): found 396, 368, 340, 312; calculated for $[^{52}Cr(CO)_4\{Me^{80}Se(CH_2)_3{}^{80}SeMe\}]^+$ *m/z* = 394, $[Cr(CO)_3\{MeSe(CH_2)_3SeMe\}]^+$ *m/z* = 366, $[Cr(CO)_2\{MeSe(CH_2)_3SeMe\}]^+$ *m/z* = 338, $[Cr(CO)\{MeSe(CH_2)_3SeMe\}]^+$ *m/z* = 310.

h). Synthesis of $[Cr(CO)_4\{o\text{-}C_6H_4(SeMe)_2\}]$

Method as for a) above but using $[Cr(CO)_4(nbd)]$ (0.12 g, 0.47 mmol) and *o*-$C_6H_4(SeMe)_2$ (0.12 g, 0.47 mmol) to give a orange precipitate (yield 0.14 g, 72 %). Required for $[C_{12}H_{10}CrO_4Se_2]$: C = 33.7, H = 2.3 %; found C = 33.4, H = 2.5 %. FAB mass spectrum (3-NOBA matrix): found 432, 404, 376, 348; calculated for $[^{52}Cr(CO)_4\{o\text{-}C_6H_4(^{80}SeMe)_2\}]^+$ *m/z* = 430, $[Cr(CO)_3\{o\text{-}C_6H_4(SeMe)_2\}]^+$ *m/z* = 402, $[Cr(CO)_2\{o\text{-}C_6H_4(SeMe)_2\}]^+$ *m/z* = 374, $[Cr(CO)\{o\text{-}C_6H_4(SeMe)_2\}]^+$ *m/z* = 346.

i). Synthesis of $[Mo(CO)_4\{MeTe(CH_2)_3TeMe\}]$

$[Mo(CO)_4(nbd)]$ (0.12 g, 0.4 mmol) was dissolved in degassed toluene (15 cm^3) and the ligand (0.13 g, 0.4 mmol) added *via* a syringe. The reaction mixture was stirred at room temperature overnight and the solution IR spectrum monitored until the reaction had reached completion. Toluene was removed *in vacuo*. The residue was dissolved in $CHCl_3$ (5 cm^3), filtered and cold *n*-pentane added to yield a pale yellow powder. This was filtered off, washed with *n*-pentane and vacuum dried (yield 0.15 g, 69 %). Required for $[C_9H_{12}MoO_4Te_2]$: C = 20.2, H = 2.3 %; found C = 20.4, H = 2.3 %. FAB mass spectrum (3-NOBA matrix):

found 536, 508; calculated for $[^{98}Mo(CO)_4\{Me^{130}Te(CH_2)_3{}^{130}TeMe\}]^+$ *m/z* = 542, $[Mo(CO)_3\{MeTe(CH_2)_3TeMe\}]^+$ *m/z* = 514.

j). Synthesis of [Mo(CO)$_4${o-C$_6$H$_4$(TeMe)$_2$}]

Method as for i) above but using [Mo(CO)$_4$(nbd)] (0.12 g, 0.4 mmol) and o-C$_6$H$_4$(TeMe)$_2$ (0.14 g, 0.4 mmol) to give a yellow precipitate (yield 0.14 g, 60 %). Required for [$C_{12}H_{10}MoO_4Te_2$]: C = 25.3, H = 1.8 %; found C = 25.5, H = 2.4 %.

k). Synthesis of [Mo(CO)$_4${PhTe(CH$_2$)$_3$TePh}]

Method as for i) above but using [Mo(CO)$_4$(nbd)] (0.12 g, 0.4 mmol) and PhTe(CH$_2$)$_3$TePh (0.18 g, 0.4 mmol) to give a pale yellow precipitate (yield 0.2 g, 74 %). Required for [$C_{19}H_{16}MoO_4Te_2$]: C = 34.6, H = 2.4 %; found C = 34.5, H = 2.4 %. FAB mass spectrum (3-NOBA matrix): found 660, 632, 604; calculated for $[^{98}Mo(CO)_4\{Ph^{130}Te(CH_2)_3{}^{130}TePh\}]^+$ *m/z* = 666, $[Mo(CO)_3\{PhTe(CH_2)_3TePh\}]^+$ *m/z* = 638, $[Mo(CO)_2\{PhTe(CH_2)_3TePh\}]^+$ *m/z* = 610.

l). Synthesis of [Mo(CO)$_4${MeS(CH$_2$)$_2$SMe}]

Method as for i) above but using [Mo(CO)$_4$(nbd)] (0.12 g, 0.4 mmol) and MeS(CH$_2$)$_2$SMe (0.05 g, 0.4 mmol) to give a yellow precipitate (yield 0.08 g, 63 %). Required for [$C_8H_{10}MoO_4S_2$]: C = 29.1, H = 3.0 %; found C = 29.2, H = 3.1 %. FAB mass spectrum (3-NOBA matrix): found 332, 304, 276; calculated for $[^{98}Mo(CO)_4\{Me^{32}S(CH_2)_2{}^{32}SMe\}]^+$ *m/z* = 332, $[Mo(CO)_3\{MeS(CH_2)_2SMe\}]^+$ *m/z* = 304, $[Mo(CO)_2\{MeS(CH_2)_2SMe\}]^+$ *m/z* = 276.

m). Synthesis of [Mo(CO)$_4${MeS(CH$_2$)$_3$SMe}]

Method as for i) above but using [Mo(CO)$_4$(nbd)] (0.12 g, 0.4 mmol) and MeS(CH$_2$)$_3$SMe (0.05 g, 0.4 mmol) to give a bright yellow precipitate (yield 0.09 g, 63 %). Required for [$C_9H_{12}MoO_4S_2$]: C = 31.4, H = 3.5 %; found C = 31.2, H = 3.5 %. FAB mass spectrum (3-NOBA matrix): found 346, 318;

calculated for $[^{98}Mo(CO)_4\{Me^{32}S(CH_2)_3{}^{32}SMe\}]^+$ *m/z* = 346, $[Mo(CO)_3\{MeS(CH_2)_2SMe\}]^+$ *m/z* = 318.

n). Synthesis of $[Mo(CO)_4\{o\text{-}C_6H_4(SMe)_2\}].½CH_2Cl_2$

Method as for i) above but using $[Mo(CO)_4(nbd)]$ (0.12 g, 0.4 mmol) and *o*-$C_6H_4(SMe_2)$ (g, 0.4 mmol) to give a yellow precipitate (yield 0.1 g, 63 %). Required for $[C_{10.5}H_{11}ClMoO_4S_2]$: C = 35.6, H = 2.6 %; found C = 35.6, H = 2.6 %.

o). Synthesis of $[Mo(CO)_4\{MeSe(CH_2)_2SeMe\}]$

Method as for i) above but using $[Mo(CO)_4(nbd)]$ (0.12 g, 0.4 mmol) and $MeSe(CH_2)_2SeMe$ (0.09 g, 0.4 mmol) to give a yellow precipitate (yield 0.1 g, 61 %). Required for $[C_8H_{10}MoO_4Se_2]$: C = 22.7, H = 2.4 %; found C = 22.8, H = 2.5 %. FAB mass spectrum (3-NOBA matrix): found 424, 398, 370; calculated for $[^{98}Mo(CO)_4\{Me^{80}Se(CH_2)_2{}^{80}SeMe\}]^+$ *m/z* = 428, $[Mo(CO)_3\{MeSe(CH_2)_2SeMe\}]^+$ *m/z* = 400, $[Mo(CO)_2\{MeSe(CH_2)_2SeMe\}]^+$ *m/z* = 372.

p). Synthesis of $[Mo(CO)_4\{MeSe(CH_2)_3SeMe\}]$

Method as for i) above but using $[Mo(CO)_4(nbd)]$ (0.12 g, 0.4 mmol) and $MeSe(CH_2)_3SeMe$ (0.09 g, 0.4 mmol) to give a light yellow precipitate (yield 0.13 g, 73 %). Required for $[C_9H_{12}MoO_4Se_2]$: C = 24.7, H = 2.7 %; found C = 24.8, H = 2.4 %. FAB mass spectrum (3-NOBA matrix): found 440, 410; calculated for $[^{98}Mo(CO)_4\{Me^{80}Se(CH_2)_3{}^{80}SeMe\}]^+$ *m/z* = 442, $[Mo(CO)_3\{MeSe(CH_2)_3SeMe\}]^+$ *m/z* = 412.

q). Synthesis of $[Mo(CO)_4\{o\text{-}C_6H_4(SeMe)_2\}]$

Method as for i) above but using $[Mo(CO)_4(nbd)]$ (0.12 g, 0.4 mmol) and *o*-$C_6H_4(SeMe_2)$ (0.11 g, 0.4 mmol) to give a orange/yellow precipitate (yield 0.14 g, 73 %). Required for $[C_{12}H_{10}ClMoO_4Se_2]$: C = 30.5, H = 2.1 %; found C = 29.7, H = 2.1 %.

r). Synthesis of [W(CO)$_4${MeTe(CH$_2$)$_3$TeMe}]

[W(CO)$_4${Me$_2$N(CH$_2$)$_3$NMe$_2$}] (0.12 g, 0.28 mmol) was dissolved in degassed toluene (15 cm^3) and the ligand (0.09 g, 0.28 mmol) added *via* a syringe. The reaction mixture was stirred at 70 °C overnight and the solution IR spectrum monitored until the reaction had reached completion. Toluene was removed *in vacuo*. The residue was dissolved in $CHCl_3$ (5 cm^3), filtered and cold *n*-pentane added to yield a pale yellow powder. This was filtered off, washed with *n*-pentane and vacuum dried (yield 0.09 g, 53 %). Required for [$C_9H_{12}WO_4Te_2$]: C = 17.3, H = 1.9 %; found C = 17.5, H = 1.9 %. FAB mass spectrum (3-NOBA matrix): found 623; calculated for [^{184}W(CO)$_4${Me^{130}Te(CH$_2$)$_3$^{130}TeMe}]$^+$ *m/z* = 628.

s). Synthesis of [W(CO)$_4${o-C$_6$H$_4$(TeMe)$_2$}]

Method as for r) above but using [W(CO)$_4$ {Me$_2$N(CH$_2$)$_3$NMe$_2$}] (0.12 g, 0.28 mmol) and o-C$_6$H$_4$(TeMe$_2$) (0.1 g, 0.28 mmol) to give a dark yellow precipitate (yield 0.13 g, 71 %). Required for [$C_{12}H_{10}O_4Te_2W$]: C = 21.9, H = 1.5 %; found C = 22.0, H = 1.7 %. FAB mass spectrum (3-NOBA matrix): found 657; calculated for [^{184}W(CO)$_4${o-C$_6$H$_4$(^{130}TeMe)$_2$}]$^+$ *m/z* = 662.

t). Synthesis of [W(CO)$_4${PhTe(CH$_2$)$_3$TePh}]

Method as for r) above but using [W(CO)$_4$ {Me$_2$N(CH$_2$)$_3$NMe$_2$}] (0.12 g, 0.28 mmol) and PhTe(CH$_2$)$_3$TePh (0.13 g, 0.28 mmol) to give a pale yellow precipitate (yield 0.13 g, 63 %). Required for [$C_{19}H_{16}O_4Te_2W$]: C = 30.5, H = 2.1 %; found C = 29.7, H = 2.1 %. FAB mass spectrum (3-NOBA matrix): found 747; calculated [^{184}W(CO)$_4${Ph^{130}Te(CH$_2$)$_3$^{130}TePh}]$^+$ *m/z* = 752.

u). Synthesis of [W(CO)$_4${MeS(CH$_2$)$_2$SMe}]

Method as for r) above but using [W(CO)$_4$ {Me$_2$N(CH$_2$)$_3$NMe$_2$}] (0.12 g, 0.28 mmol) and MeS(CH$_2$)$_2$SMe (0.04g, 0.28 mmol) to give a dark yellow precipitate (yield 0.09 g, 73 %). Required for [$C_8H_{10}O_4S_2W$]: C = 23.0, H = 2.4 %; found C

= 22.8, H = 2.4 %. FAB mass spectrum (3-NOBA matrix): found 418, 390; calculated $[^{184}W(CO)_4\{Me^{32}S(CH_2)_2{}^{32}SMe\}]^+$ *m/z* = 418, $[W(CO)_3\{MeS(CH_2)_2SMe\}]^+$ *m/z* = 390.

v). Synthesis of $[W(CO)_4\{MeS(CH_2)_3SMe\}]$

Method as for r) above but using $[W(CO)_4\ \{Me_2N(CH_2)_3NMe_2\}]$ (0.12 g, 0.28 mmol) and $MeS(CH_2)_3SMe$ (0.038 g, 0.28 mmol) to give a dark orange precipitate (yield 0.08 g, 70 %). Required for $[C_9H_{12}O_4S_2W]$: C = 25.0, H = 2.7 %; found C = 24.6, H = 2.7 %. FAB mass spectrum (3-NOBA matrix): found 432, 404; calculated $[^{184}W(CO)_4\{Me^{32}S(CH_2)_3{}^{32}SMe\}]^+$ *m/z* = 432, $[W(CO)_3\{MeS(CH_2)_3SMe\}]^+$ *m/z* = 404.

w). Synthesis of $[W(CO)_4\{MeSe(CH_2)_2SeMe\}]$

Method as for r) above but using $[W(CO)_4\ \{Me_2N(CH_2)_3NMe_2\}]$ (0.12 g, 0.28 mmol) and $MeSe(CH_2)_2SeMe$ (0.06 g, 0.28 mmol) to give a yellow precipitate (yield 0.09 g, 60 %). Required for $[C_8H_{10}O_4Se_2W]$: C = 18.8, H = 2.1 %; found C = 18.9, H = 2.1 %.

x). Synthesis of $[W(CO)_4\{MeSe(CH_2)_3SeMe\}]$

Method as for r) above but using $[W(CO)_4\ \{Me_2N(CH_2)_3NMe_2\}]$ (0.12 g, 0.28 mmol) and $MeSe(CH_2)_3SeMe$ (0.06 g, 0.28 mmol) to give a bright yellow precipitate (yield 0.11 g, 75 %). Required for $[C_9H_{12}O_4Se_2W]$: C = 20.5, H = 2.3 %; found C = 20.6, H = 2.4 %. FAB mass spectrum (3-NOBA matrix): found 526, 498; calculated $[^{184}W(CO)_4\{Me^{80}Se(CH_2)_3{}^{80}SeMe\}]^+$ *m/z* = 528, $[W(CO)_3\{MeSe(CH_2)_3SeMe\}]^+$ *m/z* = 500.

y). Synthesis of $[W(CO)_4\{o\text{-}C_6H_4(SeMe)_2\}]$

Method as for r) above but using $[W(CO)_4\ \{Me_2N(CH_2)_3NMe_2\}]$ (0.12 g, 0.28 mmol) and $o\text{-}C_6H_4(SeMe)_2$ (0.07 g, 0.28 mmol) to give a dark yellow precipitate (yield 0.11 g, 68 %). Required for $[C_{12}H_{10}O_4Se_2W]$: C = 25.7, H = 1.8 %; found C = 25.6, H = 2.0 %. FAB mass spectrum (3-NOBA matrix): found 560, 532,

504; calculated $[^{184}W(CO)_4\{o\text{-}C_6H_4(^{80}SeMe)_2\}]^+$ *m/z* = 562, $[W(CO)_3\{o\text{-}C_6H_4(SeMe)_2\}]^+$ *m/z* = 534, $[W(CO)_2\{o\text{-}C_6H_4(SeMe)_2\}]^+$ *m/z* = 506.

2.4.2 X-Ray Crystallography

$[Cr(CO)_4\{MeSe(CH_2)_2SeMe\}]$

Details of the crystallographic data collection and refinement parameters are given in Table 2.8. Data collection used a Rigaku AFC7S four-circle diffractometer equipped with an Oxford Systems open-flow cryostat operating at 150 K and using graphite-monochromated Mo-K_α X-radiation (λ = 0.71073 Å) and was undertaken by Dr G. Reid and Mr A.R.J. Genge. No significant crystal decay or movement was observed. The structure was solved by direct methods[2] and developed by iterative cycles of full-matrix least-squares refinement and difference Fourier syntheses.[3] All non-H atoms were refined anisotropically while H-atoms were placed in fixed, calculated positions with *d*(C-H) = 0.96 Å. Selected bond lengths and angles are given in Table 2.9 and Table 2.10.

2.5 REFERENCES

1. *'Comprehensive Organometallic Chemistry I and II'*, E.W. Abel, F.G.A. Stone and G. Wilkinson (eds), Pergamon, Oxford, 1982, 1995
2. D.R. Powers, G.C. Faber and G.R. Dobson, *J. Inorg. Nucl. Chem.*, 1969, **31**, 2970.
3. R.J. Angelici and J.R. Graham, *J.Am. Chem. Soc.*, 1965, **87**, 5586.
4. R.J. Angelici and J.R. Graham, *Inorg. Chem.*, 1967, **6**, 988.
5. R.J. Angelici and J.R. Graham, *Inorg. Chem.*, 1967, **6**, 992.
6. G.C. Faber and G.R. Dobson, *Inorg Chem.*, 1968, **7**, 584.
7. G.C. Faber and T.D. Walsh and G.R. Dobson, *J. Am. Chem. Soc.*, 1968, **90**, 4178.
8. J.R.Graham and R.J. Angelici, *J. Am. Chem. Soc.*, 1965, **87**, 5590.
9. F. Zingales, F. Canziani and F. Basolo, *J. Organomet. Chem.*, 1967, **7**, 461.
10. G.C. Faber and G.R. Dobson, *Inorg. Chim. Acta*, 1968, **2**, 479.
11. G.R. Dobson, *Inorg. Chem.*, 1969, **8**, 90.
12. G.R. Dobson, and G.C. Faber, *Inorg. Chim. Acta*, 1970, **4**, 87.
13. E.G. Hope, T. Kemmitt and W. Levason, *Organometallics*, 1988, **7**, 78.
14. T. Kemmitt and W. Levason, *Organometallics*, 1989, **8**, 1303.
15. E.G. Hope and W. Levason, *Coord. Chem. Rev.*, 1993, **122**, 103.
16. T. Kemmitt, W. Levason and M. Webster, *Inorg. Chem.*, 1989, **28**, 692.
17. T. Kemmitt and W. Levason, *Inorg. Chem.*, 1990, **29**, 731
18. W. Levason, S.D. Orchard, G. Reid and V. Tolhurst, *J. Chem. Soc., Dalton Trans.*, 1999, 2071.
19. E.W. Abel, K.G. Orrell, S.P. Scanlan, D. Stephenson, T. Kemmitt and W. Levason, *J.Chem. Soc., Dalton Trans.*, 1991, 591.
20. R.A. Cipriano, L.H. Hanton, W. Levason, D. Pletcher, N.A. Powell and M. Webster, *J. Chem. Soc., Dalton Trans.*, 1988, 2483.
21. J.L. Brown, T. Kemmitt and W. Levason, *J. Chem. Soc., Dalton Trans.*, 1990, 1513.

22. J.R. Black, N.R. Champness, W. Levason and G. Reid, *J. Chem. Soc., Dalton Trans.*, 1995, 3439.
23. J.R. Black, N.R. Champness, W. Levason and G. Reid, *Inorg. Chem.*, 1996, **35**, 1820.
24. A.R.J. Genge, W. Levason and G. Reid, *J. Chem. Soc., Dalton Trans.*, 1997, 4549.
25. W. Levason, S.D. Orchard and G. Reid, *Organometallics*, 1999, **18**, 1275
26. S.G. Murray and F.R. Hartley, *Chem. Rev.*, 1981, **81**, 365.
27. M. Lattman and M.A. Weiner, *Inorg. Chem.*, 1978, **17**, 1084.
28. J.F. Guttenburger, G. Popp and W. Strohmeier, *Chem. Ber.*, 1965, **98**, 2284.
29. R. Fischer, R. Mohtachemi, H. Schumann, O. Stelzer and R. Weis, *Chem. Ber.*, 1973, **106**, 48.
30. M. Herberhöld and G. Süss, *J. Chem. Res. (S)*, 1977, 246: *J. Chem. Res (M)*, 1977, 2720.
31. W. Ehrl and H. Vahrenkamp, *Chem. Ber.*, 1970, **103**, 7563.
32. J.C.A. Boeyens, S. Lotz and H.G. Raubenheimer, *J.Organomet. Chem.*, 1976, **112**, 145.
33. E.W. Abel, M.A.Z. Chowdhury, K.G. Orrell and V. Sik, *J. Organomet. Chem.*, 1984, **262**, 293.
34. H. Fischer, U. Gerbing and K. Treier, *J. Organomet. Chem.*, 1992, **433**, 127.
35. E.W. Abel, M.B. Hursthouse, M.A. Mazid, K.G. Orrell, H. Rahoo and V. Sik, *J. Organomet. Chem.*, 1992, **437**, 191.
36. J.H. Eekhovem, H. Hogenveen, R.M. Kelloggand and E. Klei, *J. Organomet. Chem.*, 1978, **161**, 183.
37. R. Donaldson, G. Hunter and R.C. Massey, *J. Chem. Soc., Dalton Trans.*, 1974, 288.
38. G. Hunter and R.C. Massey, *J. Chem. Soc., Dalton Trans.*, 1975, 209.
39. G. Hunter and R.C. Massey, *J. Chem. Soc., Dalton Trans.*, 1976, 2007.

40. E.W. Ainscough, E.J. Birch and A.M. Brodie, *Inorg. Chim. Acta*, 1976, **20**, 187.
41. E.N. Baker and N.G. Larsen, *J. Chem. Soc., Dalton Trans.*, 1976, 1769.
42. H.C.E. Mannerskantz and G. Wilkinson, *J. Chem. Soc.*, 1962, 4454.
43. R. Ros, M. Vitali and R. Graziani, *Gazz. Chim. Ital.*, 1970, **100**, 407.
44. E.W. Abel, D.E. Budgen, I. Moss, K.G. Orrell and V. Sik, *J. Organomet. Chem.*, 1984, **262**, 293.
45. E.W. Abel and G.V. Hutson, *J. Inorg. Nucl. Chem.*, 1969, **31**, 3333.
46. E.W. Abel, I. Moss, K.G. Orrell and V. Sik, *J. Organomet. Chem.*, 1987, **326**, 187.
47. D.E. Halverson, G.M. Reisener, G.R. Dobson, I. Bernal and T.L. Mulcahy, *Inorg. Chem.*, 1982, **21**, 4285.
48. G.M. Reisener, I. Bernal and G.R. Dobson, *J. Organomet. Chem.*, 1978, **157**, 23.
49. G.R. Dobson and R.A. Brown, *J. Inorg. Nucl. Chem.*, 1972, **34**, 2785.
50. G. Hunter and R.C. Massey, *J. Chem. Soc., Dalton Trans.*, 1974, 1872.
51. L.W. Houk and G.R. Dobson, *Inorg. Chem.*, 1966, **5**, 2119.
52. E.W. Abel, R.O. Bush, F.J. Hopton and C.R. Jenkins, *J. Chem. Soc., Chem. Commun.*, 1996, 58.
53. H.C.E. McFarlane and W. McFarlane, *J. Inorg. Nucl. Chem.*, 1965, **27**, 1059.
54. J.A. Connor and G.A. Hudson, *J. Chem. Soc., Dalton Trans.*, 1975, 1025.
55. I. Bernal, G.R. Dobson, D.E. Halverson, T.L. Mulcahy and G.M. Reisner, *Inorg. Chem.*, 1982, **21**, 4285.
56. G.R. Dobson and L.W. Houk, *Inorg. Chim. Acta*, 1967, **1**, 287.
57. J.J. Eisch, R.B. King, *Organomet. Syn*, 1965, **1**, 122.
58. H. Werner and R. Prinz, *Chem. Ber.*, 1967, **100**, 265.
59. R.J. Cross, G. Hunter, and R.C. Massey, *J. Chem. Soc., Dalton Trans.*, 1976, 2015.
60. E.W. Abel, S.K. Bhargava and K.G. Orrell, *Prog. Inorg. Chem.*, 1984, **32**, 1.

61. N.P. Luthra, J.D. Odom, in: S. Patai, Z. Rappoprt (eds.), '*The Chemistry of Organic Selenium and Tellurium Compounds*', Wiley, New York, 1986, Vol. **1**, Chapter 6.

62. N.F. Ramsey, *Phys. Rev.*, 1950, **77**, 567.

63. H. Schumann, A.A. Arif, A.L. Arif, A.L. Rheingold, C. Janiak, R. Hoffmann and N. Kuhn, *Inorg Chem.*, 1991, **30**, 1618.

64. E.N. Baker and B.R. Reay, *J. Chem. Soc., Dalton Trans.*, 1973, 2205.

65. H.J. Plastas, J.M. Stewart, and S.O. Grim, *Inorg Chem.*, 1973, **12**, 265.

66. R.J. Hoare and O.S. Mills, *J. Chem. Soc., Dalton Trans.*, 1972, 653.

67. O.S. Mills and A.D. Redhouse, *J.Chem. Soc. (A)*, 1968, 642.

68. M.J. Bennett, F.A. Cotton and M.D. LaPrade, *Acta Crystallogr., Sect. B,* 1971, **27**, 1899.

69. D.J. Gulliver, E.G. Hope, W. Levason, S.G. Murray, D.M. Potter and G.L. Marshall, *J. Chem. Soc., Perkin Trans. II*, 1984, 429.

70. E.G. Hope, T. Kemmitt and W. Levason, *J.Chem. Soc., Perkin Trans. II*, 1987, 487.

71. F.R. Hartley, S.G. Murray, W. Levason, H.E. Soutter and C.A. McAuliffe, *Inorg. Chim. Acta*, 1979, **35**, 265.

72. SHELXS86, Program for crystal structure solution, G.M. Sheldrick, *Acta Crystallogr. Sect. A*, 1990, **46**, 467.

73. TeXsan: Crystal Structure Analysis Package, Molecular Structure Corporation, Texas, 1995.

CHAPTER 3

Group 6 Complexes of Tritelluro-, Triseleno- and Trithio-ether Ligands.

3.1 INTRODUCTION

The aim of this chapter was to investigate the coordination chemistry of a series of tripodal Group 16 ligands, with the general formula $CH_3C(CH_2ECH_3)_3$ (E = S, Se or Te) with Cr(0), Mo(0) and W(0) carbonyls. The first examples of $[M(CO)_3\{MeC(CH_2EMe)_3\}]$ (M = Mo or W; E = Se or Te) were synthesised during this work. Figure 3.1 shows the ligand type used.

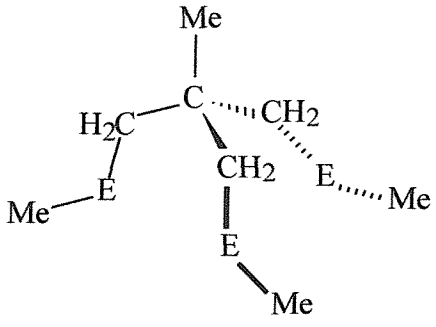

E = S, Se or Te

Figure 3.1 – The tripodal Group 16 ligands

The complexes have been studied using multinuclear NMR ($^{13}C\{^1H\}$, $^{77}Se\{^1H\}$, $^{125}Te\{^1H\}$ and ^{95}Mo) and IR spectroscopies and FAB mass spectrometry and the results are compared with those in Chapter 2.

3.1.1 Tridentate Group 16 Ligands

Recently work in our research group has been exploring the chemistry of tridentate seleno- and telluro-ether ligands with a variety of metal centres including both homoleptic and halo-complexes with palladium(II), platinum(II), rhodium(III) and iridium(III),[1,2] ruthenium(II),[3] rhodium(I) and iridium(I)-olefin and diene complexes,[4] and in homoleptic copper(I) and silver(I) species.[2] Carbonyl complexes have received less attention and reports are currently limited to the study within the group of *fac*-$[M(CO)_3(tridentate)]^+$ (M = Mn or

Re).[5,6] These studies showed that trisubstituted manganese(I) tricarbonyl cations involving Group 16 donor ligands are readily accessible in good yields *via fac*-$[Mn(CO)_3(Me_2CO)_3]^+$. The ligands used during that particular study were $MeC(CH_2EMe)_3$ (E = S, Se or Te) and the macrocycles [9]aneS_3 and [10]aneS_3.

In the time since a range of ditelluroethers was reported by Levason and co-workers[7,8,9] *ca.* 10 years ago the coordination chemistry of these ligands with a variety of transition metals has been studied in some detail.[10] However, very few tri-, tetra- or higher poly-telluroethers have been reported in the literature, reflecting difficulties in developing suitable synthetic routes to these sensitive compounds. To emphasise the rarity of these species the first reported tritelluroether complex was the manganese(I) complex *fac*-$[Mn(CO)_3\{MeC(CH_2TeMe)_3\}]CF_3SO_3$ which appeared in a communication in 1999 (Figure 3.2).[3] Since then several complexes have been synthesised and a few crystal structures have been published in scientific journals. The examples include $[Rh(COD)\{MeC(CH_2TeMe)_3\}]^+$,[4] and complexes of the new tripod $MeC(CH_2TePh)_3$ $[Mn(CO)_3\{MeC(CH_2TePh)_3\}]CF_3SO_3$[6] and $[Ir(COD)\{MeC(CH_2TePh)_3\}]^+$. There are a similar number of structurally characterised species containing the thio- and seleno-ether analogues covering a range of metal centres. $[Mn(CO)_3\{MeC(CH_2SMe)_3\}]^+$, $[Mn(CO)_3\{MeC(CH_2SeMe)_3\}]^+$ and $[Re(CO)_3\{MeC(CH_2SeMe)_3\}]^+$ were the first examples of complexes involving acyclic tridentate Group 16 donor ligands with low valent metals.[6] In each structure the tripodal ligand is facially bound in the *syn* form, analogous to $[Mn(CO)_3\{MeC(CH_2TeMe)_3\}]^+$ (Figure 3.2).

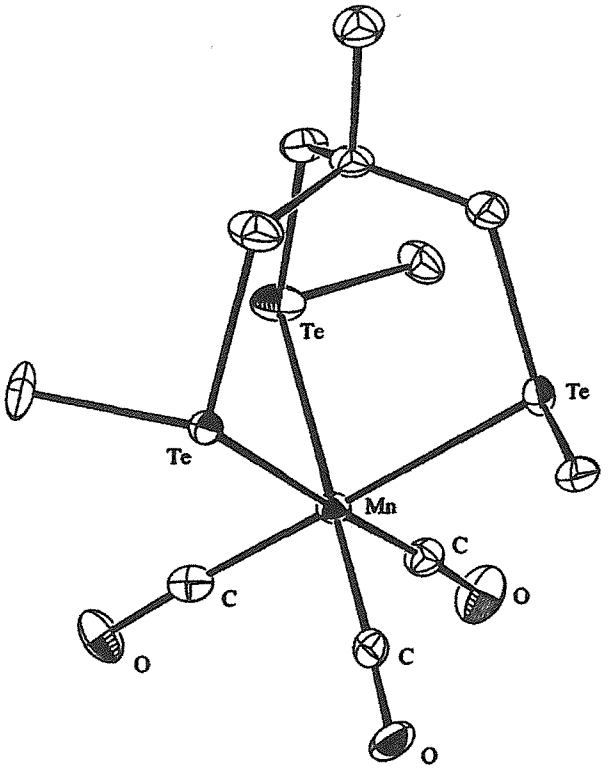

Figure 3.2 – View of the structure of the cation $[Mn(CO)_3\{MeC(CH_2TeMe)_3\}]^+$

The complexes described in this chapter are the first triselena- or tritellura-ligand complexes of Group 6 metal carbonyls. Several trithioether systems have been described in the literature. These include $[M(CO)_3\{MeS(CH_2)_2S(CH_2)_2SMe\}]$ (M = Cr, Mo),[11,12] *fac*-$[Mo(CO)_3\{[9]aneS_3\}]$,[13,29] *fac*-$[Mo(CO)_3\{[10]aneS_3\}]$,[14] and $[Mo(CO)_3L_3]$ (L = SMe_2, tht, SEt_2).[15,16] In $[M(CO)_3\{[14]aneS_4\}]$ (M = Mo, W) and $[Mo(CO)_3\{[16]aneS_4]$ the macrocycles reportedly behaved as tridentate ligands, although characterisation was very limited.[17]

Very recent reports have published the results of a study into a new thioether tripod, tris[(methylthio)methyl]silane (Figure 3.3) and its reactivity with chromium, molybdenum and tungsten carbonyl compounds.[18,19] This ligand has also been employed in other areas of chemistry, namely with bismuth(III) chloride[20] (discussed in Chapter 5), copper(I)[21] and silver.[22]

However, there are no reports of selenium or tellurium analogues. The work is solely restricted to the thioether ligand.

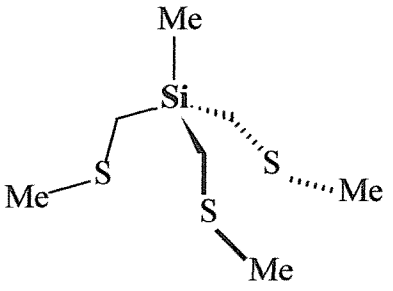

Figure 3.3 – Tris[(methylthio)methyl]silane

This ligand is very similar to the thioether employed in the present studies, differing only in the apical atom (Si in place of C). Although a number of tridentate sulfide ligands other than crown thioethers are known, including $MeC(CH_2SEt)_3$,[23] $RS(CH_2)_2S(CH_2)_2SR$ (R = Me,[24,25] Et[26]), 1,3,5-$(MeS)_3C_6H_9$, and $C_6H_6S_3$, reactivity studies with them are scant. In a manner not dissimilar to the one adopted for our own studies, Rabinovich and co-workers embarked on a systematic study of the new trithioether ligand with Group 6 metal carbonyls. The molybdenum tricarbonyl complex $[Mo(CO)_3\{MeSi(CH_2SMe)_3\}]$ was readily prepared by allowing $[Mo(CO)_6]$ to react with a slight excess of $MeSi(CH_2SMe)_3$ in refluxing methylcyclohexane, conditions under which the product precipitated and was isolated in high yield. The corresponding reactions of the chromium or tungsten hexacarbonyls $[M(CO)_6]$ (M = Cr, W) with the ligand only produced dark mixtures of unidentified products. This highlights the sensitive nature of the reaction systems of this type, something encountered during the work with $MeC(CH_2EMe)_3$ (E = S, Se or Te). However, the complexes $[M(CO)_3\{MeSi(CH_2SMe)_3\}]$ (M = Cr, W) were conveniently obtained in moderate to high yield by treating the labile nitrile derivatives $[Cr(CO)_3(MeCN)_3]$[27] or $[W(CO)_3(EtCN)_3]$[28] with the ligand in benzene/thf. Furthermore, the molecular structures of all three $[M(CO)_3\{MeSi(CH_2SMe)_3\}]$ complexes (M = Cr, Mo or W) were determined by single crystal X-ray diffraction. The complexes are isomorphous and the Cr(0) example is depicted

in Figure 3.4. Thioether complexes of Cr, Mo and W are not rare but this appears to be one of the few complete series of Group 6 metal thioether derivatives to be structurally characterised. The six-coordinate complexes present distorted octahedral geometries in the solid state, with tridentate face-capping thioether ligands. In this regard, the structures resemble those of the [9]aneS$_3$ derivatives [M(CO)$_3${[9]aneS$_3$}](M = Mo,[29] W[30]), as well as several known tricarbonyl complexes of general formula [M(CO)L$_3$] e.g. [Mn(CO)$_3${[10]aneS$_3$}]$^+$.[6]

As previously mentioned, the similarities between these and those involving the thioether tripod MeSi(CH$_2$SMe)$_3$ are obvious. Therefore, the work by Rabinovich is a very useful example to follow prior to embarking on our own studies. During the discussion section comparisons and differences between the two pieces of work will be drawn.

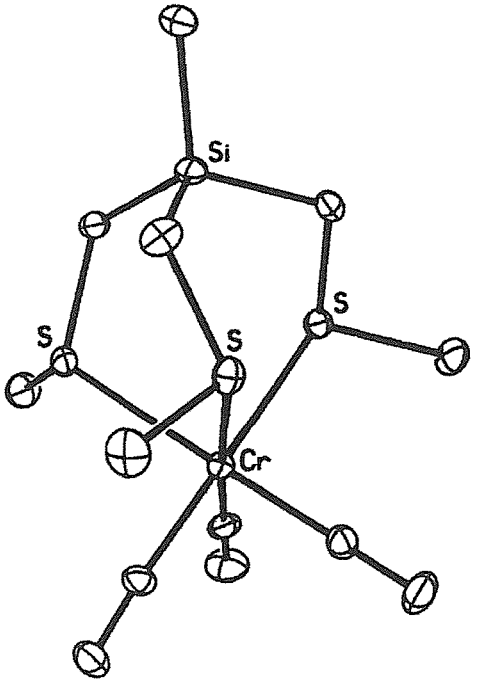

Figure 3.4 – Molecular structure of [Cr(CO)$_3${MeSi(CH$_2$SMe)$_3$}] from ref. 18

The results of the present studies may also be compared with those from previous work on $[M(CO)_4(bidentate)]$ (bidentate = various dithio-, diseleno- and ditelluro-ethers) discussed in Chapter 2.[31]

The primary aim of this chapter was to undertake a systematic study of Group 6 carbonyl derivatives of $MeC(CH_2SMe)_3$, $MeC(CH_2SeMe)_3$ and $MeC(CH_2TeMe)_3$. The employment of these three ligands should permit further comparisons between the Group 16 donors.

Further work to be discussed in this chapter is the attempted synthesis and isolation of $[Mo(CO)_3(\eta^3\text{-}[16]aneSe_4)]$ and $[Mo(CO)_2(\eta\text{-}^4[16]aneSe_4)]$. Yoshida and co-workers have reported the first example of a Mo(0) dicarbonyl complex of a thioether ligand *trans*-$[Mo(CO)_2(Me_8[16]aneS_4)]$ (Figure 3.5).[32] The aim was to determine whether the tetraselena macrocycle $[16]aneSe_4$ would accommodate a molybdenum centre within its cavity.

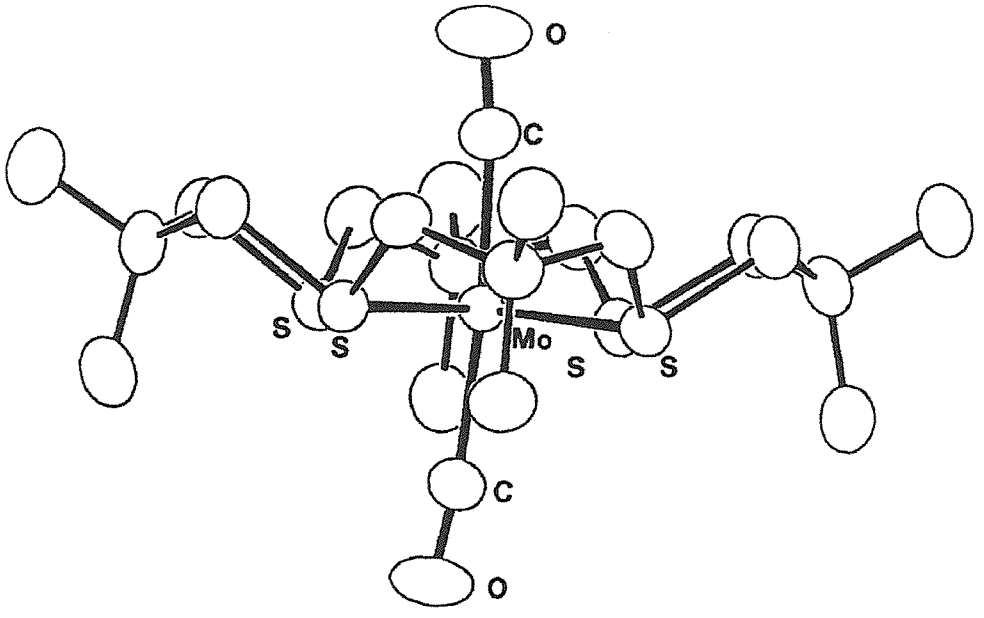

Figure 3.5 – Molecular structure of $[Mo(CO)_2(Me_8[16]aneS_4)]$ from ref. 32

3.2 RESULTS AND DISCUSSION

3.2.1 Group 6 Tricarbonyl Complexes of Group 16 Tridentate Ligands.

Although Group 6 carbonyl complexes are often regarded as among the more stable low valent complexes, the *fac*-$[M(CO)_3L^3]$ (L^3 = $MeC(CH_2SMe)_3$, $MeC(CH_2SeMe)_3$ and $MeC(CH_2TeMe)_3$) proved surprisingly difficult to isolate in the pure state, and prone to decomposition in solution, and as a result considerable care was necessary both in the syntheses and in obtaining reliable spectroscopic data.

For M = Mo or W, the starting materials in each case were the nitrile complexes $[M(CO)_3(MeCN)_3]$ made *in situ* from the hexacarbonyls in MeCN.[27,33] *Fac*-$[M(CO)_3L^3]$ (L^3 = $MeC(CH_2SMe)_3$, $MeC(CH_2SeMe)_3$ and $MeC(CH_2TeMe)_3$) have been prepared by treating the starting material with the ligand. After stirring at room temperature overnight, the solvent was removed *in vacuo*, the complex extracted with dry CH_2Cl_2, filtered and the solvent removed. The resulting solid was washed with diethyl ether which extracts any tetracarbonyl complex present (confirmed by IR spectroscopy of the solution), leaving the $[M(CO)_3L^3]$ in moderate yield as yellow or light brown products. The solids appear stable under nitrogen for several weeks, but the complexes are surprisingly unstable in solution. The identity of the products as *fac*-tricarbonyls follows from IR spectroscopic studies, the FAB mass spectra and microanalysis.

In contrast to the tripodal complexes macrocyclic thioether complexes, $[M(CO)_3S_3]$ (M = Cr, Mo or W, S_3 = [9]aneS_3 or [10]aneS_3) proved quite robust, although rather poorly soluble in most solvents.[34]

For M = Cr, the reaction of $[Cr(CO)_3(MeCN)_3]$ in situ in MeCN with $MeC(CH_2SMe)_3$ or $MeC(CH_2SeMe)_3$ gave a yellow solution which contained *fac*-$[Cr(CO)_3L^3]$, identified by *in situ* IR spectroscopic studies.

The use of solution IR spectroscopy was fundamental to the characterisation of these complexes. IR spectroscopic studies allowed the nature of these complexes to be followed throughout the reactions. During the synthesis of $[M(CO)_3L^3]$ (M = Mo, W), the two CO stretches associated with the

Group 6 metal tricarbonyl precursor disappeared and, on formation of the subsequent *fac*-tricarbonyl $[M(CO)_3L^3]$ two intense absorptions, centred at *ca.* 1930 and 1810 cm^{-1} (A_1 + E) as predicted for the facial isomer of an octahedral tricarbonyl complex, appeared.[35] Table 3.1 gives the solution IR data for the complexes. A typical IR spectrum is shown in Figure 3.6.

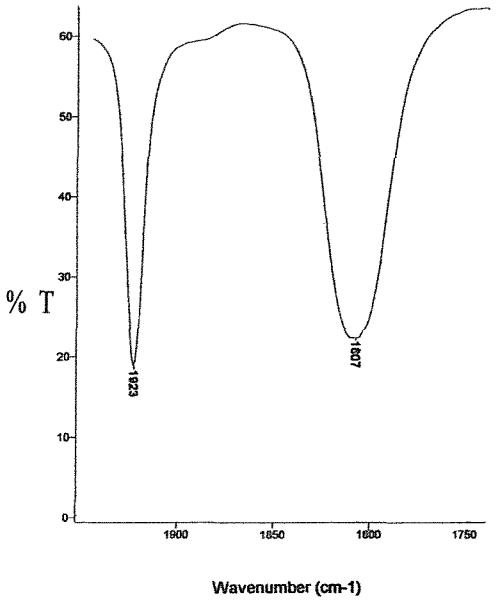

Figure 3.6 - ν(CO) region of IR spectrum of $[W(CO)_3\{MeC(CH_2SMe)_3\}]$

Table 3.1 – IR spectroscopic data (CO region)

Compound	υ (CO)/cm^{-1} [a]			
fac-$[Mo(CO)_3\{MeC(CH_2SMe)_3\}]$		1930	1816	
fac-$[W(CO)_3\{MeC(CH_2SMe)_3\}]$		1923	1807	
fac-$[Mo(CO)_3\{MeC(CH_2SeMe)_3\}]$		1927	1816	
fac-$[W(CO)_3\{MeC(CH_2SeMe)_3\}]$		1921	1809	
fac-$[Mo(CO)_3\{MeC(CH_2TeMe)_3\}]$		1930	1820	
fac-$[W(CO)_3\{MeC(CH_2TeMe)_3\}]$		1921	1821	
cis-$[Cr(CO)_4\{MeC(CH_2SMe)_3\}]$	2016	1902	1890(sh)	1854
cis-$[Mo(CO)_4\{MeC(CH_2SeMe)_3\}]$	2021	1909	1890(sh)	1855

a. Spectra measured in CH_2Cl_2 solution

FAB mass spectrometric data for each complex showed peaks corresponding to $[M(CO)_3L^3]^+$ the parent ion. The FAB mass spectrum (Figure 3.7) are shown for $[Mo(CO)_3\{MeC(CH_2SeMe)_3\}]$ in which the fragment of $[Mo\{MeC(CH_2SeMe)_3\}]^+$ (*m/z* = 446) is also observed in addition to the parent ion (*m/z* = 530). The data show good agreement with the calculated isotope distributions.

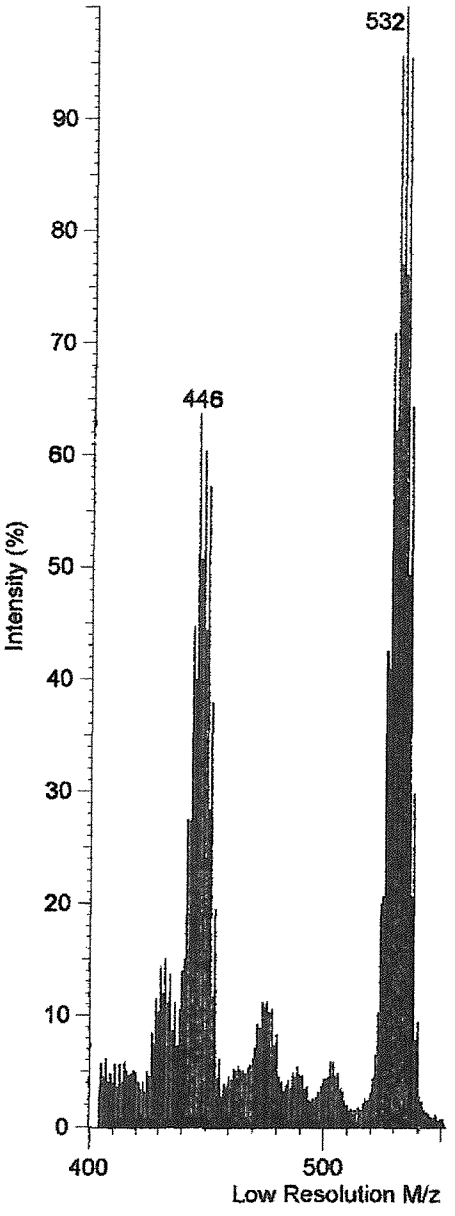

Figure 3.7 – FAB mass spectrum of $[Mo(CO)_3\{MeC(CH_2SeMe)_3\}]$

3.2.2 NMR Spectroscopic Studies

Multinuclear (^{1}H, $^{13}C\{^{1}H\}$, $^{77}Se\{^{1}H\}$, $^{125}Te\{^{1}H\}$ and ^{95}Mo) NMR spectroscopic studies were undertaken to give an insight into the character of these species in solution. The following section outlines the NMR spectroscopic data recorded for all the Group 6 metal species in this work.

^{1}H NMR Spectroscopic Studies

The ^{1}H NMR spectra of the new complexes were recorded at 300 K. Coordination of the ligand to the metal is supported by the change of chemical shift with respect to the free ligand. The ^{1}H NMR spectra consist of three sharp singlet resonances in the ratio 3:2:1. As previously mentioned, the solids appear stable under nitrogen for several weeks, but the complexes are surprisingly unstable in solution. A freshly prepared $CDCl_3$ solution of $[Mo(CO)_3\{MeC(CH_2SMe)_3\}]$ exhibits a simple ^{1}H NMR spectrum with singlets at δ 1.15 (MeC), 2.1 (MeS) and 2.45 (CH_2), however, on standing some brown solid precipitates and new resonances appear, some of which can be associated with uncoordinated $MeC(CH_2SMe)_3$ (δ 0.95, 2.0 and 2.5). The $[Mo(CO)_3\{MeC(CH_2SeMe)_3\}]$ partially decomposes in CH_2Cl_2 solution at 300 K to *cis*-$[Mo(CO)_4\{\eta^2\text{-}MeC(CH_2SeMe)_3\}]$, free ligand (both identified by a combination of ^{1}H, $^{13}C\{^{1}H\}$ NMR and IR spectroscopies) and an unidentified brown precipitate. The *fac*-$[W(CO)_3\{MeC(CH_2SeMe)_3\}]$ behaves similarly. The ^{1}H NMR spectrum of this compound is shown in Figure 3.8. The complexes of the tritelluroethers *fac*-$[M(CO)_3\{MeC(CH_2TeMe)_3\}]$ (M = Mo or W) are the most stable in the series, showing no decomposition whilst in solution over short periods of time.

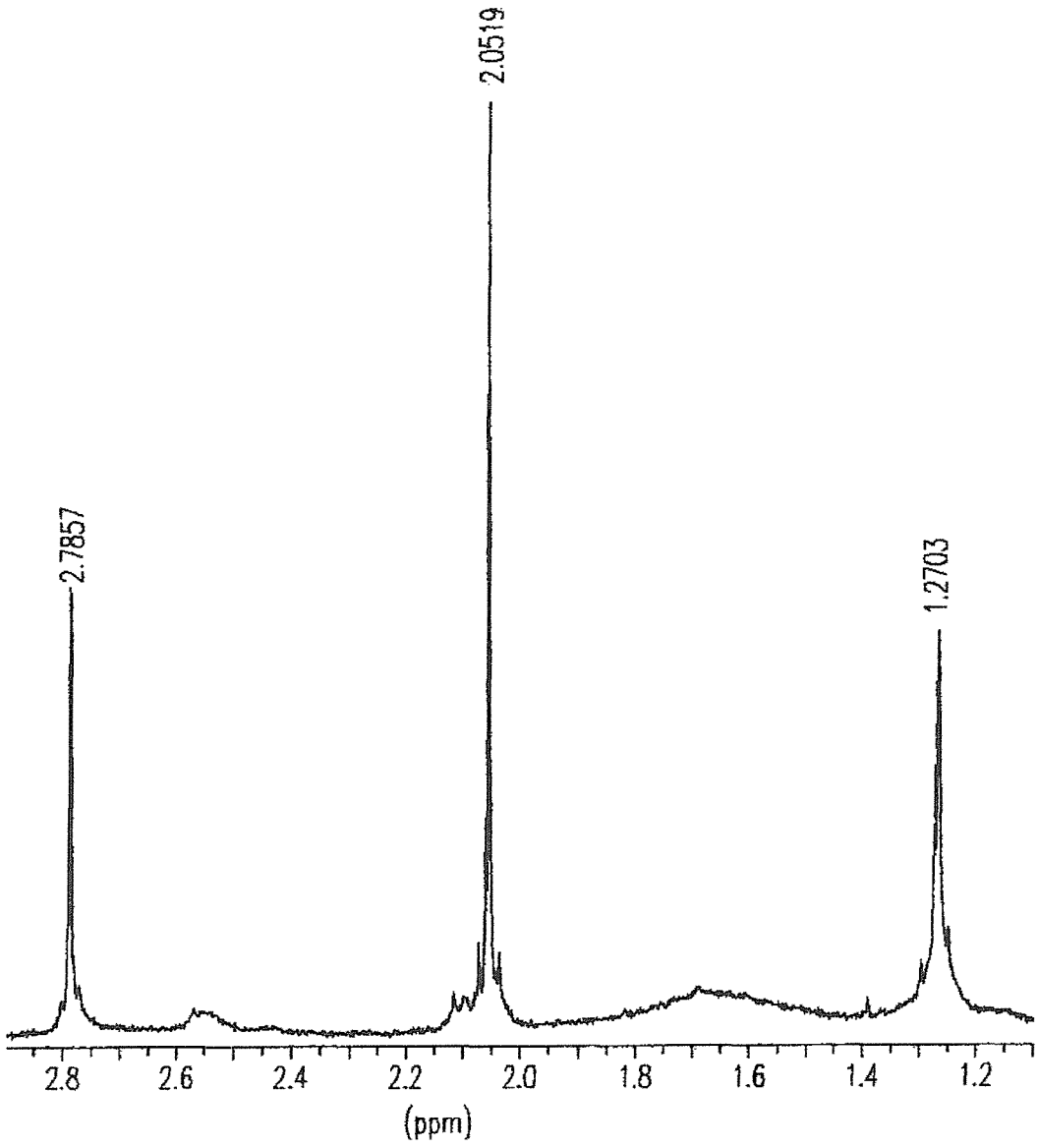

Figure 3.8 – ^{1}H NMR spectrum of $[W(CO)_3\{MeC(CH_2SeMe)_3\}]$ recorded in $CDCl_3$

$^{13}C\{^{1}H\}$ NMR Spectroscopic Studies

Data obtained by $^{13}C\{^{1}H\}$ NMR spectroscopy are shown in Table 3.2. The $^{13}C\{^{1}H\}$ NMR spectra for these derivatives were recorded at 300 K. The $^{13}C\{^{1}H\}$ NMR spectrum obtained from CH_2Cl_2-$CDCl_3$ solution at 300 K is more complex than expected for $[Mo(CO)_3\{MeC(CH_2SMe)_3\}]$, and changes with time. The $^{13}C\{^{1}H\}$ NMR spectrum was also obtained at 240 K which slowed but

did not stop the decomposition. From a freshly prepared solution immediately cooled to 240 K, the major $^{13}C\{^1H\}$ resonances are attributable to $[Mo(CO)_3\{MeC(CH_2SMe)_3\}]$ and occur at δ 221.0 (CO), 44.3 (CH_2), 41.6 (C), 27.7 (MeS) and 24.0 (MeC). Much weaker features at δ 44.2 (CH_2), 18.0 (MeS), are associated with free $MeC(CH_2SMe)_3$, and other features at 216, 208 (CO), 24.1 and 18.5 (MeS) are attributed to the tetracarbonyl *cis*-$[Mo(CO)_4\{\eta^2$-$MeC(CH_2SMe)_3\}]$, (the MeC and C resonances are not resolved from those in the tricarbonyl). After the solution had stood for some hours at room temperature, the $^{13}C\{^1H\}$ NMR resonances associated with the *fac*-tricarbonyl had greatly diminished and the free ligand and the tetracarbonyl were the major species present. The analogous *fac*-$[W(CO)_3\{MeC(CH_2SMe)_3\}]$ shows similar but slower decomposition to $MeC(CH_2SMe)_3$ and a tetracarbonyl complex in CH_2Cl_2. The ^{13}C resonance for CO of *fac*-$[W(CO)_3\{MeC(CH_2SMe)_3]$ is δ 215. The resonance frequency of the carbonyl carbon for a given metal is greater for S and Se containing complexes than the Te containing complex, i.e. the resonance is upfield w.r.t S or Se complexes. This is a consequence of the lower electronegativity of tellurium resulting in good Te→M σ-donation thus increasing the electron density in the vicinity of the carbonyl carbons leading to shielding of the carbon nucleus. We can also compare the values observed for the carbonyl carbons of the trithioether complexes with the results obtained by Rabinovich.[18] For the equivalent tris[(methylthio)methyl]silane complexes the $^{13}C\{^1H\}$ NMR spectra (in tetrahydrofuran-d_8 (THF-d_8)), the chemical shifts for the three equivalent CO groups in each compound (222.8 and 215.6 ppm for M = Mo and W, respectively) are very similar to the values observed during our studies. Similarly, the values obtained for $[M(CO)_3\{MeC(CH_2SMe)_3]$ (M = Mo or W) were virtually identical to those observed for the crown thioether compounds $[M(CO)_3\{[9]aneS_3\}]$.[30,34] When considering the species $[Mo(CO)_3\{MeC(CH_2SeMe)_3\}]$ decomposition is observed in CH_2Cl_2 solution, however, the decomposition is very slow at 240 K and at this temperature the $^{13}C\{^1H\}$ NMR data (Table 3.2) are assignable to the *fac*-tricarbonyl. The *fac*-

$[W(CO)_3\{MeC(CH_2SeMe)_3\}]$ behaves similarly. The complexes of the tritelluroether *fac*-$[M(CO)_3(MeC(CH_2TeMe)_3\}]$ (M = Mo or W) are the most stable of the series, showing no decomposition in CH_2Cl_2 at 240 K during the several hours taken to record $^{13}C\{^1H\}$ NMR spectra. At ambient temperatures in CH_2Cl_2, some decomposition is evident after several hours with weak features in the NMR spectra attributable to tetracarbonyls and some dark precipitate, but in contrast to the other systems, the free ligand ($MeC(CH_2TeMe)_3$) is not present in detectable amounts.

Table 3.2 – $^{13}C\{^1H\}$ NMR Spectroscopic Data

Compound	δ $^{13}C\{^1H\}$/ppm [a]
fac-$[Mo(CO)_3\{MeC(CH_2SMe)_3\}]$	221.0 (CO), 44.3 (CH_2), 41.3 (C), 27.7 (MeS), 24.0 (Me)
fac-$[W(CO)_3\{MeC(CH_2SMe)_3\}]$	215.0 ($^1J_{WC}$ = 178 Hz) (CO), 44.5 (CH_2), 41.5 (C), 29.6 (MeS), 24.2 (Me)
fac-$[Mo(CO)_3\{MeC(CH_2SeMe)_3\}]$	221.8 (CO), 40.7 (C), 35.2 (CH_2), 23.7 (Me), 17.5 (MeSe)
fac-$[W(CO)_3\{MeC(CH_2SeMe)_3\}]$	215.0 ($^1J_{WC}$ = 160 Hz) (CO), 40.6 (C), 36.5 (CH_2), 25.0 (Me), 19.5 (MeSe)
fac-$[Mo(CO)_3\{MeC(CH_2TeMe)_3\}]$	216.8 (CO), 34.4 (CH_2), 33.3 (C), 22.8 (Me), -9.1 (MeTe)
fac-$[W(CO)_3\{MeC(CH_2TeMe)_3\}]$	213.3 (CO), 35.0 (CH_2), 34.5 (C), 23.0 (Me), -7.0 (MeTe)
cis-$[Cr(CO)_4\{MeC(CH_2SMe)_3\}]$	226.2, 214.9 (CO), 49.0, 48.6 (CH_2), 40.3 (C), 29.0 (Me), 26.8, 18.0 (MeS) [b]
cis-$[Mo(CO)_4\{MeC(CH_2SeMe)_3\}]$	217.3, 207.9 (CO), 40.7, 37.9 (CH_2), 29.9 (Me), 16.0, 7.5 (MeSe) [b]

a. Spectra were recorded at 240 K in CH_2Cl_2 solution

b. At 300 K

$^{125}Te\{^1H\}$ NMR and $^{77}Se\{^1H\}$ NMR Spectroscopic Studies

The $^{125}Te\{^1H\}$ NMR data on these complexes are given in Table 3.3. It is notable that only a single *fac*-tricarbonyl species is present in the telluroether complexes. The $^{125}Te\{^1H\}$ NMR spectrum of $[M(CO)\{MeC(CH_2TeMe)_3\}]$ (M = Mo or W) shows a single resonance at δ 179 (Mo) and 110 (W), indicative of three equivalent Te donors and hence *fac*-tridentate coordination in solution (free $MeC(CH_2TeMe)_3$ $\delta^{125}Te$ 21). Since pyramidal inversion at a coordinated Te donor atom is expected to be slow on the NMR time scale,[10] this also implies that the ligand is in the *syn* configuration, with all three terminal Me groups pointing in the same direction giving a propeller-like arrangement. For a *fac*-$[M(CO)_3\{MeC(CH_2TeMe)_3\}]$ complex two invertomers are possible with *syn* or *anti* methyl groups (Figure 3.9).[4,6]

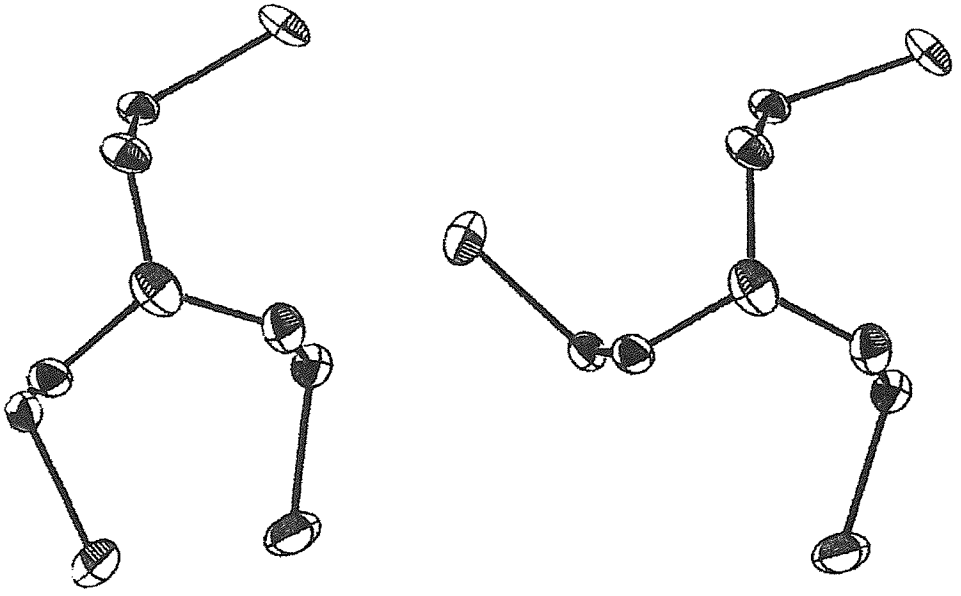

anti ***syn***

Figure 3.9 – The *anti* and *syn* forms of $MeC(CH_2EMe)_3$ viewed down the Me-C bond

Previous studies of $[M(CO)_4(L\text{-}L)]$ (L-L = dithio-, diseleno or ditelluro-ether)[31] have shown that whilst pyramidal inversion at the Group 16 atom is fast at 300 K (on the NMR time scale) for dithioethers and for some diselenoethers, the barriers are much higher for tellurium inversion, and thus we would expect to

see invertomers in the last case but, as we have seen, only a single form (the *syn* isomer) with one δ(Te) was found. Figure 3.11 shows the $^{125}Te\{^1H\}$ NMR recorded for $[W(CO)_3\{MeC(CH_2TeMe)_3\}]$. It would be reasonable to speculate that only the syn invertomer is present in significant amounts for the triselenoether complexes too. It is worth noting that in the $[M(CO)_3L^3]^+$ (M = Mn or Re)[4,6] and $[Ru(L^3)_2]^{2+}$ [3] the NMR spectra, and in several cases X-ray crystallographic data have identified only *syn* invertomers, and $[M(CO)_3\{MeSi(CH_2SMe)_3\}]$ are also *syn* in the solid state (Figure 3.10).

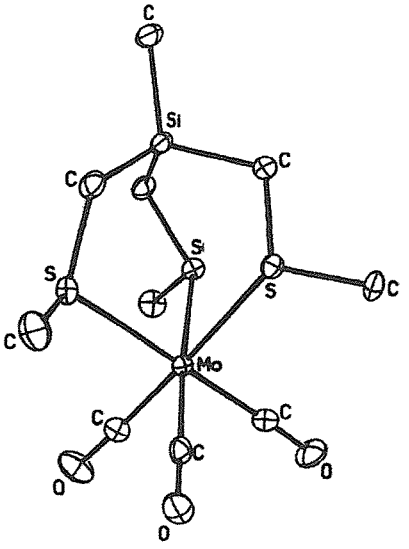

Figure 3.10 – Molecular structure of *fac*-$[Mo(CO)_3\{MeSi(CH_2SMe)_3\}]$ (showing *syn* isomer in the solid state) from ref. 18

The selenium containing complexes at 240 K in CH_2Cl_2 show a single $^{77}Se\{^1H\}$ resonance at δ 81 (Mo) and 53 (W) (free $MeC(CH_2SeMe)_3$ has δ = 23) are assignable to the *fac*-tricarbonyl. The $^{77}Se\{^1H\}$ NMR spectrum is illustrated for $[Mo(CO)_3\{MeC(CH_2SeMe)_3\}]$ in Figure 3.12.

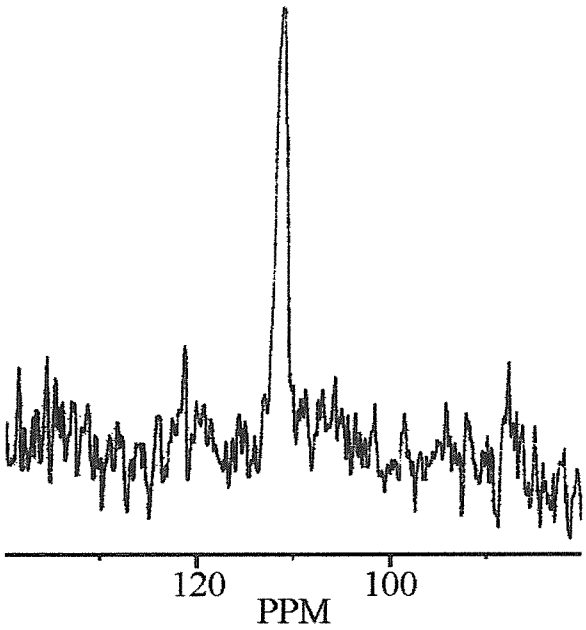

Figure 3.11 – $^{125}Te\{^1H\}$ NMR spectrum of *fac*-$[W(CO)_3\{MeC(CH_2TeMe)_3\}]$ recorded in CH_2Cl_2-10 % $CDCl_3$

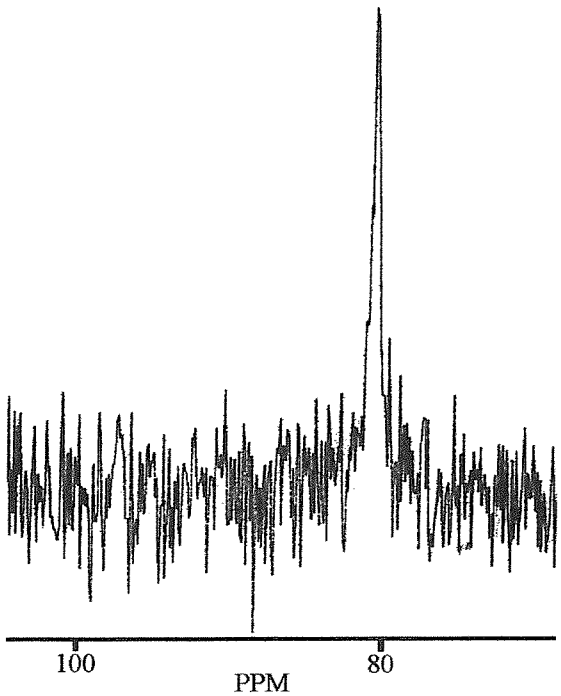

Figure 3.12 – $^{77}Se\{^1H\}$ NMR spectrum of *fac*-$[Mo(CO)_3\{MeC(CH_2SeMe)_3\}]$ recorded in CH_2Cl_2-10 % $CDCl_3$

Table 3.3 – $^{77}Se\{^1H\}$ and $^{125}Te\{^1H\}$ NMR spectroscopic data

Compound	δ ^{77}Se / ^{125}Te [a]	
fac-$[Mo(CO)_3\{MeC(CH_2SeMe)_3\}]$	81	
fac-$[W(CO)_3\{MeC(CH_2SeMe)_3\}]$	53	
fac-$[Mo(CO)_3\{MeC(CH_2TeMe)_3\}]$	179	
fac-$[W(CO)_3\{MeC(CH_2TeMe)_3\}]$	110	
cis-$[Mo(CO)_4\{MeC(CH_2SeMe)_3\}]$	31.4	20.0 [b]

a. In CH_2Cl_2-10 % $CDCl_3$ relative to neat external Me_2Se or Me_2Te.

b. Spectra recorded at 300 K.

^{95}Mo NMR Spectroscopic Studies

A ^{95}Mo NMR spectrum of freshly prepared $[Mo(CO)_3\{MeC(CH_2SMe)_3\}]$ CH_2Cl_2 solution at 300 K had δ = -1138, but this disappeared on standing, and a new resonance at –1283 grew in its place. The latter value is close to that observed for $[Mo(CO)_4\{MeS(CH_2)_3SMe\}]$ (-1294)[31], consistent with the generation of a tetracarbonyl complex. The decision to run the ^{95}Mo NMR spectra at 300 K came as a result of previous studies which have shown that ^{95}Mo NMR resonances in related complexes broaden rapidly when the samples are cooled, probably due to the substantial quadrupole moment, and spectra are best obtained at ambient temperatures.[31,36] The triseleno- and tritelluro-ether complexes each show a single resonance. The spectrum of $[Mo(CO)_3\{MeC(CH_2SeMe)_3\}]$ has been used as an example to illustrate the appearance of a ^{95}Mo NMR for these species. It is notable that the $\delta(^{95}Mo)$ shifts progressively to high frequency with trans donor Te < Se < S, consistent with increasing σ-donation as Group 16 is descended.[5,6] The shifts are *ca.* 500 ppm to high frequency of $[Mo(CO)_6]$ ($\delta(^{95}Mo)$ = -1856)[37] indicating decreased electron density on Mo(0) in these compounds. When these values are compared to those obtained for the [9]aneS_3 and [10]aneS_3 complexes, which show single resonances at –1345 and –1311 ppm respectively for $[Mo(CO)_3([9]aneS_3)]$ and

$[Mo(CO)_3([10]aneS_3)]$,[34] it can be seen that the values are similar. However, the two macrocylcic trithioether complexes are significantly more shielded than $[Mo(CO)_3\{MeC(CH_2SMe)_3\}]$. Similarly the tetracarbonyl complex *cis*-$[Mo(CO)_4\{\eta^2\text{-}MeC(CH_2SeMe)_3\}]$ is more shielded than the tricarbonyl selenoether complex *fac*-$[Mo(CO)_3\{MeC(CH_2SeMe)_3\}]$ which is a result of the fewer Group 16 donor atoms in the tetracarbonyl species leading to less electron density being displaced onto the Mo(0) centre with respect to the tricarbonyl species. Furthermore, the complex $[Mo(CO)_4([8]aneSe_2)]$[38] which also contains a bidentate ligand linked to the metal centre by two selenium donors shows a resonance at $\delta(^{95}Mo)$ –1424, which shows that the molybdenum is even more shielded in this example than the tetracarbonyl species $[Mo(CO)_2\{\eta^2\text{-}MeC(CH_2SeMe)_3\}]$.

Table 3.4 – ^{95}Mo NMR spectroscopic data

Compound	$\delta\ ^{95}Mo$ [a]
fac-$[Mo(CO)_3\{MeC(CH_2SMe)_3\}]$	-1138
fac-$[Mo(CO)_3\{MeC(CH_2SeMe)_3\}]$	-1216
fac-$[Mo(CO)_3\{MeC(CH_2TeMe)_3\}]$	-1336
cis-$[Mo(CO)_4\{MeC(CH_2SMe)_3\}]$	-1296

a. Relative to external aqueous Na_2MoO_4, recorded at 300 K recorded in CH_2Cl_2-10 % $CDCl_3$

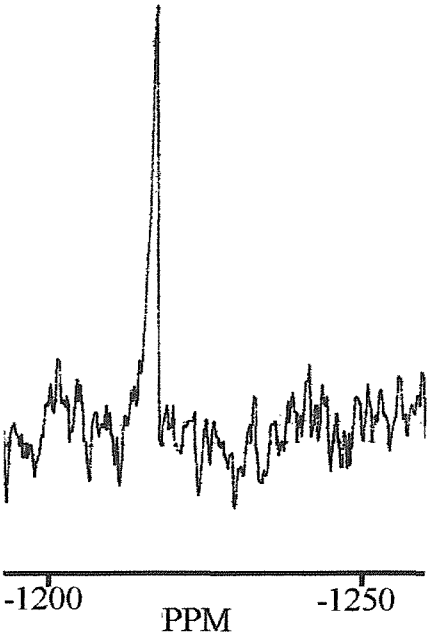

Figure 3.13 – ^{95}Mo NMR spectrum of *fac*-[Mo(CO)$_3${MeC(CH$_2$SeMe)$_3$}]

3.2.3 Tetracarbonyl Complexes

The following section outlines the procedures undertaken and the problems faced in the pursuit of the Group 6 tricarbonyl species and in particular the chromium(0) complexes.

Using the silane tridentate ligand MeSi(CH$_2$SMe)$_3$ the subsequent complexes of the Group 6 metals chromium(0), molybdenum(0) and tungsten(0) are formed as moderately air-sensitive solids. This series of Group 6 metal thioether derivatives is one of the first complete series to be structurally characterised. The work in this chapter has indicated strongly that the instability of the new complexes in solution has led to difficulties in obtaining the spectroscopic data. A solution of [Mo(CO)$_3${MeC(CH$_2$SMe)$_3$}] showed signs of decomposition during the aquisition of a ^{13}C{^{1}H} NMR spectrum and some features of the resulting spectrum are attributed to the tetracarbonyl *cis*-[Mo(CO)$_4${η^2-MeC(CH$_2$SMe)$_3$}]. As mentioned earlier, after the solution had stood for some hours at room temperature, the ^{13}C{^{1}H} NMR resonances associated with the *fac*-tricarbonyl had greatly diminished and the free ligand

and the tetracarbonyl were the major species present. Similarly the ^{95}Mo NMR spectrum showed, after a period of time, a new resonance with δ = -1283. This value is close to that observed for [Mo(CO)$_4${MeS(CH$_2$)$_3$SMe}] (-1294),[31] consistent with the generation of a tetracarbonyl complex. Confirmation of this came from an IR spectrum of the final solution used to record the ^{13}C{^{1}H} NMR spectrum, and showed ν(CO) at 2024, 1911, 1885(sh) and 1858 cm^{-1}, which may be compared with similar values 2023, 1910, 1895(sh), 1856 cm^{-1} in [Mo(CO)$_3${MeS(CH$_2$)SMe}].[31] It is thus clear that whilst pure *fac*-[Mo(CO)$_3${MeC(CH$_2$SMe)$_3$}] can be isolated, it decomposes readily in solution into *cis*-[Mo(CO)$_4${η^2-MeC(CH$_2$SMe)$_3$}], free ligand and an unidentified brown solid. Pyramidal inversion at sulfur is fast on the NMR time scales in thioether complexes of Group 6 carbonyls[31,36] but exchange between the free and coordinated MeS groups in the tetracarbonyls is not observed in the NMR spectra. The instability of the *fac*-tricarbonyl complex was greatest in the chromium-thioether system. The reaction of [Cr(CO)$_3$(MeCN)$_3$] *in situ* in MeCN with MeC(CH$_2$SMe)$_3$ gave a yellow solution which contained *fac*-[Cr(CO)$_3${MeC(CH$_2$SMe)$_3$}], identified by ν(CO) modes at 1926, 1812 cm^{-1}. However, repeated attempts to isolate a pure sample of the solid *fac* complex have been unsuccessful, either from this solution or using pre-isolated [Cr(CO)$_3$(MeCN)$_3$] in benzene.[18] Work-up of such solutions gave some green solid, large amounts of yellow [Cr(CO)$_4${η^2-MeC(CH$_2$SMe)$_3$}] which was isolated and is described below, and free ligand. An alternative route via [Cr(CO)$_6$], MeC(CH$_2$SMe)$_3$ and NaBH$_4$ in ethanol,[39] which was successful for the macrocyclic thioethers, gave only green decomposition products in this case. The instability of *fac*-[Cr(CO)$_3${MeC(CH$_2$SMe)$_3$}] is in keeping with the facile decomposition of the heavier analogues W < Mo << Cr, but is surprising when compared with the recently isolated *fac*-[Cr(CO)$_3${MeSi(CH$_2$SMe)$_3$}] which has been structurally characterised. We have described detailed studies of [M(CO)$_4$(L-L)] in Chapter 2,[31] and the tetracarbonyl complexes formed by η^2-coordination of the tripodal ligands are not fundamentally different. For

comparison two examples are described, *cis*-$[Cr(CO)_4\{\eta^2\text{-}MeC(CH_2SMe)_3\}]$ and *cis*-$[Mo(CO)_4\{\eta^2\text{-}MeC(CH_2SeMe)_3\}]$. The chromium complex was isolated during attempts to prepare the tricarbonyl from $[Cr(CO)_3(MeCN)_3]$ as described earlier, and $[Mo(CO)_4\{MeC(CH_2SeMe)_3\}]$ from reaction of $[Mo(CO)_4(MeCN)_2]$ and $MeC(CH_2SeMe)_3$. The spectroscopic data (Tables 3.1 – 3.3) are, as expected, very similar to those of the corresponding *cis*-$[M(CO)_4\{MeE(CH_2)_3EMe\}]$ (M = Cr E = S, M = Mo E = Se), which also contain 6-membered chelate rings, with extra NMR features due to the free arm of the tripodal ligand. In contrast to the *fac*-$[M(CO)_3L^3]$ these tetracarbonyls appear stable both in the solid state and in solution. The solution IR spectrum (CH_2Cl_2) of $[Cr(CO)_4\{MeC(CH_2SMe)_3\}]$ is shown in Figure 3.14. Group theory for a *cis* isomer predicts four stretches ($2A_1 + B_1 + B_2$). Difficulty in resolving the A_1 and B_1 modes at *ca.* 1900 cm^{-1} results in the observation of only three bands (plus a shoulder at *ca.* 1895 cm^{-1}) in the cases of these Cr and Mo complexes. The FAB mass spectrum is shown for the tetracarbonyl molybdenum complex showing the parent ion at m/z = 560 (Figure 3.15).

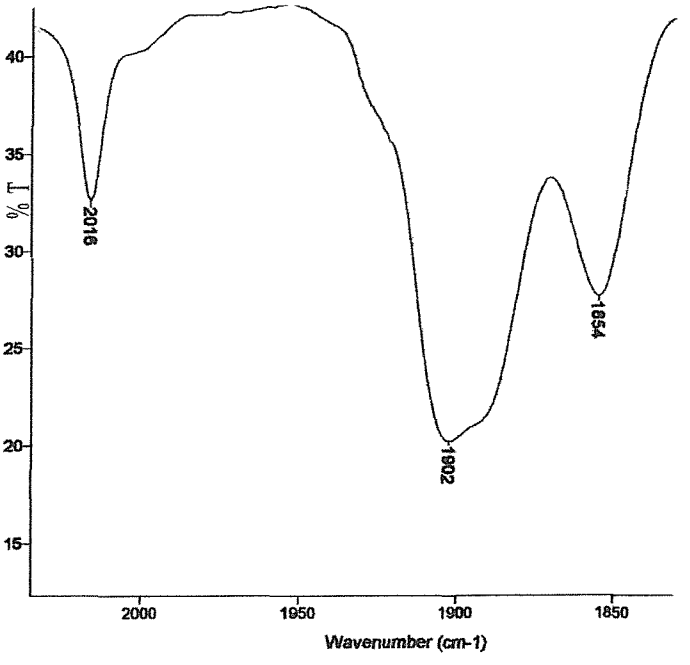

Figure 3.14 – ν(CO) region of IR spectrum of *cis*-$[Cr(CO)_4\{MeC(CH_2SMe)_3\}]$

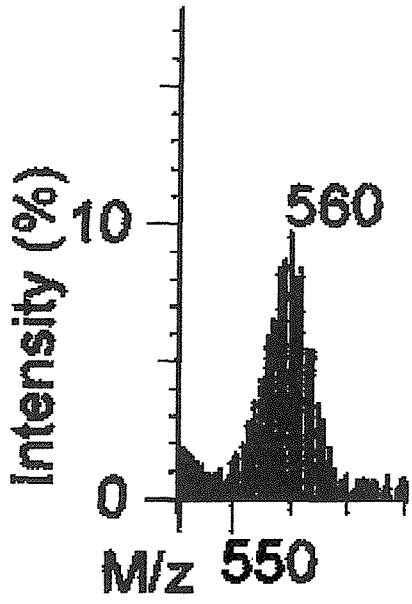

Figure 3.15 – FAB mass spectrum of *cis*-[Mo(CO)$_4${MeC(CH$_2$SeMe)$_3$}] showing the parent ion.

3.2.4 Molybdenum(0) complexes of [16]aneSe$_4$

The starting material in this case was the nitrile complex [Mo(CO)$_3$(MeCN)$_3$] made *in situ* from the hexacarbonyl in MeCN.[33] *Fac*-[Mo(CO)$_3$(η^3-[16]aneSe$_4$)] has been prepared by treating the starting material with the macrocyclic ligand. After stirring at reflux for 1 hour, the solvent was removed *in vacuo*, the complex extracted with dry CH_2Cl_2, filtered and the solvent removed. The resulting solid was washed with diethyl ether leaving [Mo(CO)$_3$(η^3-[16]aneSe$_4$)] in moderate yield as a dark yellow product. IR spectroscopic studies allowed the nature of this complex to be followed throughout the reaction. The two CO stretches associated with [Mo(CO)$_3$(MeCN)$_3$] at 1919 and 1794 cm^{-1} disappeared and, on formation of the subsequent *fac*-tricarbonyl [Mo(CO)$_3$(η^3-[16]aneSe$_4$)] two intense absorptions, centred at 1926 and 1812 cm^{-1} appeared. The IR spectrum of the complex in CH_2Cl_2 solution is shown in Figure 3.16.

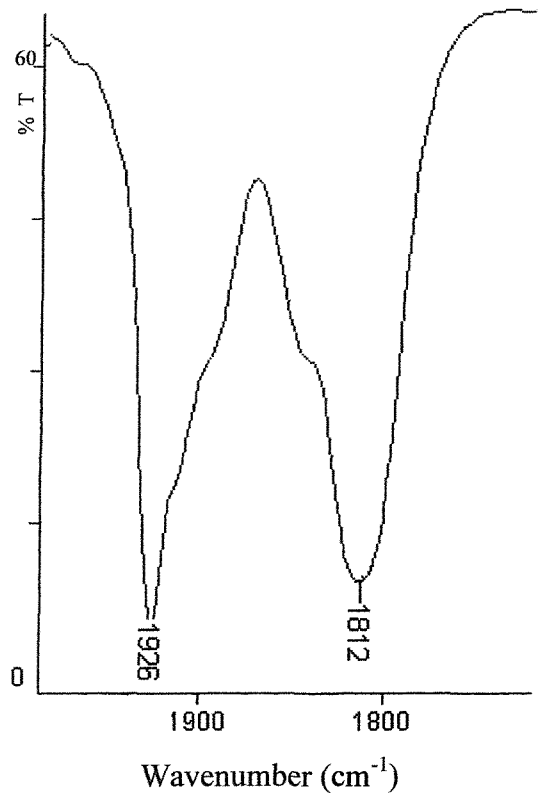

Figure 3.16 - ν(CO) region of IR spectrum of $[Mo(CO)_3(\eta^3\text{-}[16]aneSe_4)]$

APCI mass spectrometric data for the complex showed a peak corresponding to $[Mo(CO)_3(\eta^3\text{-}[16]aneSe_4)]^+$ the parent ion (*m/z* = 667) (Figure 3.17) and the fragment of $[Mo(CO)_2(\eta^3\text{-}[16]aneSe_4)]^+$ (*m/z* = 637) is also observed. The data show good agreement with the calculated isotope distributions.

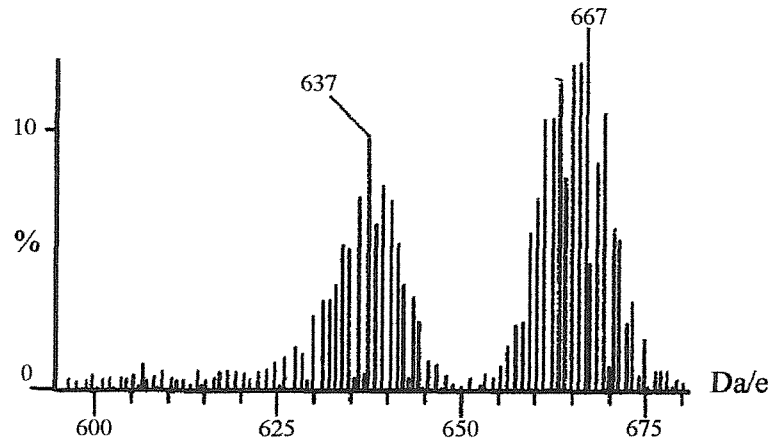

Figure 3.17 – APCI mass spectrum of $[Mo(CO)_3(\eta^3\text{-}[16]aneSe_4)]$

The next step of the reaction was the addition of trimethylamine oxide to a MeCN solution of the tricarbonyl species $[Mo(CO)_3(\eta^3\text{-}[16]aneSe_4)]$. Unfortunately, this reaction did not lead to the formation of the dicarbonyl molybdenum species. Instead the IR spectrum showed bands corresponding to a teracarbonyl compound.

3.3 CONCLUSIONS

The complexes *fac*-$[M(CO)_3L^3]$ (M = Mo or W, L^3 = $MeC(CH_2SMe)_3$, $MeC(CH_2SeMe)_3$ or $MeC(CH_2TeMe)_3$) have been prepared as light brown solids from $[M(CO)_3(MeCN)_3]$. The solution IR spectroscopic data showed two CO stretching vibrations which supports the identity of the complexes as *fac*-$[M(CO)_3L^3]$. FAB mass spectrometry confirmed the presence of $[M(CO)_3L^3]$. Multinuclear NMR studies (^1H, $^{13}C\{^1H\}$, $^{77}Se\{^1H\}$, $^{125}Te\{^1H\}$ and ^{95}Mo) were also undertaken to characterise the compounds. The complexes are surprisingly unstable in solution and would decompose over several hours to the free ligand and/or the tetracarbonyl species *cis*-$[M(CO)_4\{\eta^2MeC(CH_2EMe)_3\}]$. Attempts to isolate $[Cr(CO)_3L_3]$ have been unsuccessful but has been identified by IR spectroscopy. The instability of *fac*-$[Cr(CO)_3\{MeC(CH_2SMe)_3\}]$ is in keeping with the facile decomposition of the heavier analogues W < Mo (<< Cr), but is surprising when compared with the recently isolated *fac*-$[Cr(CO)_3\{MeSi(CH_2SMe)_3\}]$ which has been structurally characterised.[18]

3.4 EXPERIMENTAL

3.4.1 Ligand and Complex Synthesis

All preparations were performed under an argon atmosphere using standard Schlenk techniques. The $M(CO)_6$ (M = Cr, Mo or W) were obtained from Aldrich and used as received. The ligands, $MeC(CH_2SMe)_3$,[40] $MeC(CH_2SeMe)_3$,[41] and $MeC(CH_2TeMe)_3$[7] were made by literature methods.

a). Synthesis of *fac*-[$Mo(CO)_3${$MeC(CH_2SMe)_3$}]

$[Mo(CO)_6]$ (0.2 g, 0.76 mmol) was refluxed in dry degassed MeCN (50 cm^3) under argon for 16 h to give $[Mo(CO)_3(MeCN)_3]$. The ligand, $MeC(CH_2SMe)_3$ (0.17 g, 0.8 mmol) was added and the mixture stirred under argon for a further 16 h. An IR spectrum of the solution showed the absence of $[Mo(CO)_3(MeCN)_3]$. The solvent was removed *in vacuo*, and the resulting oil dissolved in CH_2Cl_2 (20 cm^3), and filtered through celite. The solvent was removed *in vacuo*, and the solid was washed with diethyl ether (20 cm^3) to remove any tetracarbonyl complex. The pale brown powder was rinsed with *n*-pentane (10 cm^3) and dried in vacuo (yield 0.15 g, 52 %). Required for $[C_{11}H_{18}MoO_3S_3]$: C = 33.8, H = 4.7 %; found C = 34.1, H = 4.7 %. FAB mass spectrum (3-NOBA matrix): found *m/z* = 392; calculated for $[^{98}Mo(CO)_3\{MeC(CH_2SMe)_3\}]^+$ *m/z* = 392. ^1H NMR spectrum (300 MHz, $CDCl_3$, 300 K): δ 1.15 (Me), 2.1 (MeS), 2.45 (CH_2).

b). Synthesis of *fac*-[$Mo(CO)_3${$MeC(CH_2SeMe)_3$}]

Method as for a) above, but using $[Mo(CO)_6]$ (0.2 g, 0.76 mmol) and $MeC(CH_2SeMe)_3$ (0.28 g, 0.8 mmol) to give a pale brown powder (yield 0.19 g, 47 %). Required for $[C_{11}H_{18}MoO_3Se_3]$: C = 24.9, H = 3.4 %; found C = 25.2, H = 3.3 %. FAB mass spectrum (3-NOBA matrix): found *m/z* = 532, 448; calculated for $[^{98}Mo(CO)_3\{MeC(CH_2{}^{80}SeMe)_3\}]^+$ *m/z* = 536, $[^{98}Mo\{MeC(CH_2{}^{80}SeMe)_3\}]^+$ *m/z* = 452. ^1H NMR spectrum (300 MHz, $CDCl_3$, 300 K): δ 1.3 (Me), 2.1 (MeS), 2.7 (CH_2).

c). Synthesis of *fac*-[Mo(CO)$_3${MeC(CH$_2$TeMe)$_3$}]

Method as for a) above, but using [Mo(CO)$_6$] (0.2 g, 0.76 mmol) and MeC(CH$_2$TeMe)$_3$ (0.40 g, 0.8 mmol) to give a pale brown powder (yield 0.23 g, 45 %). Required for [$C_{11}H_{18}MoO_3Te_3$]: C = 19.5, H = 2.7 %; found C = 20.0, H = 2.9 %. FAB mass spectrum (3-NOBA matrix): found *m/z* = 678, 594; calculated for [^{98}Mo(CO)$_3${MeC(CH$_2$^{130}TeMe)$_3$}]$^+$ *m/z* = 686, [^{98}Mo{MeC(CH$_2$^{130}TeMe)$_3$}]$^+$ *m/z* = 602. ^{1}H NMR spectrum (300 MHz, $CDCl_3$, 300 K): δ 1.3 (Me), 2.1 (MeS), 2.8 (CH_2).

d). Synthesis of *fac*-[W(CO)$_3${MeC(CH$_2$SMe)$_3$}]

[W(CO)$_6$] (0.2 g, 0.57 mmol) was refluxed in dry degassed MeCN (50 cm^3) under argon for 4 days to give [W(CO)$_3$(MeCN)$_3$]. The ligand, MeC(CH$_2$SMe)$_3$ (0.13 g, 0.6 mmol) was added and the mixture stirred for a further 16 h, at which time an IR spectrum showed the absence of [W(CO)$_3$(MeCN)$_3$]. The solvent was removed *in vacuo*, the residue dissolved in CH_2Cl_2 and the solution filtered through celite. The solvent was again removed *in vacuo*, the pale brown solid washed with diethyl ether (10 cm^3) and *n*-pentane (20 cm^3) and dried *in vacuo* (yield 0.14g, 52 %). Required for [$C_{11}H_{18}WO_3S_3$]: C = 27.6, H = 3.8 %; found C = 27.3, H = 4.0 %. FAB mass spectrum (3-NOBA matrix): found *m/z* = 478; calculated for [^{184}W(CO)$_3${MeC(CH$_2$SMe)$_3$}]$^+$ *m/z* = 478. ^{1}H NMR spectrum (300 MHz, $CDCl_3$, 300 K): δ 1.1 (Me), 2.2 (MeS), 2.6 (CH_2).

e). Synthesis of *fac*-[W(CO)$_3${MeC(CH$_2$SeMe)$_3$}]

Method as for d) above, but using [W(CO)$_6$] (0.2 g, 0.57 mmol) and MeC(CH$_2$SeMe)$_3$ (0.21 g, 0.6 mmol) to give a pale brown powder (yield 0.14 g, 39 %). Required for [$C_{11}H_{18}WO_3Se_3$]: C = 21.3, H = 2.9 %; found C = 21.5, H = 3.1 %. FAB mass spectrum (3-NOBA matrix): found *m/z* = 618; calculated for [^{184}W(CO)$_3${MeC(CH$_2$^{80}SeMe)$_3$}]$^+$ *m/z* = 622. ^{1}H NMR spectrum (300 MHz, $CDCl_3$, 300 K): δ 1.3 (Me), 2.05 (MeS), 2.8 (CH_2).

f). Synthesis of *fac*-[W(CO)$_3${MeC(CH$_2$TeMe)$_3$}]

Method as for d) above, but using [W(CO)$_6$] (0.2 g, 0.57 mmol) and MeC(CH$_2$TeMe)$_3$ (0.30 g, 0.6 mmol) to give a pale brown powder (yield 0.24 g, 55 %). Required for [$C_{11}H_{18}WO_3Te_3$]: C = 17.3, H = 2.4 %; found C = 17.3, H = 2.3 %. FAB mass spectrum (3-NOBA matrix): found *m/z* = 758; calculated for [^{184}W(CO)$_3${MeC(CH$_2$^{130}TeMe)$_3$}]$^+$ *m/z* = 766. ^{1}H NMR spectrum (300 MHz, $CDCl_3$, 300 K): δ 1.5 (Me), 2.0 (MeS), 2.2 (CH_2).

g). Synthesis of *cis*-[Cr(CO)$_4${η^2-MeC(CH$_2$SMe)$_3$}]

This was made from [Cr(CO)$_3$(MeCN)$_3$] and MeC(CH$_2$SMe)$_3$ in benzene, following the method used for [Cr(CO)$_3${MeSi(CH$_2$SMe)$_3$}].[18] The product was extracted in diethyl ether, the solvent removed and the yellow solid washed with n-pentane. Required for [$C_{12}H_{18}CrO_4S_3$]: C = 39.1, H = 4.9 %; found: C = 38.5, H = 4.3 %. ^{1}H NMR spectrum (300 MHz, $CDCl_3$, 300 K): δ 1.12 (Me), 2.2, 2.4 (MeS), 2.6, 2.7 (CH_2).

h). Synthesis of *cis*-[Mo(CO)$_3${η^2-MeC(CH$_2$SeMe)$_3$}]

[Mo(CO)$_6$] (0.2 g, 0.76 mmol) was refluxed in dry degassed MeCN (50 cm^3) under argon for 8 h to give [Mo(CO)$_4$(MeCN)$_2$] (identified *in situ* by IR spectroscopy). The ligand MeC(CH$_2$SeMe)$_3$ (0.28 g, 0.8 mmol) was added and the mixture stirred for a further 16 h. The solvent was removed *in vacuo* and the resulting oil dissolved in CH_2Cl_2 (20 cm^3) and filtered through celite. The solvent was removed *in vacuo*, the residue dissolved in diethyl ether (10 cm^3) and filtered. The solvent was again removed *in vacuo*, and the solid washed with *n*-pentane, and dried *in vacuo*. Required for [$C_{12}H_{18}MoO_4Se_3$]: C = 25.8, H = 3.2 %; found C = 25.3, H = 3.0 %. FAB mass spectrum (3-NOBA matrix): foound m/z = 560, 532; calculated for [^{98}Mo(CO)$_4${MeC(CH$_2$^{80}SeMe)$_3$}]$^+$ *m/z* = 564, [^{98}Mo(CO)$_3${MeC(CH$_2$^{80}SeMe)$_3$}]$^+$ *m/z* = 536. ^{1}H NMR spectrum (300 MHz, $CDCl_3$, 300 K): δ 1.2 (Me), 2.1, 2.45 (MeSe), 2.7, 2.8 (CH_2).

3.5 REFERENCES

1. E.G. Hope, W. Levason, S.G. Murray and G.L. Marshall, *J. Chem. Soc., Dalton Trans.*, 1985, 2185.
2. W. Levason, S.D. Orchard and G. Reid, *Inorg. Chem.*, 2000, **39**, 3853.
3. W. Levason, S.D. Orchard and G. Reid, *J. Chem. Soc., Chem. Commun.*, 1999, 1071.
4. W. Levason, S.D. Orchard, G. Reid and J.M. Street, *J. Chem. Soc., Dalton Trans.*, 2000, 2537.
5. W. Levason, S.D. Orchard and G. Reid, *J. Chem. Soc., Dalton Trans.*, 1999, 823.
6. J. Connolly, A.R.J. Genge, W. Levason, S.D. Orchard, S.J.A. Pope and G. Reid, *J. Chem. Soc., Dalton Trans.*, 1999, 2343.
7. E.G. Hope, T. Kemmitt and W. Levason, *Organometallics*, 1987, **6**, 206.
8. E.G. Hope, T. Kemmitt and W. Levason, *Organometallics*, 1988, **7**, 78.
9. T. Kemmitt and W. Levason, *Organometallics*, 1989, **8**, 1303.
10. E.G. Hope and W. Levason, *Coord. Chem. Rev.*, 1993, **122**, 109.
11. H.C.E. Mannerskantz and G. Wilkinson, *J. Chem. Soc.*, 1962, 4454.
12. M.T. Ashby, J.H. Enemark, D.L. Lichtenberger and R.B. Ortega, *Inorg. Chem.*, 1986, **25**, 3154.
13. D. Sellman and L. Zapf, Angew. Chem., 1984, **96**, 799; *Angew. Chem. Int. Ed. Engl.*, 1984, **23**, 807.
14. J.P. Carpenter, C.J. Grant, W.N. Setzer and D.G. VanDerveer, *Inorg. Chem.*, 1989, **28**, 4128.
15. F.A. Cotton and F. Zingales, *Chem. Ind. (London)*, 1960, 1219.
16. F.A. Cotton and F. Zingales, *Inorg. Chem.*, 1962, **1**, 145.
17. M. Curcic, D. Sevdic and Lj. Tusek-Bozic, *Polyhedron*, 1989, **8**, 505.
18. H.W. Yim, L.M. Tran, E.D. Dobbin and D. Rabinovich, *Inorg. Chem.*, 1999, **38**, 2211.
19. W.C. Blackwell III, D. Bunich, T.E. Concolino, A.L. Rheingold and D. Rabinovich, *Inorg. Chem. Commun.*, 2000, **3**, 325.

20. H.W. Yim, K-C. Lam, A.L. Rheingold and D. Rabinovich, *Polyhedron*, 2000, **19**, 849.
21. H.W. Yim, L.M. Tran, E.E. Pullen, D. Rabinovich, L.M. Liable-Sands, T.E. Concolino and A.L. Rheingold, *Inorg. Chem.*, 1999, **38**, 6234.
22. H.W. Yim, H.V. Pham, L.M. Liable-Sands, A.L. Rheingold and D. Rabinovich, within reference 19.
23. J. Chatt, G.J. Leigh and A.P. Storace, *J. Chem. Soc., A*, 1971, 1380.
24. M.T. Ashby, J.H. Enemark, D.L. Lichtenberger and R.B. Ortega, *Inorg. Chem.*, 1986, **25**, 3154.
25. P.K. Baker, S.D. Harris, M.C. Durrant, D.L. Hughes and R.L. Richards, *J. Chem. Soc., Dalton Trans.*, 1994, 1401.
26. O.P. Siclovan and R.J. Angelici, *Inorg. Chem.*, 1998, **37**, 432.
27. D.P. Tate, W.R. Knipple and J.M. Augl, *Inorg. Chem.*, 1962, **2**, 433.
28. G.J. Kubas and L.S. Van der Sluys, *Inorg. Synth.*, 1990, **28**, 29.
29. M.T. Ashby and D.L. Lichtenger, *Inorg. Chem.*, 1985, **24**, 636.
30. H. –J. Kim, Y. Do, H.W. Lee, J.H. Jeong and Y.S. Sohn, *Bull. Korean Chem. Soc.*, 1991, **12**, 257.
31. A.J. Barton, W. Levason and G. Reid, *J. Organomet. Chem.*, 1999, **579**, 235.
32. T. Yoshida, T. adachi, T. Ueda, M. Watanabe, M. Kaminaka and T. Higuchi, *Angew. Chem. Int. Ed. Engl.*, 1987, **26**, 1171.
33. G.J. Kubas, *Inorg. Synth.*, 1990, **27**, 4.
34. A.J. Barton, J. Connolly, W. Levason, A. Mendia-Jalon, S.D. Orchard and G. Reid, *Polyhedron*, 2000, **19**, 1373.
35. P.S. Braterman, *Struct. Bonding, Berlin*, 1976, **26**, 1.
36. E.W. Abel, D.E. Budgen, I. Moss, K.G. Orrell and V. Sik, *J. Organomet. Chem.*, 1989, **362**, 105.
37. M. Minelli, J.H. Enemark, R.T.C. Brownlee, M.J. O'Connor and A.G. Wedd, *Coord. Chem. Rev.*, 1985, **68**, 169.
38. M.K. Davies, M.C. Durrant, W. Levason, G. Reid and R.L. Richards, *J. Chem. Soc., Dalton Trans.*, 1999, 1077.

39. J. Chatt, G.J. Leigh and N. Thankarajan, *J. Organomet. Chem.*, 1971, **29**, 105.

40. R. Ali, S.J. Higgins and W. Levason, *Inorg. Chim. Acta*, 1984, **84**, 65.

41. D.J. Gulliver, E.G. Hope, W. Levason, S.G. Murray, D.M. Potter and G.L. Marshall, *J. Chem. Soc., Perkin Trans. II*, 1984, 429.

CHAPTER 4

Group 16 Complexes of Osmium, Platinum, Palladium and Rhodium

4.1 INTRODUCTION

The aim of this chapter was to investigate the complexation of a range of bidentate Group 15 and Group 16 ligands, with the aim of generating Os(II) compounds of the form $[OsCl_2(L\text{-}L)_2]$ and the cationic $[OsCl(PPh_3)(L\text{-}L)_2]^+$. See Figure 4.1 for the ligands used. Furthermore, investigations have been carried out into Pt(II), Pd(II) and Rh(III) complexes of the organo-selenium macrocycle $[24]aneSe_6$.

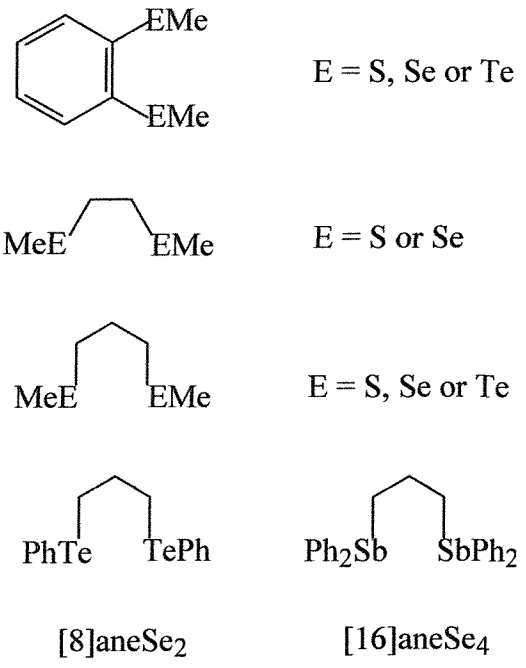

Figure 4.1 – The bidentate ligands.

The coordination chemistry of these Os(II) complexes has been investigated using IR, UV-Vis and multinuclear (^1H, $^{31}P\{^1H\}$ and $^{125}Te\{^1H\}$) spectroscopies, ES^+ mass spectrometry, cyclic voltammetry and single crystal X-ray diffraction.

4.1.1 Group 16 Osmium Complexes

Osmium forms compounds in formal oxidation states ranging from 8 to –2 and as a consequence has an extremely rich coordination chemistry.[1] However, the absence of labile osmium precursors in the medium oxidation states can make some types of complex difficult to prepare.

The ability of tertiary phosphine and arsine ligands to stabilize medium and higher oxidation states of the Group 8 metals is well known.[2] A wide range of bidentate and polydentate phosphine and arsine complexes of Os(II), Os(III) and Os(IV) are readily made from starting from OsO_4, HX and ROH (X = Cl, Br or I) or $[OsX_6]^{2-}$. Likewise, charged sulphur-donor ligands, dithiocarbamates, and 1,1-dithiolenes are similarly effective,[3,4] but obtaining complexes with neutral Group 16 donors has proved considerably more difficult. The reaction of osmium tetraoxide or potassium tetrahydroxodioxo-osmate(VI), $K_2[OsO_2(OH)_4]$, in concentrated hydrochloric acid with 2,5-dithiahexane in alcohol gave poor yield of the green complex $[Os\{MeS(CH_2)_2SMe\}Cl_4]$, but attempts to extend this to other thioethers were not very successful.[5] Poor yields were also generated by direct reaction of $[OsX_6]^{2-}$ with dithioethers. The general route reacted together sodium hexachloro-osmate(IV) and the thioether in refluxing 2-ethoxyethanol. This afforded $[Os(L\text{-}L)Cl_4]$ (L-L = $MeS(CH_2)_2SMe$, *cis*-MeSCH=CHSMe, o-$C_6H_4(SMe)_2$, $PhS(CH_2)_2SPh$, PhSCH=CHSPh or o-$C_6H_4(SPh)_2$).[5] Osmium tetraoxide, aqueous HBr, and various dithioethers yielded only brown oils. However, moderate success was achieved when $K_2[OsBr_6]$ reacted with the ligands in 2-ethoxyethanol to form $[Os(L\text{-}L)Br_4]$ (L-L = $MeS(CH_2)_2SMe$ or MeSCH=CHSMe).[5] Attempts to prepare iodo-complexes from $K_2[OsI_6]$ gave intractable green oils.[5] Similar low yielding reactions are experienced when dealing with diselenoethers.[6] Refluxing $Na_2[OsCl_6]$ and $MeSe(CH_2)_2SeMe$ gave black uncharacterised materials, which contrasts with the green complex when the dithioether analogue was used. However, if the mixture was heated to reflux, then immediately cooled and concentrated *in vacuo*, the green $[Os\{MeSe(CH_2)_2SeMe\}Cl_4]$ could be precipitated with diethyl ether. The complexes $[Os(L\text{-}L)Cl_4]$ complexes (L-L = $MeSe(CH_2)_3SeMe$, $PhSe(CH_2)_2SePh$

or MeSCH=CHSeMe) were obtained by similar routes. The red $[Os\{MeSe(CH_2)_2SeMe\}Br_4]$ was obtained using $Na_2[OsBr_6]$.

Further investigations into the OsO_4-HX (X =Cl or Br)-dithioether-ethanol reactions have been carried out, and found that under mild conditions, *trans*-dioxo-osmium(VI) complexes can be isolated.[7,8] Until work by Levason and Harbron, despite a wide variety of related *trans*-$[OsO_2]^{2+}$ (osmyl) complexes being known,[9] no examples with thio- or seleno-ethers had been reported. The addition of L-L (L-L = $MeS(CH_2)_2SMe$, o-$C_6H_4(SMe)_2$ or o-$C_6H_4(PPh_2)(SMe)$) to a solution of OsO_4 in a mixture of concentrated HX (X = Cl or Br) and ethanol at room temperature gave the complexes $[OsO_2X_2(L\text{-}L)]$ in moderate yields. In contrast $PhS(CH_2)_2SPh$ did not react with the OsO_4-HX-EtOH mixture, even after several days at room temperature. The diselenoether $MeSe(CH_2)_2SeMe$ gave poor yield of the Os(VI) complex but $PhSe(CH_2)_2SePh$ was rapidly oxidised by OsO_4-HX-EtOH, and no evidence for an Os(VI) complex was obtained. The osmyl complexes $[OsO_2X_2(L\text{-}L)]$ are however unstable, further reduction to, for example, $[OsX_2(L\text{-}L)_2]$ does not appear possible by this route.

In the search for a route to *trans*-$[OsCl_2(L\text{-}L)_2]$ from Os(II) we used the recently characterised *trans*-$[OsCl_2(dmso)_4]$.[17,18] Efficient syntheses of dimethyl sulfoxide complexes of osmium are highly desirable at the moment as a result of the attractive chemistry being offered by its neighbour ruthenium. Ruthenium(II) complexes incorporating sulfoxide ligands have attracted a great deal of interest recently. Octahedral *cis*- and *trans*-$[RuCl_2(dmso)_4]$ possess mutagenic properties and exhibit antitumour activity. In addition, sulfoxide complexes of ruthenium(II) have been utilised as precatalysts for homogeneous hydrogenation.[10] The sulfoxides in these complexes are readily displaced by a wide variety of ligands under mild conditions and thus serve as moderately stabilised precurors to a range of derivatives.[11,12,13,14] Sulfoxide complexes are therefore of importance for a variety of reasons. As far as our investigations were concerned, the opportunity of introducing moderate donor ligands, such as dithio-, diseleno- and ditelluro-ethers, and displacing moderately labile dmso ligands from Os(II) systems was of high importance. Until very recently only

two studies of the osmium analogues had appeared.[15,16] No structural or reactivity studies of the complexes were extant However, the use of *cis*- and *trans*-$[OsCl_2(dmso)_4]$ as precursors to osmium(II) complexes have been reported.[17,18] The incorporation of chiral-at-phosphorus ligands has recently been communicated by M.G. Humphrey.[18] These studies have afforded efficient routes to lightly stabilised precursors of osmium(II) which are important as entry points to derivative chemistry. Close examination of Ru(II) complexes of ditelluroethers could give clues when considering routes into the synthesis of Os(II) ditelluroether complexes. A recent journal article gave a good illustration of how far the chemistry of ruthenium with organo-tellurium ligands has come.[23] Ruthenium(II) compounds of this type are close analogues of the osmium compounds I am striving to synthesise. Direct reaction of the ditelluroethers with $RuCl_3.nH_2O$ proved generally unsatisfactory, although one example *trans*-$[RuCl_2\{o\text{-}C_6H_4(TeMe)_2\}_2]$ has been obtained by this route.[19] Entry into the ruthenium chemistry was achieved by reaction of the ligands with $[RuCl_2(PPh_3)_3]$ in the presence of NH_4PF_6, $[RuCl_2(dmso)_4]$ or $[Ru(dmf)_6][CF_3SO_3]_3$.[20] The first reaction gave *trans*-$[RuCl(PPh_3)(L\text{-}L)_2]PF_6$ as orange-brown powders, whilst use of $[RuCl_2(dmso)_4]$ afforded *trans*-$[RuCl_2(L\text{-}L)_2]$. A more general route to *trans*-$[RuX_2(L\text{-}L)_2]$ (X = Cl, Br or I) was reaction of $[Ru(dmf)_6][CF_3SO_3]_3$ with L-L and LiX in EtOH. The ruthenium(II) complexes are air-stable in the solid state. The success of these reaction systems gave us sufficient encouragement in our pursuit of synthetic routes into the chemistry of Os(II) complexes with ditelluroethers and other Group 16 bidentate ligands, namely dithio- and diseleno-ethers.

The aim of this research was to extend the previous studies of ditelluroether complexes with platinum group metals, Pt or Pd,[21,22,23] Ir,[21,22] Ru or Rh,[23] to osmium and the results of the investigation will be discussed. Dr V. Tolhurst made a considerable contribution to the work of ruthenium with ditelluroethers followed by some preliminary work on osmium. This became the spring board for my own study.[24]

Work within the group also covered the chemistry of Ru(II) compounds of ditertiary stibine ligands.[25] The majority of knowledge of stibine coordination chemistry is based upon $SbPh_3$.[26] As this work is usually carried out within studies involving phosphorus and arsenic analogues assumptions are made on the donor capacity of the antimony containing ligands. Detailed studies have shown that one assumption, namely that stibines were poorer donors than phosphines was incorrect.[27,28] Reports have also shown that SbR_3 ligands exhibit different behaviour compared to PR_3 and AsR_3 ligands. Unusual observations during the studies of the distibinomethane complexes with metal carbonyls[29,30] showed that on coordination the C-Sb-C bond angles increase, whereas C-P-C or C-As-C angles in P or As analogues do not vary significantly between the free and coordinated ligands. A similar effect was found in complexes of $Ph_2Sb(CH_2)_3SbPh_2$ bonded to platinum group metal halides including ruthenium(II).[25] Ruthenium(II) complexes of $Ph_2Sb(CH_2)_3SbPh_3$ are easily prepared by reaction of $[Ru(dmf)_6][CF_3SO_3]_3$ with $Ph_2Sb(CH_2)_3SbPh_2$ in ethanol in the presence of the appropriate lithium halide. The products $[RuX_2\{Ph_2Sb(CH_2)_3SbPh_2\}_2]$ (X = Cl, Br or I) are identified as *trans* isomers following diffuse reflectance UV-Vis spectra which show two weak d-d bands and was confirmed by the crystal structure of the bromide which is shown in Figure 4.2. These results are interesting because they show the efficiency of the reactions of ditertiary stibines with a metal from Group 8 and also illustrate the nature and structure of the final product.

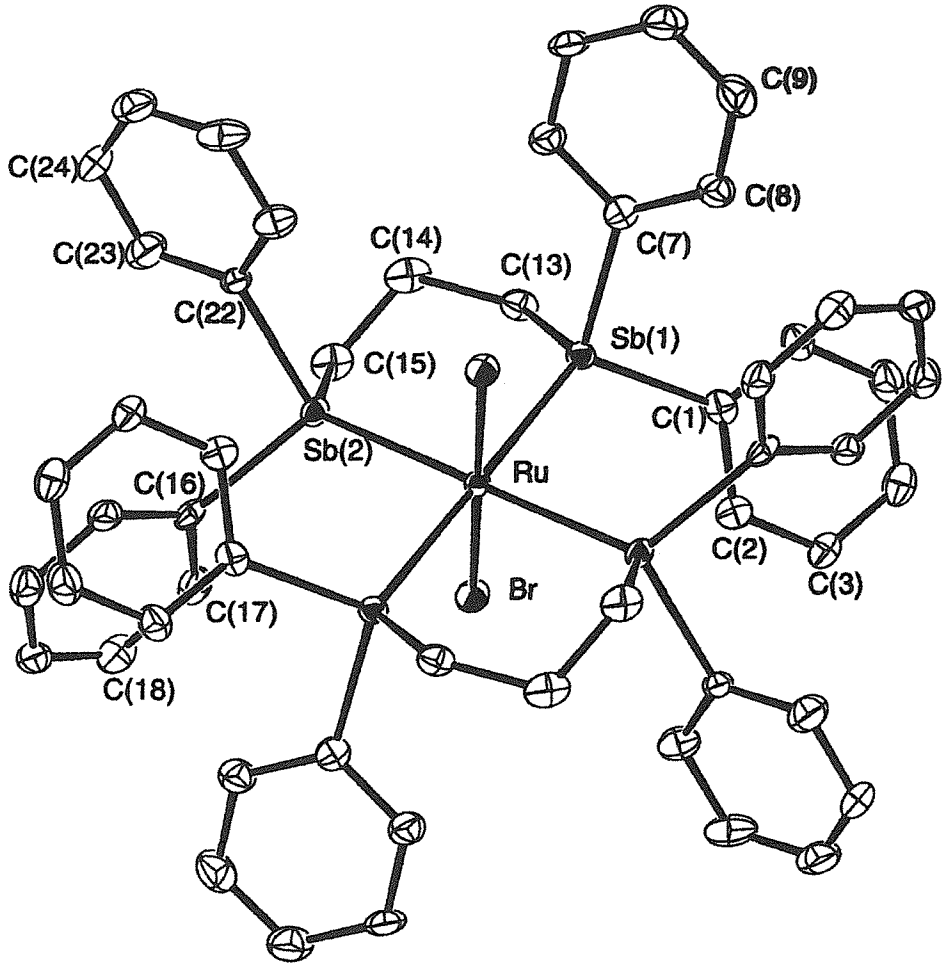

Figure 4.2 – Molecular structure of $[RuBr_2\{Ph_2Sb(CH_2)_3SbPh_2\}_2]$

4.1.2 Platinum Group Metal Complexes of Macrocyclic Selenoethers

The coordination chemistry of N- and S- donor macrocycles has attracted intense interest.[31,32] In comparison, reports on metal-ion complexes of the selenium congeners are relatively few and have dealt mainly with the ligand 1,5,9,13-tetraselenacyclohexadecane [16]aneSe$_4$.[33,34] Within the last decade reports of complexes of [16]aneSe$_4$, with Rh(III),[35,36] Ir(III),[36] Pd(II), and Pt(II),[37] Ru(II)[38] and Ru(III) and Pt(IV)[39] have appeared. Studies of the metals with the hexaselenoether ligand [24]aneSe$_6$ have been undertaken. This is mainly the work of the Southampton research group.

The only reported example of a crystallographically characterised complex involving a [24]aneSe$_6$ is [(PdCl)$_2${[24]aneSe$_6$}]$^{2+}$.[34] In this structure [24]aneSe$_6$ chelates two individual palladium atoms in a tridentate fashion, while a chlorine atom occupies the fourth coordination site in each case, to form the [(PdCl)$_2${[24]aneSe$_6$}]$^{2+}$ cation shown in Figure 4.3.

The thioether complexes [M([18]aneS$_6$)][BPh$_4$]$_2$ (M = Pt or Pd) reported by Schröder and co-workers[40] have been shown to adopt unusual geometries in the solid state. Furthermore, they have been shown to be important precursors in obtaining metal complexes in unusual oxidation states. For example, [Pd([18]aneS$_6$)]$^{2+}$ undergoes a reversible one electron oxidation to afford [Pd([18]aneS$_6$)]$^{3+}$.[32] Hence a study of the coordination chemistry of [24]aneSe$_6$ with Pt(II) and Pd(II) was undertaken. So far, the only reported complex involving [24]aneSe$_6$ with Pd(II) has been the synthesis of the aforementioned complex [(PdCl)$_2$([24]aneSe$_6$)][BF$_4$]$_2$.[34]

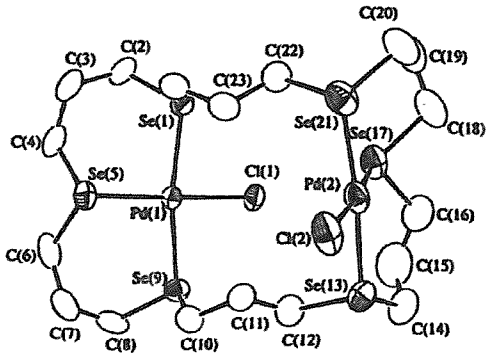

Figure 4.3 – Molecular structure of [(PdCl)$_2${[24]aneSe$_6$}]$^{2+}$

There is a paucity of Rh(III) acylic multidentate selenoether complexes reported in literarure. To date, the only fully characterised complexes have been those reported by Levason and co-workers.[35,36,41,42] These are limited in the main to the bidentate selenoether complexes [Rh{MeSe(CH$_2$)$_2$SeMe}Cl$_4$]$^-$, *cis*- and *trans*-[Rh{MeSe(CH$_2$)$_2$SeMe}$_2$Cl$_2$]$^+$ and *trans*-[Rh{PhSe(CH$_2$)$_2$SePh}$_2$Cl$_2$]$^+$; and the tridentate selenoether complexes [Rh{MeC(CH$_2$SeMe)$_3$}Cl$_3$] and [Rh{Se(CH$_2$CH$_2$CH$_2$SeMe)$_2$}Cl$_3$]. A fairly recent publication by this research

group reported the coordination chemistry of the macrocyclic selenoether complex $[Rh([16]aneSe_4)Cl_2][BF_4]$.[35,36] The coordination chemistry of Rh(III) with hexathiamacrocyclic ligands has been documented.[43] In particular, the reaction of $[RhCl(C_8H_{12})_2]_2$ with two equivalents of $[18]aneS_6$ in the presence of acid affords the $[Rh([18]aneS_6)]^{3+}$ system. A crystal structure of this cation was not reported but it was assigned the *meso* structure on the basis of $^{13}C\{^1H\}$ NMR spectroscopy. The crystal structure of the closely related thioether system $[Rh([9]aneS_3)_2]^{3+}$ shows the macrocycles bound in a facial manner to the metal.[44,45] Taking all of the above into consideration we were therefore interested in the investigation of the coordination chemistry of $[24]aneSe_6$ with Rh(III).

While several macrocyclic thioether ruthenium complexes are known, e.g. *cis*-$[RuCl_2\{[14]aneS_4\}]^{0/+}$,[46] *cis*-$[RuCl(PPh_3)\{[14]aneS_4\}]^+$,[47] $[Ru\{[9]aneS_3\}_2]^{2+}$, $[Ru\{[12]aneS_3\}_2]^{2+}$[48,49,50] and $[Ru(PPh_3)\{[15]aneS_5\}]^{2+}$,[51] there are very few examples involving macrocyclic selenoethers. Work within this group led to the formation of an array of compounds including *cis*-$[RuCl_2\{[8]aneSe_2\}_2]$, *cis*- and *trans*-$[RuX_2\{[16]aneSe_4\}]$ (X = Cl, Br or I) and *trans*-$[RuCl(PPh_3)\{[16]aneSe_4\}]PF_6$.[38]

The aim of the research into platinum group metals was to undertake studies of the metals with the ligand $[24]aneSe_6$.

4.2 RESULTS AND DISCUSSION

4.2.1 Osmium(II) Complexes of Ditelluroether Ligands

It was found that the reaction of OsO_4-conc. HCl-EtOH with each of the three ditelluroether ligands (L-L = o-$C_6H_4(TeMe)_2$, or $RTe(CH_2)_3TeR$ (R = Me or Ph)) at 0° C gave brownish-purple solids. These solids lacked the very strong $\nu(OsO_2)$ IR vibrations at *ca.* 850 cm^{-1} typical of *trans*-$[OsO_2Cl_2(L'\text{-}L')]$ (L'-L' = dithioether or diselenoether),[7,8] ruling out the formation of osmyl species. A similar result was reported with Me_2Te,[7,8] were the organo-tellurium ligand was rapidly oxidised by OsO_4-HX-EtOH. Since telluroethers are both stronger reducing agents and less able to stabilise high oxidation states then their lighter analogues,[21,22,23] their failure to stabilise Os(VI) is not unexpected, but it was hoped that reduction would lead to Os(III) or Os(IV) complexes. The brownish purple solids have UV-Vis spectra typical of Os(IV), in fact the major features are very similar to those of $[OsCl_6]^{2-}$,[52] and were weakly paramagnetic, which would suggest either Os(IV) and/or Os(III) compounds were present. However, after long accumulations each sample gave a single sharp ^{125}Te NMR resonance at very high frequencies ($\delta(^{125}Te)$ *ca.* 800-900) which would seem to indicate that at least some of the tellurium was present in a diagmagnetic material, the shifts being in the range typical of R_2TeCl_2 species.[53] A pale brown crystal was grown from MeCN solution from the $PhTe(CH_2)_3TePh$ reaction and the structure solution revealed the diamagnetic tellurium compound $PhCl_2Te(CH_2)_3TePhCl_2$.MeCN. The structure is shown in Figure 4.4 and selected bond length and angle data are in Tables 4.2 and 4.3. The structure is typical of R_2TeCl_2 type compounds, with $PhCl_2TeCH_2TePhCl_2$ the closest structurally characterised example.[54] The environment about each Te is based upon a distorted trigonal bipyramid with axial $TeCl_2$ groups and with one equatorial position vacant, presumably occupied by the lone pair. The Te-Cl bonds 2.504(2) – 2.524(1) Å lie within the usual range,[54] and the structure is

unexceptional, but serves to identify unequivocally a significant product of the aforementioned reaction.

Crystal Structure of $PhTeCl_2(CH_2)_3TePhCl_2$.MeCN

A pale brown crystal was grown from MeCN from the products of the reaction of $PhTe(CH_2)_3TePh$ with OsO_4-HCl-EtOH. Selected interatomic distances and bond angles are listed in Tables 4.2 and 4.3. The single crystal structure of $[PhTeCl_2(CH_2)_3TePhCl_2]$.MeCN reveals that the primary bonds to tellurium are arranged in the expected bipyramid with the chlorine atoms axial and the phenyl and methylene groups in equatorial positions. The primary bond lengths to tellurium fall within the range found for other R_2TeCl_2[55-61] compounds, notably $PhCl_2TeCH_2TePhCl_2$ which is the closest structually characterised example.[54] The Te-C bonds (2.168(6) and 2.150(6) Å) are at the upper end of their range. The usual distortion from ideal trigonal-bipyramidal geometry, in which the ligands are bent away from the presumed site of the nonbonding pair of electrons, is observed. The C-Te-C bond angle (94.6(2) °) falls in the range for R_2TeCl_2 structures (90.06(8) – 99.2(2) °).[55,59] Likewise, the Cl-Te-Cl angle (176.54(5) °) falls within the range of literature recorded values (169.1 - 178.8(1) °).[60,61]

Table 4.1 – Crystallographic data collection and refinement parameters for $PhTeCl_2(CH_2)_3TePhCl_2.MeCN$

Formula	$C_{17}H_{19}Cl_4NTe_2$
Formula Weight	634.37
Colour, morphology	brown, column
Crystal Dimensions/mm	0.46 x 0.17 x 0.12
Crystal System	monoclinic
Space Group	$P2_1/n$
a / Å	7.931(3)
b / Å	26.889(4)
c / Å	10.695(3)
α/ °	90
β/ °	110.20(2)
γ/ °	90
V / Å^3	2140(1)
Z	4
F(000)	1216
D_{calc}/ g cm^{-3}	1.984
μ(Mo-K_α)/ cm^{-1}	32.28
Unique observed reflections	3872
Observed reflections with [$I_o > 2\sigma(I_o)$]	2785
No. of parameters	217
Goodness of fit	1.16
R[a]	0.028
Rw[b]	0.034

a. $R = \Sigma (|F_{obs}|_i - |F_{calc}|_i)^2 / \Sigma |F_{obs}|_i$

b. $R_w = \sqrt{[\Sigma w_i(|F_{obs}|_i - |F_{calc}|_i)^2 / \Sigma w_i |F_{obs}|_i^2]}$

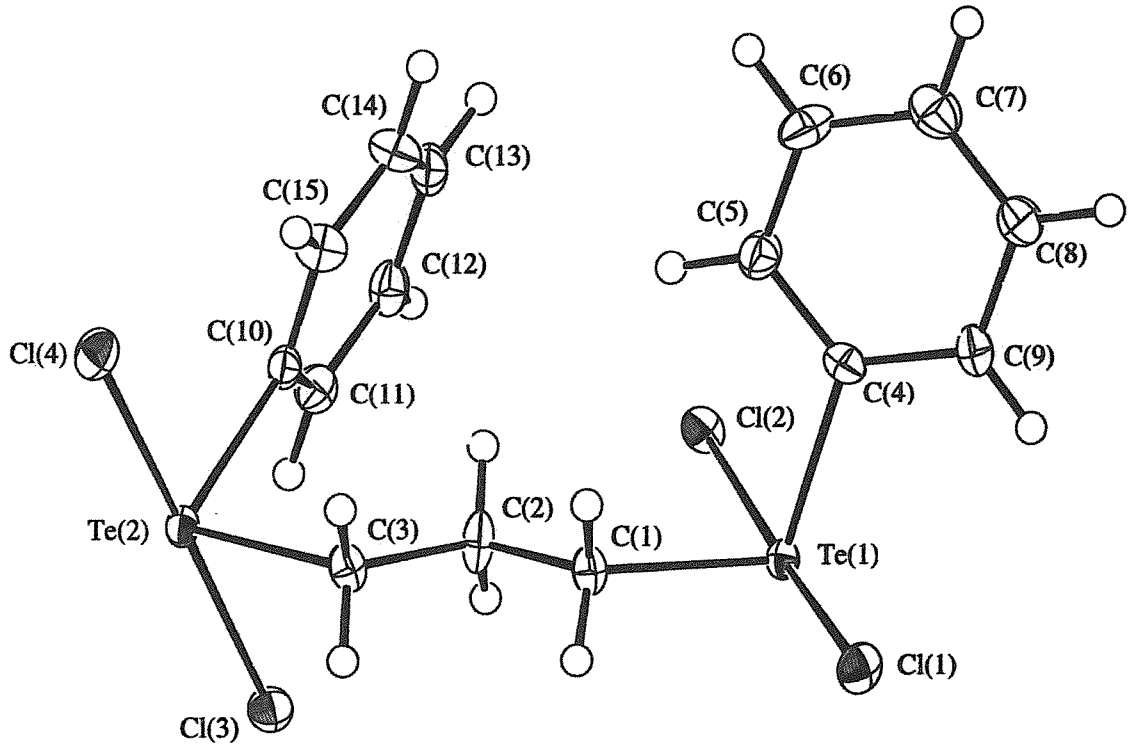

Figure 4.4 – View of the structure of $PhCl_2Te(CH_2)_3TePhCl_2$.MeCN with numbering scheme adopted. Ellipsoids are shown at 40 % probability.

Table 4.2 – Selected bond lengths (Å) for $PhCl_2Te(CH_2)_3TePhCl_2.MeCN$

Te(1)	Cl(1)	2.507(1)
Te(1)	Cl(2)	2.524(1)
Te(1)	C(1)	2.169(5)
Te(1)	C(4)	2.131(6)
Te(2)	Cl(3)	2.520(2)
Te(2)	Cl(4)	2.504(2)
Te(2)	C(3)	2.169(6)
Te(2)	C(10)	2.150(6)

Table 4.3 –

Selected bond angles (degrees) for $PhCl_2Te(CH_2)_3TePhCl_2.MeCN$

Cl(1)	Te(1)	Cl(2)	175.01(5)
Cl(1)	Te(1)	C(1)	85.3(2)
Cl(1)	Te(1)	C(4)	89.3(2)
Cl(2)	Te(1)	C(1)	93.1(2)
Cl(2)	Te(1)	C(4)	86.2(2)
C(1)	Te(1)	C(4)	99.1(2)
Cl(3)	Te(2)	Cl(4)	176.54(5)
Cl(3)	Te(2)	C(3)	88.1(2)
Cl(3)	Te(2)	C(10)	91.3(2)
Cl(4)	Te(2)	C(3)	89.7(2)
Cl(4)	Te(2)	C(10)	91.5(2)
C(3)	Te(2)	C(10)	94.6(2)
Te(1)	C(1)	C(2)	114.7(4)
C(1)	C(2)	C(3)	110.8(5)
Te(2)	C(3)	C(2)	112.3(4)

Similar brownish purple materials are formed on refluxing $[NH_4]_2[OsCl_6]$ with the ditelluroether in alcohols. Notably none of the crude materials gave ^{125}Te NMR resonances in the ranges we subsequently observed for the $[OsCl_2(L\text{-}L)_2]$ complexes, discussed below. Although attempts to separate any pure osmium species from these reactions were unsuccessful, it is clear that the target $[OsCl_2(L\text{-}L)_2]$ are not present in significant amounts.

An alternative route to *trans*-$[OsCl_2(L\text{-}L)_2]$ from Os(II) starting materials was sought, although as indicated previously in this chapter, most Os(II) materials are kinetically very inert and introducing moderate donor ligands like telluroethers, (and also dithio- and diseleno-ethers), is not easy.

The preparation of *trans*-$[OsCl_2(dmso)_4]$ was carried out in accordance with the published procedure,[18] from aqueous $[NH_4]_2[OsCl_6]$, dmso and $SnCl_2.2H_2O$. $[OsCl_2(L\text{-}L)_2]$ (L-L = o-$C_6H_4(TeMe)_2$, $RTe(CH_2)_3TeR$ (R = Ph or Me)) have been prepared by addition of L-L to trans-$[OsCl_2(dmso)_4]$ and refluxing in ethanol for 18 h. On completion, precipitation with Et_2O afforded the products in poor to moderate yields as orange or red solids. The isolated complexes are air stable and generally poorly soluble in chlorocarbons or MeCN, which to some extent limited solution spectroscopic studies.

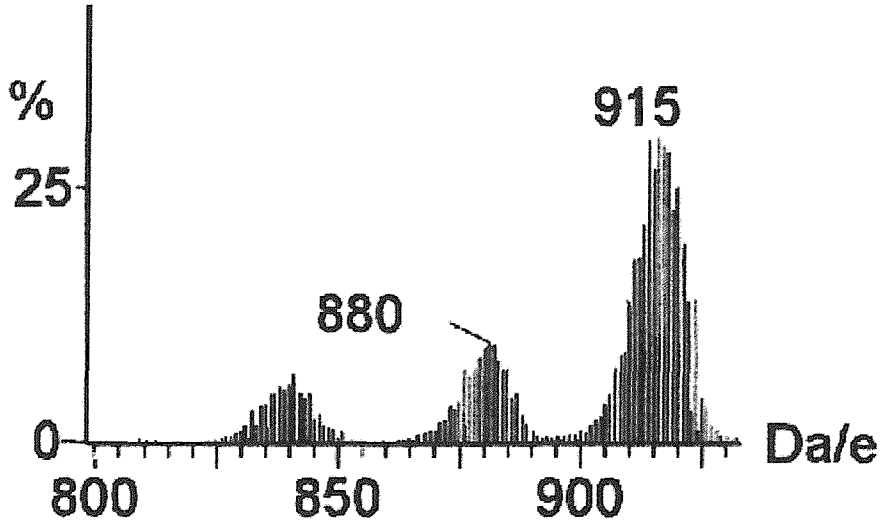

Figure 4.5 – ES^+ mass spectrum of $[OsCl_2\{MeTe(CH_2)_3TeMe\}_2]$

ES^+ mass spectrometric data for $[OsCl_2(L\text{-}L)_2]$ (L-L = o-$C_6H_4(TeMe)_2$, $MeTe(CH_2)_3TeMe$) showed peaks with the correct isotopic distributions corresponding to $[OsCl_2(L\text{-}L)_2]^+$. Additional fragments corresponding to sequential chlorine loss were observed for the complex $[OsCl_2\{MeTe(CH_2)_3TeMe\}_2]$ (Figure 4.5).

The three $[OsCl_2(L\text{-}L)_2]$ complexes have very similar spectroscopic properties including two d-d bands in the range 21000 – 26000 cm^{-1} as expected

for a low spin d^6 complex with local D_{4h} symmetry.[52] The poor solubility made it very difficult to obtain ^{125}Te NMR spectra, but after a very long accumulations several resonances were present in each complex, consistent with a mixture of invertomers, showing that pyramidal inversion is slow on the NMR time scale in these systems. However, it is not possible to assign resonances to individual isomers. The possible combinations of *meso* or *DL* ditelluroethers for *trans*-$[M(L\text{-}L)_2X_2]$ moieties result in five possible isomers (invertomers) as shown in Figure 4.6.

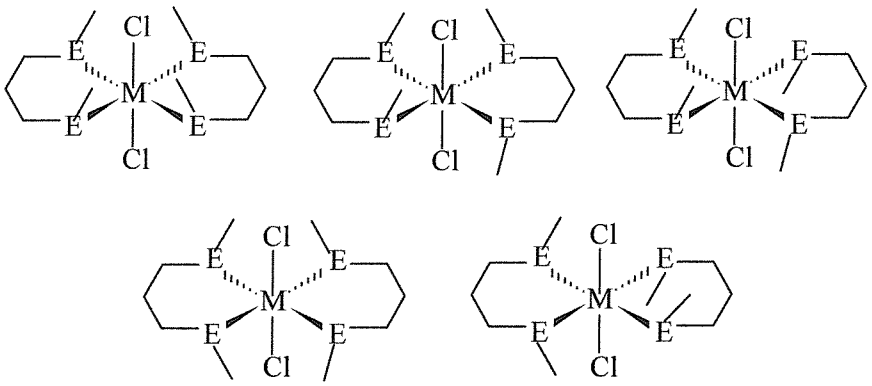

Figure 4.6 The five invertomers for *trans*-$[M(L\text{-}L)_2X_2]$

Notably, for comparable complexes, the $\delta(^{125}Te)$ are found at considerably higher frequency in the ruthenium complexes[23] compared with the present osmium complexes. An example of this can be seen by considering the $\delta(^{125}Te)$ for $[MCl_2\{PhTe(CH_2)_3TePh\}_2]$ (M = Os or Ru). The osmium complex covers the range: 478 – 548 (δ), whereas for the ruthenium analogue the peaks are found within the region: 545.6 – 653.4 (δ). This affect is also found for corresponding ruthenium and osmium phosphines.[62]

Crystal Structure of $[OsCl_2\{PhTe(CH_2)_3TePh\}_2]$

Red crystals were obtained by the slow evaporation of a $CHCl_3$ solution of the complex. The single crystal structure of $[OsCl_2\{PhTe(CH_2)_3TePh\}_2]$ (Figure 4.7, Table 4.4) shows a *trans* pseudo-octahedral molecule with the osmium on the inversion centre and with both ditelluroethers in the *meso* form.

Although the crystals are not isomorphous, the structure is very similar to that previously found in trans-[$RuCl_2\{PhTe(CH_2)_3TePh\}_2$].[23] The Os-Cl bond length, 2.450(4) Å, is comparable with those found in [$OsCl_2\{Ph_2P(CH2)_2PPh_2\}_2$][63] (2.434(1) Å) and *trans*-[$OsCl_2\{H_2C{=}C(PPh_2)_2\}_2$] (2.431(1) Å).[64] There are no literature data on Os(II)-TeR_2 bonds, but those in the present complex (2.616(1), 2.6135(9) Å) are, as might be expected, similar to the Ru-Te bonds in the Ru(II) analogue (2.6247(3), 2.6194(3) Å).[23]

Table 4.4 – Crystallographic data collection and refinement parameters for $[OsCl_2\{PhTe(CH_2)_3TePh\}_2]$

Formula	$C_{30}H_{32}Cl_2OsTe_4$
Formula Weight	1164.09
Colour, morphology	red, block
Crystal Dimensions/mm	0.26, 0.16, 0.12
Crystal System	monclinic
Space Group	$P2_1/n$
a / Å	8.684(5)
b / Å	7.225(6)
c / Å	25.205(2)
α/ °	90
β/ °	94.00(2)
γ/ °	90
V / Å^3	1577
Z	2
$F(000)$	1060
D_{calc}/ g cm^{-3}	2.451
μ(Mo-K_α)/ cm^{-1}	78.54
Unique observed reflections	3040
Observed reflections with $[I_o > 2\sigma(I_o)]$	2254
No. of parameters	169
Goodness of fit	2.7
R[a]	0.052
Rw[b]	0.058

a. $R = \Sigma (|F_{obs}|_i - |F_{calc}|_i)^2 / \Sigma |F_{obs}|_i$

b. $R_w = \sqrt{[\Sigma w_i(|F_{obs}|_i - |F_{calc}|_i)^2 / \Sigma w_i |F_{obs}|_i^2]}$

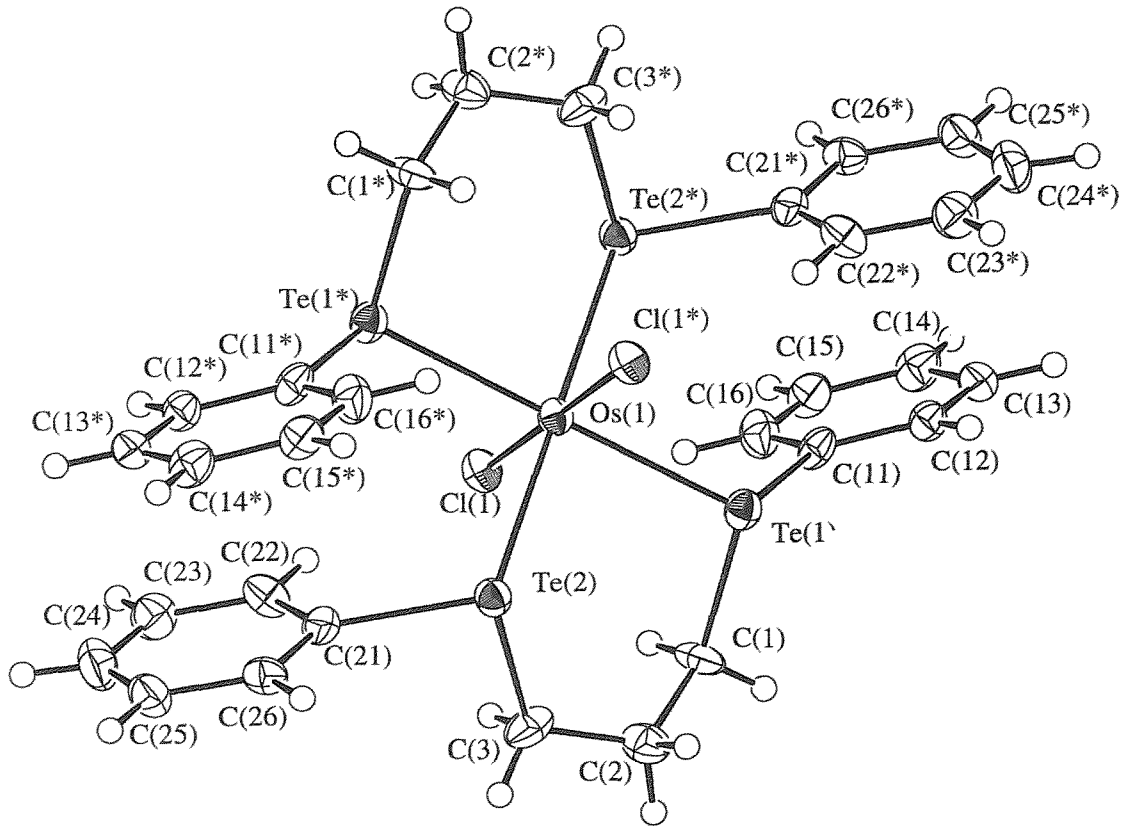

Figure 4.7 – View of the structure of $[OsCl_2\{PhTe(CH_2)_3TePh\}_2]$ with numbering scheme adopted. Ellipsoids are shown at 40 % probability. Atoms marked are related by a crystallographic inversion centre. H-atoms are omitted for clarity.

Table 4.5 – Selected bond lengths (Å) and angles (degrees) for $[OsCl_2\{PhTe(CH_2)_3TePh\}_2]$

Os(1)	Te(1)	2.6135(9)
Os(1)	Te(2)	2.616(1)
Os(1)	Cl(1)	2.450(4)
Te(1)	C(1)	2.18(1)
Te(1)	C(11)	2.13(1)
Te(2)	C(3)	2.18(1)
Te(2)	C(21)	2.14(1)

Te(1)	Os(1)	Cl(1)	86,85(8)
Te(1)	Os(1)	Te(2)	86.65(3)
Te(1)	Os(1)	Cl(1)	93.15(8)
Te(2)	Os(1)	Cl(1)	93.12(9)

4.2.2 Electrochemical Studies

The electrochemistry of the ditelluroether complexes was studied in order to determine whether the telluroether ligands would stabilise Os(III). Cyclic voltammetry was conducted on a series of the Os(II) ditelluroether complexes in CH_2Cl_2 (0.1 mol.dm^{-3} $^nBu_4NBF_4$ supporting electrolyte) at a double platinum electrode and was used to study the oxidation of these complexes. The cyclic voltammograms of each complex were recorded at room temperature and were performed at the scan rates of 0.2, 0.1 and 0.05 V s^{-1}. Each revealed a single reversible oxidation for each. The values are given in Table 4.6.

Table 4.6 – Reversible oxidation potentials for the Os(II) ditelluroether complexes

Complex	Oxidation Potential / V[a]
$[OsCl_2\{MeTe(CH_2)_3TeMe\}_2]$	+0.35
$[OsCl_2\{PhTe(CH_2)_3TePh\}_2]$	+0.18
$[OsCl_2\{o\text{-}C_6H_4(TeMe)_2\}_2]$	+0.43

a. Measured versus SCE.

These results contrast with the quasi-reversible or irreversible oxidations observed in the ruthenium analogues,[23] reflecting the expected greater stability of the M(III) state for osmium.

4.2.3 Osmium(II) Complexes of Dithio- and Diseleno-ether Ligands

Although $[OsCl_2(dmso)_4]$ provided a satisfactory starting material for the synthesis of the ditelluroether complexes it is still not ideal, and attempts to prepare $[OsCl_2(L'\text{-}L')_2]$ (L'-L' = dithioether or diselenoether) proved to be less than straightforward.

An immense amount of effort was committed to this area of research within the laboratory. The success of the ditelluroether reactions led to extension of the field of interest to encompass similar dithio- and diseleno-ether ligands. Preliminary reactions involving $MeE(CH_2)_3EMe$ (E = S or Se) with $[OsCl_2(dmso)_4]$ in refluxing MeOH, i.e. following the procedure adopted for the ditelluroether ligands, failed to yield any of the desired products. Instead, evidence from ES^+ mass spectrometry indicated the formation of one species, namely $[OsCl(dmso)\{MeE(CH_2)_3EMe\}_2]^+$. Similarly, the IR spectrum clearly showed the presence of S=O stretches. Much manipulation of the reaction parameters followed. The temperature, time-scale, ligand type were all altered during a very frustrating and unrewarding period of laboratory work. The changes in procedure were being made to shift the balance of product ratio away from the compound containing a dmso ligand to the desired compound *trans*-$[OsCl_2(L\text{-}L)_2]$. The following paragraphs essentially describes the procedure

which satisfied the criteria of producing the desired complex, although by no means cleanly. The reaction of $[OsCl_2(dmso)_4]$ with L'-L' (L'-L' = $MeE(CH_2)_3EMe$ (E = S or Se), $MeS(CH_2)_2SMe$, $PhSe(CH_2)_3SePh$ or o-$C_6H_4(SMe)_2$) in dmf at 120° C generated grey-to-brown product mixtures containing $[OsCl(dmso)(L'\text{-}L')_2]^+$, $[OsCl_2(dmso)_2(L'\text{-}L')]$ and the target compound $[OsCl_2(L'\text{-}L')_2]$ as explained below. Futile attempts were made to separate the products and it was not possible to obtain useful amounts of the last complexes. Similar disappointing results were discovered for the reactions incorporating the selenoether macrocylclic ligands [8]aneSe_2 and [16]aneSe_4. IR spectroscopy and mass spectrometry proved to be very useful tools during this investigation. $[OsCl_2(dmso)_4]$ shows very distinctive S=O stretches at 1083 and 1028 cm^{-1}. IR spectra of the product mixtures show the presence of prominent stretches in the region where S=O are expected to be found. Supporting evidence for the failure to cleanly synthesise the desired $[OsCl_2(L'\text{-}L')_2]$ is given by the ES^+ mass spectra of the product mixtures. For the reactions with L'-L' = $MeS(CH_2)_2SMe$, $MeE(CH_2)_3EMe$ (E = S or Se), o-$C_6H_4(SMe)_2$, [8]aneSe_2 and [16]aneSe_4 the recorded spectra show a mixture of $[OsCl_2(L'\text{-}L')_2]$ and $[OsCl(dmso)\{L'\text{-}L'\})]^+$ in fairly high abundance. The ES^+ mass spectrum data (Figure 4.8) is shown for the reaction involving the diselenoether $MeSe(CH_2)_3SeMe$, in which $[OsCl(dmso)\{MeSe(CH_2)_3SeMe\}_2]^+$, $[OsCl_2\{MeSe(CH_2)_3SeMe\}_2]$ and the loss of Cl from $[MCl_2(L\text{-}L)]^+$ were observed. The data show good agreement with the calculated isotope distributions. The ES^+ mass spectra are chosen to illustrate the general spectrum obtained for a compound in this area of research after many changes in reaction parameters had been implemented. It is interesting to note that from successful attempts to grow single crystals from solutions of this mixture the structure revealed *trans*-$[OsCl_2(dmso)_2\{MeSe(CH_2)_3SeMe\}]$ (Figure 4.9) despite the peak pattern corresponding to this species (646 amu) is of low abundance. This again highlights the sensitive nature of these compounds and the frustrating aspects of the chemistry of Os(II) and organosulfur and organoselenium ligands.

Crystal Structure of $[OsCl_2(dmso)_2\{MeSe(CH_2)_3SeMe\}]$

Yellow crystals were obtained from CH_2Cl_2 solution of the product mixture after the reaction of $[OsCl_2(dmso)_4]$ with $MeSe(CH_2)_3SeMe$. The single crystal structure showed them to be of $[OsCl_2(dmso)_2\{MeSe(CH_2)_3SeMe\}]$ (Figure 4.8, Tables 4.7 – 4.9) and reveals a octahedron about the central osmium atom. The chlorine atoms adopt axial positions with the chelate ligand adopting the *meso* conformation. The Os-Cl bond distances of 2.49(1) and 2.34(1) Å are similar to those previously reported *trans*-disposed chlorines in osmium complexes (2.431(1) – 2.477(2) Å).[18,24,63,64,69] The Os-S bond lengths (2.293(9) and 2.317(9) Å) differ very slightly from the Os-S bond length of the precursor compound $[OsCl_2(dmso)_4]$ which has average Os-S bond length of 2.343(2) Å.

Table 4.7 – Crystallographic data collection and refinement parameters for $[OsCl_2(dmso)_2\{MeSe(CH_2)_3SeMe\}]$

Formula	$C_9H_{24}Cl_2Se_2OsS_2O_2$
Formula Weight	647.43
Colour, morphology	yellow, plate
Crystal Dimensions/mm	0.28, 0.16, 0.13
Crystal System	orthorhombic
Space Group	$Pna2_1$
a / Å	24.003(3)
b / Å	8.918(3)
c / Å	8.380(3)
α/ °	90
β/ °	90
γ/ °	90
V / Å^3	1793(1)
Z	4
F(000)	1216
D_{calc}/ g cm^{-3}	2.398
μ(Mo-K_α)/ cm^{-1}	116.88
Unique observed reflections	1860
Observed reflections with [$I_o > 2\sigma(I_o)$]	1243
No. of parameters	117
Goodness of fit	2.29
R[a]	0.061
Rw[b]	0.072

a. $R = \Sigma (| F_{obs} |_i - | F_{calc} |_i)^2 / \Sigma | F_{obs} |_i$

b. $R_w = \sqrt{[\Sigma w_i(| F_{obs} |_i - | F_{calc} |_i)^2 / \Sigma w_i | F_{obs} |_i^2]}$

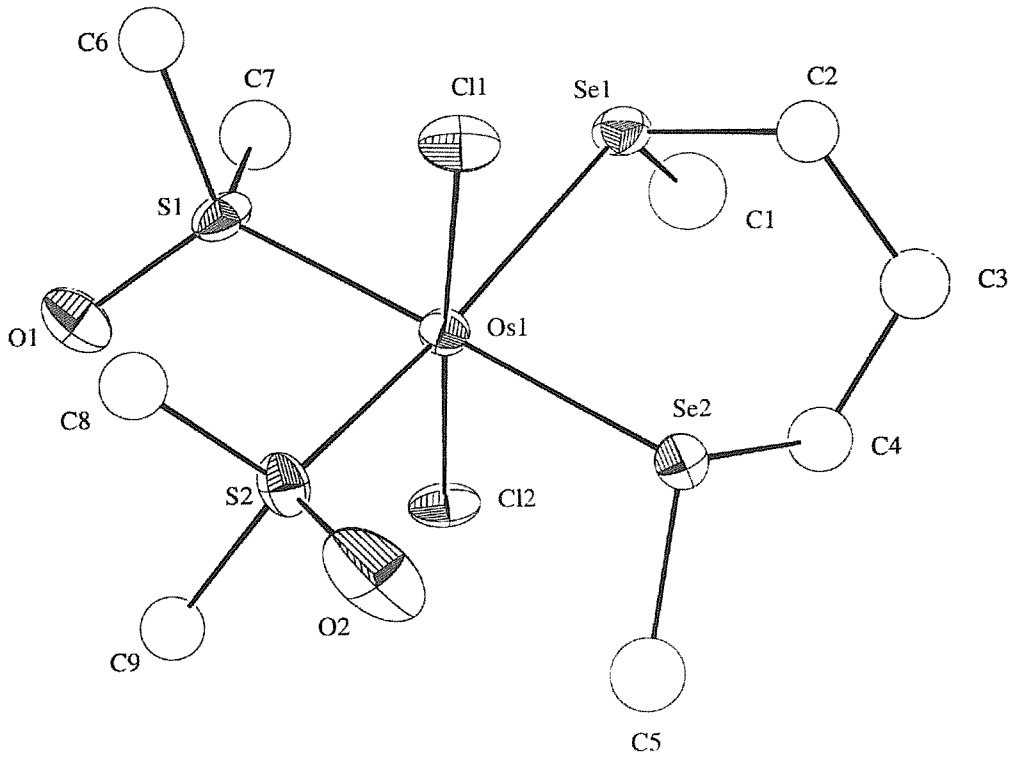

Figure 4.8 – View of $[OsCl_2(dmso)_2\{MeSe(CH_2)_3SeMe\}]$ with numbering scheme adopted. Ellipsoids are shown at 40 % probability.

Table 4.8 –

Selected bond lengths (Å) for $[OsCl_2(dmso)_2\{MeSe(CH_2)_3SeMe\}]$

Os(1)	Se(1)	2.522(4)	Os(1)	Se(2)	2.513(4)
Os(1)	Cl(1)	2.49(1)	Os(1)	Cl(2)	2.34(1)
Os(1)	S(1)	2.293(9)	Os(1)	S(2)	2.317(9)
Se(1)	C(1)	1.81(5)	Se(1)	C(2)	1.89(4)
Se(2)	C(4)	1.82(5)	Se(2)	C(5)	1.84(4)
S(1)	O(1)	1.51(2)	S(1)	C(6)	1.81(5)
S(1)	C(7)	1.79(4)	S(2)	O(2)	1.52(3)
S(2)	C(8)	1.76(4)	S(2)	C(9)	1.77(4)
C(2)	C(3)	1.63(6)	C(3)	C(4)	1.54(5)

Table 4.9 –

Selected bond angles (degrees) for $[OsCl_2(dmso)_2\{MeSe(CH_2)_3SeMe\}]$

Se(1)	Os(1)	Se(2)	90.4(1)	Se(1)	Os(1)	Cl(1)	83.0(3)
Se(1)	Os(1)	Cl(2)	94.6(3)	Se(1)	Os(1)	S(1)	91.5(3)
Se(1)	Os(1)	S(2)	169.5(3)	Se(2)	Os(1)	Cl(1)	86.7(3)
Se(2)	Os(1)	Cl(2)	91.4(3)	Se(2)	Os(1)	S(1)	178.0(3)
Se(2)	Os(1)	S(2)	88.8(2)	Cl(1)	Os(1)	Cl(2)	176.9(4)
Cl(1)	Os(1)	S(1)	92.8(3)	Cl(1)	Os(1)	S(2)	86.5(4)
Cl(2)	Os(1)	S(1)	89.2(3)	Cl(2)	Os(1)	S(2)	95.9(4)
S(1)	Os(1)	S(2)	89.2(4)	Os(1)	Se(1)	C(1)	113(1)
Os(1)	Se(1)	C(2)	104(1)	C(1)	Se(1)	C(2)	104(2)
Os(1)	Se(2)	C(4)	100(1)				

The ES^+ mass spectrum of the reaction involving $PhSe(CH_2)_3SePh$, however, reveals the parent molecule minus a phenyl group (C_6H_5), (Figure 4.9). However, evidence points to it not being a clean sample with peaks attributable to the loss of a phenyl group from $[OsCl(dmso)\{PhSe(CH_2)_3SePh\}_2]^+$ present. Once again, the data show good agreement with the calculated isotope distribution.

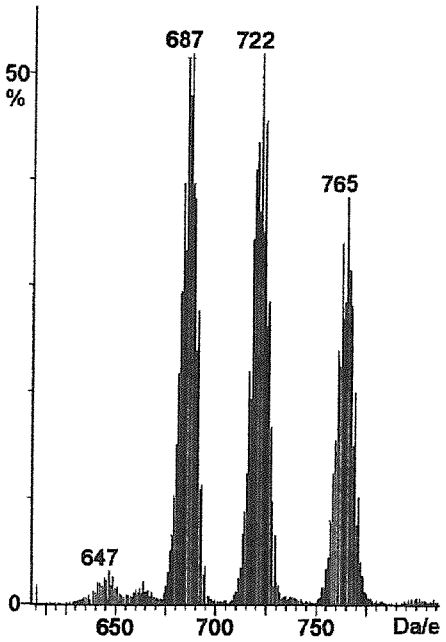

Figure 4.9 – ES^+ mass spectrum of the product of attempt to make $[OsCl_2\{MeSe(CH_2)_2SeMe\}_2]$

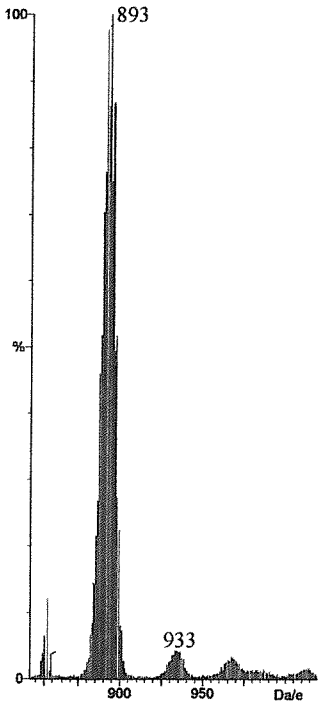

Figure 4.10 – ES^+ mass spectrum of crude $[OsCl_2\{PhSe(CH_2)_3SePh\}_2]$

The reaction of $[OsCl_2(PPh_3)_3]$ with 2 equivalents of the Group 16 ligands in gently refluxing EtOH in the presence of $[PF_6]^-$ generated moderate yields of $[OsCl(PPh_3)(L\text{-}L)_2]PF_6$ (L-L = $RTe(CH_2)_3TeR$, R = Me or Ph), $[OsCl(PPh_3)\{MeS(CH_2)_2SMe\}_2]PF_6$ and $[OsCl(PPh_3)\{MeSe(CH_2)_3SeMe\}_2]PF_6$ as yellow or brown solids.

The isolated solids were relatively air stable which show $[OsCl(PPh_3)(L\text{-}L)_2]^+$ as the highest mass ions in their ES^+ mass spectra.

The UV-Vis spectra are uninformative, showing only the $\pi \rightarrow \pi^*$ transitions of the Ph-groups and charge transfer transitions in the near-UV which tail into the visible obscuring the d-d bands, although the absence of significant features below 20,000 cm^{-1} confirms the oxidation state as Os(II).

The ^1H NMR spectra of the ditelluroether compounds are complex and not very helpful, but the $^{31}P\{^1H\}$ NMR spectra are more useful. For $[OsCl(PPh_3)\{PhTe(CH_2)_3TePh\}_2]PF_6$, in addition to the septet at δ -145 due to $[PF_6]^-$ there are two singlets at –10.5 and –11.8 with approximate intensities 2:1 showing the presence of two major invertomers. The corresponding $^{125}Te\{^1H\}$ NMR spectrum showed five doublets in the range δ 450-565 with $^2J(^{125}Te\text{-}^{31}P)$ of *ca.* 60-90 Hz. In the case of $[OsCl(PPh_3)\{MeTe(CH_2)_3TeMe\}_2]PF_6$ the $^{31}P\{^1H\}$ NMR spectrum reveals one major invertomer δ -14.5 and there are four doublets in the $^{125}Te\{^1H\}$ NMR spectrum and four δ(Me) resonances in the ^1H NMR spectrum. This is consistent with one invertomer as the major solution form with one *meso* and one *DL* ditelluroether.

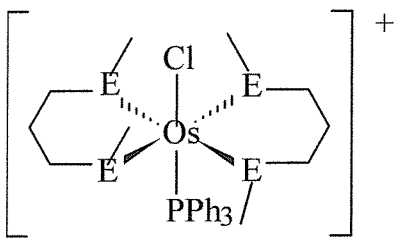

Figure 4.11 –

The major solution invertomer of $[OsCl(PPh_3)\{MeTe(CH_2)_3TeMe\}_2]PF_6$

The pattern of invertomers in these two cases is very similar to that observed in the ruthenium analogues.[23] For the $[OsCl(PPh_3)\{MeSe(CH_2)_3SeMe\}_2]PF_6$ the $^{31}P\{^1H\}$ NMR spectrum shows a singlet at –14.0 and the septet at –145. There are singlets for the Me and CH_2 groups of the diselenoether in the ^1H NMR. Whilst at first sight this might be taken to indicate one isomer with high symmetry, it was not possible to observe a ^{77}Se NMR spectrum from this complex, which suggests that pyramidal inversion is occuring. Finally, for $[OsCl(PPh_3)\{MeS(CH_2)_2SMe\}_2]PF_6$ there is a singlet in the $^{31}P\{^1H\}$ NMR spectrum at δ -15.1, and broad singlets at δ 2.44 and 2.7 (in addition to the Ph mulitplet) in the ^1H NMR spectrum, consistent with fast inversion in the dithioether complex. The poor solubility and the number of possible invertomers make these systems poorly suited to VT NMR studies, but comparison of the room temperature spectra shows the usual trends in pyramidal inversion barriers Te > Se > S are present.[65,66]

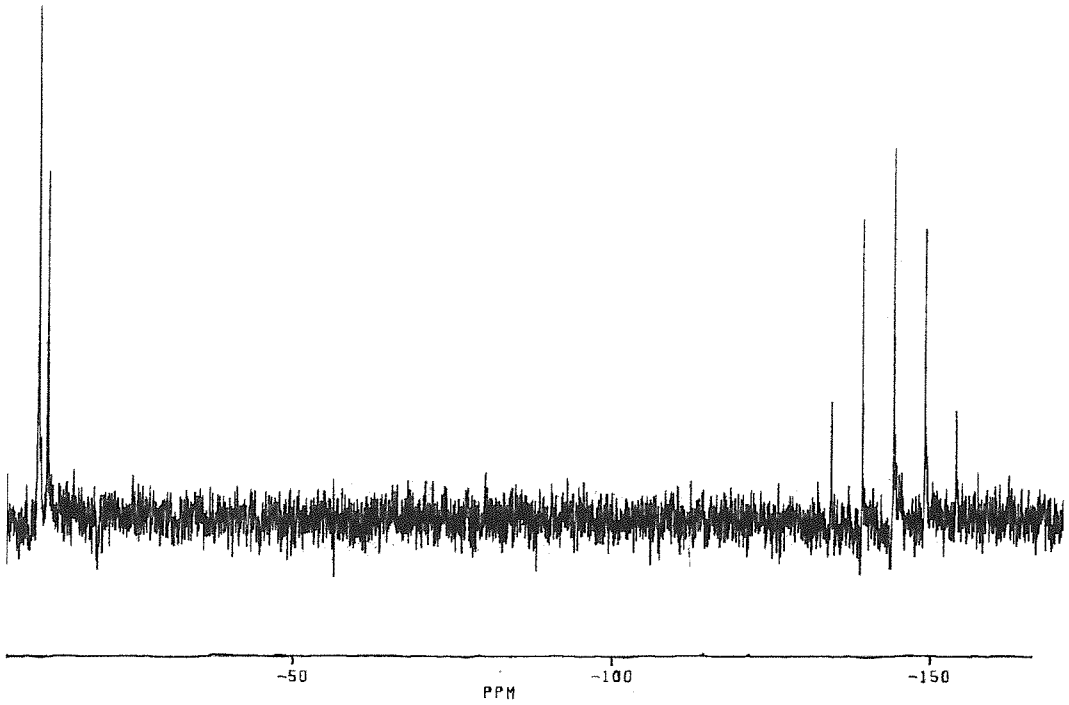

Figure 4.12 –

$^{31}P\{^1H\}$ NMR Spectrum of $[OsCl(PPh_3)\{PhTe(CH_2)_3TePh\}_2]PF_6$

Taking a look at the general product from the analogous Ru(II) work it should be highlighted that the results obtained there and the Os(II) results mentioned within this chapter share many close similarities. The reaction of with $[RuCl_2(PPh_3)_3]$ with L-L (L-L = $RTe(CH_2)_3TeR$ (R = Te or Ph) or o-$C_6H_4(MeTe)_2$) affords *trans*-$[RuCl(PPh_3)(L\text{-}L)_2]PF_6$. The structure of *trans*-$[RuCl(PPh_3)\{MeTe(CH_2)_3TeMe\}_2]^+$ was used as supporting evidence which shows the ligands adopting one *meso* and one *DL* form (Figure 4.13). Furthermore, in the case of $^{31}P\{^1H\}$ and $^{125}Te\{^1H\}$ NMR spectroscopy for the ruthenium complexes with the ligands $PhTe(CH_2)_3TePh$ and $MeTe(CH_2)_3TeMe$ show the same number of resonances as the osmium examples discussed previously. All in all there is substantial evidence to support the proposal of the Os(II) systems being similar to the published Ru(II) data.[23]

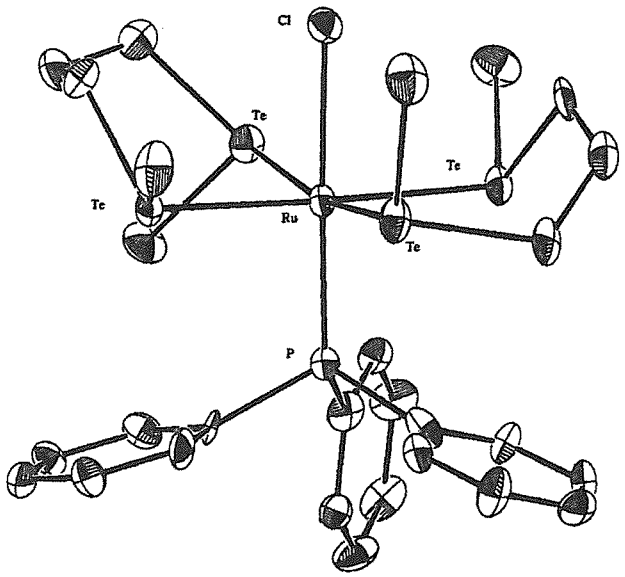

Figure 4.13 – View of the structure of $[RuCl(PPh_3)\{MeTe(CH_2)_3TeMe\}_2]^+$ from ref 23.

4.2.4 Osmium(II) Complexes of Distibine Ligands

As a further test of the usefulness of $[OsCl_2(dmso)_4]$ it was reacted with $Ph_2Sb(CH_2)_3SbPh_2$ in ethanol, and readily yielded good amounts of yellow *trans*-

$[OsCl_2\{Ph_2Sb(CH_2)_3SbPh_2\}_2]$. The spectroscopic data are unexceptional and compare well with the corresponding data on *trans*-$[OsCl_2(Ph_3Sb)_4]$[67] and *trans*-$[OsCl_2(diphosphine)_2]$.[68] The ES^+ mass spectrum reveals peaks with the correct isotopic distribution corresponding to $[OsCl_2(L\text{-}L)_2]^+$. The UV-Vis spectrum revealed an intense CT absorption at 30,860 and a less intense absorption at 22,230 cm^{-1} corresponding to a d-d transition. In reference to $[RuBr_2\{Ph_2Sb(CH_2)_3SbPh_2\}_2]$ the identification of this species as the *trans* isomer followed from the diffuse reflectance UV/Vis spectra which shows two weak d-d bands at 22,500 and 18,900 cm^{-1}.

Crystal Structure of $[OsCl_2\{Ph_2Sb(CH_2)_2SbPh_2\}_2]$

Yellow crystals were obtained from CH_2Cl_2 solution of the complex. The structure solution of $[OsCl_2\{Ph_2Sb(CH_2)_2SbPh_2\}_2]$ (Figure 4.14 and Tables 4.11 – 4.12) revealed a *trans* pseudo-octahedral molecule with the osmium on the inversion centre. The Os-Cl distance of 2.477(2) Å slightly shorter than to those previously reported *trans*-disposed chlorines in osmium complexes (2.431(1) – 2.448(2) Å),[18,63,64,69] including the precursor $[OsCl_2(dmso)_4]$ which has Os-Cl distance of 2.414(2) Å. The Os-Sb distances, 2.5933(8) and 2.6030(4) Å are very similar to those in *trans*-$[OsCl_2(Ph_3Sb)_4]$ (2.611(2) – 2.630(2) Å).[70] The X-ray structural determination confirms that the distibine ligands lie in the equatorial plane of the molecule. Another example of a single crystal X-ray structure of a Group 8 metal coordinated to four Sb atoms in a similar way to the Os(II) structure discussed above is the Ru(II) structure $[RuBr_2\{SbMe_2Ph\}_4]$ which has two axial halides and all four stibines in the equatorial plane.[62] The employment of the ditertiary stibine ligand with Ru(II) has been reported and structural analysis recorded. Similarities between this structure and the one deduced for the osmium species begin with the metal (Ru/Os) positioned on a centre of symmetry. Furthermore, the isomer present for the ruthenium analogue is the *trans* form.

Table 4.10 – Crystallographic data collection and refinement parameters for $[OsCl_2\{Ph_2Sb(CH_2)_3SbPh_2\}_2]$

Formula	$C_{56}H_{56}Cl_6OsSb_4$
Formula Weight	1618.98
Colour, morphology	yellow, rhomb.
Crystal Dimensions/mm	0.28, 0.16, 0.13
Crystal System	triclinic
Space Group	P-1
a / Å	12.096(3)
b / Å	12.226(3)
c / Å	11.510(4)
α/ °	107.43(2)
β/ °	114.96(3)
γ/ °	96.17(2)
V / Å^3	1417.4(9)
Z	1
F(000)	774
D_{calc}/ g cm^{-3}	1.897
μ(Mo-K$_\alpha$)/ cm^{-1}	44.28
Unique observed reflections	4983
Observed reflections with [$I_o > 2\sigma(I_o)$]	4308
No. of parameters	297
Goodness of fit	2.01
R[a]	0.036
Rw[b]	0.052

a. $R = \Sigma (| F_{obs} |_i - | F_{calc} |_i)^2 / \Sigma | F_{obs} |_i$

b. $R_w = \sqrt{[\Sigma w_i(| F_{obs} |_i - | F_{calc} |_i)^2 / \Sigma w_i | F_{obs} |_i^2]}$

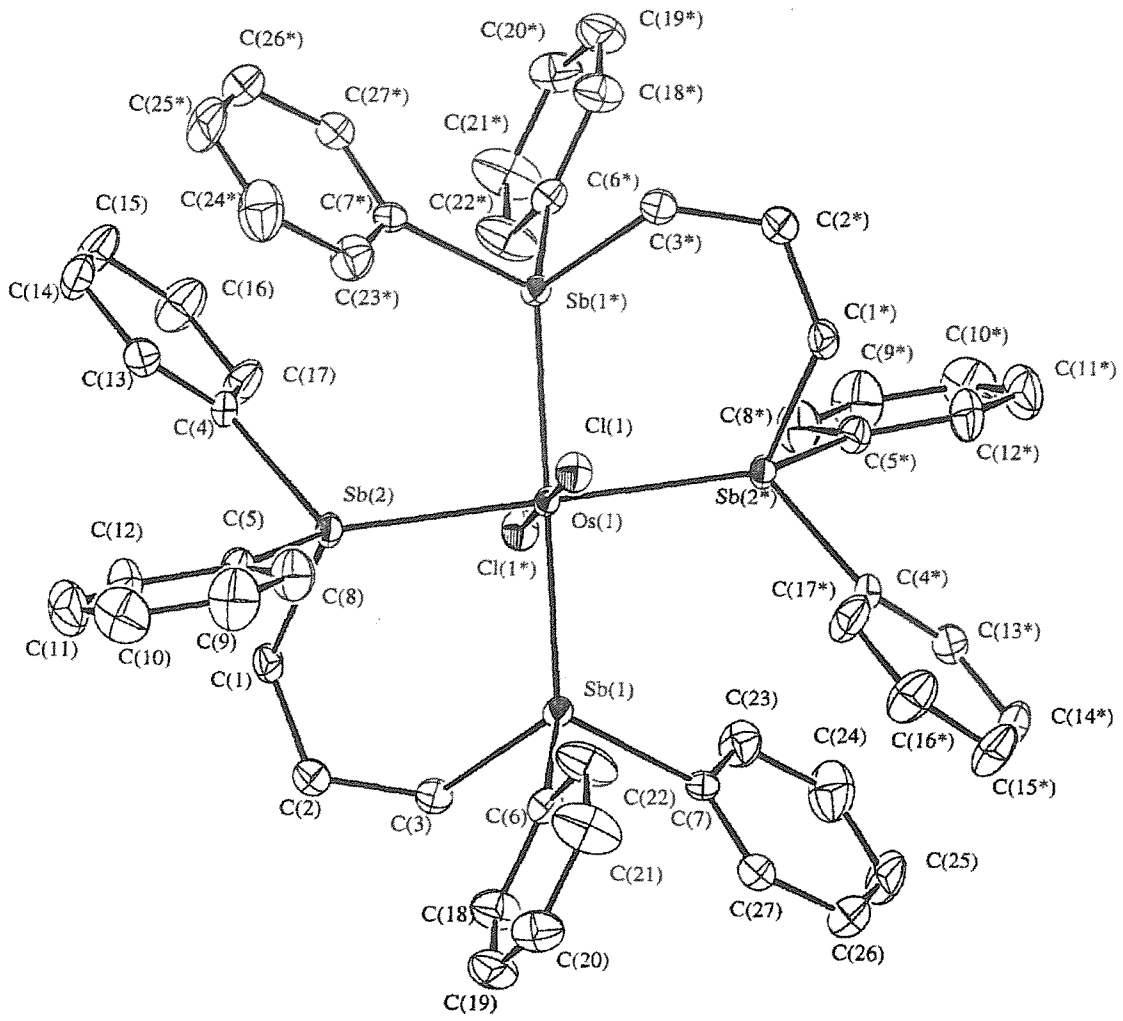

Figure 4.14 – View of $[OsCl_2\{Ph_2Sb(CH_2)_3SbPh_2\}_2]$ with numbering scheme adopted. Ellipsoids are shown at 40 % probability. Atoms marked * are related by a crystallographic inversion centre. H-atoms are omitted for clarity.

Table 4.11 – Selected bond lengths (Å) for $[OsCl_2\{Ph_2Sb(CH_2)_3SbPh_2\}_2]$

Os(1)	Sb(1)	2.5933(8)
Os(1)	Sb(2)	2.6030(4)
Os(1)	Cl(1)	2.477(2)
Sb(1)	C(3)	2.154(7)
Sb(1)	C(6)	2.137(7)
Sb(1)	C(7)	2.149(7)
Sb(2)	C(1)	2.143(7)
Sb(2)	C(4)	2.137(7)
Sb(2)	C(5)	2.144(7)

Table 4.12 – Selected bond angles (degrees) for $[OsCl_2\{Ph_2Sb(CH_2)_3SbPh_2\}_2]$

Sb(1)	Os(1)	Sb(2)	85.73(1)
Sb(1)	Os(1)	Cl(1)	95.53(4)
Sb(2)	Os(1)	Cl(1)	96.76(4)
Os(1)	Sb(1)	C(3)	114.2(2)
Os(1)	Sb(1)	C(6)	124.2(2)
Os(1)	Sb(1)	C(7)	117.1(2)
C(3)	Sb(1)	C(6)	100.1(3)
C(3)	Sb(1)	C(7)	96.9(3)
C(6)	Sb(1)	C(7)	99.7(3)
Os(1)	Sb(2)	C(1)	114.3(2)
Os(1)	Sb(2)	C(4)	118.9(2)
Os(1)	Sb(2)	C(5)	123.6(2)
C(1)	Sb(2)	C(4)	95.7(3)
C(1)	Sb(2)	C(5)	98.5(3)
C(4)	Sb(2)	C(5)	100.8(3)

4.2.5 Pt(II) and Pd(II) complexes of [24]aneSe$_6$

The first reaction carried out followed the procedure by Pinto in the creation of [(PdCl)$_2${[24]aneSe$_6$}][BF$_4$]$_2$.[34] This was then extended to cover the analogous reaction with Pt(II). The reaction of two equivalents of MCl$_2$ (M = Pt or Pd) with one equivalent of [24]aneSe$_6$ and two equivalents of NaBF$_4$ in refluxing MeCN afford the complexes of stoichiometry [(MCl)$_2${[24]aneSe$_6$}][BF$_4$]$_2$. These have been characterised by a combination of elemental analysis, IR spectroscopy, mass spectrometry and multinuclear NMR studies. The data observed for the 2:1 compound of PdCl$_2$:[24]aneSe$_6$ in MeCN was consistent with that found by Pinto.[34] The analyses of the reaction of PtCl$_2$ with the selenoether macrocycle was consistent with the formula [(PtCl)$_2${[24]aneSe$_6$}][BF$_4$]$_2$. The ^{195}Pt NMR spectrum at 200 K clearly shows a peak at δ -4261 and a less significant peak at δ -4236 (Figure 4.15).

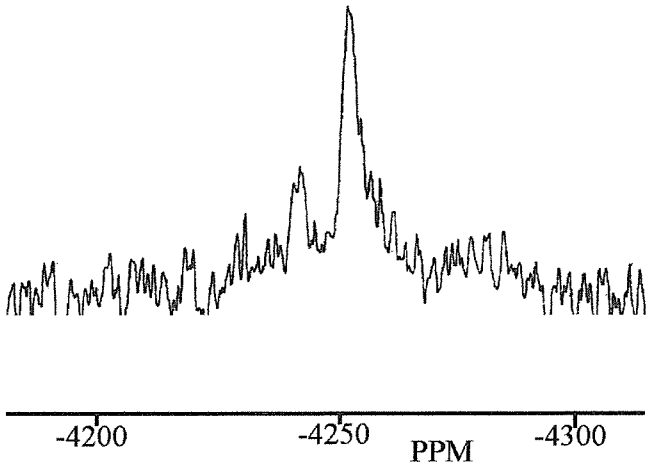

Figure 4.15 – ^{195}Pt NMR spectrum of [(PtCl)$_2${[24]aneSe$_6$}][BF$_4$]$_2$

When examining the ^{77}Se{^{1}H} NMR spectrum for this complex no signal is observed at room temperature and only a very broad signal at δ 337 is noticed when the experiment is run at 240 K. Another broad signal is observed, this time in the ^{1}H NMR spectrum recorded at room temperature. Resonances are found at

$\delta(\alpha\text{-}CH_2)$ 3.1 and $\delta(\beta\text{-}CH_2)$ 2.46. Attempts to grow single crystals of this complex were unsuccessful.

The reaction of [24]aneSe_6 with one equivalent of $PtCl_2$ and two equivalents of $TlPF_6$ in refluxing $MeNO_2$ affords the complex of the stoichiometry $[Pt\{[24]aneSe_6\}][PF_6]_2$. This complex has been characterised by a combination of elemental analysis, IR spectroscopy, mass spectrometry and multinuclear NMR studies.

The analyses are consistent with 1 : 1 : 2 ratio of ligand : metal : PF_6^-. The IR spectra shows the presence of [24]aneSe_6, with bands between 1000 and 1400 cm^{-1}, as well as the expected stretching and bending vibrations of the PF_6^- counter ion. The ES^+ mass spectra in MeCN shows peaks at m/z = 1066 with the correct isotopic distribution pattern which can be attributed to $[Pt\{[24]aneSe_6\}PF_6]^+$. Once more crystal growing attempts proved to be futile.

The rhodium(III) complex $[RhCl_2\{[24]aneSe_6\}]BF_4$ was prepared from $RhCl_3.3H_2O$ and [24]aneSe_6 in refluxing aqueous ethanol. The product was isolated, in good yield, as an orange microcrystalline solid upon addition of the non-coordinating counter ion BF_4^-. The IR spectrum of $[RhCl_2\{[24]aneSe_6\}]BF_4$ shows a metal halide stretch at 350 cm^{-1} and the distinctive peaks corresponding to the stretches of BF_4^- at 1062 and 521 cm^{-1}. The presence of the ligand is also shown by the IR spectrum with bands at 1293, 1359 and 1409 cm^{-1}. The ES^+ mass spectrum shows an isotope pattern consistent with $[RhCl_2\{[24]aneSe_6\}]^{2+}$.

The reaction of $[RuCl_2(PPh_3)_2]$, [24]aneSe_6 and NH_4PF_6 in refluxing EtOH resulted in the formation of the yellow compound $[RuCl(PPh_3)\{[24]aneSe_6\}]PF_6$. The ES^+ mass spectrum reveals peak patterns in region attributable to the species $[RuCl(PPh_3)\{[24]aneSe_6\}]^+$, and species due to the loss of PPh_3 group at m/z = 1124 and 864 respectively. The $^{31}P\{^1H\}$ NMR spectrum of the species shows in addition to the septet at δ -145 due to $[PF_6]^-$ a singlet at 45.7 assigned to the PPh_3 ligand. This compares well to $[RuCl(PPh_3)\{[16]aneSe_4\}]PF_6$ which gives a value of δ 41 for the PPh_3 ligand. Overall the solubility of the [24]aneSe_6 complexes have been poor and this has

hampered NMR studies. Also, the quest for single crystals of at least one of the systems has not been fruitful and has been a major disappointment during this work.

4.3 CONCLUSIONS

The complexes *trans*-$[OsCl_2(L\text{-}L)_2]$ (L-L = o-$C_6H_4(TeMe)_2$, $RTe(CH_2)_3TeR$ (R = Me or Ph)) have been prepared from *trans*-$[OsCl_2(dmso)_4]$ and the ditelluroethers in ethanol in poor to moderate yields. The limitations of $[OsCl_2(dmso)_4]$ as a satisfactory starting material were highlighted in reactions with analogous dithio- and diseleno-ether ligands where mixtures of products were recovered which were not readily separated. A substantial amount of effort and dedication was channelled into the attempted syntheses of osmium(II) complexes with sulfur and selenium ligands but to no avail. Other ways must be sought in order to design more fruitful routes into this chemistry. The reaction of $[OsCl_2(PPh_3)_3]$ with the ditelluroethers or $MeS(CH_2)_2SMe$ or $MeSe(CH_2)_2SeMe$ in ethanol in the presence of NH_4PF_6 gave *trans*-$[OsCl(PPh_3)(L\text{-}L)_2]PF_6$ in moderate yields.

The X-ray crystallographic studies revealed unexceptional structures that compare well with literature examples.

Studies involving the selenoether macrocycle [24]aneSe_6 with platinum group metals failed to produce single crystals suitable for X-ray crystallographic study but there is evidence to support the formation of complexes with Pt(II), Rh(III) and Ru(II).

4.4 EXPERIMENTAL

4.4.1 Ligand and Complex Synthesis

All preparations were perfomed under a dinitrogen atmosphere using standard Schlenk techniques. The $[NH_4]_2[OsCl_6]$ was synthesised from OsO_4 and converted into *trans*-$[OsCl_2(dmso)_4]$ and $[OsCl_2(PPh_3)_3]$ by literature methods.[18,71,72] The ligands were synthesised following the literature procedures.[34,73-77]

a). Synthesis of $[OsCl_2\{MeTe(CH_2)_3TeMe\}_2]$

$[OsCl_2(dmso)_4]$ (90 mg, 0.155mmol) and $MeTe(CH_2)_3TeMe$ (100 mg, 0.307 mmol) were refluxed in MeOH (70 cm^3) for 16 h. The solvent was removed *in vacuo* and CH_2Cl_2 added (2 cm^3). The orange solution was filtered and Et_2O added to the precipitate an orange solid (yield 0.05 g, 36 %). Required for $[C_{10}H_{24}Cl_2OsTe_4]$: C = 13.1, H = 2.6 %; found: C = 12.9, H = 2.6 %. ^1H NMR ($CDCl_3$, 300 MHz): δ 1.94-3.15 (m, CH_2 + CH_3). $^{125}Te\{^1H\}$ NMR ($CDCl_3/CH_2Cl_2$, 113 MHz): δ 236, 267, 274, 286, 293, 329, 339. IR spectrum (CsI disc): 2922 (m), 2855 (w), 1358 (s), 1262 (w), 1091 (s), 1068 (w), 920 (w), 835 (m), 615 (w), 598 (w), 430 (w), 297 (m), 224 (w). UV-Vis spectrum (CH_2Cl_2): ν_{max} = 22125 (ε_{mol} = 330), 20580 (sh) cm^{-1} (250 $dm^3mol^{-1}cm^{-1}$).

b). Synthesis of $[OsCl_2\{PhTe(CH_2)_3TePh\}_2]$

Method as for $[OsCl_2\{MeTe(CH_2)_3TeMe\}_2]$ above, but using $[OsCl_2(dmso)_4]$ (0.09 g, 0.155 mmol) and $PhTe(CH_2)_3TePh$ (0.14 g, 0.32 mmol) to afford a red solid (yield 40 mg, 32 %). Required for $[C_{30}H_{32}Cl_2OsTe_4]$: C = 31.0, H = 2.8 %; found: C = 30.8, H = 2.8 %. ^1H NMR ($CDCl_3$, 300 MHz): δ 3.0-3.5 (6H, CH_2), 7.4-7.9 (10H, Ph). $^{125}Te\{^1H\}$ NMR ($CDCl_3/CH_2Cl_2$, 113 MHz): δ 478, 489, 513, 523, 548. IR spectrum (CsI disc):3042 (m), 2921 (w), 1571 (m), 1474 (s), 1433 (s), 1415 (m), 1396 (m), 1359 (s), 1200 (m), 1061 (m), 1018 (m), 996 (m), 754 (w), 730 (s), 691 (s), 614 (w), 490 (w), 453 (w), 259 (w), 227 (w). UV-Vis

spectrum (CH_2Cl_2): ν_{max} = 21000 (ε_{mol} = 180), 24600 (540), 38300 cm^{-1} (18235 $dm^3mol^{-1}cm^{-1}$).

c). Synthesis of $[OsCl_2\{o\text{-}C_6H_4(TeMe)_2\}_2]$

Method as for $[OsCl_2\{MeTe(CH_2)_3TeMe\}_2]$ above, but using $[OsCl_2(dmso)_4]$ (0.09 g, 0.155 mmol) and o-$C_6H_4(TeMe)_2$ (0.11 g, 0.31 mmol) to afford a orange solid (yield 0.04 g, 29 %). Required for $[C_{16}H_{20}Cl_2OsTe_4]$: C = 19.5, H = 2.1 %; found: C = 19.4, H = 1.9 %. ^1H NMR ($CDCl_3$, 300 MHz): δ 2.05-2.3 (6H, CH_3), 7.2-7.8 (4H, C_6H_4). $^{125}Te\{^1H\}$ NMR ($CDCl_3/CH_2Cl_2$, 113 MHz): 656, 663, 671, 672, 673. ES^+ mass spectrum (MeCN): found *m/z* = 992, 948; calculated for $[^{192}Os\{C_6H_4(^{130}TeMe)_2\}_2{}^{35}Cl + MeCN]^+$ *m/z* = 1000, $[^{192}Os\{C_6H_4(^{130}TeMe)_2\}_2{}^{35}Cl]^+$ *m/z* = 959. IR spectrum (CsI disc): 2923 (w), 2851 (w), 1358 (s), 1260 (w), 1080 (s), 1019 (m), 835 (m), 753 (m), 685 (w), 614 (w), 548 (w), 427 (w), 326 (w), 302 (w). UV-Vis spectrum (CH_2Cl_2): ν_{max} = 22600 (ε_{mol} = 590), 33200 (sh) cm^{-1} (6300 $dm^3mol^{-1}cm^{-1}$).

d). Synthesis of $[OsCl(PPh_3)\{MeS(CH_2)_2SMe\}_2]PF_6$

$[OsCl_2(PPh_3)_3]$ (0.1 g, 0.095 mmol) and $MeS(CH_2)_2SMe$ (0.06 g, 0.29mmol) were refluxed together in ethanol (10 cm^3) for 2 h, during which time the colour changed from green to orange. After cooling to room temperature, NH_4PF_6 (0.06 g, 0.32 mmol) was added and the solution concentrated to 3 cm^3 to give an orange solid, which was filtered off and recrystallised from CH_2Cl_2 and Et_2O (yield 0.069 g, 70 %). Required for $[C_{26}H_{35}ClF_6OsP_2S_4]$: C = 35.5, H = 4.0 %; found: C = 35.0, H = 3.3 %. ES^+ mass spectrum (MeCN): found *m/z* = M^+ 734; calculated for $[^{192}Os^{35}Cl(PPh_3)\{MeS(CH_2)_2SMe\}_2]^+$ *m/z* = 734. IR spectrum (CsI disc): 2930 (w), 1435 (m), 1357 (m), 1091 (m), 839 (s), 750 (m), 699 (s), 516 (m), 504 (m). ^1H NMR spectrum (300 MHz, $CDCl_3$): δ 2.6 (s), 2.74 (s). $^{31}P\{^1H\}$ (145 MHz, $CH_2Cl_2/CDCl_3$): δ -15.1 (s), -147 (septet).

e). Synthesis of $[OsCl(PPh_3)\{MeSe(CH_2)_3SeMe\}_2]PF_6$

Method as for $[OsCl(PPh_3)\{MeS(CH_2)_2SMe\}_2]PF_6$ above, but using $[OsCl_2(PPh_3)_3]$ (0.1 g, 0.095 mmol) and $MeSe(CH_2)_3SeMe$ (0.06 g, 0.27mmol) to afford a brown solid (yield 0.07 g, 70 %). Required for $[C_{28}H_{39}ClF_6OsP_2Se_4]$: C = 30.9, H = 3.2 %; found: C = 30.2, H = 3.0 %. ES^+ mass spectrum (MeCN): found *m/z* = M^+ 949; calculated for $[^{192}Os^{35}Cl(PPh_3)\{Me^{80}Se(CH_2)_3{}^{80}SeMe\}_2]^+$ *m/z* = 953. IR spectrum (CsI disc): 2927 (w), 2850 (w), 1434 (w), 1089 (m), 999 (w), 840 (s), 751 (m), 699 (s), 558 (s), 537 (m), 499 (w), 440 (w). ^1H NMR (300 MHz, $CDCl_3$): δ 1.72 (q), 2.25 (s), 2.85 (t), 7.4-7.7 (m). $^{31}P\{^1H\}$ (145 MHz, $CH_2Cl_2/CDCl_3$): δ -14.0 (s), -147 (septet).

g). Synthesis of $[OsCl(PPh_3)\{MeTe(CH_2)_3TeMe\}_2]PF_6$

Method as for $[OsCl(PPh_3)\{MeS(CH_2)_2SMe\}_2]PF_6$ above, but using $[OsCl_2(PPh_3)_3]$ (0.1 g, 0.095 mmol) and $MeTe(CH_2)_3TeMe$ (g, mmol) to afford a yellow solid (yield g, 75 %). Required for $[C_{28}H_{39}ClF_6OsP_2Te_4]$: C = 26.1, H = 3.0 %; found: C = 26.5, H = 2.1 %. ES^+ mass spectrum (MeCN): found *m/z* = M^+ 1143; calculated for $[^{192}Os^{35}Cl(PPh_3)\{Me^{130}Te(CH_2)_3{}^{130}TeMe\}_2]^+$ *m/z* = 1153. IR spectrum (CsI disc): 2921 (w), 1634 (w), 1417 (w), 1201 (w), 1088 (m), 841 (s), 753 (w), 688 (m), 556 (m), 539 (m), 517 (w), 278 (w). ^1H NMR spectrum (300 MHz, $CDCl_3$): δ 1.57 (m), 1.78 (s), 1.96 (s), 2.02 (s), 2.25 (s), 3.2-3.4 *m), 7.4-7.6 (m). $^{31}P\{^1H\}$ NMR spectrum (145 MHz, $CH_2Cl_2/CDCl_3$): δ -13.0 (s), -147 (septet). $^{125}Te\{^1H\}$ NME spectrum (114 MHz, $CH_2Cl_2/CDCl_3$): δ 361, 411, 422, 430.

h). Synthesis of $[OsCl(PPh_3)\{PhTe(CH_2)_3TePh\}_2]PF_6$

Method as for $[OsCl(PPh_3)\{MeS(CH_2)_2SMe\}_2]PF_6$ above, but using $[OsCl_2(PPh_3)_3]$ (0.1 g, 0.095 mmol) and $PhTe(CH_2)_3TePh$ (g, mmol) to afford a yellow solid (yield g, 87 %). Required for $[C_{48}H_{47}ClF_6OsP_2Te_4]$: C = 37.5, H = 3.0 %; found: C = 37.9, H = 2.4 %. ES^+ mass spectrum (MeCN): found *m/z* = M^+ 1391; calculated for $[^{192}Os^{35}Cl(PPh_3)\{MeTe(CH_2)_3TeMe\}_2]^+$ *m/z* = 1401. IR

spectrum (CsI disc): 3050 (w), 2932 (w), 1477 (w), 1435 (m), 1363 (m), 1088 (m), 1017 (w), 938 (s), 735 (s), 688 (s), 558 (m), 536 (m), 454 (w), 250 (m). ^{1}H NMR spectrum (300 MHz, $CDCl_3$): δ 2.2 (m), 2.9-3.3 (m), 7.0-7.8 (m). $^{31}P\{^{1}H\}$ (145 MHz, $CH_2Cl_2/CDCl_3$): δ -10.5 (s), -11.8 (s), -145 (septet). $^{125}Te\{^{1}H\}$ NMR spectrum (114 MHz, $CH_2Cl_2/CDCl_3$): δ 454, 463, 499, 540, 565.

i). Synthesis of $[OsCl_2\{Ph_2Sb(CH_2)_3SbPh_2\}_2]$

$[OsCl_2(dmso)_4]$ (0.05 g, 0.09 mmol) and $Ph_2Sb(CH_2)_3SbPh_2$ (0.16 g, 0.27 mmol) were refluxed together in ethanol (10 cm^3) for 3 h. The solvent was removed *in vacuo*. CH_2Cl_2 was added to the residue and this solution was filtered. The addition of Et_2O precipitated an orange solid (yield 0.045 g, 35 %). Required for $[C_{54}H_{52}Cl_2OsSb_4].CH_2Cl_2$: C = 43.1, H = 3.4 %; found: C = 43.1, H = 2.8 %. ES+ mass spectrum (MeCN) *m/z* = M^+ 1450; calculated for $[^{192}Os^{35}Cl_2\{Ph_2{}^{121}Sb(CH_2)_3{}^{121}SbPh_2)_2]^+$ *m/z* = 1446. IR spectrum (CsI disc): 3066 (m), 3049 (m), 1480 (w), 1432 (s), 1360 (m), 1102 (m), 1069 (s), 998 (m), 727 (s), 695 (s), 451 (s), 267 (m). UV-Vis spectrum (CH_2Cl_2): ν_{max} = 30860 (sh), (ε_{mol} = 2200), 22230 (sh) cm^{-1} (250 $dm^3mol^{-1}cm^{-1}$). $^{13}C\{^{1}H\}$ NMR ($CH_2Cl_2/CDCl_3$): δ 15.8, 24.3, 128 – 137. CV (CH_2Cl_2): reversible +0.3 V versus SCE.

j). Reaction of $[OsCl_2(dmso)_4]$ with $MeS(CH_2)_2SMe$

$[OsCl_2(dmso)_4]$ (0.05 g, 0.09 mmol) and $MeS(CH_2)_2SMe$ (0.04 g, 0.27 mmol) were heated at 120° C for 24 hours in DMF (10 cm^3). Most of the solvent was removed *in vacuo* and diethyl ether was added which precipitated a brown solid. ES^+ mass spectrum (MeCN): found *m/z* = 549; calculated for $[^{192}Os^{35}Cl(Me_2{}^{32}SO)\{MeS(CH_2)_2SMe\}_2]^+$ *m/z* = 549.

k). Reaction of $[OsCl_2(dmso)_4]$ with $MeS(CH_2)_3SMe$

$[OsCl_2(dmso)_4]$ (0.05 g, 0.09 mmol) and $MeS(CH_2)_3SMe$ (0.04 g, 0.27 mmol) were heated at 120° C for 24 hours in DMF (10 cm^3). Most of the solvent was

removed *in vacuo* and diethyl ether was added which precipitated a brown solid. ES^+ mass spectrum (MeCN): found *m/z* = 577; calculated for $[^{192}Os^{35}Cl(Me_2{}^{32}SO)\{MeS(CH_2)_3SMe\}_2]^+$ *m/z* = 577.

l). Reaction of $[OsCl_2(dmso)_4]$ with o-$C_6H_4(SMe)_2$

$[OsCl_2(dmso)_4]$ (0.05 g, 0.09 mmol) and o-$C_6H_4(SMe)_2$ (0.05 g, 0.27 mmol) were heated at 120° C for 24 hours in DMF (10 cm^3). Most of the solvent was removed *in vacuo* and diethyl ether was added which precipitated a brown solid. ES^+ mass spectrum (MeCN): found *m/z* = 645; calculated for $[^{192}Os^{35}Cl(Me_2{}^{32}SO)\{o\text{-}C_6H_4(SMe)_2\}_2]^+$ *m/z* = 645.

m). Reaction of $[OsCl_2(dmso)_4]$ with $MeSe(CH_2)_3SeMe$

$[OsCl_2(dmso)_4]$ (0.05 g, 0.09 mmol) and $MeSe(CH_2)_3SeMe$ (0.06 g, 0.27 mmol) were heated at 120° C for 24 hours in DMF (10 cm^3). Most of the solvent was removed *in vacuo* and diethyl ether was added which precipitated a brown solid. ES^+ mass spectrum (MeCN): found *m/z* = 765, 722, 687; calculated for $[^{192}Os^{35}Cl(Me_2{}^{32}SO)\{Me^{80}Se(CH_2)_3SeMe\}_2]^+$ *m/z* = 769; $[^{192}Os^{35}Cl_2\{Me^{80}Se(CH_2)_3SeMe\}_2]^+$ *m/z* = 726; $[^{192}Os^{35}Cl_2\{Me^{80}Se(CH_2)_3SeMe\}_2]^+$ *m/z* = 691.

n). Reaction of $[OsCl_2(dmso)_4]$ with $PhSe(CH_2)_3SePh$

$[OsCl_2(dmso)_4]$ (0.05 g, 0.09 mmol) and $PhSe(CH_2)_3SePh$ (0.07 g, 0.27 mmol) were heated at 120° C for 24 hours in DMF (10 cm^3). Most of the solvent was removed *in vacuo* and diethyl ether was added which precipitated a brown solid. ES^+ mass spectrum (MeCN): found *m/z* = 972, 893 calculated for $[^{192}Os^{35}Cl_2\{Ph^{80}Se(CH_2)_3SePh\}_2]^+$ *m/z* = 974; $[^{192}Os^{35}Cl_2\{Ph^{80}Se(CH_2)_3SePh\}\{PhSe(CH_2)_3Se\}]^+$ *m/z* = 897.

o). Reaction of $[OsCl_2(dmso)_4]$ with [8]aneSe$_2$

$[OsCl_2(dmso)_4]$ (0.05 g, 0.09 mmol) and [8]aneSe$_2$ (0.07 g, 0.27 mmol) were heated at 120° C for 24 hours in DMF (10 cm^3). Most of the solvent was removed *in vacuo* and diethyl ether was added which precipitated a brown solid. ES$^+$ mass spectrum (MeCN): found *m/z* = 787, 751 calculated for $[^{192}Os^{35}Cl(Me_2SO)\{[8]aneSe_2\}_2]^+$ *m/z* = 793; $[^{192}Os^{35}Cl_2\{[8]aneSe_2\}_2]^+$ *m/z* = 750.

p). Reaction of $[OsCl_2(dmso)_4]$ with [16]aneSe$_4$

$[OsCl_2(dmso)_4]$ (0.05 g, 0.09 mmol) and [16]aneSe$_4$ (0.13 g, 0.27 mmol) were heated at 120° C for 24 hours in DMF (10 cm^3). Most of the solvent was removed *in vacuo* and diethyl ether was added which precipitated a brown solid. ES$^+$ mass spectrum (MeCN): found *m/z* = 789, 747 calculated for $[^{192}Os^{35}Cl(Me_2SO)\{[16]aneSe_4\}]^+$ *m/z* = 793; $[^{192}Os^{35}Cl_2\{[16]aneSe_4\}]^+$ *m/z* = 750.

q). Synthesis of $[(PdCl)_2\{[24]aneSe_6\}][BF_4]_2$[34]

$PdCl_2$ (37 mg, 0.142 mmol) in MeCN (3 cm^3) under N_2 was heated to effect dissolution and then cooled to ambient temperature. [24]aneSe$_6$ (52 mg, 0.07 mmol) was added, and the mixture was stirred for 5 min. $NaBF_4$ (46 mg, 0.42 mmol) was then added. The mixture was stirred for 15 min and then filtered. The addition of diethyl ether afforded the product as a yellow solid.

r). Synthesis of $[(PtCl)_2\{[24]aneSe_6\}][BF_4]_2$

$PtCl_2$ (38 mg, 0.142 mmol) in MeCN (3 cm^3) under N_2 was heated to effect dissolution and then cooled to ambient temperature. [24]aneSe$_6$ (52 mg, 0.07 mmol) was added, and the mixture was stirred for 5 min. $NaBF_4$ (46 mg, 0.42 mmol) was then added. The mixture was stirred for 15 min and then filtered. The addition of diethyl ether to the clear solution afforded the product as an off-white solid (yield 0.06 g, 72 %). Required for $[C_{18}H_{36}B_2Cl_2F_8PtSe_6]$: C = 15.9, H = 2.7 %; found: C = 15.6, H = 2.7 %. $^{77}Se\{^1H\}$ NMR spectrum (68.68 MHz,

CD_3CN/MeCN, 240 K): δ 337 (v.br). $^{195}Pt\{^1H\}$ NMR spectrum (77.4 MHz, CD_3CN/MeCN, 200 K): δ -4236, -4261. ^1H NMR spectrum (300 MHz, CD_3CN, 298 K): δ 3.1 (α-CH_2), 2.46 (β-CH_2). IR spectrum (CsI disc): 1359 (s), 1262 (s), 1094 (s), 804 (m), 521 (m), 319 (m) cm^{-1}.

s). Synthesis of $[Pt([24]aneSe_6)][PF_6]_2$

$PtCl_2$ (25 mg, 0.09 mmol), [24]aneSe_6 (65 mg, 0.09 mmol) and $TlPF_6$ (62 mg, 0.18 mmol) were added to $MeNO_2$ (70 cm^3) and were refluxed together for 24 h to produce a colourless solution plus white precipitate. TlCl was removed by filtration, and the filtrate was reduced in volume to *ca.* 2 cm^3 and cold diethyl ether (30cm^3) was added slowly to afford a white solid which was collected and dried *in vacuo* (yield 0.74g, 76 %). Required for $[C_{18}H_{36}Cl_2F_{12}P_2PtSe_6]$: C = 17.8, H = 3.0 %; found: C = 18.4, H = 2.9. %. ES^+ mass spectrum (MeCN) found *m/z* = 1066; calculated for $[^{195}Pt\{[24]ane^{80}Se_6\}PF_6]^+$ *m/z* = 1072. IR spectrum (CsI disc): 2959 (s), 1431 (s), 1379 (s), 1260 (s), 1097 (s), 836 (vs), 740 (m), 558 (s), 435 (w) cm^{-1}.

t). Synthesis of $[RhCl_2\{[24]aneSe_6\}]BF_4$

The compound [24]aneSe_6 (0.116 g, 0.16 mmol) was added to EtOH (100 cm^3) and the solution was brought to reflux; $RhCl_3.3H_2O$ (51 mg, 0.16 mmol) in water (10 cm^3) was added dropwise over 0.5 h and the mixture refluxed for 2 h to give an orange solution. The solution was cooled and an excess of NH_4BF_4 (0.26 g, 0.24 mmol) was the added and the solution concentrated to *ca.* 5 cm^3 prior to treatment with diethyl ether (50 cm^3) which afforded an orange solid which was dried *in vacuo* (yield 0.08 g, 58 %). Required for $[C_{18}H_{36}BCl_2F_4PtSe_6]$: C = 24.0, H = 3.6 %; found: C = 24.2, H = 3.7 %. ES^+ mass spectrum (MeCN) found *m/z* = 900; calculated for $[^{103}Rh^{35}Cl_2\{[24]ane^{80}Se_6\}]^+$ *m/z* = 905. IR spectrum (CsI disc): 2920 (m), 1409 (s), 1293 (s), 1062 (vs), 886 (s), 840 (s), 799 (s), 767 (s), 521 (s), 350 (s). ^1H NMR spectrum (300 MHz, CD_3CN, 298 K): δ 3.0-2.7 (α-CH_2), 2.4-2.1 (β-CH_2).

u). Synthesis of $[RuCl(PPh_3)\{[24]aneSe_6\}]PF_6$

A mixture of $[RuCl_2(PPh_3)_3]$ (0.118 g, 0.12 mmol) and [24]aneSe$_6$ (0.09 g, 0.12 mmol) was reluxed under N_2 in MeOH for 4 h. The resulting yellow solution was allowed to stir at room temperature for 16 h. The salt NH_4PF_6 (60 mg, 0.36 mmol) was then added and the solution reduced to *ca.* 2cm^3 to give a yellow precipitate which was filtered off, recrystalised from CH_2Cl_2 and dried *in vacuo* (yield 0.09g, 59 %). ES$^+$ mass spectrum (MeCN) found *m/z* = 1125, 863; calculated for $[^{101}Ru^{35}Cl(PPh_3)\{[24]ane^{80}Se_6\}]^+$ *m/z* = 1130; $[RuCl\{[24]aneSe_6\}]^+$ *m/z* = 868. IR spectrum (CsI disc): 2930 (m), 1435 (s), 1360 (s), 1090 (s), 840 (vs), 748 (m), 698 (m), 558 (m), 529 (m), 325 (m). $^{31}P\{^1H\}$ NMR spectrum (145.8 MHz, CD_3CN, MeCN): δ -146.3 (septet, PF_6^-), 45.7 (PPh_3).

4.4.2 X-Ray Crystallography

$[OsCl_2\{Ph_2Sb(CH_2)_3SbPh_2\}_2].2CH_2Cl_2$

and $[OsCl_2(dmso)_2\{MeSe(CH_2)_3SeMe\}]$

The selected crystals were mounted on a glass fibre. Details of the crystallographic data collection and refinement parameters are given in Tables 4.7 and 4.10. Data collection used a Rigaku AFC7S four-circle diffractometer operating at 150 K using graphite-monochromated Mo Kα X-ray radiation (λ = 0.71073 Å), and was undertaken by Dr G. Reid and Dr A.R.J. Genge. For $[OsCl_2\{Ph_2Sb(CH_2)_3SbPh_2\}_2].2CH_2Cl_2$ the data were corrected for absorption using psi-scans. The structure was solved by heavy atom methods[78] and developed by iterative cycles of full matrix least-squares refinement[79] and difference Fourier syntheses. All fully occupied non-H atoms were refined anisotropically and H-atoms were placed in fixed, calculated positions. This species was found to have crystallographic inversion symmetry, with the Os atom occupying an inversion centre. Two half CH_2Cl_2 solvent molecules, disordered across crystallographic inversion centres, were also identified in the asymmetric unit in the structure of $[OsCl_2\{Ph_2Sb(CH_2)_3SbPh_2\}_2]$. Selected bond

lengths and angles are given in Tables 4.11 and 4.12. For $[OsCl_2(dmso)_2\{MeSe(CH_2)_2SeMe\}]$ preliminary psi scans did not provide a satisfactory absorption correction, hence, with the model at isotropic convergence, the data were corrected for absorption using DIFABS.[80] All atoms except carbons were refined anisotropically. The Flack parameter indicated that the correct enantiomorph of $[OsCl_2(dmso)_2\{MeSe(CH_2)_3SeMe\}]$ was refined. Selected bond lengths and angles are given in Tables 4.8 and 4.9.

The data collection and X-ray crystallography experimental information for $PhTeCl_2(CH_2)_3TeCl_2Ph.MeCN$ and $[OsCl_2\{PhTe(CH_2)_3TePh\}_2]$ can be found in literature.[24]

4.5 REFERENCES

1. W.P. Griffith, in; '*Comprehensive Coordination Chemistry*,' G. Wilkinson, R.R. Gillard, J.A. McCleverty (Eds.), Vol. 4, Pergamon, Oxford, 1987, 519.
2. L.F. Warren and M.A. Bennett, *Inorg. Chem.*, 1976, **15**, 3126.
3. J. Willemse, J.A. Cras, J.J. Steggerda and C.P. Kreitzers, *Struct. Bonding, Berlin*,1976, **28**, 83.
4. D. Coucouvanis, *Prog. Inorg. Chem.*, 1970, **11**, 233.
5. D.J. Gulliver, W. Levason, K.G. Smith, M.J. Selwood and S.G. Murray, *J. Chem. Soc., Dalton Trans.*, 1980, 1872.
6. E.G. Hope, W. Levason, M. Webster and S.G. Murray, *J. Chem. Soc., Dalton Trans.*, 1986, 1003.
7. S.K. Harbron and W. Levason, *J. Chem. Soc., Dalton Trans.*, 1985, 205.
8. S.K. Habron and W. Levason, *J. Chem. Soc., Dalton Trans.*, 1987, 633.
9. D.J. Gulliver and W. Levason, *Coord. Chem. Rev.*, 1982, **46**, 1.
10. J.S. Jaswal, S.J. Rettig and B.R. James, *Can. J. Chem.*, 1990, **68**, 1808.
11. I.P. Evans, A. Spencer and G. Wilkinson, *J. Chem. Soc., Dalton Trans.*, 1973, 204.
12. E. Alessio, B. Milani, M. Bolle, G. Mestroni, G. P. Faleschini, F. Todone, S. Geremia and M. Calligaris, *Inorg. Chem.*, 1995, **34**, 4722.
13. D.C.R. Hockless, S.B. Wild, A.M. McDonagh, I.R. Whitall and M.G. Humphrey, *Acta Crystallogr., Sect. C*, 1996, **52**, 1639.
14. B. Chaudret, G. Commenges and R. Poilblanc, *J. Chem. Soc., Dalton Trans.*, 1984, 1635.
15. P.G. Antonov, Y.N. Kukushkin, W.I. Konnov and Y.P. Kostikov, *Koord. Khim.*, 1980, **6**, 1585.
16. P.G. Antonov and I.A. Amantova, *Zh. Obshch. Khim.*, 1988, **58**, 2523.
17. A.M. McDonagh, M.G. Humphrey and D.C.R. Hockless, *Aust. J. Chem.*, 1998, **51**, 807.

18. A.M. McDonagh, M.G. Humphrey and D.C.R. Hockless, *Tetrahedron: Asymmetry*, 1997, **8**, 3579.
19. N.R. Champness, W. Levason, S.R. Preece and M. Webster, *Polyhedron*, 1994, **13**, 881.
20. R.J. Judd, R. Cao, M. Biner, T. Armbruster, H.-B Burgi, A.E. Merbach and A. Ludi, *Inorg. Chem.*, 1995, **34**, 5080.
21. T. Kemmitt, W. Levason and M. Webster, *Inorg. Chem.*, 1989, **28**, 692.
22. T. Kemmitt and W. Levason, *Inorg. Chem.*, 1990, **29**, 731.
23. W. Levason, S.D. Orchard, G. Reid and V. Tolhurst, *J. Chem. Soc., Dalton Trans.*, 1999, 2071.
24. A.J. Barton, W. Levason, G. Reid and V. Tolhurst, *Polyhedron*, 2000, **19**, 235.
25. N.J. Holmes, W. Levason and M. Webster, *J. Chem. Soc., Dalton Trans.*, 1998, 3457.
26. N.R. Champness and W. Levason, *Coord. Chem. Rev.*, 1993, **133**, 115.
27. P.E. Garrou and G.E. Hartwell, *J. Organomet. Chem.*, 1974, **69**, 445.
28. M.F. Ludmann, D. Dartiguenave and Y. Dartiguenave, *Inorg. Chem.*, 1977, **16**, 440.
29. A.M. Hill, W. Levason, M. Webster and I. Albers, *Organometallics*, 1997, **16**, 5641.
30. A.M. Hill, N.J. Holmes, A.R.J. Genge, W. Levason, M. Webster and S. Rutschow, *J. Chem. Soc., Dalton Trans.*, 1998, 825.
31. S.R. Cooper and S.C. Rawle, *Struct. Bonding (Berlin)*, 1990, **72**, 1.
32. A.J. Blake and M.J. Schröder, *Adv. Inorg. Chem.*, A.G. Sykes, Ed, New York, 1990, **35**, 2.
33. R.J. Batchelor, F.W.B. Einstein, I.D. Gay, J.H. Gu, B.D. Johnston and B.M. Pinto, *J. Am. Chem. Soc.*, 1989, **111**, 6582.
34. R.J. Batchelor, F.W.B. Einstein, I.D. Gay, J. Gu, B.M. Pinto and X. Zhou, *Inorg. Chem*, 1996, **33**, 3667.
35. P.F. Kelly, W. Levason, G. Reid and D.J. Williams, *J. Chem. Soc., Chem. Commun.*, 1993, 1716.

36. W. Levason, J.J. Quirk and G. Reid, *J. Chem. Soc., Dalton Trans.*, 1996, 3713.
37. N.R. Champness, P.F. Kelly, W. Levason, G. Reid, A.M.Z. Slawin and D.J. Williams, *Inorg. Chem.*, 1995, **34**, 651.
38. W.Levason, J.J. Quirk, G. Reid and S.M. Smith, *J. Chem. Soc., Dalton Trans.*, 1997, 3719.
39. W. Levason, J.J. Quirk, G. Reid and C.S. Frampton, *Inorg Chem.*, 1994, **33**, 6120.
40. A.J. Blake, R.O. Gould, A.J. Lavery and M. Schröder, *Angew. Chem. Int. Ed. Engl.*, 1986, **25**, 274.
41. D.J. Gulliver, E.G. Hope, W. Levason, S.G. Murray and G.L. Marshall, *J. Chem. Soc., Dalton Trans.*, 1985, 1265.
42. E.G. Hope, W. Levason, S.G. Murray, M. Webster and S.G. Murray, *J. Chem. Soc., Dalton Trans.*, 1985, 2185.
43. J.J. Jenkinson, W. Levason, R.J. Perry and M.D. Spicer, *J. Chem. Soc., Dalton Trans.*, 1989, 453.
44. D. Collinson, G. Reid and M. Schröder, *Polyhedron*, 1992, **11**, 3165.
45. A.J. Blake, R.O. Gould, A.J. Holder, T.I. Hyde and M. Schröder, *J. Chem. Soc., Dalton Trans.*, 1988, 1861.
46. T. –F. Lai and C. –K. Poon, *J. Chem. Soc., Dalton Trans.*, 1982, 1465.
47. N. W. Alcock, J.C. Cannadine, G.R. Clark and A.F. Hill, *J. Chem. Soc., Dalton Trans.*, 1993, 1131.
48. S.C. Rawle and S.R. Cooper, *J. Chem. Soc., Chem. Commun.*, 1987, 308.
49. S.C. Rawle, T.J. Sewell and S.R. Cooper, *Inorg Chem.*, 1987, **26**, 3769.
50. M.N. Bell, A.J. Blake, H.-J. Kuppers, M. Schroder and K. Wieghardt, *Angew. Chem., Int. Ed. Engl.*, 1987, **26**, 250.
51. A.J. Blake, G. Reid and M. Schröder, *Polyhedron*, 1992, **11**, 2501.
52. A.B.P. Lever, *Inorganic Electronic Spectroscopy*, Elsevier, New York, 2nd edn., 1984.

53. N.P. Luthra and J.D. Odom, in: S. Patai and Z. Rappoport (Eds), *The Chemistry of Organic Selenium and Tellurium Compounds, Vol. 1*, Wiley, New York, 1986, 189.

54. R.J. Batchelor, F.W.B. Einstein, C.H.W. Jones and R.D. Sharma, *Organometallics*, 1987, **6**, 2164.

55. J.D. Korp, I. Bernal, J.C. Turley and G.E. Martin, *Inorg Chem.*, 1980, **19**, 2556.

56. C.L.Raston, R.J. Secomb and A.H. White, *J. Chem. Soc., Dalton Trans.*, 1976, 2307.

57. E.E. Castellano, J. Zuckerman-Schpector, J.T.B. Ferreira and J.V. Comassetto, *Acta Crystallogr., Sect. C*, 1986, **42**, 44.

58. R.K. Chadha, J.E. Drake and J.L. Hencher, *Can. J. Chem.*, 1983, **61**, 1222.

59. R.H. Jones and T.A. Hamor, *J. Organomet. Chem.*, 1984, **262**, 151.

60. R.K. Chadha, J.E. Drake and M.A. Khan, *Acta Crystallogr. Sect. C*, 1983, **39**, 45.

61. D. Kobelt and E.F. Paulus, *J. Organomet. Chem.*, 1971, **C63**, 27.

62. N.J. Holmes, W. Levason and M. Webster, *J. Chem. Soc., Dalton Trans.*, 1997, 4223.

63. W. Levason, N.R. Champness and M. Webster, *Acta Crystallogr., Sect. C*, 1993, **49**, 1884.

64. F.A. Cotton, M.P. Diebold and M. Matusz, *Polyhedron*, 1987, **6**, 1131.

65. E.W. Abel, S.K. Bhargava and K.G. Orrell, *Prog. Inorg. Chem.*, 1984, **32**, 1.

66. E.W. Abel, K.G. Orrell, S.P. Scanlan, D. Stephenson, T. Kemmitt and W. Levason, *J. Chem. Soc., Dalton Trans.*, 1991, 591.

67. N.R. Champness, W. Levason, R.A.S. Mould, D. Pletcher and M. Webster, *J. Chem. Soc., Dalton Trans.*, 1991, 591.

68. N.R. Champness, W. Levason, D. Pletcher, M.D. Spicer and M. Webster, *J. Chem. Soc., Dalton Trans.*, 1992, 2201.

69. A.J. Blake, N.R. Champness, R.J. Forder, C.S. Frampton, C.A. Frost, G. Reid and R.H. Simpson, *J. Chem. Soc., Dalton Trans.*, 1994, 3377.

70. N.R. Champness, W. Levason and M. Webster, *Inorg. Chim. Acta*, 1993, **208**, 189.

71. F.P. Dwyer and J.W. Hogarth, *Inorg. Synth.*, 1957, **5**, 206.

72. P.R. Hoffman and K.G. Caulton, *J. Am. Chem. Soc.*, 1975, **97**, 4221.

73. E.G. Hope, T. Kemmitt and W. Levason, *Organometallics*, 1988, **7**, 78.

74. T. Kemmitt and W. Levason, *Organometallics*, 1989, **8**, 1303.

75. D.J. Gulliver, E.G. Hope, W. Levason, S.G. Murray, D.M. Potter and G.L. Marshall, *J. Chem. Soc., Perkin Trans. II*, 1984, 429.

76. E.G. Hope, T. Kemmitt and W. Levason, *J. Chem. Soc., Perkin Trans. II*, 1987, 487.

77. F.R. Hartley, S.G. Murray, W. Levason, H.E. Soutter and C.A. McAuliffe, *Inorg. Chim. Acta*, 1979, **35**, 265.

78. P.T. Beurskens, G. Admiraal, G. Beurskens, W.P. Bosmans, S. Garcia Granda, R.O. Gould, J.M.M. Smits and C. Smykalla, PATTY, The DIRDIF Program System, Technical Report of the Crystallography Laboratory, University of Nijmegen, The Netherlands, 1992.

79. TEXSAN: Crystal Structure Analysis Package, Molecular Structure Corporation, TX, 1995.

80. N. Walker and D. Stuart, *Acta Crystallogr., Sect. A*, 1983, **39**, 158.

CHAPTER 5

Bismuth(III) Halide Complexes of Tridentate and Macrocyclic Group 16 Ligands

5.1 INTRODUCTION

This chapter aims to examine the complexes formed between the bismuth(III) halides and a variety of tridentate and macrocyclic ligands of differing architecture from Group 16.

Group 15 constitutes the third column of the p-block of the periodic table and comprises the elements nitrogen, phosphorus, arsenic, antimony and **bismuth**, which are often referred to as the pnictogens or pnictides. The ground state electronic configuration for bismuth is $[Xe]4f^{14}5d^{10}6s^26p^3$ which results in common oxidation states of +3 (III) and +5 (V). All the possible compounds BiX_3 (X = F, Cl, Br or I) are known, stable compounds. BiF_3 is prepared by dissolving Bi_2O_3 in HF with the formation of $BiF_3.3HF$ (H_3BiF_6) which yields BiF_3 on heating.[1] BiF_3 does not readily form complexes. $BiCl_3$ can be prepared by dissolving bismuth metal in aqua regia, giving the dihydrate $BiCl_3.2H_2O$ on evaporation. Distillation, which decomposes the hydrate, gives $BiCl_3$ as colourless deliquescent crystals.[2] $BiCl_3$ has pyramidal molecular structure in the vapour phase.[3] However, the solid-state structure bismuth has three short Bi-Cl bonds and five longer-distance interactions which leads to a bicapped trigonal prismatic geometry ($BiCl_8$ units).[4] $BiBr_3$ is prepared by a similar route to the chlorides.[5] Bismuth bromide was also shown to be a pyramidal molecule in the vapour phase.[6] In the solid phase $BiBr_3$ exists in two forms,[7] with a transition temperature of 158° C:

$$\alpha\text{-}BiBr_3 \quad \rightleftharpoons \quad \beta\text{-}BiBr_3$$

The low-temperature α-$BiBr_3$ has a distorted $BiBr_6$ octahedral structure, with the three short Bi-Br bonds and three longer interactions. The high-temperature β-$BiBr_3$ has an $AlCl_3$-type structure. Useful laboratory procedures for the preparation of BiI_3 are also available.[8] The solid-phase structure of bismuth triiodide shows a symmetrical octahedron with the pnictogen atom at the centre.[9]

In the +3 oxidation state the elements of Group 15 have a lone pair of electrons. It is not clear whether this lone pair of electrons will be stereochemically active in a particular compound but a number of trends have been observed.[10] The stereochemical activity of this lone pair appears to decrease with increasing coordination number, increasing atomic number of the halogen (Cl > Br > I) and with increasing atomic number in Group 15 (i.e. As > Sb > Bi).

A large amount of work has been done involving anionic complexes of the bismuth(III) halides. These have been discussed in detail in previous reviews[11,12] and since this study involves neutral complexes they will not be discussed here. Alonzo *et al.*[13] examined the products formed from the reactions of bismuth(III) halides with a variety of nitrogen and phosphorus chelating ligands such as 1,10-phenantholine and 1,2-bis(diphenylphosphino)ethane (dppe). Using a combination of analytical, mass spectrometry and IR spectroscopic techniques they studied a number of solids in which the ligands are believed to be chelated. The only structurally characterised examples of multidentate amine complexes of bismuth(III) involve the macrocyclic ligands Me_3[9]aneN_3[14] and [12]aneN_4[15] with bismuth(III) chloride and perchlorate respectively. In both cases the structures feature the pyramidal bismuth(III) species with the tri- or tetra-dentate macrocycle capping the Bi(III) ion.

Although, bismuth(III) complexes containing tertiary phosphine ligands were virtually unknown until recently, there now exists a variety of complexes. The first neutral bismuth(III) complex containing a tertiaryphosphine ligand, $[Bi_2Br_6(PMe_3)_4]$, was synthesised and crystallographically characterised by Norman and co-workers.[16] The yellow solid adopts a centrosymmetric edge-shared bioctahedral structure, with the bismuth(III) atoms in a near to ideal octahedral geometry. Norman *et al.*[16] have since studied various phosphine complexes of the Group 15 halides including $[Bi_2Br_6(dmpe)_2]$ (Figure 5.1), $[Bi_4Br_{12}(PEt_3)_4]$ and $[BiBr_6(PMe_2Ph)_2(OPMe_2Ph)_2]$. The reaction of bismuth(III) bromide with two equivalents of PEt_3 in thf solution produced the tetramic bismuth(III) complex $[Bi_4Br_{12}(PEt_3)_4]$ (Figure 5.2) which possesses C_i symmetry

with two unique bismuth atoms each bonded to one phosphine atom and five bromine atoms. The structure may be viewed as two linked edge-shared bioctahedral units, again with the bismuth(III) atoms having almost perfect octahedral gemoetry. The other complexes all contain an edge-shared, bioctahedral structure.

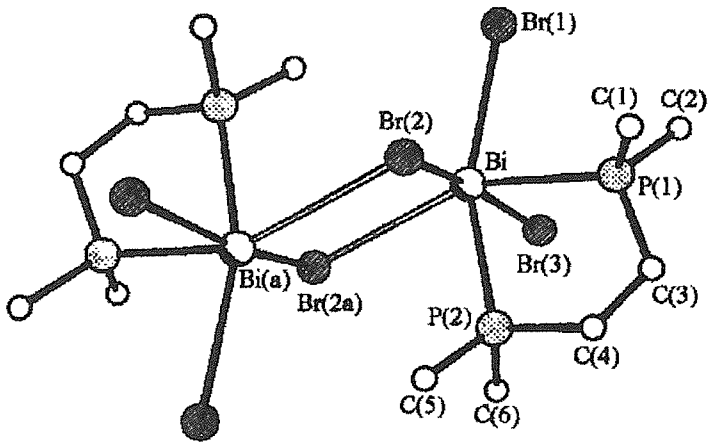

Figure 5.1 – View of the molecular structure of $[Bi_2Br_6(dmpe)_2]$ taken from ref. 16

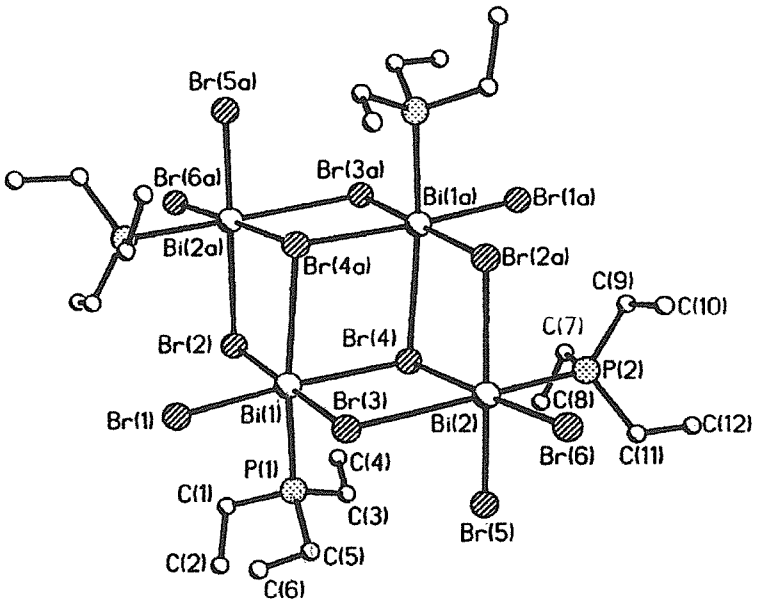

Figure 5.2 – View of the molecular structure of $[Bi_4Br_{12}(PEt_3)_4]$ taken from ref 16

The reaction of bismuth(III) chloride with dppm and dppe in acetonitrile solution has been investigated by Willey *et al.*[17] The resulting complexes, $[Bi_2Cl_6(dppm)_2]$ and $[Bi_4Cl_{12}(dppe)_5]$, respectively, were studied by single crystal X-ray diffraction. $[Bi_2Cl_6(dppm)_2]$ (Figure 5.3) has a centrosymmetric structure consisting of coplanar halide-bridged Bi_2Cl_6 units with each of the two dppm ligands in a bidentate bridging mode between the two metal centres. The overall coordination geometry at each bismuth(III) atom is approximately octahedral. In contrast the structure of $[Bi_4Cl_{12}(dppe)_5]$ has two crystallographically independent molecules in the asymmetric unit which may be identified as $[Bi_2Cl_6(dppe)_2]$ and $[Bi_2Cl_6(dppe)_3]$ (Figure 5.4). For the former species, the centrosymmetric structure is made up of halide bridged Bi_2Cl_6 units with bidentate chelate attachment of a dppe ligand to each bismuth atom giving rise to an overall edge-shared bioctahedral geometry. The $[Bi_2Cl_6(dppe)_3]$ species is a centrosymmetric dimer containing two $BiCl_3(dppe)$ moieties connected by a bridging dppe ligand. Thus both chelating and bridging dppe ligands are observed.

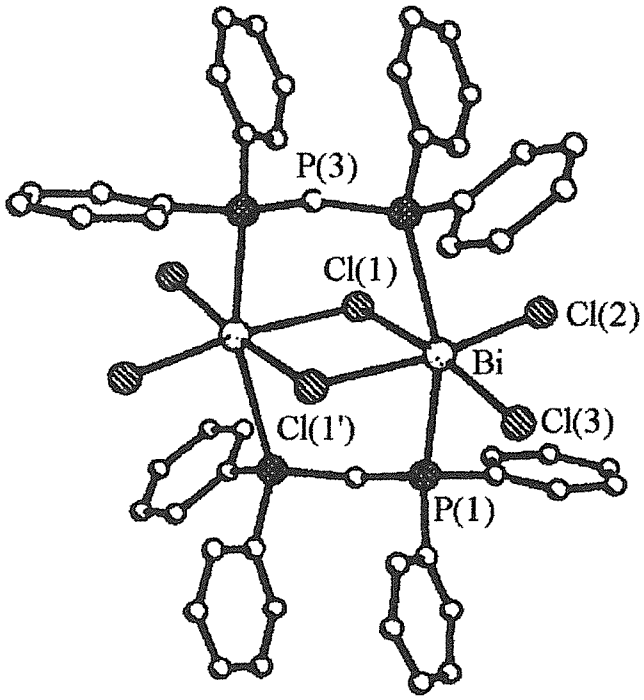

Figure 5.3 – View of the centrosymetric $[Bi_2Cl_6(dppm)_2]$ dimer taken from ref. 17

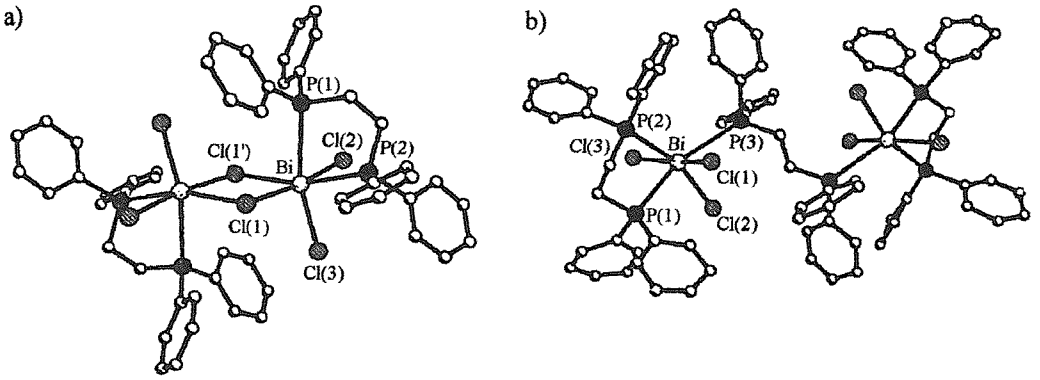

Figure 5.4 – View of the centrosymmetric dimeric structures of a) $[Bi_2Cl_6(dppe)_2]$ and b) $[Bi_2Cl_6(dppe)_3]$ taken from ref. 17

The reason for the complexes adopting these edge-shared, bioctahedral dimers in the majority of cases is unclear. Norman and Pickett[11] observe that the Bi-X *trans* to a phosphine ligand is typically *ca.* 0.2 Å greater than similar Bi-X bonds *trans* to X. This observation is attributed to the large *trans* influence of the phosphine *vs.* halide. They also note that of the four possible isomers (Figure 5.5) for structures of this type (**A-D**), isomer **A** is formed.

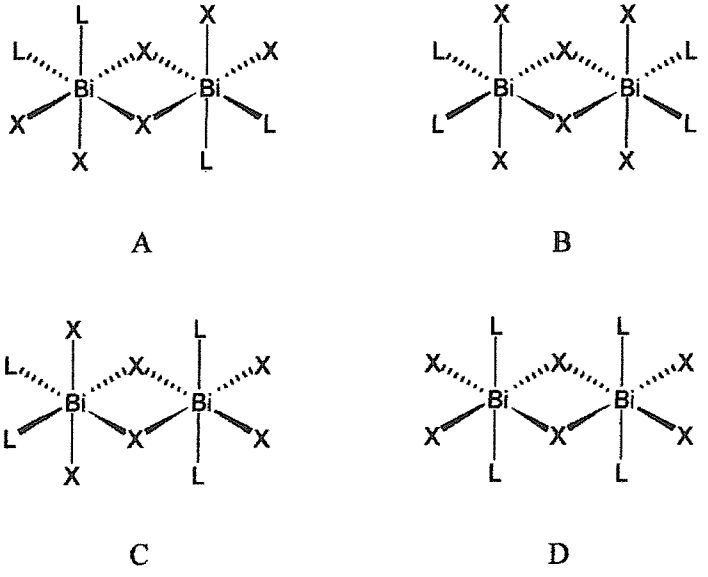

Figure 5.5 – Possible isomers for $[Bi_2X_6(L)_4]$

On steric grounds isomer **C** would be the favoured isomer and Norman and Pickett suggests that the preference for isomer **A** can be assigned to an

electronic effect arising from the *trans* influence of the phosphine ligands. If a phosphine were placed *trans* to a bridging halide (as in isomer **B**), this would weaken the Bi-X bond, effectively creating a pair of $[BiX_2L_2]^+$ cations in close proximity which is not energetically favoured.

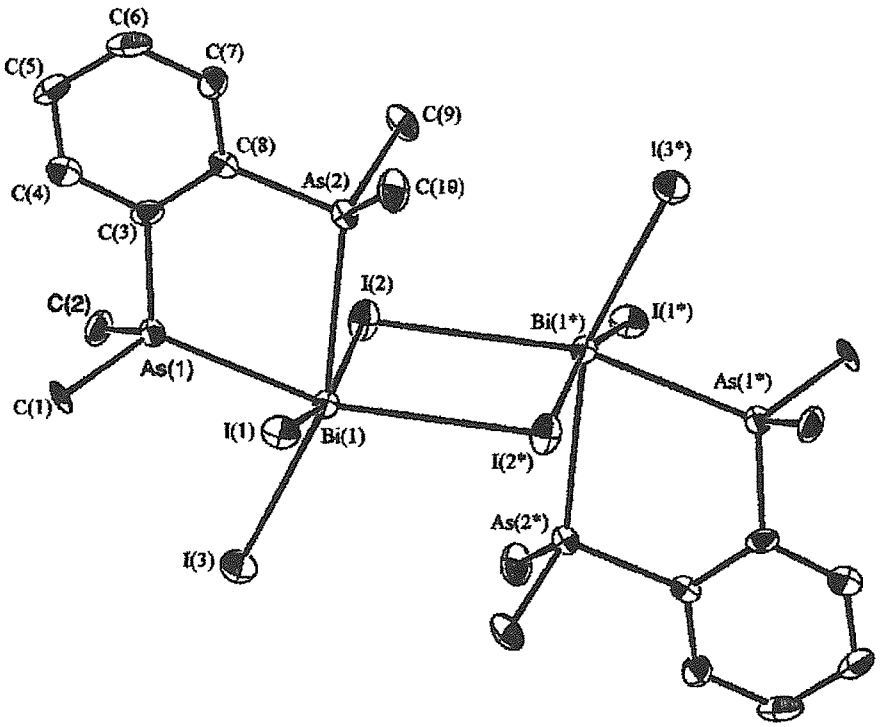

Figure 5.6 – View of the dimeric structure of $[Bi_2I_6\{o\text{-}C_6H_4(AsMe)_2\}_2]$ taken from ref. 18

In contrast to amine[13,14,15] and phosphine[16,17] complexes of Bi(III) very little work has been done on other Group 15 donors, namely arsines.[18] Recent work within the Southampton research group has produced a range of complexes of type $[BiX_3(L\text{-}L)]$ (X = Cl, Br or I; L-L = $Ph_2As(CH_2)_2AsPh_2$ or o-$C_6H_4(AsMe_2)_2$ (diars)), and $[BiX_3(L\text{-}L\text{-}L)]$ (X = Cl, Br or I; L-L-L = $MeC(CH_2AsMe_2)_3$) by reaction of BiX_3 with the appropriate ligand in MeCN. A view of the first structurally characterised example of a Bi(III) – arsine complex, the dimeric $[Bi_2I_6\{o\text{-}C_6H_4(AsMe)_2\}_2]$, is shown in Figure 5.6. The X-ray structure shows that the complex adopts the same form as the phosphine

complexes characterised, i.e. the structure features the edge-shared, bioctahedral dimer with each Bi atom bound to two terminal I atoms, two μ_2-bridging I atoms and two mutually *cis* As atoms from the chelating diars ligands.

For Group 16 donor systems the preference is again for the harder oxygen-donor ligands. The crown ethers in particular have been studied in great detail and all show a monomeric BiX_3 unit capped by the multidentate ligand (Figure 5.7).[19-23]

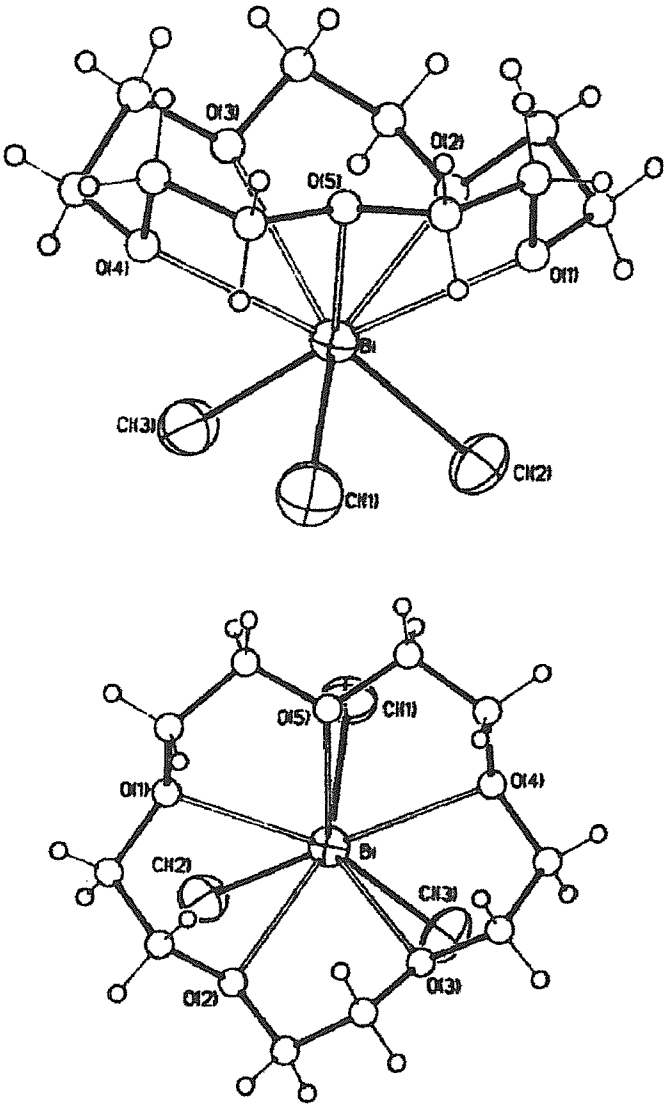

Figure 5.7 – Top and side view of [$BiCl_3$(15-crown-5)] taken from ref. 21

A number of monodentate ligand systems (e.g. *fac*-$[BiX_3(thf)_3]$ (X = Cl or Br)[24,25] and $[BiX_3(dmso)_3]$ (X = Cl or Br)[26,27]) have also been characterised structurally, and these do not adopt the edge-shared, bioctahedral unit observed for the chelates. Instead they form mononuclear octahedral 1:3 Bi:ligand systems. A series of acyclic ethylene glycols of varying denticities have also been studied by Rogers and co-workers.[20] The interdonor linkages in these species are no larger than dimethylene, and all form monomeric units with Bi centres of no more than 7-coordinate with O_4X_3 donor sets. The example of $[BiCl_3(pentaethyleneglycol)]$ is shown in Figure 5.8.

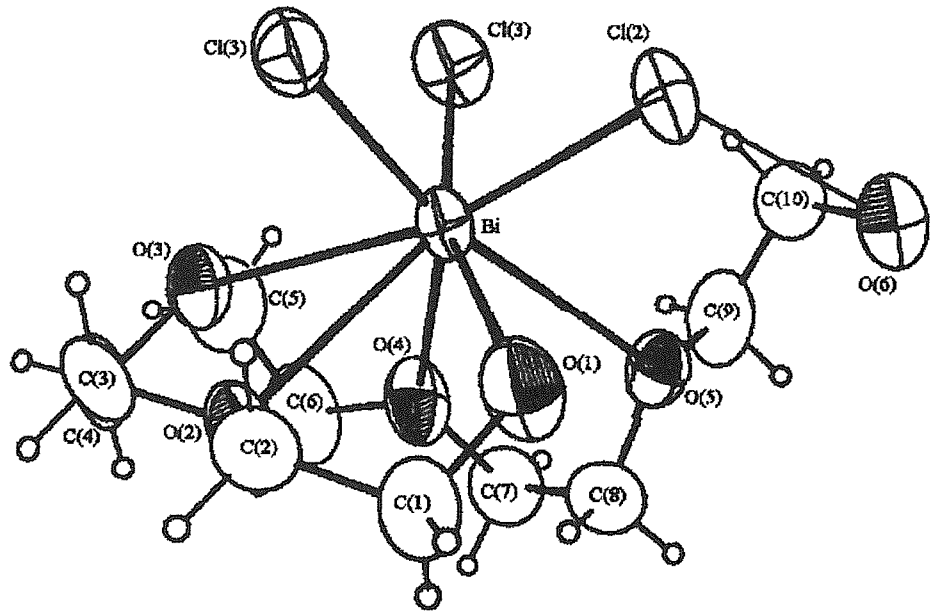

Figure 5.8 – View of the monomeric structure of $[BiCl_3(pentaethyleneglycol)]$ taken from ref. 20

The ether donor is preferred to the hydroxyl donor in the cases where five oxygen donors are present within the ligand. Eveland *et al.*[24] have also characterised the products formed from the reaction of $BiCl_3$ with $MeO(CH_2)_2O(CH_2)_2OMe$ and $EtO(CH_2)_2O(CH_2)_2OEt$. In both cases the product formed adopts the edge-shared, bioctahedral dimers commonly observed in Bi(III) complexes.

A large number of complexes have been reported containing bismuth(III) and sulfur donor ligands, amongst the first examples to be structurally characterised being those containing the tris(diethyldithiocarbamato) ligand and associated derivatives.[28] Thus, the parent complex bismuth(III) tris(diethyldithiocarbamate) was shown to consist of six-coordinate bismuth atoms in distorted dodecahedral geometry (taking into account the stereochemically lone pair) weakly linked into dimers.

The research group in Southampton has been interested for some time in the synthesis and properties of thio-, seleno- and telluro-ether ligands and the coordination chemistry of these with a wide range of d-block elements has now been investigated (discussed in Chapters 2-4).[29] More recently these studies have been extended to include the heavier p-block elements such as Sn(IV) and Bi(III).[30-34] Compared to transition metal chemistry, main group coordination chemistry has in general received less attention. To some extent this may be attributed to the absence of good spectroscopic probes through which to monitor the chemistry, e.g. they are often colourless and/or labile in solution. Furthermore, complexes of the p-block elements may adopt a very wide range of geometries. This has already been noted with examples of Group 15 donors. This point is further demonstrated by the recent report describing the preparation and crystal structure of a highly unusual open framework lattice, $[Bi_4Cl_{12}\{MeS(CH_2)_3SMe\}_4].H_2O$, incorporating psuedo-cubane Bi_4Cl_{12} units linked by bridging dithioether ligands to yield an infinite three dimensional array with large open channels.[33] Figure 5.9 shows a view of a portion of the $[Bi_4Cl_{12}\{MeS(CH_2)_3SMe\}_4]_n$ structure and Figure 5.10 shows the view down the c-axis of the three-dimensional polymer, illustrating the channels running through the structure.

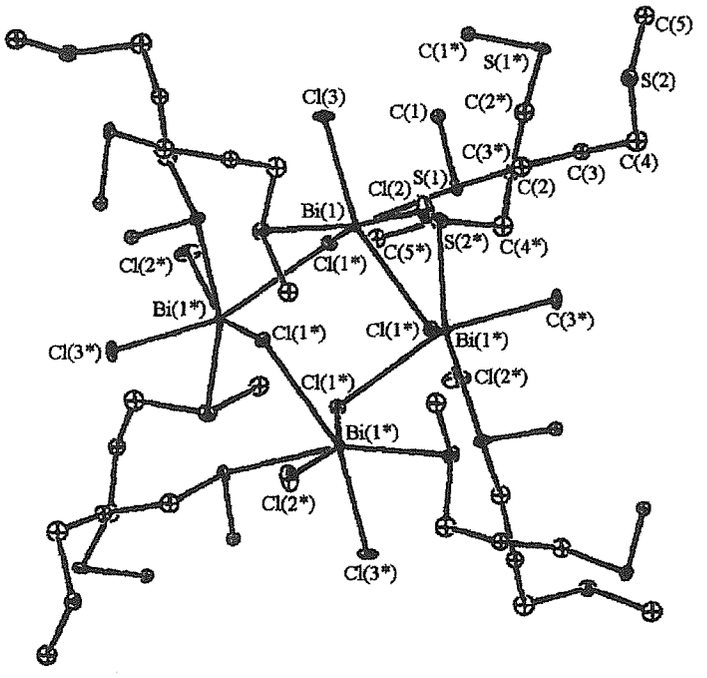

Figure 5.9 – View of a portion of the $[Bi_4Cl_{12}\{MeS(CH_2)_3SMe\}_4]_n$ structure taken from ref. 33

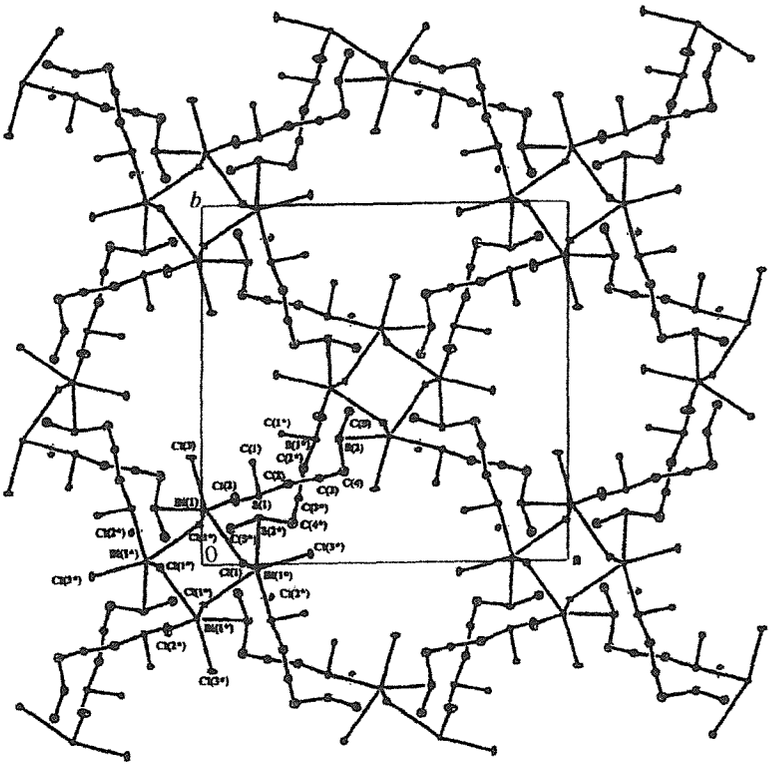

Figure 5.10 – View down the c-axis of $[Bi_4Cl_{12}\{MeS(CH_2)_3SMe\}_4]_n$ taken from ref. 33

The work was extended to investigate the interaction of bismuth(III) halides with a wider variety of thioether and also selenoether ligands.[34] A range of compounds of stoichiometry $[BiX_3(L\text{-}L)_2]$ (X = Cl, Br or I; L-L = $MeS(CH_2)_2SMe$), $[Bi_2X_6\{PhS(CH_2)_2SPh\}]$ (X = Cl or Br), $[BiX_3(L\text{-}L)]$ (L-L = $MeE(CH_2)_3EMe$ (E = S or Se) or $MeSe(CH_2)_2SeMe$) have been isolated from reaction of BiX_3 with L-L in dry MeCN solution. Prior to this work there were no structurally characterised examples of bismuth(III) selenoether compounds and examples of thioether derivatives were limited to the aforementioned $[Bi_4Cl_{12}\{MeS(CH_2)_3SMe\}_4].H_2O$,[33] $[Me_3S]_2[Bi_2I_8(Me_2S)_2]$,[35] (produced from the reaction of BiI_3 in neat Me_2S), and a small number of macrocyclic thioether complexes including $[BiCl_3([12]aneS_4)]$, $[BiCl_3([15]aneS_5)]$. $[BiCl_3([18]aneS_6)]$ and $[(BiCl_3)_2([24]aneS_8)]$.[36,37,38] It is significant that all of these characterised bismuth(III) halide complexes involving crown thioethers reflect the dominance of the pyramidal BiX_3 unit on the structure adopted. The five weaker secondary halide interactions which are evident within the structure of the parent Bi(III) halide (Figure 5.11) are replaced with weak Bi-S interactions, generating 7-, 8- or 9-coordinate compounds. Figure 5.11 shows the projection of the structure of $BiCl_3$ on the *ab* plane, showing the chlorine bridging that is present between a single $BiCl_3$ molecule and its neighbours. Two unit cells in the z direction are involved. In these thiacrown species the weak thioether interactions form around the direction of the Bi-based lone pair. The stereochemically active lone pair on bismuth can clearly be seen being directed towards the weakly interacting S-donors in the structures of $[(BiCl_3)_2([24]aneS_8)]$[38] (Figure 5.12) $[BiCl_3([15]aneS_5)]$ (Figure 5.13) and $[BiCl_3([12]aneS_4)]$[36] (Figure 5.14).

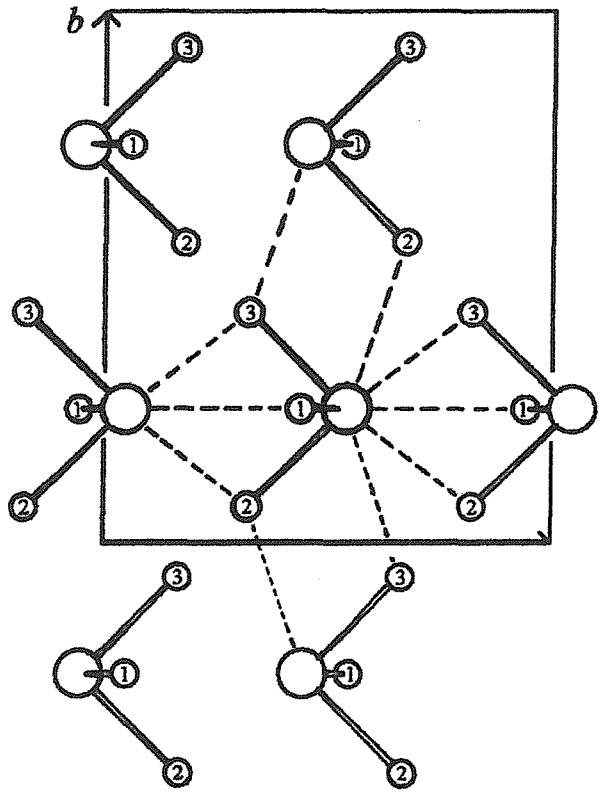

Figure 5.11 – Projection of the structure of $BiCl_3$ on the *ab* plane taken from ref. 37

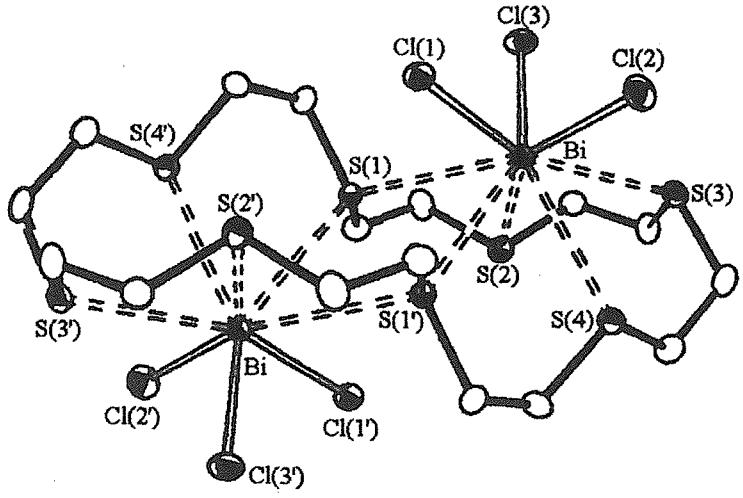

Figure 5.12 – View of $[(BiCl_3)_2([24]aneS_8)]$ taken from ref. 37

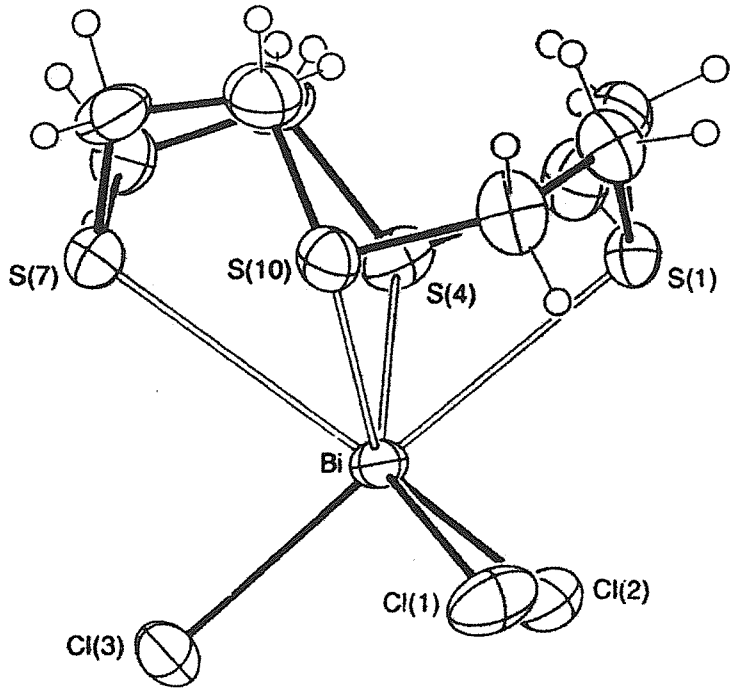

Figure 5.13 – View of [$BiCl_3$([12]aneS_4)] taken from ref. 36

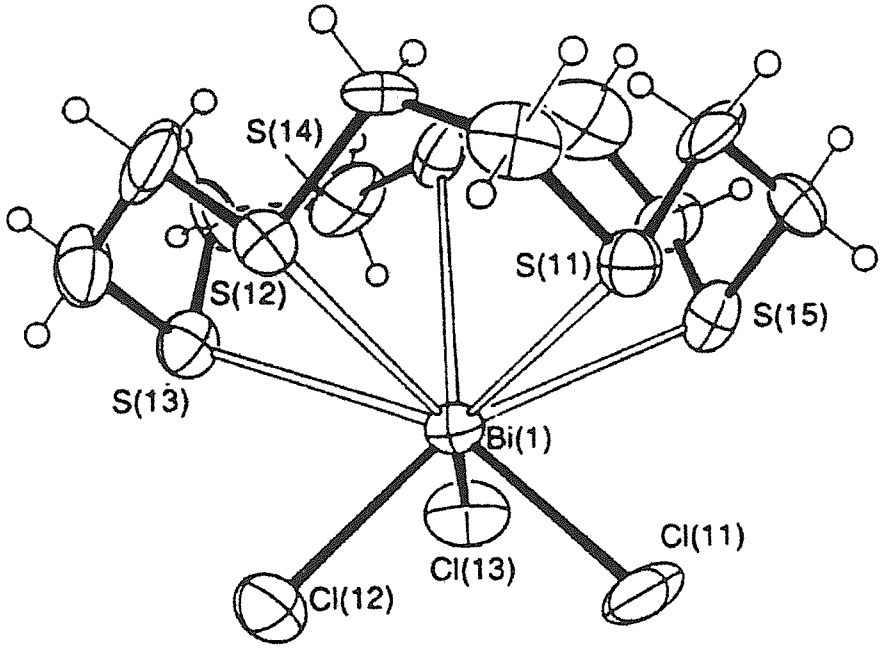

Figure 5.14 – View of [$BiCl_3$([15]aneS_5)] taken from ref. 36

The recent work by the research group in Southampton has generated crystal structures of a number of Bi(III) complexes which exhibit a wide variety of different structural motifs for relatively small alterations in ligand architecture. The structure of $[BiBr_3\{MeS(CH_2)_3SMe\}]$ (Figure 5.15) shows Bi_2Br_6 units linked by four different, bridging dithioether ligands to give an infinite two-dimensional sheet. The orientation of the bismuth lone pair is implied from the elongated Bi-μ-Br distances. Sawyer and Gillespie have noted previously that the weak interactions form around the direction of the maximum electron density of the lone pair, but not directly over it.[39] The structure adopted for this compound contrasts starkly with that of the chloro analogue, $[Bi_4Cl_{12}\{MeS(CH_2)_3SMe\}_4].H_2O$ discussed above.

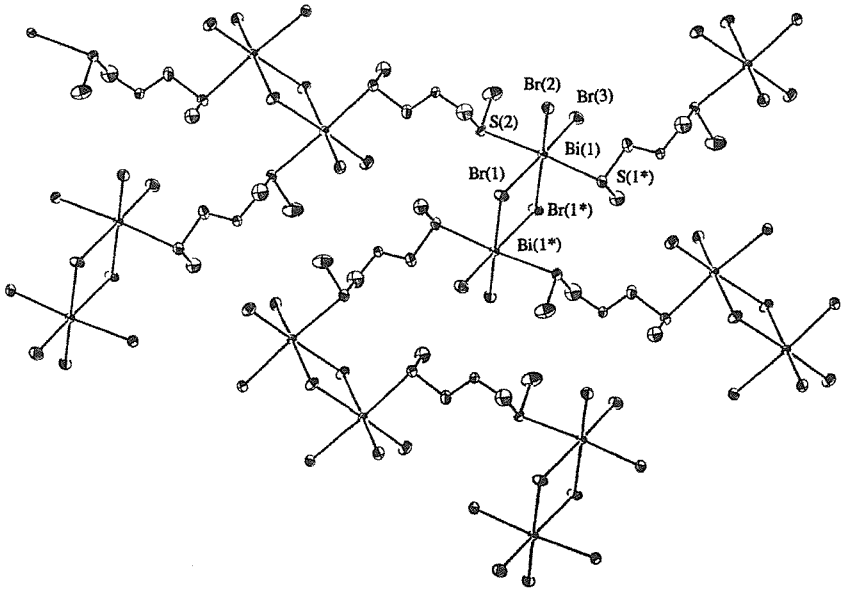

Figure 5.15 – View of a portion of the structure of $[BiBr_3\{MeS(CH_2)_3SMe\}]$ taken from ref. 34

Crystals were also obtained for the dithioether compound $[BiBr_3\{MeS(CH_2)_2SMe\}_2]$ (Figure 5.16). The structure of this species is different to the one described above, showing discrete mononuclear units. In this case the bismuth(III) species is seven coordinate and adopts a distorted pentagonal bipyramidal geometry. The donor set is derived from three terminal Br and four S-donors from two chelating dithioethers.

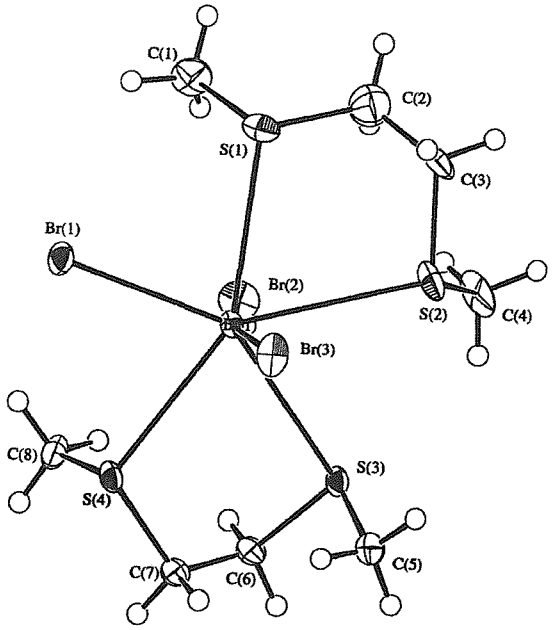

Figure 5.16 – View of the structure of $[BiBr_3\{MeS(CH_2)_2SMe\}_2]$ taken from ref. 34

Altering the terminal substituent on the dithioether ligand also has a dramatic effect upon the structure adopted. The crystal structure of $[Bi_2Br_6\{PhS(CH_2)_2SPh\}]$ (Figure 5.17) shows that the species adopts an infinite two-dimensional sheet structure which incorporates infinite chains of almost orthogonal Bi_2Br_6 dimer units cross-linked by bridging $PhS(CH_2)_2SPh$ ligands to give a two-dimensional sheet. Dithioether ligands of this type and other Group 16 ligands have previously been shown to bind to Cu(I) and Ag(I) centres and in a small number of cases also yield polymeric arrays, although quite different in detail to this complex.[40,41,42]

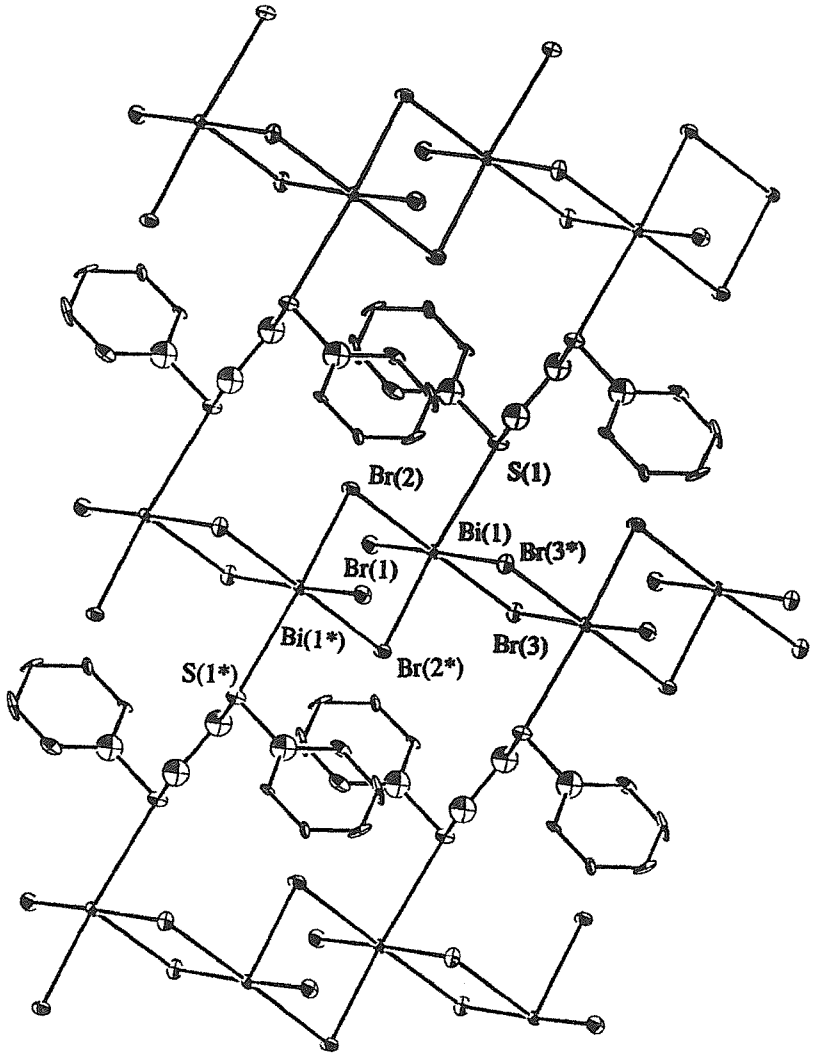

Figure 5.17 – View of a portion of the structure of $[Bi_2Br_6\{PhS(CH_2)_2SPh\}]$ taken from ref. 34

As previously stated, there were no structurally characterised examples of bismuth(III) selenoether compounds until the recent work.[34] Crystals were obtained from a 1:1 ratio of $BiCl_3$ and $MeSe(CH_2)_3SeMe$. The structure of this compound shows (Figure 5.18) a very similar two-dimensional sheet array to $[BiBr_3\{MeS(CH_2)_3SMe\}]$ mentioned earlier, with edge-shared bioctahedral Bi_2Cl_6 dimers linked by diselenoether ligands. The crystal structure of $[BiBr_3\{MeSe(CH_2)_3SeMe\}]$ has also been established (Figure 5.19). It is isostructural with $[BiBr_3\{MeS(CH_2)_3SMe\}]$.

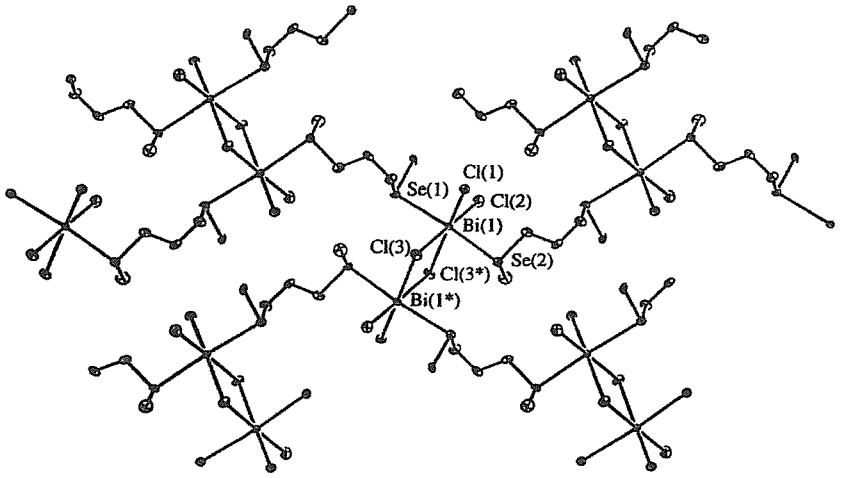

Figure 5.18 – View of a portion of the structure of [$BiCl_3${$MeSe(CH_2)_3SeMe$}] taken from ref. 34

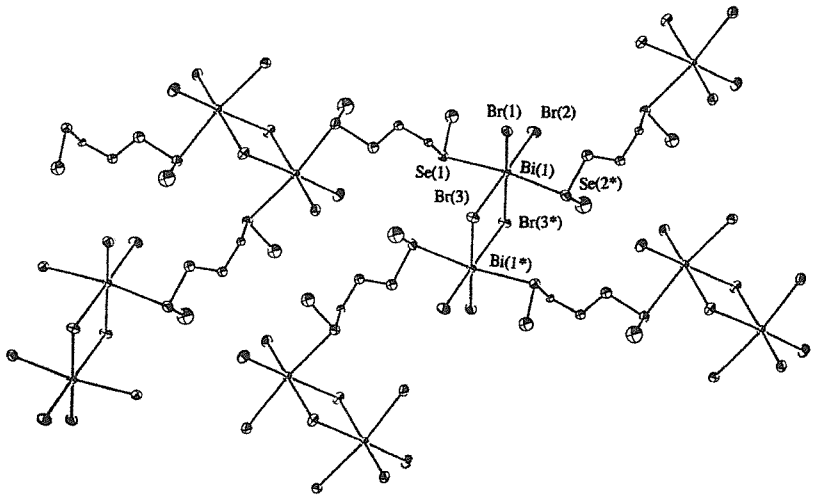

Figure 5.19 – View of a portion of the structure of [$BiBr_3${$MeSe(CH_2)_3SeMe$}] taken from ref. 34

Significantly, the Bi-Se distances in these compounds are shorter to the Bi-S distances in the macrocyclic thioether complexes. This suggests that while the Bi-S interactions are described as weak, secondary interactions, those involving Se are considerably stronger, and presumably reflect the orientation of the bismuth lone pair which is towards the thioether ligand in the macrocyclic derivatives, but towards the bridging Br ligands in the selenoether complexes mentioned here.

This work is still in its infancy and the recent work carried out by myself, to be discussed later in this chapter, is the next step into the chemistry of Group 16 multidentate ligands with p-block elements. In order to investigate this chemistry further and to establish the range of structures and coordination modes possible for these systems have been extended to investigate the interaction of bismuth(III) halides with a wider variety of thioether and selenoether ligands including macrocyclic selenoethers (Figure 5.20).

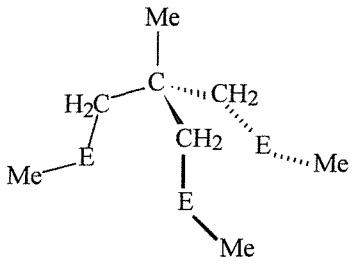

E = S or Se

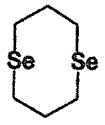

[8]aneSe$_2$

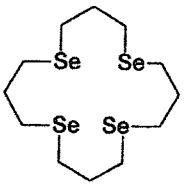

[16]aneSe$_4$

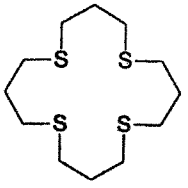

[16]aneS$_4$

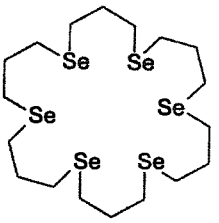

[24]aneSe$_6$

Figure 5.20 The tridentate and macrocyclic ligands

5.2 RESULTS AND DISCUSSION

5.2.1 Synthesis and Properties of Tridentate Group 16 Complexes of BiX_3

A range of complexes of the stoichiometry $[BiX_3L^3]$ (L^3 = $MeC(CH_2SMe)_3$ or $MeC(CH_2SeMe)_3$) has been isolated from reaction of BiX_3 with L^3 in dry MeCN solution. The solid thioether and selenoether complexes are relatively stable to moist air and can be kept for many weeks in a N_2-purged dry-box. Microanalytical data consistent with these formulations were obtained for all freshly prepared solids. The IR spectra of the chloro derivatives show up to three peaks in the range 230-280 cm^{-1} assigned to ν(Bi-Cl); these compare to values of 242 and 288 cm^{-1} for the parent species, $BiCl_3$.[16] By the very nature of these Bi(III) species, their characterisation is restricted to analytical data, IR spectroscopy and single crystal X-ray diffraction studies. The very poor solubility of these compounds in non-coordinating solvents such as CH_2Cl_2 and $CHCl_3$ severely hindered attempts to obtain meaningful ^1H and $^{77}Se\{^1H\}$ NMR spectra.

5.2.2 Single Crystal X-ray Diffraction Studies of $[BiCl_3\{MeC(CH_2SeMe)_3\}]$ and $[Bi_2I_6\{MeC(CH_2SeMe)_3\}_2]$

Prior to this study the only complexes of the bismuth(III) halides with selenoether ligands characterised structurally were restricted to bidentate ligands.[33,34] The tripod selenoether, $MeC(CH_2SeMe)_3$ might have been expected to cap the BiX_3 units in a *fac* conformation. However, the structures obtained for $[BiCl_3\{MeC(CH_2SeMe)_3\}]$ and $[Bi_2I_6\{MeC(CH_2SeMe)_3\}_2]$ exhibit very different structural motifs.

Crystals obtained from the reaction of $BiCl_3$ with $MeC(CH_2SeMe)_3$ shows centrosymmetric Bi_2Cl_6 units linked by tripodal selenoether ligands (Figure 5.20). The bismuth(III) ions are 7-coordinate, with the donor set comprising two bridging Cl (2.776(8), 3.151(10) Å), two terminal Cl (2.622(9), 2.55(1) Å), one bidentate selenoether (2.962(4), 3.156(4) Å) and one monodentate selenoether (3.117(4) Å). This product may be considered as

Bi_2Cl_6 units with additional bidentate selenoether coordination at each Bi, with the third Se-donor from each tripod cross-linking these to give a 2-dimensional sheet, with a Se_3Cl_4 donor set at each Bi. The coordination of the third Se-donor results in a severe twisting of the Bi_2Cl_6 unit from planarity. The Bi-Se bond distances seen here are in good agreement with the previously reported selenoether complexes, e.g. $[BiCl_3\{MeSe(CH_2)_3SeMe\}]_n$ (2.989(3) and 3.035(3) Å).[33] The Bi-Cl bond distances are also consistent with previous literature examples including $[BiCl_3\{MeSe(CH_2)_3SeMe\}]_n$ (2.555(7), 2.570(7), 2.829(7) and 2.883(7) Å).[33,36-38] The Bi-Cl bond distances for the terminal Cl atoms in $[BiCl_3\{MeC(CH_2SeMe)_3\}]$ are considerably shorter than those of the μ_2-bridging Cl atoms as has been observed for the examples in previous studies and consistent with the observations of Sawyer and Gillespie[39] that the stereochemically active lone pair of electrons of Bi lie within the Bi_2Cl_6 plane.

The crystals of $[Bi_2I_6\{MeC(CH_2SeMe)_3\}_2]$ were very weakly diffracting, and hence the structure quality is rather poor. However, while comparisons of bond lengths and angles are not warranted, it is worth noting that this species is different from $[BiCl_3\{MeC(CH_2SeMe)_3\}]$ above, showing (Figure 5.21) a discrete dimeric species, analogous to the literature examples of dimethylene backboned diphosphine complexes,[11,12,16,17,43] (an example of which is shown in Figure 5.1) derived from twisted Bi_2I_6 units with one bidentate tripod selenoether coordinated to each Bi leaving one arm of the tripod uncoordinated. The geometry at Bi is therefore a distorted octahedron. Selected bond lengths: Bi(1)-I(1) 2.923(7), Bi(1)-I(2) 3.133(7), Bi(1)-I(2*) 3.260(7), Bi(1)-I(3) 2.917(9), Bi(1)-Se(1) 2.96(1), Bi(1)-Se(2) 3.19(1) Å

Table 5.1 – Crystallographic data collection and refinement parameters for $[BiCl_3\{MeC(CH_2SeMe)_3\}]$

Formula	$C_8H_{18}BiCl_3Se_3$
Formula Weight	666.45
Colour, morphology	Yellow, plate
Crystal Dimensions/mm	0.26, 0.23, 0.04
Crystal System	Monoclinic
Space Group	$P2_1/a$
a / Å	11.402(7)
b / Å	16.919(5)
c / Å	11.893(6)
α/ °	90
β/ °	99.23(4)
γ/ °	90
V / Å^3	2264(1)
Z	4
$F(000)$	1208
D_{calc}/ g cm^{-3}	1.955
μ(Mo-K_α)/ cm^{-1}	129.28
Unique observed reflections	4136
Observed reflections with $[I_o > 2\sigma(I_o)]$	1880
No. of parameters	136
Goodness of fit	1.14
R[a]	0.06
Rw[b]	0.088

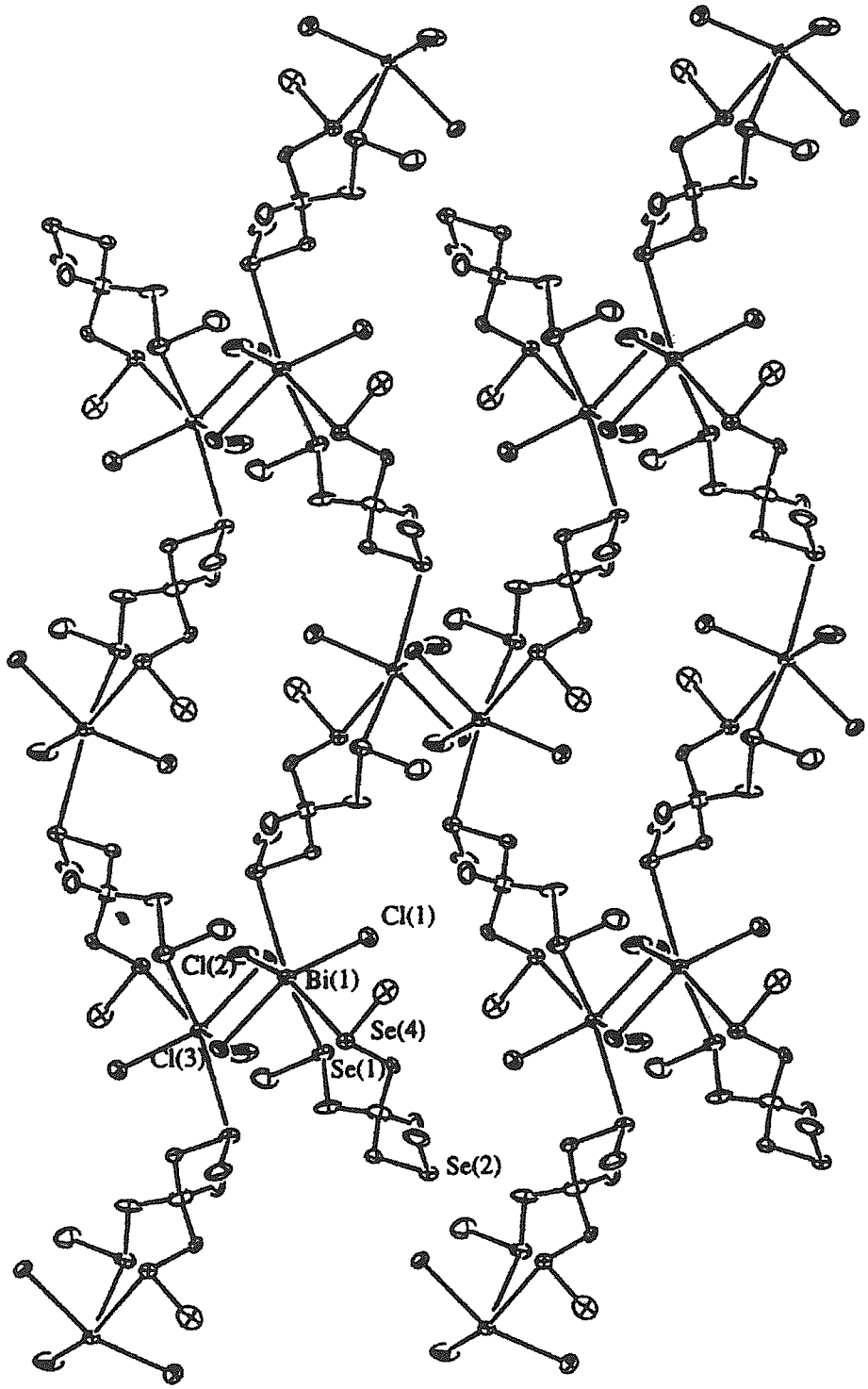

Figure 5.21 – View of a portion of the structure of $[BiCl_3\{MeC(CH_2SeMe)_3\}]$ with the numbering scheme adopted.

Table 5.2 – Selected bond lengths (Å) for [$BiCl_3${$MeC(CH_2SeMe)_3$}]

Bi(1)	Se(1)	2.962(4)	Bi(1)	Cl(2)	2.55(1)
Bi(1)	Se(2)	3.117(4)	Bi(1)	Cl(3)	2.776(8)
Bi(1)	Se(4*)	3.156(4)	Bi(1)	Cl(3*)	3.151(10)
Bi(1)	Cl(1)	2.622(9)			

Table 5.3 – Selected bond angles (degrees) for [$BiCl_3${$MeC(CH_2SeMe)_3$}]

Se(1)	Bi(1)	Se(2*)	153.6(1)	Se(2*)	Bi(1)	Cl(2)	79.4(2)
Se(1)	Bi(1)	Se(4)	78.0(1)	Se(2*)	Bi(1)	Cl(3)	115.6(2)
Se(1)	Bi(1)	Cl(1)	81.1(2)	Se(2*)	Bi(1)	Cl(3*)	65.9(2)
Se(1)	Bi(1)	Cl(2)	80.3(3)	Se(4)	Bi(1)	Cl(1)	85.4(2)
Se(1)	Bi(1)	Cl(3)	81.0(2)	Se(4)	Bi(1)	Cl(2)	157.5(2)
Se(1)	Bi(1)	Cl(3*)	140.0(2)	Se(4)	Bi(1)	Cl(3)	80.5(2)
Se(2*)	Bi(1)	Se(4)	123.2(1)	Se(4)	Bi(1)	Cl(3*)	64.8(2)
Se(2*)	Bi(1)	Cl(1)	85.0(2)	Cl(1)	Bi(1)	Cl(2)	97.1(4)
Cl(1)	Bi(1)	Cl(3)	159.2(3)	Cl(1)	Bi(1)	Cl(3*)	108.8(3)
Cl(2)	Bi(1)	Cl(3)	90.3(3)	Cl(2)	Bi(1)	Cl(3*)	133.7(3)
Cl(3)	Bi(1)	Cl(3*)	79.0(3)				

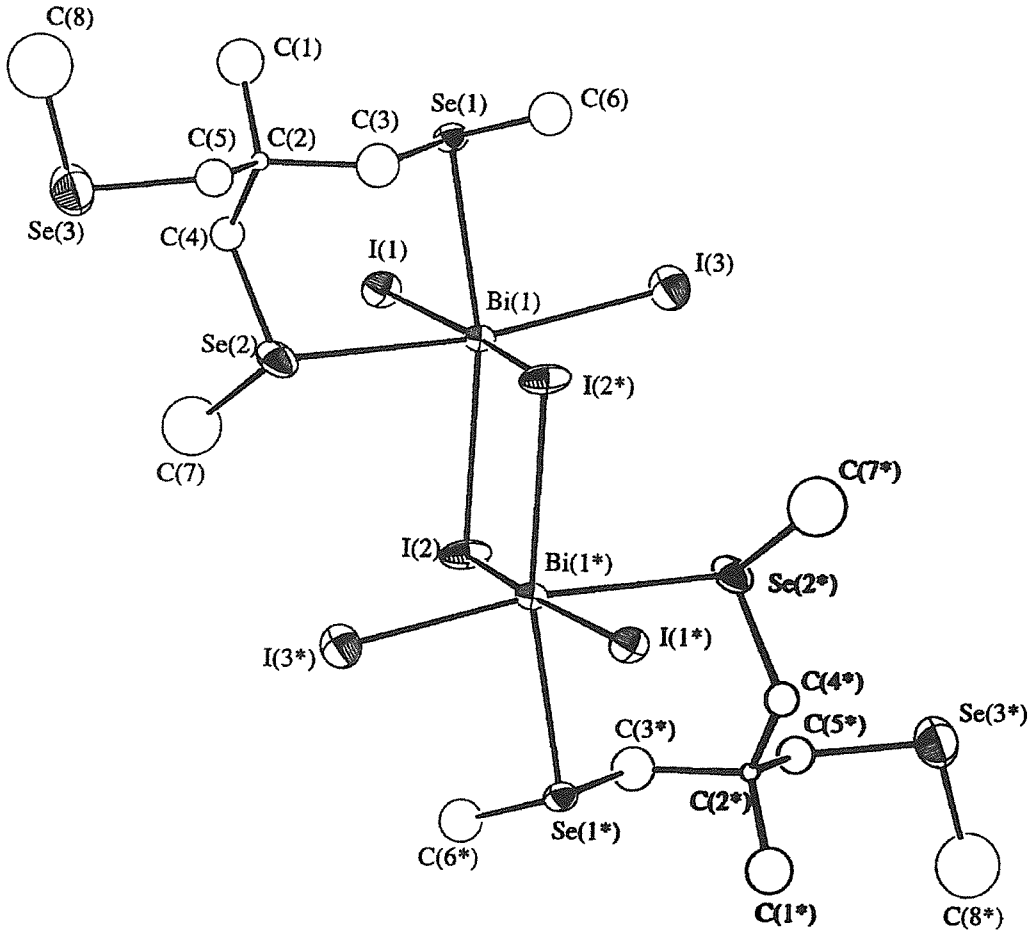

Figure 5.22 – View of the structure of $[Bi_2I_6\{MeC(CH_2SeMe)_3\}_2]$ with the numbering scheme adopted.

Soon after the publication of the structures discussed above a $BiCl_3$ structure was reported containing the tripodal thioether $MeSi(CH_2SMe)_3$.[44] Crystals obtained by slow evaporation of a saturated acetonitrile solution of $[BiCl_3\{MeSi(CH_2SMe)_3\}]$ exhibit an extended structure, with each asymmetric unit consisting of a dinuclear Bi_2Cl_6 group and two bridging unidentate/bidentate thioether ligands in a similar manner to $[Bi_2Cl_6\{MeC(CH_2SeMe)_3\}_2]$ (Figure 5.21). However, in contrast to the seven-coordinate selenoether species, this example shows two six-coordinate bismuth centres which are linked by a single chloro ligand. The complex could be envisioned as a dinuclear derivative of stoichiometry $[Bi_2Cl_6\{MeSi(CH_2SMe)_3\}_2]$. There are two distinctive coordination environments for the bismuth centres: (i) BiS_3X_3, with one arm of a thioether ligand and two from another bonded to a $BiCl_3$ centre, as for Bi(1), and (ii) BiS_2X_4, with two arms of a thioether ligand and the bridging Cl atom attached to the other $BiCl_3$ moiety, as in Bi(2). This binding mode of $MeSi(CH_2SMe)_3$ has been observed before in Cu(I) coordination polymers.[45]

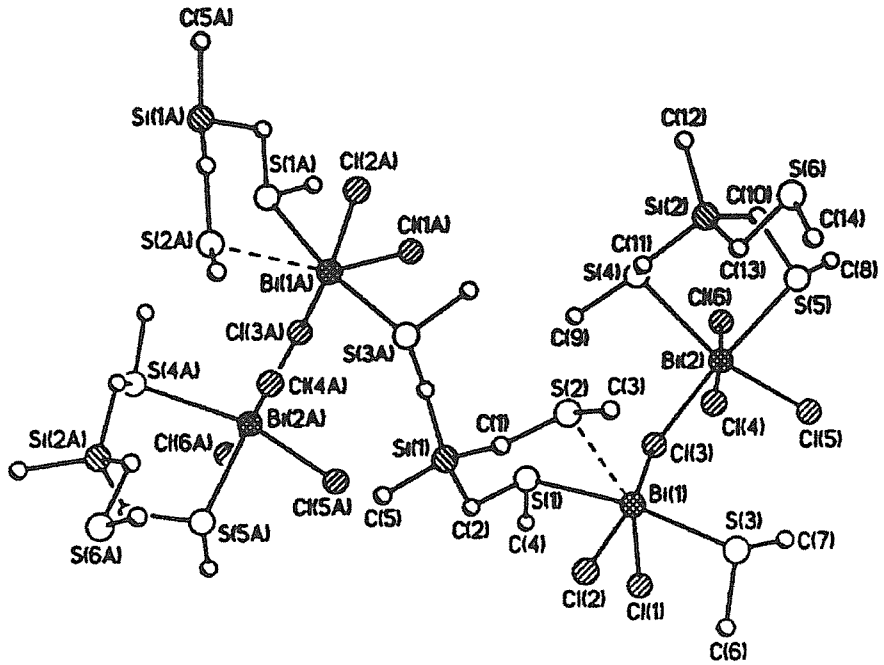

Figure 5.23 – Two repeating units of the extended structure of $[Bi_2Cl_6\{MeSi(CH_2SMe)_3\}_2]$ taken from ref. 44

This example adds to the array of structural motifs available in the diverse and interesting chemistry of heavy p-block elements with Group 16 ligands.

As previously mentioned Group 16 ligands have been shown to bind to Ag(I) centres yielding polymeric arrays. An example containing a selenoether ligand is $[Ag_n\{PhSe(CH_2)_3SePh\}_{2n}]^{n+}$ (Figure 5.24). The extended polymeric structure is reported to be a consequence of the length of the methylene backbone of the ligand, enabling the ligand to bridge adjacent metal ions.[40]

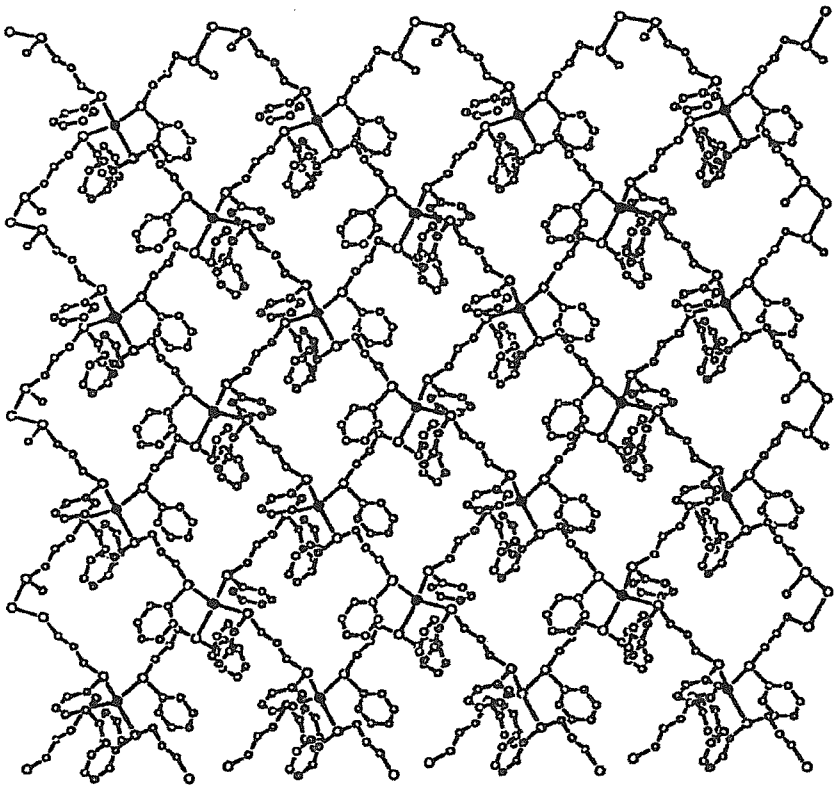

Figure 5.24 – View of a portion of the polymeric structure of $[Ag_n\{PhSe(CH_2)_3SePh\}_{2n}]^{n+}$ taken from ref. 40

5.2.3 Synthesis and Structures of Macrocyclic Selenoether Compounds of BiX_3

Reaction of BiX_3 (X = Cl or Br) with one molar equivalent of [8]aneSe_2 in anhydrous MeCN solution yields yellow solutions from which microcrystalline, air-stable, red powders with stoichiometry [BiX_3([8]aneSe_2)] were obtained. Similarly, reaction of BiX_3 with one molar equivalent of [16]aneSe_4 or [24]aneSe_6 in anhydrous MeCN yields deep orange [BiX_3([16]aneSe_4)], bright yellow [BiX_3([16]aneS_4)] or yellow-orange [BiX_3([24]aneSe_6)]. The IR spectra of the chloro derivatives show several features in the range 230-280 cm^{-1} which are probably associated with ν(Bi-Cl). Owing to the poor solubilities of the compounds in non-coordinating solvents, UV-visible spectra were recorded by diffuse reflectance. The spectra reveal only ill defined absorptions tailing from the UV into the visible region. Similarly, it was not possible to obtain useful NMR spectroscopic data (^1H or $^{77}Se\{^1H\}$) due to the poor solubilities. Attempts to heat these solutions to increase the solubility results in decomposition, while dissolution in coordinating solvents readily displaces the selenoether ligand. Similar problems were encountered in the Group 16 tridentate ligand complexes mentioned above and in other dithioether and diselenoether complexes of Bi(III).[34]

5.2.4 Single Crystal X-ray Diffraction Studies

A crystal structure determination was undertaken on [$BiCl_3$([8]aneSe_2)] in order to determine the structural arrangement present and to provide a comparison with the closest acyclic selenoether analogue, the recently reported [$BiCl_3${$MeSe(CH_2)_3SeMe$}], the structure of which was discussed earlier. Crystals of [$BiCl_3$([8]aneSe_2)] were obtained by slow evaporation from a solution of the complex in MeCN. The structure shows (Figure 5.25, Tables 5.5 and 5.6) an infinite one-dimensional ladder structure derived from almost coplanar Bi_2Cl_6 'rungs' which are linked by four bridging [8]aneSe_2 'uprights'. The Se-donor atoms adopt mutually *trans* coordination sites on each Bi ion, giving Bi-Se 2.977(4) – 3.067(4) Å. It is interesting that complexes of the form

$[Bi_2X_6L_4]$ and $[Bi_2X_6(L\text{-}L)_2]$ (L and L-L = phosphine ligands) invariably adopt bioctahedral structures in which the L and L-L ligands occupy mutually *cis* coordination sites.[11,16] Examples of related bismuth(III) halide compounds incorporating *trans* related ligands (as in the example above) are much rarer. The $Bi\text{-}Cl_{terminal}$ bond distances of *ca.* 2.5 Å and $Bi\text{-}Cl_{bridging}$ distances of *ca.* 2.8 Å are similar to those observed in other related chlorobismuth species. The structure adopted by this [8]aneSe$_2$ complex may be compared with that of $[BiCl_3\{MeSe(CH_2)_3SeMe\}]$. Rather than one-dimensional network seen for $[BiCl_3([8]aneSe_2)]$, $[BiCl_3\{MeSe(CH_2)_3SeMe\}]$ adopts an infinite two-dimensional sheet structure in which staggered Bi_2Cl_6 units are linked *via* four different bridging diselenoether ligands; the Se donors are mutually *trans*.[34]

Table 5.4 – Crystallographic data collection and refinement parameters

Complex	**$[BiCl_3([8]aneSe_2)]$**	**$[BiBr_3([16]aneSe_4)]$**
Formula	$C_6H_{12}BiCl_3Se_2$	$C_{12}H_{24}BiBr_3Se_4$
Formula Weight	557.42	932.85
Colour, morphology	red, column	orange, block
Crystal Dimensions/mm	0.40, 0.16, 0.14	0.42, 0.17, 0.14
Crystal System	Monoclinic	Triclinic
Space Group	$P2_1$	P-1
a / Å	9.362(6)	11.963(30
b / Å	12.142(9)	12.022(2)
c / Å	11.356(3)	9.509(2)
α/ °	90	91.30(2)
β/ °	99.67(3)	109.78(2)
γ/ °	90	118.64(2)
V / Å^3	1272(1)	100.7(6)
Z	4	2
$F(000)$	1000	840
D_{calc}/ g cm^{-3}	2.909	2.814
μ(Mo-K_α)/ cm^{-1}	201.53	200.62
Unique observed reflections	2367	3867
Observed reflections with $[I_o > 2\sigma(I_o)]$	1929	2902
No. of parameters	157	181
Goodness of fit	1.855	2.03
R[a]	0.043	0.044
Rw[b]	0.055	0.056

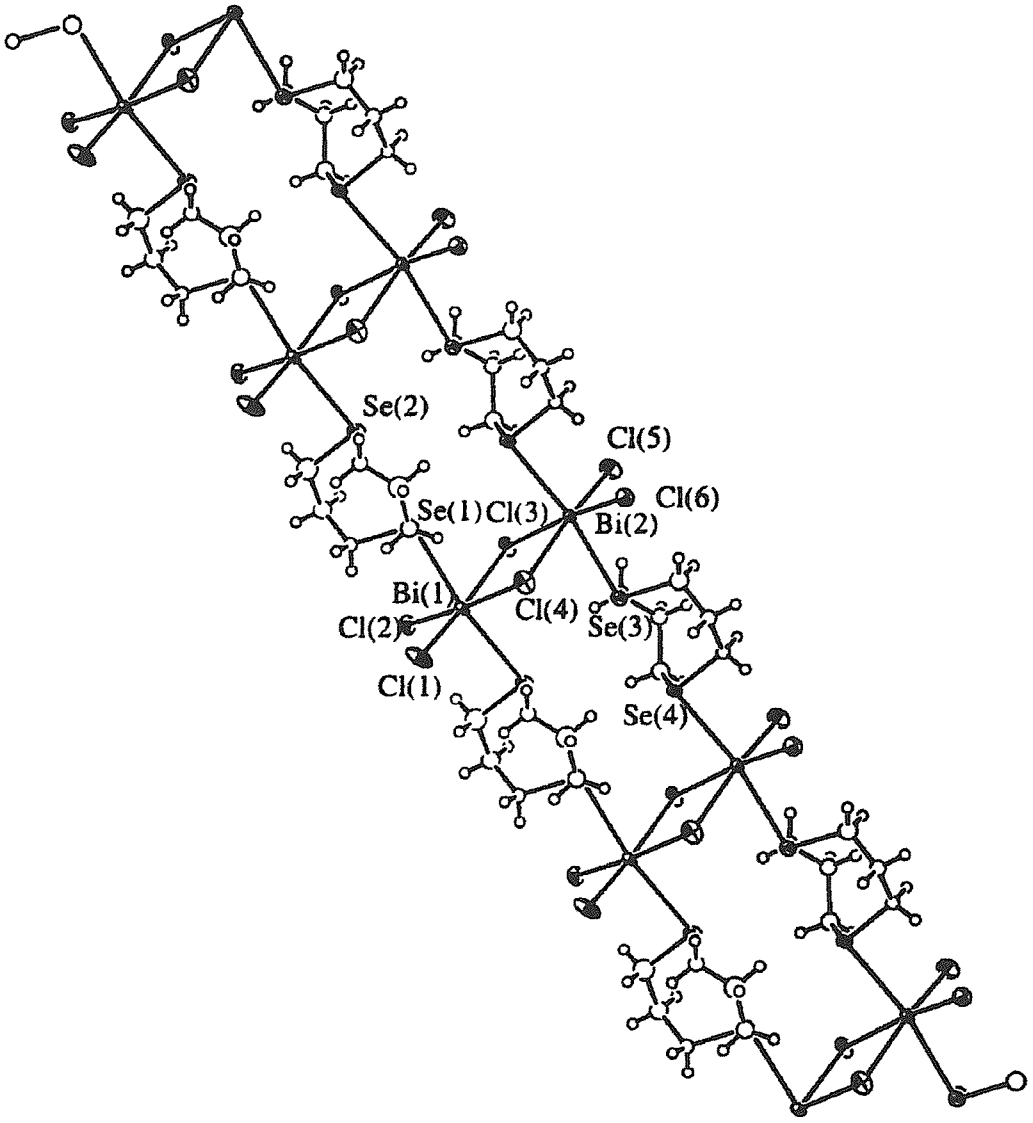

Figure 5.25 – View of a portion of the structure of the infinite 1-dimensional ladder adopted by $[BiCl_3([8]aneSe_2)]$ with the numbering scheme adopted. Ellipsoids are drawn at the 40 % probability level.

Table 5.5 – Selected bond lengths (Å) for $[BiCl_3([8]aneSe_2)]$

Bi(1)	Se(1)	2.988(4)	Bi(2)	Se(3)	2.977(4)
Bi(1)	Se(2)	3.044(4)	Bi(2)	Se(4)	3.067(4)
Bi(1)	Cl(1)	2.61(1)	Bi(2)	Cl(3)	2.836(8)
Bi(1)	Cl(2)	2.522(8)	Bi(2)	Cl(4)	2.95(1)
Bi(1)	Cl(3)	2.77(1)	Bi(2)	Cl(5)	2.50(1)
Bi(1)	Cl(4)	2.832(8)	Bi(2)	Cl(6)	2.573(8)

Table 5.6 – Selected bond angles (degrees) for $[BiCl_3([8]aneSe_2)]$

Se(1)	Bi(1)	Se(2)	171.4(1)
Se(3)	Bi(2)	Se(4)	168.9(1)
Cl(1)	Bi(1)	Cl(2)	93.9(3)
Cl(3)	Bi(1)	Cl(4)	84.5(3)
Cl(3)	Bi(2)	Cl(4)	81.3(2)
Cl(5)	Bi(2)	Cl(6)	94.8(3)
Bi(1)	Cl(3)	Bi(2)	99.0(3)
Bi(1)	Cl(4)	Bi(2)	95.2(3)

A very similar structural motif is observed for the tetraselenoether species $[BiBr_3([16]aneSe_4)]$ (Figure 5.26, Table 5.7). In this case the one-dimensional arrangement is derived from almost planar Bi_2Br_6 units, with each Bi linked to the next Bi_2Br_6 units by bridging $[16]aneSe_4$ ligands. Coordination is *via* one Se-donor atom to each Bi, i.e. μ-bridging $[16]aneSe_4$. The macrocycles are bonded (and therefore bridge) *via* mutually *trans* selenium donors and adopt an exocyclic conformation. Within this centrosymmetric structure each Bi is coordinated *via* a *trans*-Se_2Br_4 donor set, Bi-Se(1) 2.952(2), Bi-Se(3) 3.095(2), Bi-Br(1) 2.693(2), Bi-Br(2) 2.711(2), Bi-Br(3) 3.002(2) and Bi-Br(3*) 3.058(2) Å. The other two mutually *trans* selenium atoms, Se(2) and Se(4), within each $[16]aneSe_4$ unit remain non-coordinating.

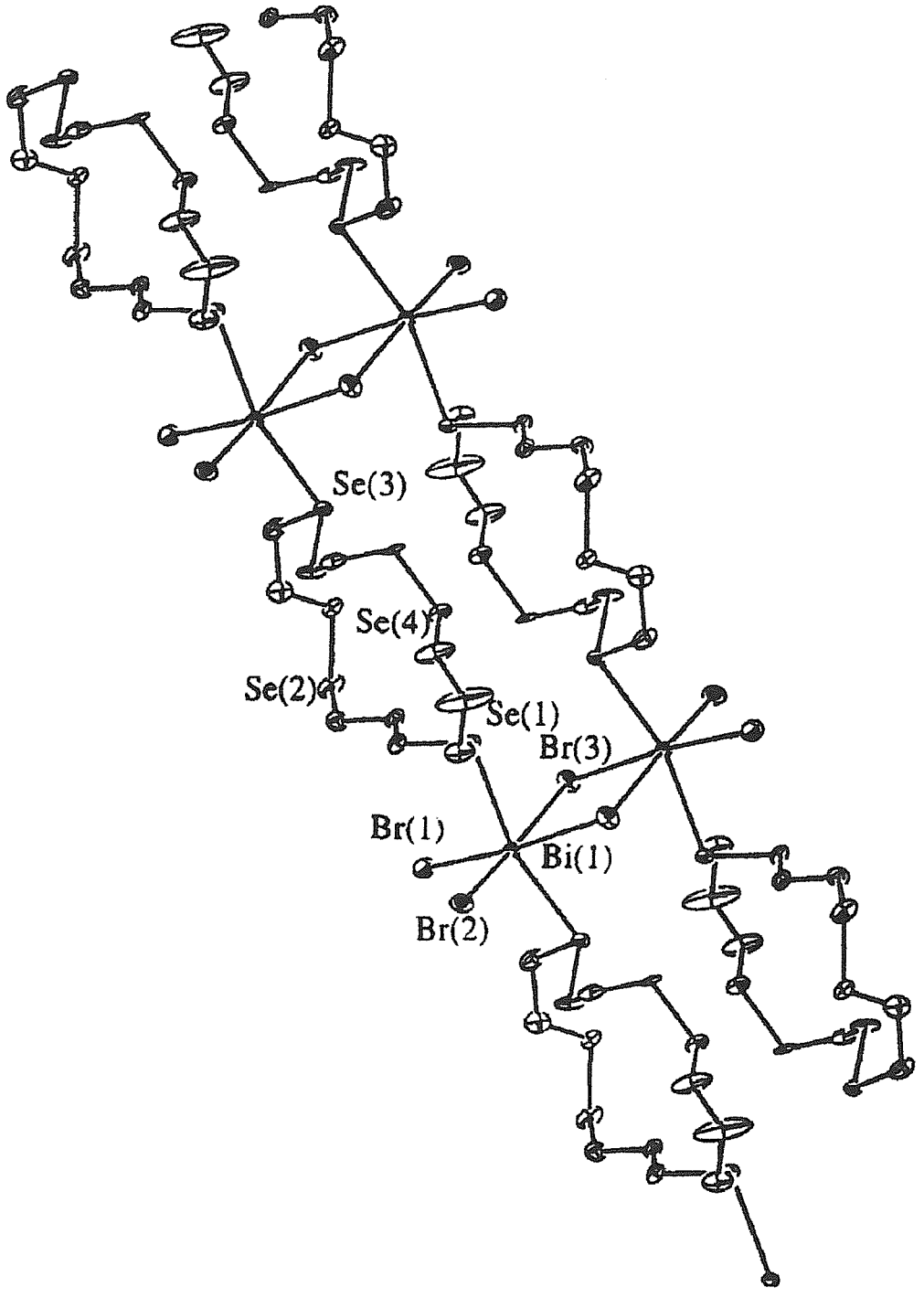

Figure 5.26 – View of the structure of a portion of the infinite 1-dimensional ladder adopted by [$BiBr_3$([16]aneSe_4)] with the numbering scheme adopted. Hydrogen atoms are omitted for clarity and ellipsoids are drawn at the 40% probability level.

Table 5.7 – Selected bond lengths (Å) and angles (degrees) for [$BiBr_3$([16]aneSe_4)]

Bi(1)	Se(1)	2.952(2)	Bi(1)	Br(2)	2.711(2)
Bi(1)	Se(3)	3.095(2)	Bi(1)	Br(3)	3.002(2)
Bi(1)	Br(1)	2.693(2)	Bi(1)	Br(3*)	3.058(2)

Se(1)	Bi(1)	Se(3*)	162.86(4)	Br(3)	Bi(1)	Br(3*)	86.04(5)
Br(1)	Bi(1)	Br(2)	91.16(6)	Bi(1)	Br(3)	Bi(1*)	93.96(5)

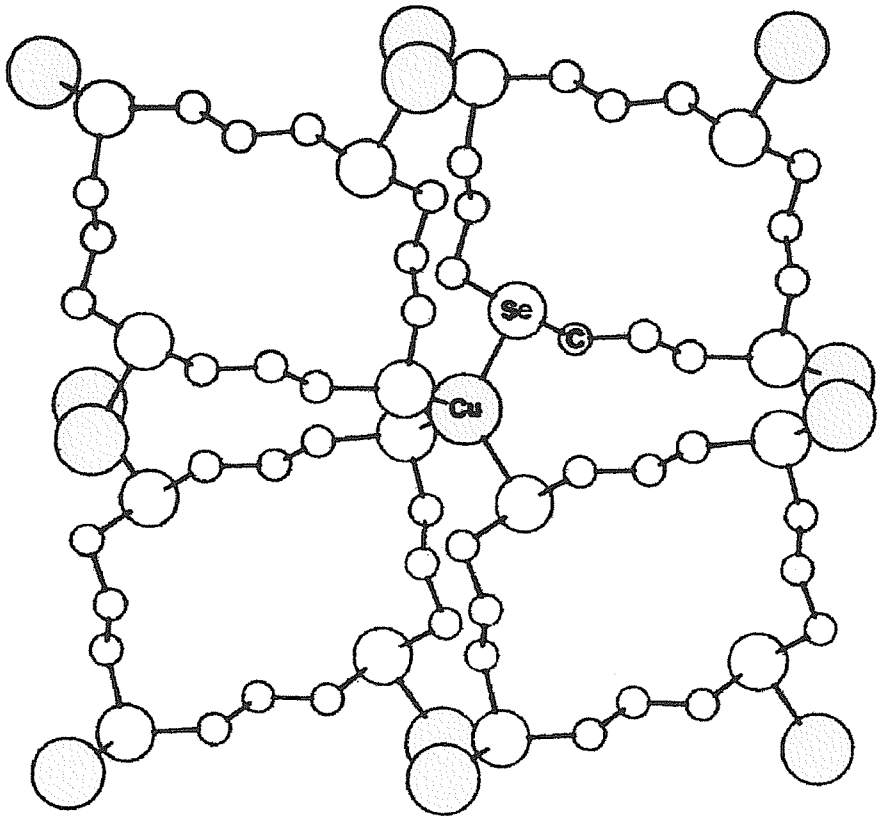

Figure 5.27 – View of the 3-dimensionally polymeric complex cation [Cu([16]aneSe_4)]$^+$ taken from ref. 46

The Bi-Se distances in these two bismuth(III) halogeno compounds incorporating cyclic selenoethers are very similar to those observed in the other structurally characterised bismuth selenoether species, e.g. $[BiX_3\{MeSe(CH_2)_3SeMe\}]$[33] (X = Cl or Br, *d*(Bi-Se) = 2.978(2)-3.0362(2) Å) and the tridentate ligand containing complex discussed earlier $[BiCl_3\{MeC(CH_2SeMe)_3\}]$ (*d*(Bi-Se) = 2.962-3.156(4) Å). The stereochemical activity of the Bi-based lone pair appears to be minimal in the new compounds. It is also noteworthy that while the compounds reported here are the first structurally characterised macrocyclic selenoether complexes involving bismuth, there are also only two other structurally characterised species which involve exocyclic [16]aneSe$_4$, they are $[Cu_n([16]aneSe_4)_n]^{n+}$ reported by Pinto and co-workers[46] (Figure 5.26) and the antimony(III) complex discussed in Chapter 6 $[(SbBr_3)_2([16]aneSe_4)]$.[47]

In view of the potential availability of the two remaining Se atoms, Se(2) and Se(4), in $[BiBr_3([16]aneSe_4)]$ for coordination, attempts were made to establish whether it might be possible to cross-link the chains of $[BiBr_3([16]aneSe_4)]$ through coordination of additional Bi to these atoms. However, treatment of $[BiBr_3([16]aneSe_4)]$ with one molar equivalent of $BiBr_3$ in MeCN solution gave no apparent reaction. Similarly, treatment of [24]aneSe$_6$ with two molar equivalents of BiX_3 yields only 1:1 species $[BiX_3([24]aneSe_6)]$, although this may simply reflect the lower solubility of the 1:1 species.

As stated previously several macrocyclic thioether complexes of $BiCl_3$ have been reported, including $[BiCl_3([12]aneS_4)]$, $[BiCl_3([15]aneS_5)]$, $[BiCl_3([18]aneS_6)]$ and $[(BiCl_3)_2([24]aneS_8)]$. Without exception, these adopt discrete molecular structures. In fact, all of the structurally characterised bismuth(III) halogeno complexes involving crown ethers and crown thioethers reflect the dominance of the pyramidal BiX_3 unit on the structures adopted, with weak Bi-O or Bi-S interactions replacing the secondary Bi-X interactions in the parent trihalides, generating 7-, 8- or 9-coordinate compounds.[20,36,37,48] A stereochemically active lone pair on the Bi, directed towards the weakly interacting S- or O-donors, is implied for these species. The selenoether

macrocyclic complexes reported here are therefore markedly different in their coordination modes and geometries from those of the lighter Group 16 analogues, generating infinite chain structures. In view of these results a decision was made to investigate the factors which influence the structures adopted. The group have noted previously that while ligands of the form $MeE(CH_2)_2EMe$ (E = S or Se) typically yield chelate complexes, introduction of an additional CH_2 unit (in $MeE(CH_2)_3EMe$) can lead to a tendency to bridge metal centres, e.g. in $[Ag_n\{MeE(CH_2)_3EMe\}_{2n}]^{n+}$ and in the bismuth(III) species $[BiX_3\{MeE(CH_2)_3EMe\}]$. Since macrocyclic selenoether ligands involving dimethylene linkages are unstable (these would otherwise provide the direct analogues of the macrocyclic thioether complexes above), an alternative strategy was adopted, to investigate the coordination of [16]aneS_4 (the direct analogue of [16]aneSe_4) with BiX_3. The 1:1 complexes $[BiX_3([16]aneS_4)]$ were obtained in good yield, however considerable efforts to obtain crystals suitable for a structure analysis, have not been successful.

5.3 CONCLUSIONS

For the tripodal ligands $MeC(CH_2SMe)_3$ and $MeC(CH_2SeMe)_3$, the anticipated formation of a discrete octahedral species, $[BiX_3L_3]$, was not forthcoming and in contrast, the occurrence of the dinuclear Bi_2X_6 subunit is observed. This results in the selenoether ligand functioning as a bidentate chelate and, in the case of $[BiCl_3\{MeC(CH_2SeMe)_3\}]$, the third arm bridging to an adjacent Bi. This structure is one of the first bismuth-selenoether species which adopt infinite, polymeric structures. The crystals of $[Bi_2I_6\{MeC(CH_2SeMe)_3\}_2]$ exhibit a discrete dimeric species analogous to the literature examples of dimethylene linked diphosphine complexes. Both of the compounds reported here adopt topologies that are markedly different in structure from the thiacrown bismuth(III) derivatives reported previously.

The results obtained from the studies involving macrocyclic selenoethers show that cyclic selenoethers serve to add to the structural diversity and contrast with those identified for the acyclic selenoether complex analogue. The structure adopted by the [8]aneSe$_2$ and the [16]aneSe$_4$ complexesare infinite 1-dimensional ladders which display the edge-shared, bioctahedral Bi_2X_6 dimers identified in other bismuth(III) halide complexes. This is in stark contrast to the structures determined for bismuth(III) halogeno complexes involving crown ethers and crown thioethers which reflect the dominance of the pyramidal BiX_3 unit, with weak Bi-O or Bi-S interactions replacing the secondary Bi-X interactions in the parent trihalides.

Clearly more work is needed to investigate the factors which govern the topologies adopted by these bismuth(III) adducts. The structures obtained during these studies refer to compounds from which it was possible to grow crystals suitable for X-ray characterisation. Different conditions e.g. solvents may lead to different structural motifs.

5.4 EXPERIMENTAL

5.4.1 Ligand and Complex Synthesis

The bismuth(III) chloride, bromide and iodide, [16]aneS$_4$ and anhydrous CH_2Cl_2 were purchased from Aldrich Chemicals. The ligands $MeC(CH_2SMe)_3$, $MeC(CH_2SeMe)_3$, [8]aneSe$_2$, [16]aneSe$_4$ and [24]aneSe$_6$ were all produced by literature methods.[49,50,51]

a). Synthesis of [$BiCl_3${$MeC(CH_2SMe)_3$}]

The compound $BiCl_3$ (0.11 g, 0.35 mmol) was treated with $MeC(CH_2SMe)_3$ (0.08 g, 0.35 mmol) in MeCN (10 cm^3) to give a yellow solid (yield 0.04 g, 35 %). Required for [$C_8H_{18}BiCl_3S_3$]: C = 14.6, H = 2.7 %; found: C = 14.4; H = 2.5 %. IR spectrum (Nujol mull, CsI plates): 233, 246 cm^{-1}.

b). Synthesis of [$BiCl_3${$MeC(CH_2SeMe)_3$}]

Method as for [$BiCl_3${$MeC(CH_2SMe)_3$}] but using $BiCl_3$ (0.11 g, 0.35 mmol) and $MeC(CH_2SeMe)_3$ (0.12 g, 0.35 mmol) to give a yellow solid (yield 0.18 g, 77 %). Required for [$C_8H_{18}BiCl_3Se_3$]: C = 14.4, H = 2.7; found: C = 14.0, H = 2.8 %. IR spectrum (Nujol mull, CsI plates): 230, 246.

c). Synthesis of [$BiBr_3${$MeC(CH_2SeMe)_3$}]

Method as for [$BiCl_3${$MeC(CH_2SMe)_3$}] but using $BiBr_3$ (0.16 g, 0.35 mmol) and $MeC(CH_2SeMe)_3$ (0.11 g, 0.35 mmol) to give a yellow-orange solid (yield 0.07 g, 46 %). Required for [$C_8H_{18}BiBr_3Se_3$]: C = 12.0, H = 2.3; found: C = 12.3, H = 2.4 %.

d). Synthesis of [BiI_3{$MeC(CH_2SeMe)_3$}]

Method as for [$BiCl_3${$MeC(CH_2SMe)_3$}] but using BiI_3 (0.21 g, 0.35 mmol) and $MeC(CH_2SeMe)_3$ (0.11 g, 0.35 mmol) to give a dark red solid (yield 0.13 g, 38 %). Required for [$C_8H_{18}BiI_3Se_3$]: C = 10.2, H = 1.9; found: C = 10.0, H = 1.7 %.

e). Synthesis of [$BiCl_3$([8]aneSe_2)]

A solution of $BiCl_3$ (0.16 g, 0.52 mmol) in dry, degassed MeCN (4 cm^3) was added to a stirred solution of [8]aneSe_2 (0.24 g, 1.04 mmol) in CH_2Cl_2 (2 cm^3) at room temperature. A yellow solution formed almost immediately. Concentrating the solution *in vacuo* gave a red solid which was filtered off, washed with CH_2Cl_2 and dried *in vacuo* (yield 0.157 g, 55 %). Required for [$C_6H_{12}BiCl_3Se_2$]: C = 13.0, H = 2.2 %; found: C = 13.2, H =2.2 %. IR spectrum (Nujol, CsI): 244, 258, 273 cm^{-1}.

f). Synthesis of [$BiBr_3$([8]aneSe_2)]

Method as for [$BiCl_3$([8]aneSe_2)] but using $BiBr_3$ (0.23 g, 0.52 mmol) and [8]aneSe_2 (0.24 g, 1.04mmol) to give a red solid (yield 0.24 g, 66 %). Required for [$C_6H_{12}BiBr_3Se_2$]: C = 10.4, H = 1.7 %; found: C = 10.7, H = 1.9 %.

g). Synthesis of [$BiCl_3$([16]aneSe_4)]

Method as for [$BiCl_3$([8]aneSe_2)] but using $BiCl_3$ (0.16 g, 0.52 mmol) and [16]aneSe_4 (0.25 g, 0.52 mmol) to give a deep orange solid (yield 0.15 g, 35 %). Required for [$C_{12}H_{24}BiCl_3Se_4$]: C = 18.0, H = 3.0 %; found: C = 18.2, H = 3.0 %. IR spectrum (Nujol, CsI): 247 and 256 cm^{-1}.

h). Synthesis of [$BiBr_3$([16]aneSe_4)]

Method as for [$BiCl_3$([8]aneSe_2)] but using $BiBr_3$ (0.23 g, 0.52 mmol) and [16]aneSe_4 (0.25 g, 0.52 mmol) to give an orange solid (yield 0.30 g, 60 %). Required for [$C_{12}H_{24}BiBr_3Se_4$]: C = 15.4, H = 2.6 %; found: C = 15.5, H = 2.6 %.

i). Synthesis of [$BiCl_3$([24]aneSe_6)]

Method as for [$BiCl_3$([8]aneSe_2)] but using $BiCl_3$ (0.16 g, 0.52 mmol) and [24]aneSe_6 (0.19 g, 0.26 mmol) to give a yellow solid (yield 0.16 g, 60 %). Required for [$C_{18}H_{36}BiCl_3Se_6$]: C = 20.5, H = 3.2 %; found: C = 20.5, H = 3.2 %. IR spectrum (Nujol, CsI): 235 and 255 cm^{-1}.

j). Synthesis of [$BiBr_3$([24]aneSe_6)]

Method as for [$BiCl_3$([8]aneSe_2)] but using $BiBr_3$ (0.23 g, 0.52 mmol) and [24]aneSe_6 (0.19 g, 0.26 mmol) to give an orange solid (yield 0.17 g, 57 %). Required for [$C_{18}H_{36}BiBr_3Se_6$]: C = 18.4, H = 3.1 %; found: C = 18.0, H = 2.8 %.

k). Synthesis of [$BiCl_3$([16]aneS_4)]

Method as for [$BiCl_3$([8]aneSe_2)] but using $BiCl_3$ (0.16 g, 0.52 mmol) and [16]aneS_4 (0.15 g, 0.52 mmol) to give a bright yellow solid (yield 0.22 g, 68 %). Required for [$C_{12}H_{24}BiCl_3S_4$]: C = 23.6, H = 3.9 %; found: C = 24.0, H = 3.9 %. IR spectrum (Nujol, CsI): 264 and 271 cm^{-1}.

l). Synthesis of [$BiBr_3$([16]aneS_4)]

Method as for [$BiCl_3$([8]aneSe_2)] but using $BiBr_3$ (0.23 g, 0.52 mmol) and [16]aneS_4 (0.15 g, 0.52 mmol) to give a bright yellow solid (yield 0.36 g, 92 %). Required for [$C_{12}H_{24}BiBr_3S_4$]: C = 19.3, H = 3.2 %; found: C = 19.6, H = 3.0 %.

5.4.2 X-ray Crystallography

Crystals were obtained by slow evaporation from solutions of the appropriate complexes in MeCN. Data collection used a Rigaku AFC7S four-circle diffractometer and graphite-monochromated Mo-Kα X-radiation (λ = 0.71073 Å) at 150 K.

[$BiCl_3${$MeC(CH_2SeMe)_3$}]

Details of the crystallographic data collection and refinement parameters are given in Tables 5.1. The data were corrected for absorption using ψ-scans. The structure was solved by heavy atoms method[52] and developed by iterative cycles of full-matrix least-squares refinement and Fourier difference syntheses.[53] All fully occupied non-H atoms were refined anisotropically.

[$BiCl_3$([8]aneSe_2)] and [$BiBr_3$([16]aneSe_4)]

Details of the crystallographic data collection and refinement parameters are given in Table 5.4. Structure solution and refinement were solved by direct methods[54] and developed by iterative cycles of full-matrix least-squares refinement and Fourier difference syntheses. For [$BiCl_3$([8]aneSe_2)] a Bi_2Cl_6 unit and two [8]aneSe_2 ligands were identified in the asymmetric unit. Attempts to refine these C atoms anisotropically led to non-positive definite thermal parameters, presumably since the scattering is dominated by the heavy Bi and Se atoms. The C atoms were therefore refined isotropically for the [8]aneSe_2 structure. The Flack parameter confirmed the correct choice of enantiomorph for this species.[55]

5.5 REFERENCES

1. W. Kwasnik, '*Handbook of Preparative Inorganic Chemistry*', Vol.1, Academic Press, London, 1963.
2. P.W. Schenk, '*Handbook of Preparative Inorganic Chemistry*', Vol.1, Academic Press, London, 1963, 621
3. A. Haaland, J. Houghen, S. Samdal and J. Tremmel, *Acta Chem. Scand.*, 1988, **42A**, 409.
4. S.C. Nyburgm G.A. Ozin and J.T. Szymanski, *Acta Cryst.*, 1971, **B27**, 2298.
5. '*Handbook of Preparative Inorganic Chemistry*', Vol.1, P.W. Schenk, Academic Press, London, 1963, 623.
6. H.A. Skinner and L.E. Sutton, *Trans. Faraday Soc.*, 1940, **36**, 681.
7. H. von Benda, *Z. Kristallogr.*, 1980, **151**, 271.
8. G.W. Watt, W.W. Hakki and G.R. Choppin, *Inorg. Syn.*, 1953, **4**, 114.
9. J. Trotter and T. Zobel, *Z. Kristallogr.*, 1966, **123**, 67.
10. '*Advanced Inorganic Chemistry*', F.A. Cotton, G. Wilkinson, C.A. Murillo and M. Bochmann, 6th Edition, Wiley, London, 1999.
11. N.C. Norman and N.L. Picket, *Coord. Chem. Rev.*, 1995, **145**, 27.
12. '*Chemistry of Arsenic, Antimony and Bismuth,*' N.C. Norman (Ed.), Blackie, New York, 1997, p. 159.
13. G. Alonzo, M. Consiglio, N. Bertazzi and C. Preti, *Inorg. Chim. Acta*, 1985, **105**, 51.
14. G.R. Willey, L.T. Daly and M.D. Rudd, *Polyhedron*, 1995, **14**, 315.
15. R. Luckay, I. Cukrowski, J. Mashishi, J.H. Reibenspies, A.H. Bond, R.D. Rogers and R.D. Hancock, *J. Chem. Soc., Dalton Trans.*, 1997, 901.
16. W. Clegg, M.R.J. Elsegood, W. Graham, N.C. Norman, N.L. Pickett and K. Tavakkoli, *J. Chem. Soc., Dalton Trans.*, 1994, 1743.
17. G.R. Willey, L.T. Daly and M.G.B. Drew, *J. Chem. Soc., Dalton Trans.*, 1996, 1063.
18. G.J. Sutton, *Aust. J. Chem.*, 1958, **11**, 415.

19. N.W. Alcock, M. Ravindran and G.R. Willey, *J. Chem. Soc., Chem. Commun.*, 1989, 1063.
20. R.D. Rogers, A.H. Bond, S. Aguinaga and A. Reyes, *J. Am. Chem. Soc.*, 1992, **114**, 2967.
21. N.W. Alcock, M. Ravindran and G.R. Willey, *Acta Crystallogr., Sect. B*, 1993, **49**, 507.
22. R. Weber, H. Kosters and G. Bergerhoff, *Z. Kristallogr.*, 1993, **207**, 175.
23. M.G.B. Drew, D.G. Nicholson, I. Sylte and A. Vasudevan, *Inorg. Chim. Acta*, 1990, **171**, 11.
24. J.R. Eveland and K.H. Whitmire, *Inorg. Chim. Acta*, 1996, **249**, 41.
25. C.J. Carmalt, W. Clegg, M.R.J. Elsegood, R.J. Errington, J. Havelock, P. Lightfoot, N.C. Norman and A.J. Scott, *Inorg. Chem.*, 1996, **35**, 3709.
26. P.G. Jones, D. Henschel, A. Weitze and A. Blaschette, *Z. Anorg. Allg. Chem.*, 1994, **620**, 1037.
27. G.A. Bowmaker, J.M. Harrowfield, P.C. Junk, B.W. Skelton and A.H. White, *Aust. J. Chem.*, 1998, **51**, 285.
28. F. Knodler, W. Schwartz and A. Schmidt, *Z. Naturforsch., Teil B.*, 1987, **42**, 1282.
29. E.G. Hope and W. Levason, *Coord. Chem. Rev.*, 1993, **122**, 109.
30. S.E. Dann, A.R.J. Genge, W. Levason and G. Reid, *J. Chem. Soc., Dalton Trans.*, 1996, 4471.
31. S.E. Dann, A.R.J. Genge, W. Levason and G. Reid, *J. Chem. Soc., Dalton Trans.*, 1997, 2207.
32. A.R.J. Genge, W. Levason and G. Reid, *J. Chem. Soc., Dalton Trans.*, 1997, 4549.
33. A.R.J. Genge, W. Levason and G. Reid, *J. Chem. Soc., Chem. Commun.*, 1998, 2159.
34. A.J. Barton, A.R.J. Genge, W. Levason and G. Reid, *J. Chem. Soc., Dalton Trans.*, 2000, 859.
35. W. Clegg, N.C. Norman and N.L. Pickett, *Polyhedron*, 1993, **12**, 1251.

36. G.R. Willey, M.T. Lakin and N.W. Alcock, *J. Chem. Soc., Dalton Trans.*, 1992, 591.

37. G.R. Willey, M.T. Lakin and N.W. Alcock, *J. Chem. Soc., Dalton Trans.*, 1992, 1339.

38. A.J. Fenske, W-S. Li, V. Lippolis and M. Schröder, *J. Chem. Soc., Dalton Trans.*, 1998, 3968.

39. J.F. Sawyer and R.J. Gillespie, *Prog. Inorg. Chem.*, 1986, **34**, 65.

40. J.R. Black, N.R. Champness, W. Levason and G. Reid, *J. Chem. Soc., Dalton Trans.*, 1995, 3439.

41. J.R. Black, N.R. Champness, W. Levason and G. Reid, *Inorg. Chem.*, 1996, **35**, 1820.

42. J.R. Black, N.R. Champness, W. Levason and G. Reid, *Inorg. Chem.*, 1996, **35**, 4432.

43. G.R. Willey, M.D. Rudd, C.J. Samuel and M.G.B. Drew, *J. Chem. Soc., Dalton Trans.*, 1995, 759.

44. H.-W. Yim, K. Lam, A.L. Rheingold and D. Rabinovich, *Polyhedron*, 2000, **19**, 849.

45. H.-W. Yim, L.-M. Tran, E.E. Pullen, D. Rabinovich, L.M. Liable-Sands, T.E. Concolino and A.L. Rheingold, *Inorg. Chem.*, 1999, **38**, 6235.

46. R.J. Batchelor, F.W.B. Einstein, I.D. Gay, J.-H. Gu and B.M. Pinto, *J. Organomet. Chem.*, 1991, **411**, 147.

47. A.J. Barton, N.J. Hill, W. Levason and G.Reid, *J. Chem. Soc., Chem. Commun., submitted.*

48. A.J.Blake, D. Fenske, W.-S. Li, V. Lippolis and M. Schroder, *J. Chem. Soc., Dalton. Trans.*, 1998, 3961.

49. R. Ali, S.J. Higgins and W. Levason, *Inorg. Chim. Acta*, 1984, **84**, 65.

50. D.J. Gulliver, E.G. Hope, W. Levason, S.G. Murray, D.M. Potter and G.L. Marshall, *J. Chem. Soc., Perkin Trans. II*, 1984, 429.

51. R.J. Batchelor, F.W.B. Einstein, I.D. Gay, J.H. Gu, B.D. Jonston and B.M. Pinto, *J. Am. Chem. Soc.*, 1989, **111**, 6582.

52. PATTY, The DIRDIF Program System, P.T. Beurskens, G. Admiraal, G. Beurskens, W.P. Bosman, S. Barcia-Granda, R.O. Gould, J.M.M. Smits and C. Smykalla, Technical Report of the Crystallography Laboratory, University of Nijmegen, 1992.
53. TEXSAN, Crystal Structure Analysis Package, Molecular Structure Corporation, Houston, TX, 1995.
54. SHELX 86, G.M. Sheldrick, *Acta Crystallogr., Sect. A*, 1990, **46**, 467.
55. H.D. Flack, *Acta Crystallogr., Sect. C.*, 1983, **39**, 876.

CHAPTER 6

Antimony(III) Halide Complexes of Tridentate and Macrocyclic Group 16 Ligands

6.1 INTRODUCTION

The aim of this chapter was to investigate the complexation of a range of tridentate and macrocyclic Group 16 ligands with antimony(III) halides. An emphasis was placed on obtaining single crystal structural data to permit detailed comparisons with the bismuth(III) species in Chapter 5.

There has been substantial interest for some time in the synthesis and properties of thio-, seleno- and telluro-ether ligands and the coordination chemistry of these with a wide range of d-block elements has been investigated by the research group in Southampton and others.[1] However, derivatives of the p-block elements are much less known. This imbalance has been slightly addressed by work into Sn(IV) and the Bi(III), the latter being discussed in Chapter 5.[2-7] A wide range of structural motifs has been discovered for Bi(III) halide complexes with Group 16 ligands and hence we were interested to investigate the chemistry of Sb(III) halides with these ligands.

The similarities between antimony and bismuth stem from the similar electron configuration and the electronegativities of the elements of Group 15. Despite being in the same group, however, the properties of the elements vary to a considerable degree as the group is descended. Thus, using values from either the Pauling or Allred-Rochow scales of electronegativity (amongst the two most widely used), it can be seen that antimony should be considered, together with bismuth (which has the lowest electronegativity of all Group 15 elements), as metallic. The two elements have similar values for electronegativity (χ(Pauling) 2.05, 2.02 and χ(Allred-Rochrow) 1.82 and 1.67 respectively). It should be noted that the similarity in electronegativity of the two elements is a result of bismuth having a higher than expected value. This apparent anomaly derives from the filling of the 4f orbitals prior to bismuth which leads to a higher effective nuclear charge as a result of inefficient screening of the nuclear charge by the 4f electrons. Therefore, investigations into the chemistry of bismuth(III) should be accompanied by subsequent studies into analogous antimony species.

The Lewis acidity of the elements in the +3 oxidation state is perhaps less well appreciated since the presence of a lone pair of electrons generally leads to the expectation of Lewis basic behaviour, which is well documented. For antimony (and bismuth) in the +3 oxidation state, it is apparent that whatever basicity such compounds may exhibit, a considerable degree of Lewis acidity is also evident especially where the Group 15 element is bonded to significantly more electronegative atoms or groups. Thus, antimony (and bismuth) trihalides are sufficiently Lewis acidic to exhibit quite an extensive coordination chemistry with ligands such as phosphines (PR_3) and phosphine oxides (OPR_3).[8,9]

SbX_3 are stable compounds which are readily available by straightforward syntheses. SbF_3 is relatively less reactive than the other antimony(III) halides. $SbCl_3$ shares the same pyramidal molecular structure as $BiCl_3$ in the vapour phase,[10] whilst in solid $SbCl_3$ the antimony,[11] like bismuth,[12] has three short E-Cl bonds and five longer-distance interactions. However, although both have bicapped trigonal prismatic geometries (ECl_8 units), the ratio of the three short Sb-Cl bond lengths to the five longer Sb-Cl bond lengths is greater than the corresponding ratio in the case of bismuth. This coupled with the greater radius of the bismuth(III) over antimony(III) leads to the greater tendency for bismuth to adopt stronger secondary bonding and higher coordinating numbers. Antimony(III) chloride forms a clear solution with water, dilution results in precipitation of insoluble oxychlorides of various compositions, for example SbOCl, $Sb_4O_5Cl_2$ and $Sb_8O_{11}Cl_2$. Prior to reactions with $SbCl_3$, discussed in this chapter, the trihalide was purified to remove the unwanted oxychloride species. Antimony tribromide has been shown to be pyramidal in the gas phase and the solid phase exists in two forms as α-$SbBr_3$[13] and β-$SbBr_3$,[14] as observed for $BiBr_3$.[15] The solid-phase structure of antimony triiodide shows a slightly distorted octahedron (*c.f.* symmetrical octahedral in BiI_3).[16] The pnictogen atom progressively moves to the centre of the I_6 octahedron as Group 15 is descended. Antimony triiodide has two crystal modifications, the red trigonal crystalline form just described and a greenish-yellow monoclinic phase.[17] The structure of monoclinic SbI_3 is intermediate

between the trigonal (close-packed iodine layers) and a layered molecular structure with discrete SbI_3 units forming strongly distorted SbI_6 octahedra.

The chemistry of Group 15 donor ligands with antimony(III) halides has been investigated. Complexes containing nitrogen donors, for example $[SbCl_3(PhNH_2)]$ and $[SbCl_3(N_2C_{10}H_8)]$ ($N_2C_{10}H_8$ = 2,2-bipyridyl) have had their structures determined. The structure of the former adopts a disphenoidal geometry with the stereochemically active lone pair on the antimony lying in the equatorial plane.[18] In contrast, the 1:1 complex formed between antimony(III) chloride and 2,2-bipyridyl, $[SbCl_3(N_2C_{10}H_8)]$, exhibits a weakly associated dimeric structure in which the antimony(III) centres adopt a distorted octahedral geometry.[19]

Until recently complexes of antimony(III) containing tertiary phosphine ligands were virtually unknown, although their possible existence was indicated by early workers principally from NMR studies.[20,21] No X-ray crystallographic information was available until 1993 when Norman and co-workers reported the ionic complex $[H(py)_2][SbI_4(dmpe)]$ which was prepared serendipitously from the dissolution of a compound of formula $[SbI_3(dmpe)]$ in pyridine.[22] Further examples of anionic complexes are known and since this study involves neutral complexes they will not be discussed here. Further studies by the same workers have established a trimethylphosphine complex of antimony(III) iodide, $[SbI_3(PMe_3)]_n$, prepared by the direct reaction of SbI_3 with PMe_3 in thf solution.[23] The structure is best described as a polymer of dimers, the dimeric units consisting of two antimony atoms with a square-based pyramidal geometry coordinated by a PMe_3 ligand in the apical site and four iodine atoms in the basal plane (Figure 6.1). The basal planes of the pyramids are then linked through an edge. Two coordinated iodine atoms form weak bridging interactions to adjacent dimer units to form the polymeric array. The bond angles in the complex are all close to idealised values, implying that the antimony(III) lone pair has no appreciable stereochemical activity. In Figure 6.1 the thf of recrystallisation have been omitted and the weaker bridging interactions between the dimer units are indicated by dotted lines.

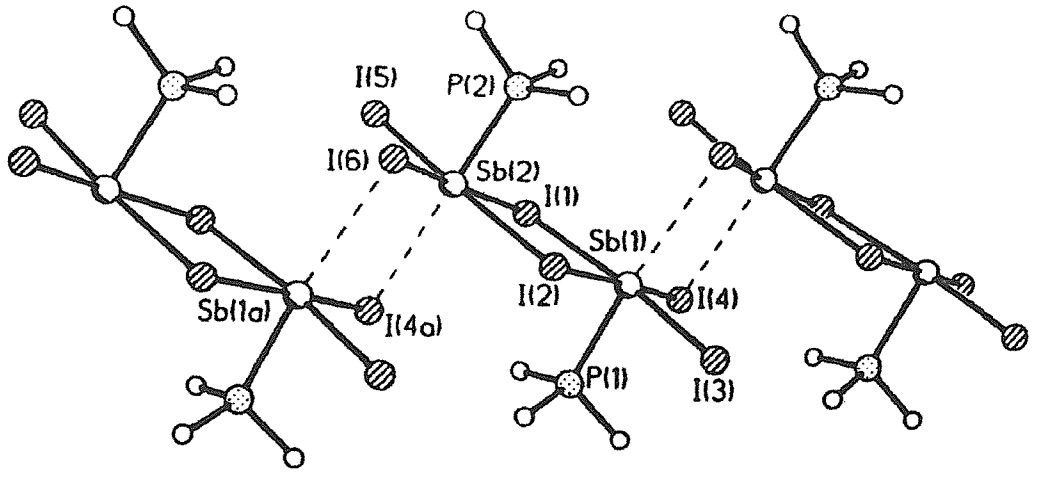

Figure 6.1 – View of part of the crystal structure of $[Sb_2I_6(PMe_3)_2]$ taken from ref. 23

In addition to the (mono)tertiaryphosphine derivative described above, two isomeric forms of the ditertiaryphosphine-antimony(III) bromide complex of empirical formula $[SbBr_3(dmpe)]$ have been described.[23] The first of these, $[Sb_2Br_6(dmpe)_2]$ (Figure 6.2), has the commonly observed dimeric edge-shared bioctahedral structure (the product from the reaction betweeen $BiBr_3$ and dmpe also afforded a crystalline compound displaying the edge-shared, bioctahedral geometry (Figure 6.3)), whereas the second, $[Sb_4Br_{12}(dmpe)_4]$ (Figure 6.5), may be described as a centrosymmetric tetramer.

Looking at the first structure, the major difference between this complex and the Bi(III) analogue is the asymmetry of the bromide bridges. For the antimony compound the relevant distances are Sb-Br(2) 2.8280(12) and Sb-Br(2a) 3.5954(12) with Δ = 0.767 Å whereas for the bismuth derivative the corresponding Bi-Br distances are 2.887 and 3.345 Å (Δ = 0.458 Å). Clearly, the bridge asymmetry is considerably smaller for bismuth than it is for antimony, consistent with secondary bonding interactions being more pronounced for bismuth. This feature is quite general in that, in isomorphous pairs of antimony and bismuth structures, bridge asymmetry is greatest for antimony and least for

bismuth; this feature is also encountered in the structures of the parent halides SbI_3 and BiI_3.[24,25]

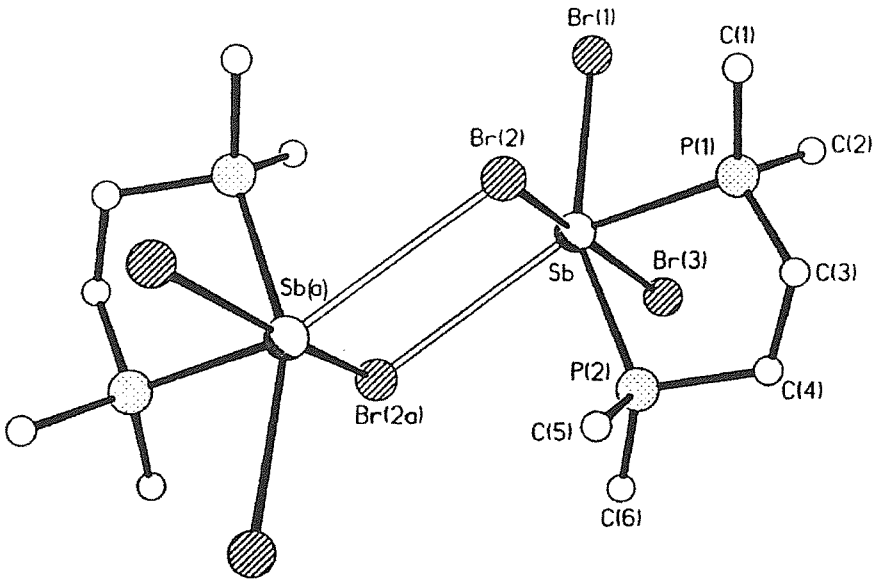

Figure 6.2 – A view of the molecular structure of $[Sb_2Br_6(dmpe)_2]$ taken from ref. 23

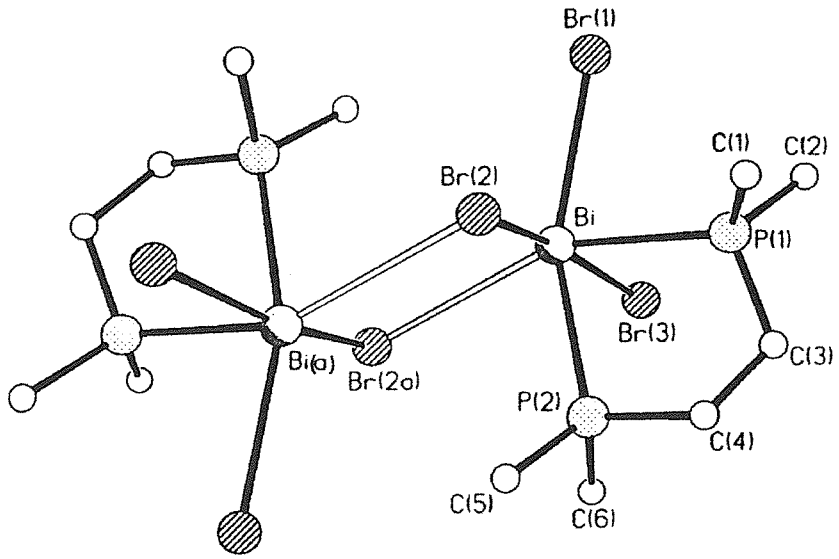

Figure 6.3 – A view of the molecular structure of $[Bi_2Br_6(dmpe)_2]$ taken from ref. 23

The central part of the tetramer in the structure of $[Sb_4Br_{12}(dmpe)_4]$ (Figure 6.5) is similar to the dimer unit present in $[Sb_2Br_6(dmpe)_2]$ in having the isomeric structure shown in Figure 6.4 with highly asymmetric Sb-Br-Sb bridges (Sb(1)-Br(2) 2.787(2), Sb(1)-Br(2a) 3.293(2), Δ = 0.706 Å), the value being much closer to $[Sb_2Br_6(dmpe)_2]$ than to $[Bi_2Br_6(dmpe)_2]$ providing independent confirmation of the trend towards greater asymmetry for antimony.

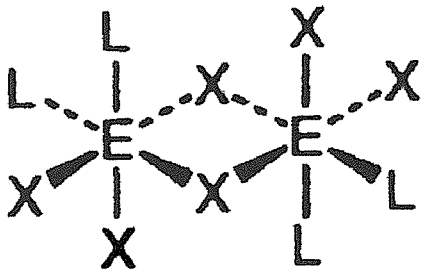

Figure 6.4 – The isomeric structure adopted by $[Sb_4Br_{12}(dmpe)_4]$ and $[Sb_2Br_6(dmpe)_2]$

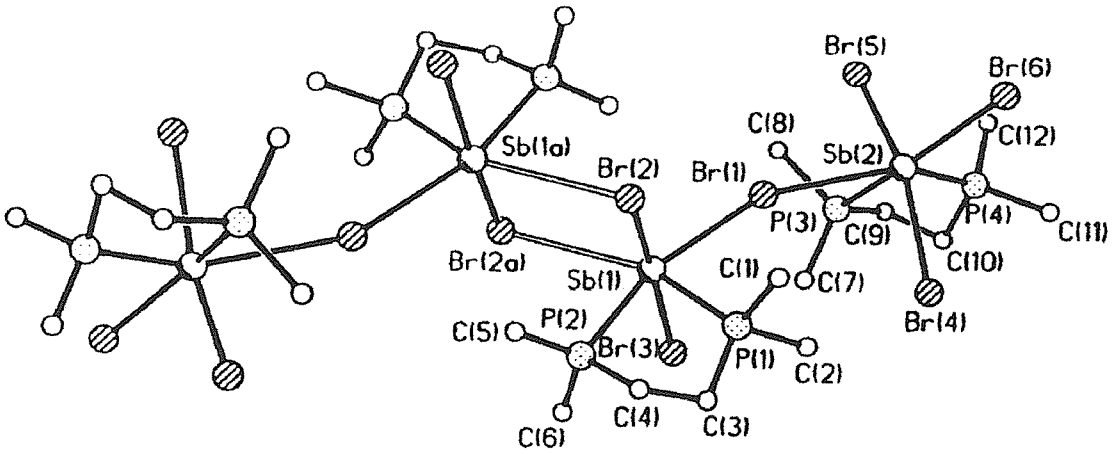

Figure 6.5 – View of the structure of $[Sb_4Br_{12}(dmpe)_4]$ taken from ref. 23

For Group 16 donors, the crown ethers have been studied in great detail and all show a monomeric SbX_3 unit capped by the multidentate ligand. $[SbCl_3(15\text{-crown-}5)]$ was the first compound of this type to be isolated and characterised by X-ray crystallography.[26]

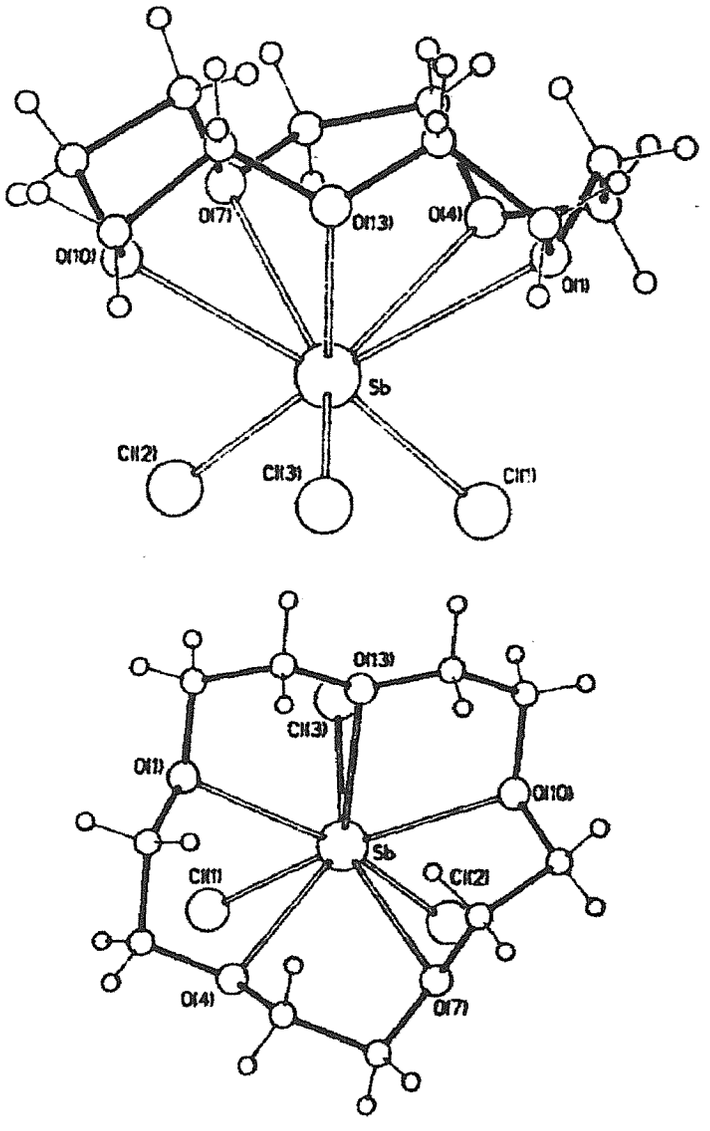

Figure 6.6 – Top and side view of the structure of [$SbCl_3$(15-crown-5)] taken from ref. 27

The structure shows that the compound has all five O atoms bonded to a pyramidal $SbCl_3$ unit in a half sandwich structure (Figure 6.6). Other structurally characterised examples of antimony(III) complexes containing crown ethers include [$SbCl_3$(12-crown-4)][27] (Figure 6.7) and [$SbCl_3$(18-crown-6)].[28] The complexes show closely similar basic structures. The $SbCl_3$ units retain the pyramidal geometry of the parent halides,[11] a common phenomenon also observed for the analogous BiX_3 complexes of these macrocycles.[27,29,30]

The crowns form puckered rings, so that the oxygen lone pairs are all directed towards the central atom. The Sb-O distances are exceptionally long, *ca.* 0.6 Å longer than the Sb-Cl bonds, therefore, these interactions are clearly very weak.

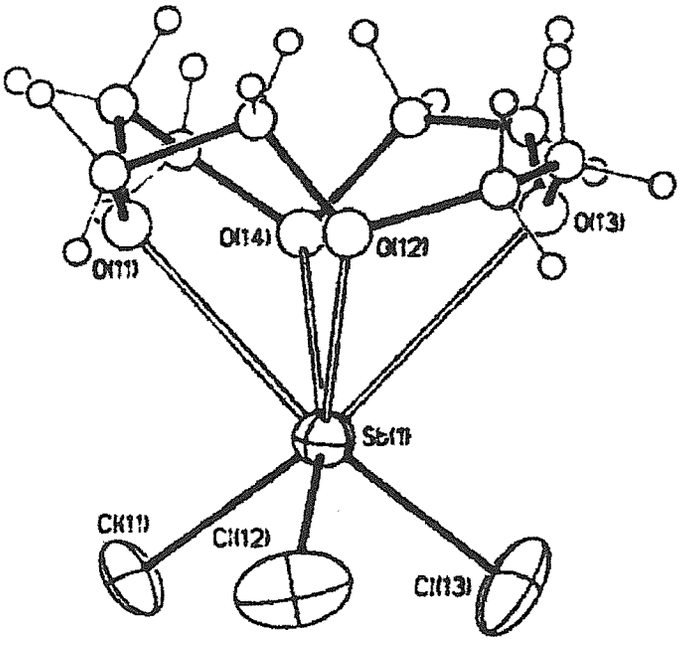

Figure 6.7 – View of the structure of [$SbCl_3$(12-crown-4)] taken from ref. 27

The first structurally characterised antimony(III) bromide compound with a crownether, 15-crown-5 was reported about a decade ago.[31] The antimony atom is surrounded by five oxygen atoms in a manner analogous to the chloride example shown in Figure 6.6.

Recent reports have provided crystal structures for the compounds [(SbX_3)(dibenzo-24-crown-8)] (X = Cl or Br).[32] These structures differ slightly from the examples discussed previously. The dominant feature in the case of the chloride is that there are two $SbCl_3$ moities which coordinate to opposite sides of the crown (Figure 6.8). Each metal centre binds to five crown oxygens of which two are in bridging positions. This type of conformation has previously been observed for [($BiCl_3$)$_2$([24]aneS_8)] where the ligand adopts a sigmoidal shape, similar to the one observed for the antimony(III) example, to coordinate the two

metal centres.[33] The $SbCl_3$ units in the aforementioned example show little conformational variation to those of the parent trichloride. In the bromide analogue, again the two metal centres reside on opposite sides of the ligand, but unlike the chloride example coordination is *via* four M-O bonds and the ligand adopts a more planar conformation.

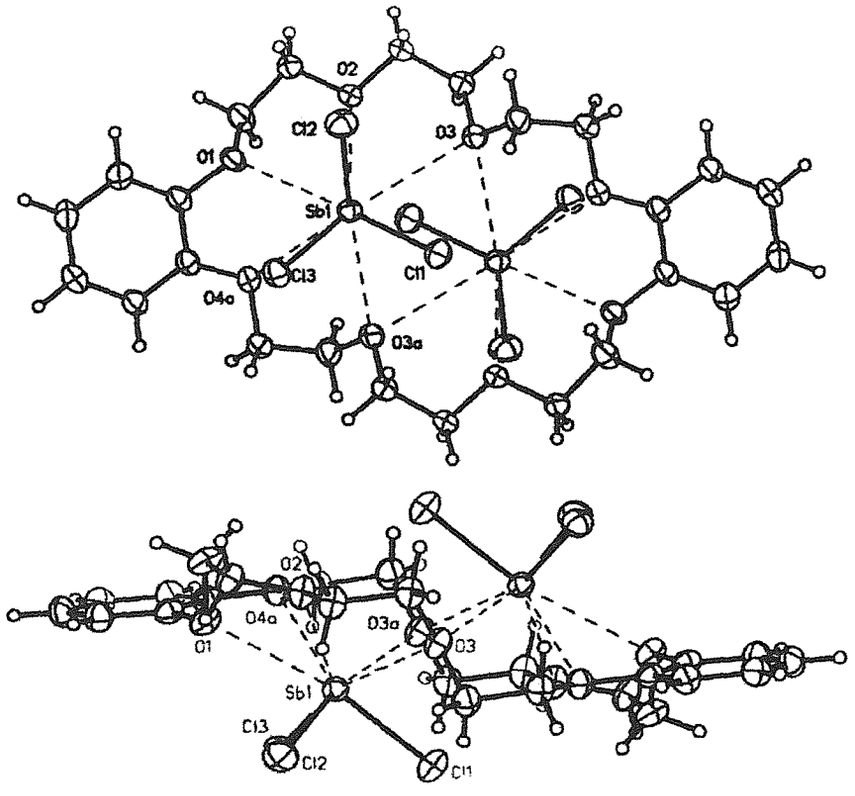

Figure 6.8 – View of structure of $[(SbCl_3)_2$(dibenzo-24-crown-8)] taken from ref. 32

Studies into thioether crown complexes of antimony(III) have also confirmed that the effect of the lone pair is to leave the geometry of the $SbCl_3$ unit essentially unchanged following coordination of the macrocycle. The complexes $[SbCl_3([9]aneS_3)]$, $[SbCl_3([15]aneS_5)]$, $[(SbCl_3)_2([18]aneS_6)]$ and $[SbI_3([9]aneS_3)]$.[34,35] have been isolated and apart from the $[15]aneS_5$ species, X-ray characterisation has been obtained for all of the complexes. In both of the trichloride complexes, the Sb atoms are weakly coordinated to the sulfur atoms with Sb-S distances in the range 2.968(2)-3.460(3) Å. The Sb-Cl distances in

$[SbCl_3([9]aneS_3)]$ (2.374(3)-2.451(3)) and $[(SbCl_3)_2([18]aneS_6)]$ (2.381(3)-2.471(2) Å) are similar to those of the pyramidal core unit in crystalline $SbCl_3$ itself (2.340(2) and 2.368(1) Å).[11] In $[(SbCl_3)_2([18]aneS_6)]$ the antimony centres are six coordinate with each of the three crown sulfur atoms *trans* to a chlorine atom in an irregular *fac*-octahedral array. One of the trio of sulfur atoms is noticeably further away from the metal centre than the other two. A similar (2 + 1) Sb-S bonding mode has been noted in $[SbCl_3(EtNHCSCSNHEt)_{1.5}]$[36] and $[SbCl_3(S_2C_5H_{10})]$[37] ($S_2C_5H_{10}$ = 1,4-dithiacycloheptane) suggesting that this is a prefered geometry for antimony(III).

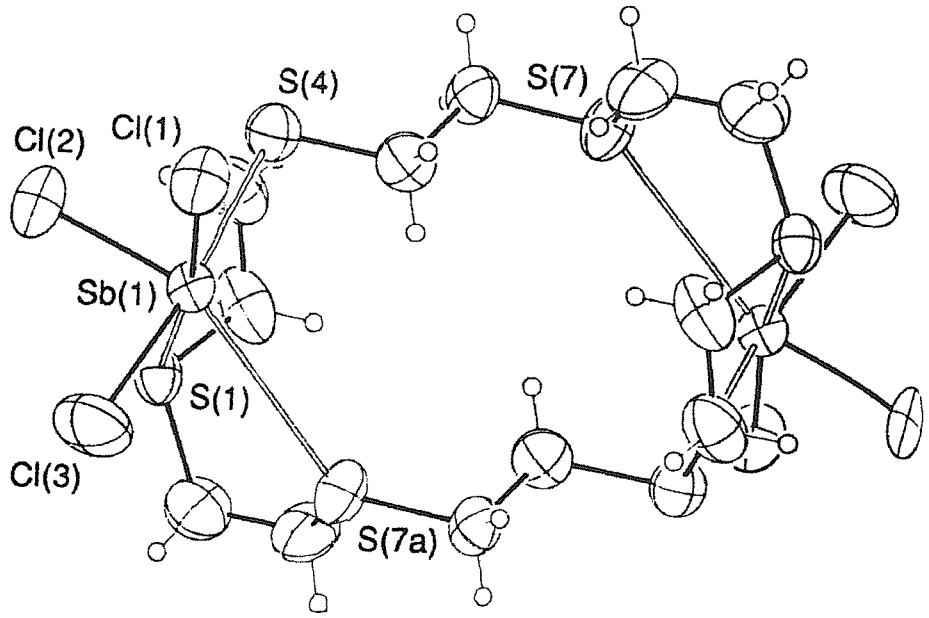

Figure 6.9 – View of the structure of $[(SbCl_3)_2([18]aneS_6)]$ taken from ref. 29

In $[SbCl_3([9]aneS_3)]$ the metal centres adopt a completely different stereochemistry and there is a chain structure. As a general comparison the Sb-S distances are quite similar to the Sb-O distances in the analogous $SbCl_3$ crown ether complexes (above) indicating a relative order of binding thiacrown > oxa-crown. SbI_3 forms a 1:1 adduct with $[9]aneS_3$. The crystal structure exhibits a discrete complex with a distorted octahedral coordination of antimony(III) and there is no significant stereochemical influence of the antimony(III) lone pair.

Once again the structure is another example of the common structural type observed for thia- and oxa-crown ethers of E(III) (E = Sb or Bi).

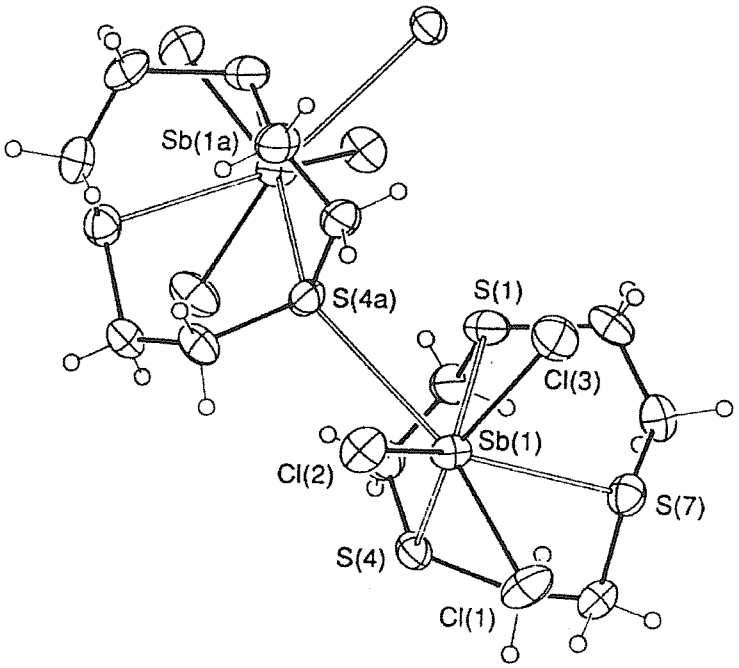

Figure 6.10 – View of the structure of [$SbCl_3$([9]aneS_3)] taken from ref. 29

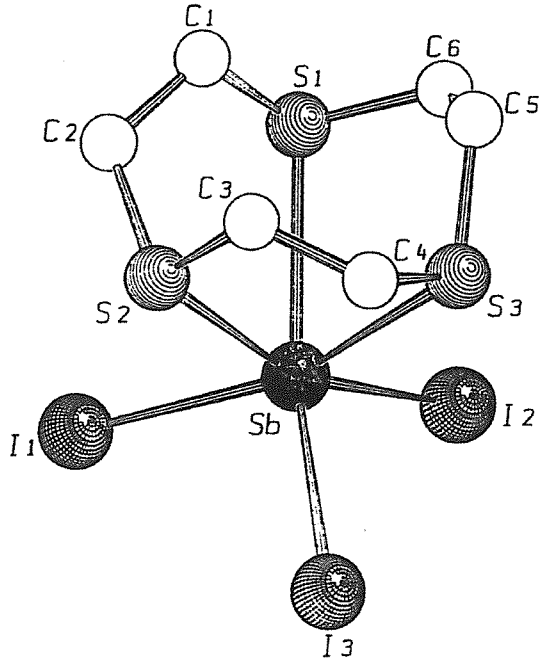

Figure 6.11 – View of the structure of [SbI_3([9]aneS_3)] taken from ref. 35

As previously mentioned, like the bismuth(III) species, antimony(III) is regarded as a soft acid centre and is thus expected to preferentially coordinate ligands bearing soft donor atoms such as sulfur and phosphorus over those containing, for example, nitrogen or oxygen donors. Studies of antimony(III) complexes of dithio-oxamide and dithiomalonamide ligands (RHNC(S)C(S)NHR and RHNC(S)CH_2C(S)NHR, R = alkyl), where both N and S donor atoms are available to the antimony(III) atom, revealed this to be so.[38,39] In all cases, bidentate ligand attachment via the two sulfur donors was observed, with the nitrogen donors remaining uncoordinated.

The aim of the work discussed in this chapter was to conduct an investigation into the reaction of antimony(III) halides with a range of tridentate and macrocyclic Group 16 ligands. The affects of changing halide are studied, and comparisons and differences are drawn with antimony(III) structures containing other Group 16 ligands and bismuth(III) halide compounds described in an earlier chapter.

6.2 RESULTS AND DISCUSSION

6.2.1 Synthesis and Properties of Tridentate Group 16 Complexes of SbX_3

A range of complexes of stoichiometry $[SbX_3\{MeC(CH_2EMe)_3\}]$ (X = Cl, Br or I; E = S, Se or Te) has been isolated from reaction of SbX_3 and $MeC(CH_2EMe)_3$ in MeCN. This array of complexes include the first SbX_3-telluroether compounds. Concentration of the resultant solutions produced solids, ranging from white for $[SbCl_3\{MeC(CH_2SMe)_3\}]$ through yellows for $[SbX_3\{MeC(CH_2SeMe)_3\}]$ (X = Cl, Br or I) to orange for $[SbX_3\{MeC(CH_2TeMe)_3\}]$ (X = Cl, Br or I), which were filtered, washed with anhydrous diethyl ether and dried *in vacuo*. Due to the moisture sensitivity of the antimony(III) halides, all reactions were carried out under an atmosphere of dry nitrogen using standard Schlenk techniques. All complexes were stored in a dinitrogen purged dry-box. Satisfactory microanalysis were recorded for all freshly prepared solids and IR spectra of the $SbCl_3$ species show several features in the range 250-350 cm^{-1} assigned to ν(Sb-Cl) (*c.f.* 220-270 cm^{-1} in the parent halide, $SbCl_3$). The poor solubility of the complexes in non-coordinating solvents such as CH_2Cl_2 and $CHCl_3$ meant that NMR spectroscopy did not provide any useful information. Their characterisation is thus restricted to analytical data, IR spectroscopy and single crystal X-ray diffraction studies.

6.2.2 Single Crystal X-ray Diffraction Studies.

As previously mentioned, prior to this study Group 16 complexes of antimony(III) halides characterised structurally were restricted to crown ether and crown thioether complexes which generally feature pyramidal SbX_3 units capped by the macrocycle (Figures 6.6 – 6.11).[27-35] The structures obtained for the three examples $[SbCl_3\{MeC(CH_2SMe)_3\}]$, $[SbBr_3\{MeC(CH_2SeMe)_3\}]$ and $[SbI_3\{MeC(CH_2SMe)_3\}]$ exhibit a variety of different structural motifs for relatively small alterations in substituent architecture. The crystals discussed within this section were obtained by slow evaporation from a solution of the complex in MeCN.

Crystals obtained from the reaction of $SbCl_3$ with $MeC(CH_2SMe)_3$ show that the 5-coordinate species $[SbCl_3\{MeC(CH_2SMe)_3\}]$ is formed as an infinite one-dimensional "helical" structure derived from $SbCl_3$ units each linked to the next $SbCl_3$ unit by bridging $MeC(CH_2SMe)_3$ ligands. Coordination is *via* one S-donor to each antimony(III), i.e. each metal centre coordinates to sulfur atoms from two different thioether ligands, which function as bidentates. The infinitely repeating motif (Figure 6.12) retains some of the characteristics of the parent halide with bond lengths indicative of primary Sb-Cl bonds and weak secondary Sb-S interactions. In fact the bond lengths of Sb-Cl (2.391(2) – 2.407(2) Å) are extremely similar to those observed in $SbCl_3$ (average 2.359 Å)[11] and previous antimony(III) complexes incorporating cyclic thioether ligands (*c.f.* 2.374(3) – 2.451(3) Å for $[SbCl_3([9]aneS_3)]$ and 2.381(3) – 2.471(2) Å for $[(SbCl_3)_2([18]aneS_6)]$).[34] The weak secondary Sb-S bond lengths seen here in $[SbCl_3\{MeC(CH_2SMe)_3\}]$ (Sb(1)-S(1) 3.172(2); Sb(1)-S(3) 3.106(2) Å) are also show similarity to those observed in the previously characterised thiacrown complexes (*c.f.* 3.32 Å (average) for $[(SbCl_3)_2([18]aneS_6)]$ and 3.163 Å (average) for $[SbCl_3([9]aneS_3)]$).[34] The secondary interactions of sulfur to bismuth in $BiCl_3$ complexes involving thioether ligands have also been shown to be in the order of *ca.* 3.1 Å.[6,33,40,41]

Table 6.1 – Crystallographic data collection and refinement parameters

Complex	**$[SbCl_3\{Me(CH_2SMe)_3\}]$**	**$[SbI_3\{Me(CH_2SMe)_3\}]$**
Formula	$C_8H_{18}Cl_3S_3Sb$	$C_8H_{18}I_3S_3Sb$
Formula Weight	438.52	712.87
Colour, morphology	colourless, block	yellow, rhomb
Crystal Dimensions/mm	0.32, 0.28, 0.26	0.30, 0.30, 0.25
Crystal System	orthorhombic	triclinic
Space Group	$P2_12_12_1$	P-1
a / Å	9.479(1)	11.198(7)
b / Å	18.736(1)	12.017(8)
c / Å	9.056(2)	7.584(3)
α/ °	90	93.98(5)
β/ °	90	98.28(5)
γ/ °	90	114.44(5)
V / Å^3	1608.4(3)	910(1)
Z	4	2
F(000)	864	648
D_{calc}/ g cm^{-3}	1.811	2.602
μ(Mo-K_α)/ cm^{-1}	25.72	68.74
Unique observed reflections	1669	3194
Observed reflections with $[I_o > 2\sigma(I_o)]$	1495	2786
No. of parameters	136	136
Goodness of fit	1.63	7.41
R[a]	0.029	0.081
Rw[b]	0.033	0.122

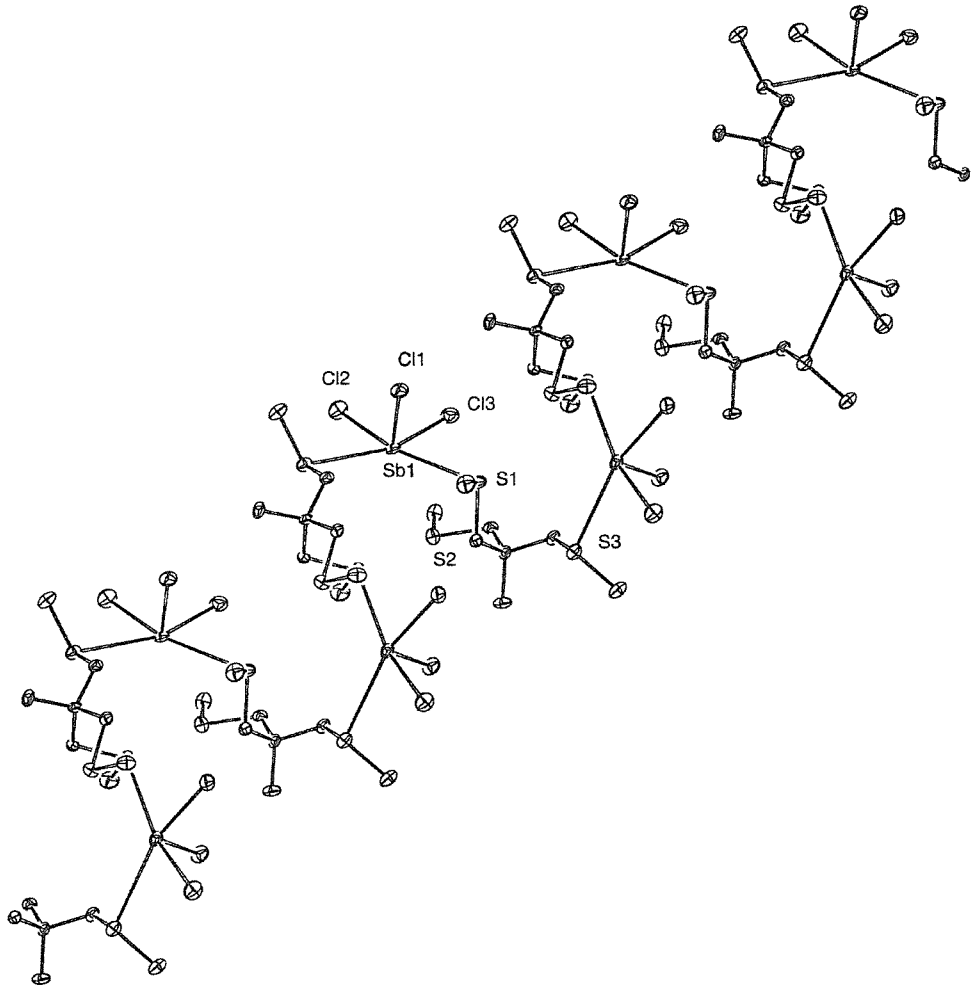

Figure 6.12 – View of a portion of the structure of $[SbCl_3\{MeC(CH_2SMe)_3\}]$ with the numbering scheme adopted.

Table 6.2 – Selected bond lengths (Å) for $[SbCl_3\{MeC(CH_2SMe)_3\}]$

Sb(1)	Cl(1)	2.391(2)	Sb(1)	Cl(2)	2.407(2)
Sb(1)	Cl(3)	2.398(2)	Sb(1)	S(1)	3.172(2)
Sb(1)	S(3)	3.106(2)	S(1)	C(1)	1.804(9)
S(1)	C(2)	1.822(7)	S(2)	C(5)	1.829(8)
S(2)	C(6)	1.804(8)	S(3)	C(7)	1.813(7)
S(3)	C(8)	1.811(7)			

Table 6.3 – Selected bond angles (degrees) for $[SbCl_3\{MeC(CH_2SMe)_3\}]$

Cl(1)	Sb(1)	Cl(2)	95.51(8)	Cl(1)	Sb(1)	Cl(3)	91.79(8)
Cl(1)	Sb(1)	S(1)	81.35(6)	Cl(1)	Sb(1)	S(3)	80.86(6)
Cl(2)	Sb(1)	Cl(3)	88.79(8)	Cl(2)	Sb(1)	S(1)	167.29(7)
Cl(2)	Sb(1)	S(3)	77.23(7)	Cl(3)	Sb(1)	S(1)	79.05(7)
Cl(3)	Sb(1)	S(3)	163.41(7)	S(1)	Sb(1)	S(3)	114.13(5)
Sb(1)	S(1)	C(1)	107.5(3)	Sb(1)	S(1)	C(2)	101.4(2)
C(1)	S(1)	C(2)	100.5(4)	Sb(1)	S(3)	C(8)	108.8(3)
Sb(1)	S(3)	C(7)	99.8(3)				

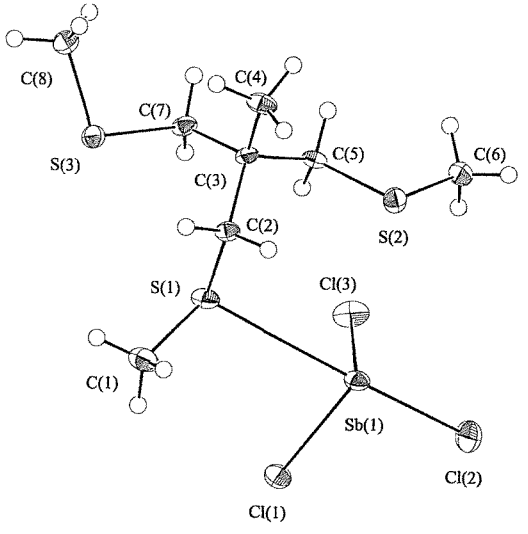

Figure 6.13 – View of the $[SbCl_3\{MeC(CH_2SMe)_3\}]$ asymmetric unit with numbering scheme adopted. Ellipsoids are drawn at 40 % probability.

Crystals were also obtained for the 1:1 reaction of SbI_3 with the tripodal thioether ligand, $MeC(CH_2SMe)_3$, in MeCN. The structure determined for this example proves to illustrate the diversity of structural form possible with the simple change of the halogen from chlorine to iodine. Instead of the 5-coordinate antimony(III) we observe a 6-coordinate species. In this species, the secondary bonds between the antimony atom and an iodine ligand from an adjacent SbI_3 unit form an edge-shared bioctahedron which serve to create an infinite one-dimensional array. Within this polymeric structure each antimony atom is in a distorted octahedral environment, coordinated to two sulfur donor atoms, two terminal iodine ligands and two μ^2-bridging iodine atoms. The bridging unit is asymmetric, with bond lengths indicative of primary Sb-I bonds (2.861(2) Å) and secondary Sb-I bonds (3.516(2) Å).[42] Furthermore, the Sb-I bond distances for the terminal I atoms in $[SbI_3\{MeC(CH_2SMe)_3\}]$ are considerably shorter than those of the μ^2-bridging I atoms as was observed for the examples in previous studies involving SbX_3 and BiX_3 (X = Cl or Br). The distances of the Sb-S interactions (Sb-S(1) 3.021(6) Å, Sb-S(2*) 2.973(6) Å) are comparable to those previously found in literature (*ca.* 2.890(2) Å) for the SbI_3 thiacrown complex.[35] The bond angles S(1)-Sb(1)-I(2) (174.0(1) °), I(3)-Sb(1)-I(1*) (177.39(7) °) and I(1)-Sb(1)-I(1*) (85.05(6) °) indicate that the geometry about the antimony(III) atom is distorted from idealized octahedral. The asymmetric unit is shown in Figure 6.14 and a portion of the polymeric network is shown in Figure 6.15.

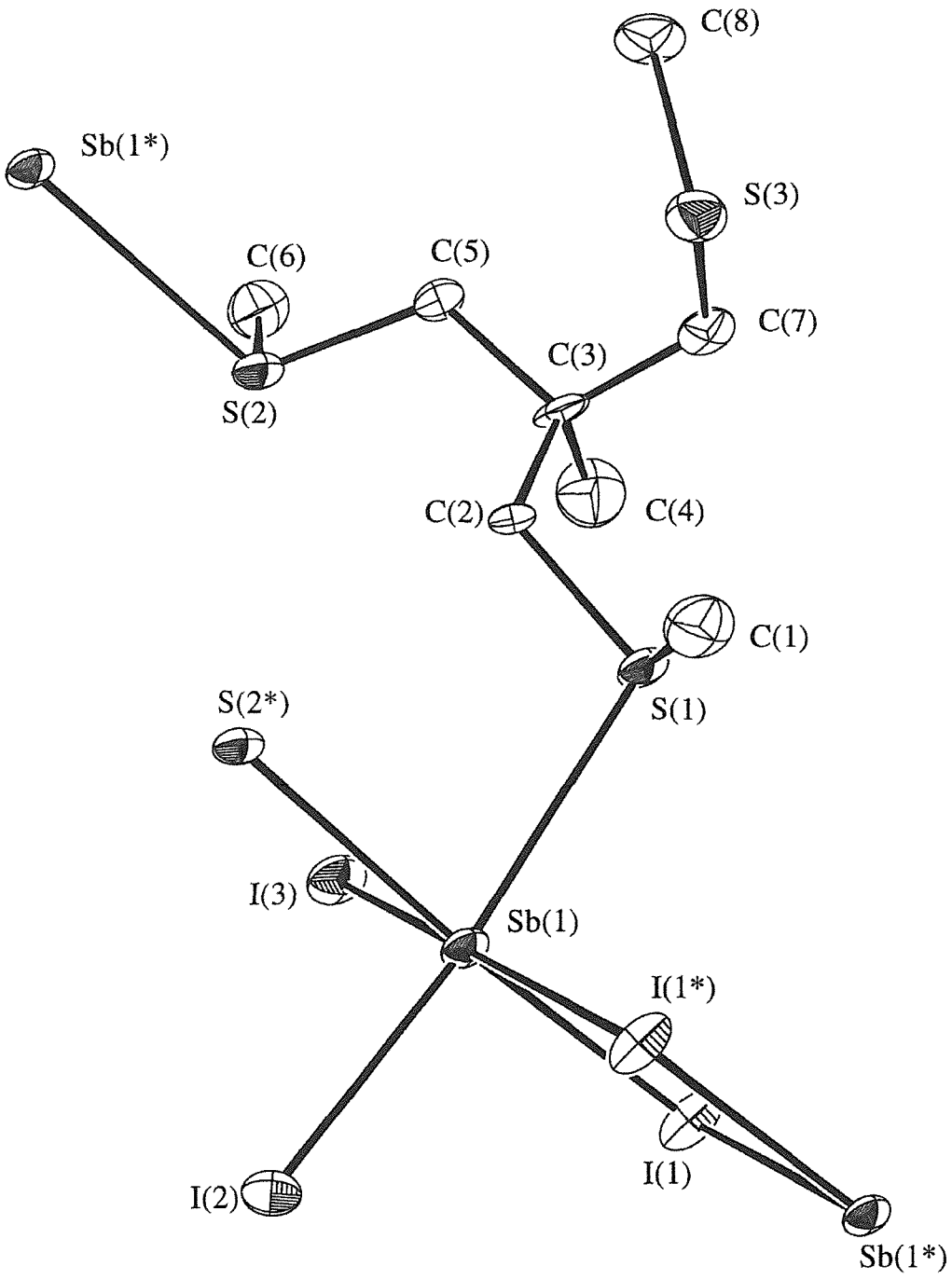

Figure 6.14 – View of the $[SbI_3\{MeC(CH_2SMe)_3\}]$ asymmetric unit with numbering scheme adopted. Ellipsoids are drawn at 40 % probability. Neighbouring atoms are included marked with an asterisk (*) (related by a crystallographic inversion centre).

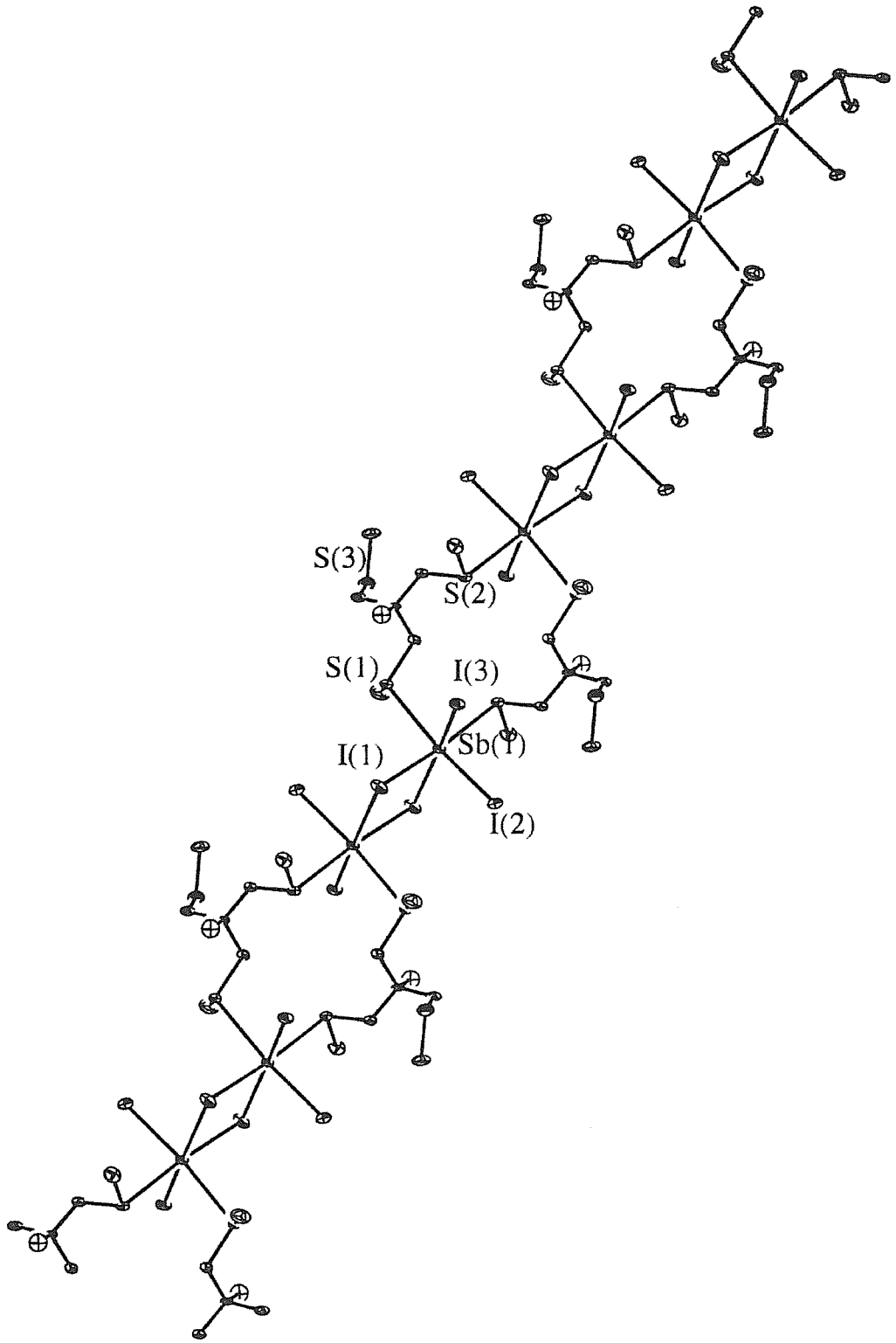

Figure 6.15 – View of a portion of the structure of $[SbI_3\{MeC(CH_2SMe)_3\}]$ with numbering scheme adopted.

Table 6.4 – Selected bond lengths (Å) for $[SbI_3\{MeC(CH_2SMe)_3\}]$

I(1)	Sb(1)	2.861(2)	I(1)	Sb(1*)	3.516(2)
I(2)	Sb(1)	2.847(2)	I(3)	Sb(1)	2.771(2)
Sb(1)	S(1)	3.021(6)	Sb(1)	S(2*)	2.973(6)
S(1)	C(1)	1.77(3)	S(1)	C(2)	1.83(2)
S(2)	C(5)	1.84(2)	S(2)	C(6)	1.83(3)
S(3)	C(7)	1.82(3)	S(3)	C(8)	1.80(3)
C(2)	C(3)	1.52(3)	C(3)	C(4)	1.54(3)
C(3)	C(5)	1.51(3)	C(3)	C(7)	1.55(4)

Table 6.5 – Selected bond angles (degrees) for $[SbI_3\{MeC(CH_2SMe)_3\}]$

Sb(1)	I(1)	Sb(1*)	94.95(6)	I(1)	Sb(1)	I(1*)	85.05(6)
I(1)	Sb(1)	I(2)	95.16(7)	I(1)	Sb(1)	I(3)	92.35(7)
I(1)	Sb(1)	S(1)	90.6(1)	I(1)	Sb(1)	S(2*)	175.0(1)
I(1*)	Sb(1)	I(2)	85.61(6)	I(1*)	Sb(1)	I(3)	177.39(7)
I(1*)	Sb(1)	S(1)	96.5(1)	I(1*)	Sb(1)	S(2*)	97.8(1)
I(2)	Sb(1)	I(3)	94.65(7)	I(2)	Sb(1)	S(1)	174.0(1)
I(2)	Sb(1)	S(2*)	89.1(1)	I(3)	Sb(1)	S(1)	83.5(1)
I(3)	Sb(1)	S(2*)	84.8(1)	S(1)	Sb(1)	S(2*)	85.0(2)
Sb(1)	S(1)	C(1)	100(1)	Sb(1)	S(1)	C(2)	107.9(8)
C(1)	S(1)	C(2)	101(1)	Sb(1)	S(2)	C(5)	105.8(8)
Sb(1*)	S(2)	C(6)	100.1(9)				

A similarity between this structure and that of the analogous chloride complex is the preference of the ligand to bridge instead of chelating. This bonding mode has also been observed during subsequent work within the Southampton research group on dithio- and diseleno-ether complexes of antimony(III) halides.[43] The specific example in question is the structure of $[SbCl_3\{MeSe(CH_2)_3SeMe\}]$ in which the similarities include the edge-shared bioctahedral SbX_3 unit and two bridging ligands, with equivalent sized carbon back bone, linking neighbouring antimony(III) atoms. The linkage differs in the case of the tripodal thioether complex by the non-bonding third arm of the ligand.

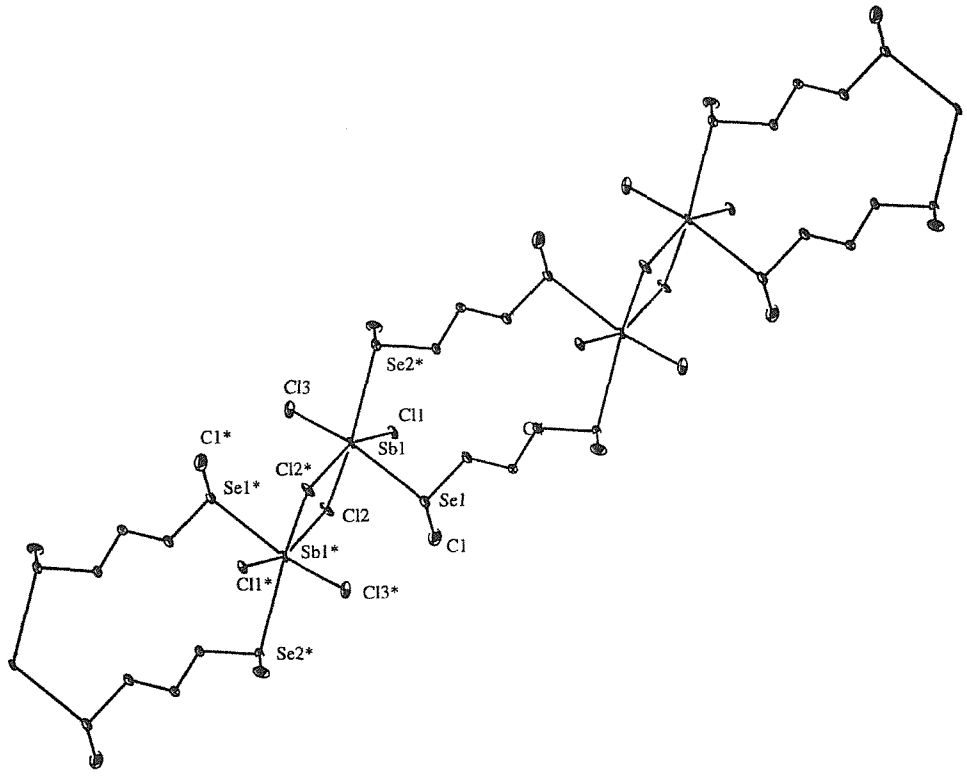

Figure 6.16 – View of the extended structure of $[SbCl_3\{MeSe(CH_2)_3SeMe\}]$ taken from ref. 43

Prior to the work discussed in this chapter there were no structurally characterised examples of antimony(III) selenoether compounds. The following example of an antimony(III) bromide complex serves as the first involving such ligands. Crystals suitable for X-ray diffraction studies were grown by the slow evaporation of solvent from a solution the reaction mixture of $SbBr_3$ with $MeC(CH_2SeMe)_3$ in MeCN. The crystals show antimony(III) atoms which are 6-coordinate and can be considered as distorted octahedral environments. The motif is infinitely repeated, giving rise to a one-dimensional coordination polymer (Figure 6.18). The coordination set comprises three terminal Br and a *fac*-coordinated trio of Se-donors; from one bidentate selenoether and one monodentate selenoether. The bond lengths of the halide to the central antimony(III) atom (Sb-Br in this case) are once again indicative of primary interactions (Sb-Br(1), Sb-Br(2) and Sb-Br(3), 2.625(4), 2.574(4) and 2.580(3) Å respectively) which are in keeping with the bond lengths incorporated in the parent antimony(III) halide (average Sb-Br 2.49 Å).[14] They also bear a close resemblance to the Sb-Br bond lengths in the only other antimony(III) bromide complexes to involve Group 16 ligands reported in literature, $[SbBr_3$(15-crown-5)] (Figure 6.17) and $[(SbBr_3)_2$(dibenzo-24-crown-8)].[31,32] The Sb-Br bond lengths in these particular complexes range from 2.5230(15) – 2.587(2) Å.

After verifying the retention of the structural identity of the parent $SbBr_3$ and considering the bonding modes of the oxo-crown and thi-cown macrocycles, the tripodal selenoether might have been expected to cap the SbX_3 unit in a *fac* coordination. It is true to say that a trio of selenium donors do adopt this arrangement. However, as previously noted the donors are from two separate ligands (Figure 6.17).

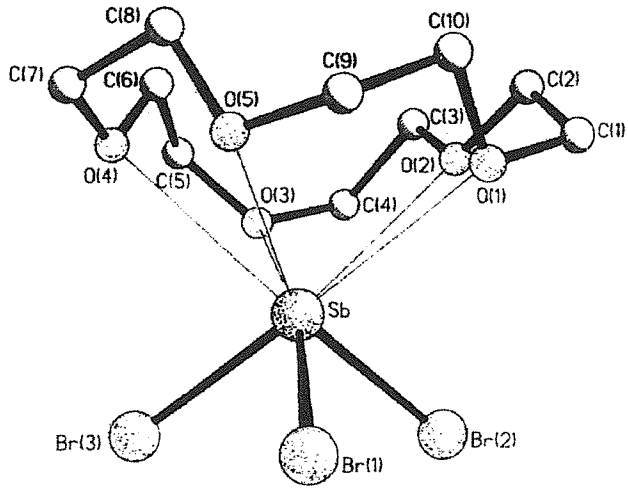

Figure 6.17 – View of the structure of [$SbBr_3$(15-crown-5)] taken from ref. 31

Single crystal X-ray diffraction studies have been previously carried out on two bismuth(III) complexes incorporating this selenoether ligand, [$BiCl_3${$MeC(CH_2SeMe)_3$}] and [Bi_2I_6{$MeC(CH_2SeMe)_3$}$_2$].[6] Discussions are included in Chapter 5. However, I would like to draw comparisons between the structure of [$SbBr_3${$MeC(CH_2SeMe)_3$}] and the two-dimensional array observed for [$BiCl_3${$MeC(CH_2SeMe)_3$}] (Figure 6.18).

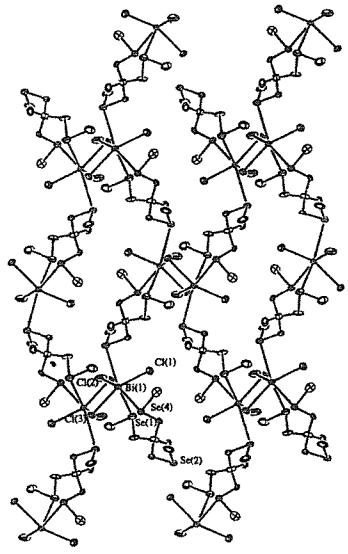

Figure 6.18 – View of the structure of [$BiCl_3${$MeC(CH_2SeMe)_3$}] taken from ref. 4

Each bismuth(III) atom is coordinated to a donor set which includes one bidentate and one monodentate selenoether ligand which bond in a manner similar to the one observed in $[SbBr_3\{MeC(CH_2SeMe)_3\}]$ i.e, the ligand links one metal centre to its neighbour. However, investigations have shown that, after consideration of atom radii of Sb and Br, there is no bridging from one antimony(III) to another *via* two bridging halides as seen for the bismuth(III) complex which results in the polymeric array extending in one dimension as opposed to two-dimensions. The asymmetric unit is shown in Figure 6.19 and a portion of the one-dimensional network is shown in Figure 6.20.

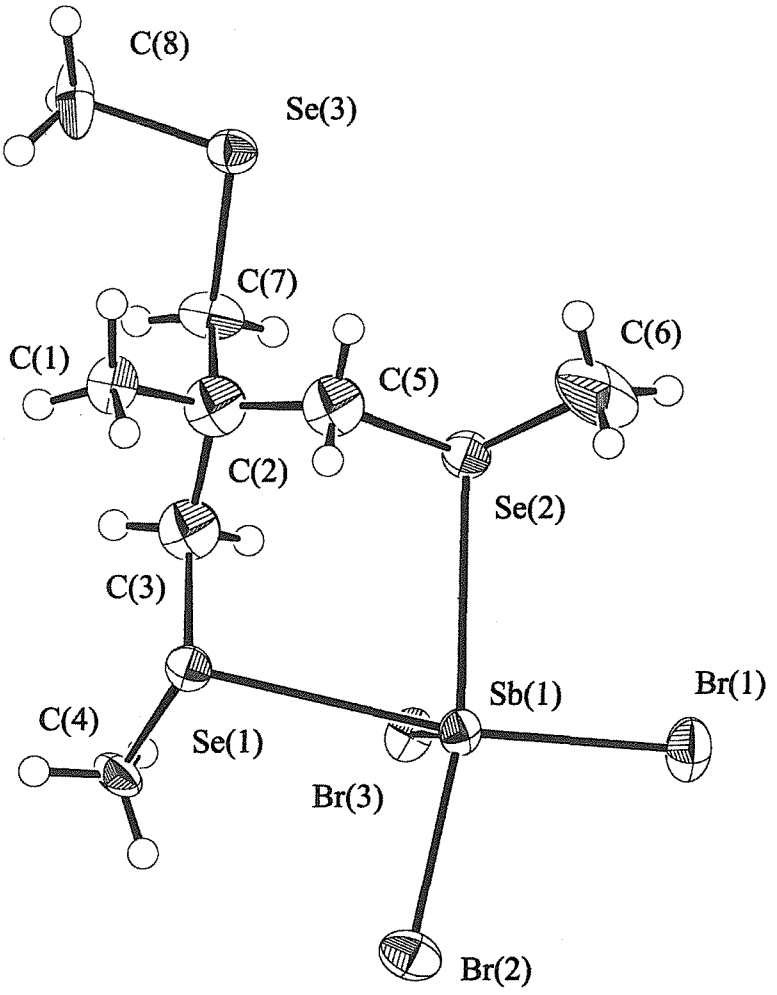

Figure 6.19 – View of the $[SbBr_3\{MeC(CH_2SeMe)_3\}]$ asymmetric unit with numbering scheme adopted. Ellipsoids are drawn at 40 % probability.

Table 6.6 – Crystallographic data collection and refinement parameters for $[SbBr_3\{MeC(CH_2SeMe)_3\}]$

Formula	$C_8H_{18}Br_3SbSe_3$
Formula Weight	712.57
Colour, morphology	yellow, rhomoid
Crystal Dimensions/mm	0.20, 0.12, 0.12
Crystal System	monoclinic
Space Group	Cc
a / Å	11.9999(3)
b / Å	15.2832(4)
c / Å	9.9029(3)
α/ °	90
β/ °	104.4770(12)
γ/ °	90
V / Å^3	1758.49(8)
Z	4
$F(000)$	1296
D_{calc}/ g cm^{-3}	2.691
μ(Mo-K_α)/ cm^{-1}	145.9
Unique observed reflections	2095
Observed reflections with $[I_o > 2\sigma(I_o)]$	1281
No. of parameters	134
Goodness of fit	1.51
R[a]	0.063
Rw[b]	0.068

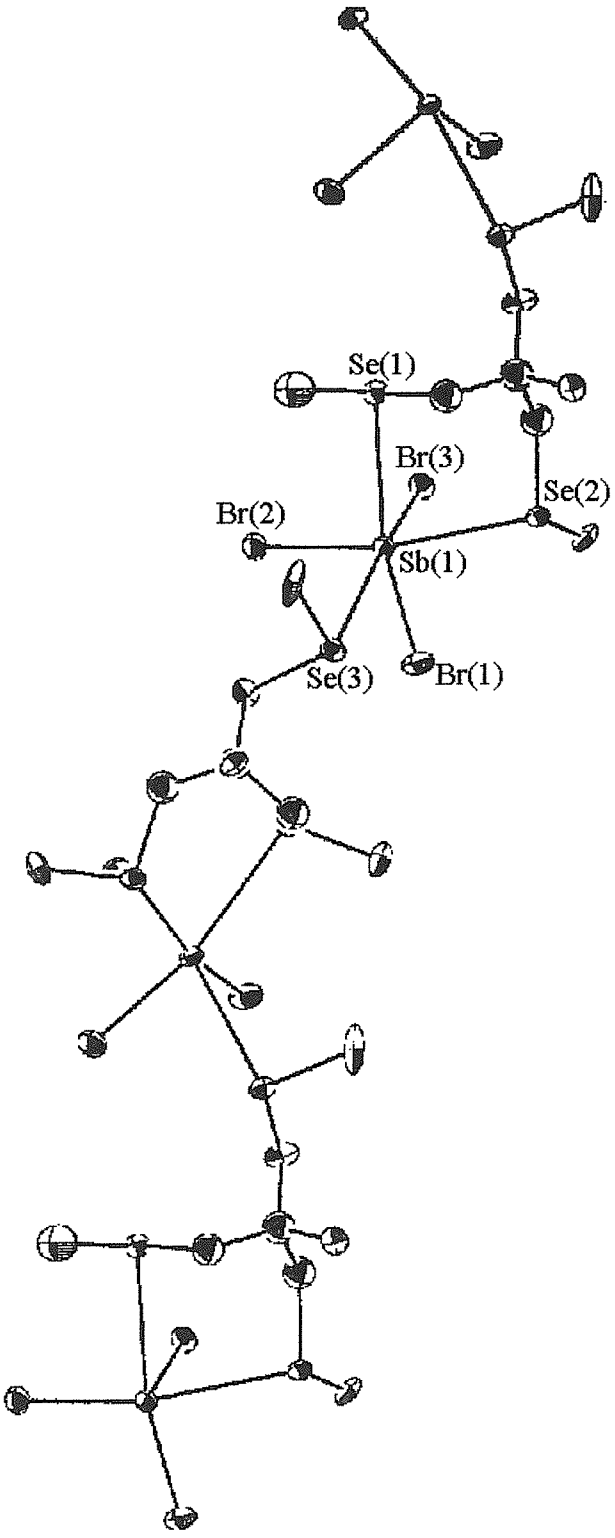

Figure 6.20 – View of a portion of the structure of [$SbBr_3${$MeC(CH_2SeMe)_3$}] with the numbering scheme adopted.

Table 6.7 – Selected bond lengths (Å) for $[SbBr_3\{MeC(CH_2SeMe)_3\}]$

Sb(1)	Br(1)	2.625(4)	Sb(1)	Br(2)	2.574(4)
Sb(1)	Br(3)	2.580(3)	Sb(1)	Se(1)	3.162(3)
Sb(1)	Se(2)	3.188(4)	Sb(1)	Se(3)	3.195(4)
Se(1)	C(3)	1.93(3)	Se(1)	C(4)	1.92(3)
Se(2)	C(5)	2.03(3)	Se(2)	C(6)	1.93(4)
Se(3)	C(7)	1.97(3)	Se(3)	C(8)	1.91(3)

Table 6.8 – Selected bond angles (degrees) for $[SbBr_3\{MeC(CH_2SeMe)_3\}]$

Br(1)	Sb(1)	Br(2)	98.47(12)	Br(1)	Sb(1)	Br(3)	90.94(11)
Br(1)	Sb(1)	Se(1)	168.70(12)	Br(1)	Sb(1)	Se(2)	91.30(11)
Br(1)	Sb(1)	Se(3)	85.78(10)	Br(2)	Sb(1)	Br(3)	91.20(12)
Br(2)	Sb(1)	Se(1)	90.57(11)	Br(2)	Sb(1)	Se(2)	166.70(12)
Br(2)	Sb(1)	Se(3)	77.88(11)	Br(3)	Sb(1)	Se(1)	82.06(9)
Br(3)	Sb(1)	Se(2)	79.57(10)	Br(3)	Sb(1)	Se(3)	167.98(10)
Se(1)	Sb(1)	Se(2)	78.76(9)	Se(1)	Sb(1)	Se(3)	102.83(9)
Se(2)	Sb(1)	Se(3)	112.03(9)	Sb(1)	Se(1)	C(3)	98.0(7)
Sb(1)	Se(1)	C(4)	101.6(8)	C(3)	Se(1)	C(4)	96.8(13)
Sb(1)	Se(2)	C(5)	97.7(9)	Sb(1)	Se(2)	C(6)	104.4(13)
C(5)	Se(2)	C(6)	97.1(18)	Sb(1)	Se(3)	C(7)	108.5(8)
Sb(1)	Se(3)	C(8)	97.2(13)	C(7)	Se(3)	C(8)	97.3(14)

6.2.3 Synthesis and Structures of Macrocyclic Selenoether Complexes of SbX_3

Reaction of SbX_3 (X = Cl, Br or I) with one molar equivalent of [8]aneSe$_2$ in anhydrous MeCN solution yields yellow, orange or red microcrystalline powders with stoichiometry [SbX_3([8]aneSe$_2$)]. Similarly, reaction of SbX_3 with one molar equivalent of [16]aneSe$_4$ or [24]aneSe$_6$ in anhydrous MeCN yields white ($SbCl_3$ complexes), yellow ($SbBr_3$ complexes) or red and orange (SbI_3 complexes). Once again, due to the poor solubility of the products, NMR spectroscopic data were not obtained. The characterisation was restricted to analytical data, IR spectroscopy and single crystal X-ray diffraction studies. The microanalysis results indicate that the complexes formed from the reaction of [16]aneSe$_4$ with SbX_3 have the stoichiometry [(SbX_3)$_2$([16]aneSe$_4$)]. Similarly, isolated products from reactions involving [24]aneSe$_6$ have the stoichiometry [SbX_3([24]aneSe$_6$)].

6.2.4 Single Crystal X-ray Diffraction Studies of [($SbBr_3$)$_2$([16]aneSe$_4$)]

A crystal structure determination was undertaken on [($SbBr_3$)$_2$([16]aneSe$_4$)] in order to determine the structural arrangement present and to provide a comparison with the structure adopted by this macrocycle with $BiBr_3$. Crystals of [($SbBr_3$)$_2$([16]aneSe$_4$)] were obtained by slow evaporation from a solution of the complex in MeCN. The structure shows an infinite two-dimensional structure derived from [16]aneSe$_4$ units linked to four neighbouring macrocycles by $SbBr_3$ units. Hence, the 5-coordinate antimony(III) centre is bonded to one selenium donor from two separate macrocycles. All four selenium atoms within each [16]aneSe$_4$ are involved in bonding. Once again we observe a structure with the three Sb-X bond lengths showing close similarity to those found in the parent halide and those of previously reported examples. Hence, Sb-Br(1), Sb-Br(2) and Sb-Br(3) have bond lengths 2.687(1), 2.537(1) and 2.601(1) Å respectively (*c.f.* $SbBr_3$ (average 2.49 Å) and [$SbBr_3${$MeC(CH_2SeMe)_3$}] (*ca.* 2.625 Å)).[43]

Table 6.9 – Crystallographic data collection and refinement parameters

Complex	**$[(SbBr_3)_2([16]aneSe_4)]$**
Formula	$C_6H_{12}Se_2Br_3Sb$
Formula Weight	603.54
Colour, morphology	yellow, rhomb.
Crystal Dimensions/mm	0.36, 0.20, 0.18
Crystal System	monoclinic
Space Group	$P2_1/n$
a / Å	10.276(2)
b / Å	13.540(3)
c / Å	10.755(2)
α/ °	90
β/ °	113.71(1)
γ/ °	90
V / Å^3	1370.1(4)
Z	4
$F(000)$	1088
D_{calc}/ g cm^{-3}	2.926
μ(Mo-K_α)/ cm^{-1}	160.58
Unique observed reflections	2536
Observed reflections with $[I_o > 2\sigma(I_o)]$	1724
No. of parameters	109
Goodness of fit	1.61
R[a]	0.035
Rw[b]	0.039

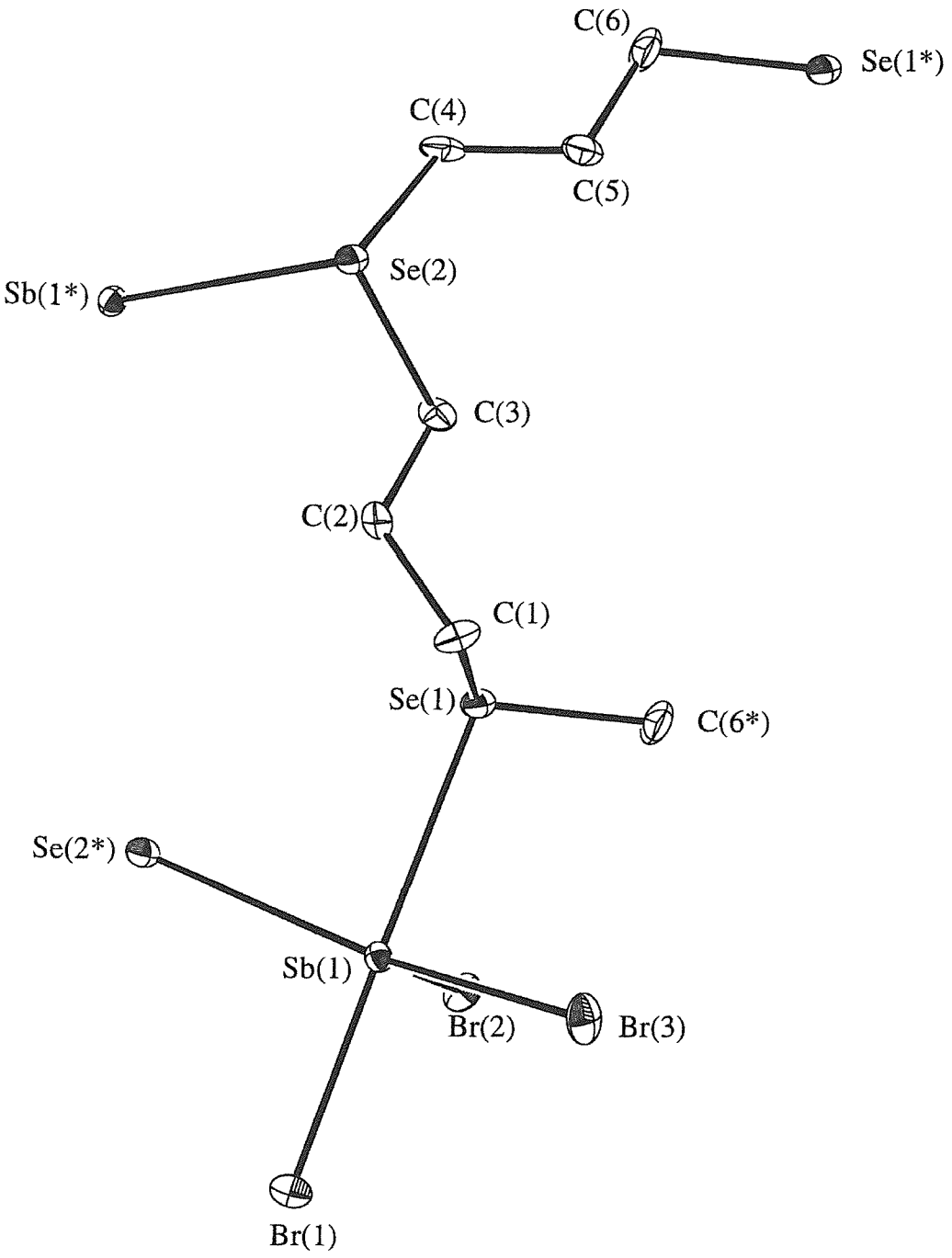

Figure 6.21 – View of the $[(SbBr_3)_2([16]aneSe_4)]$ asymmetric unit, including nearest symmetry related neighbours, with numbering scheme adopted. Ellipsoids are drawn at 40 % probability

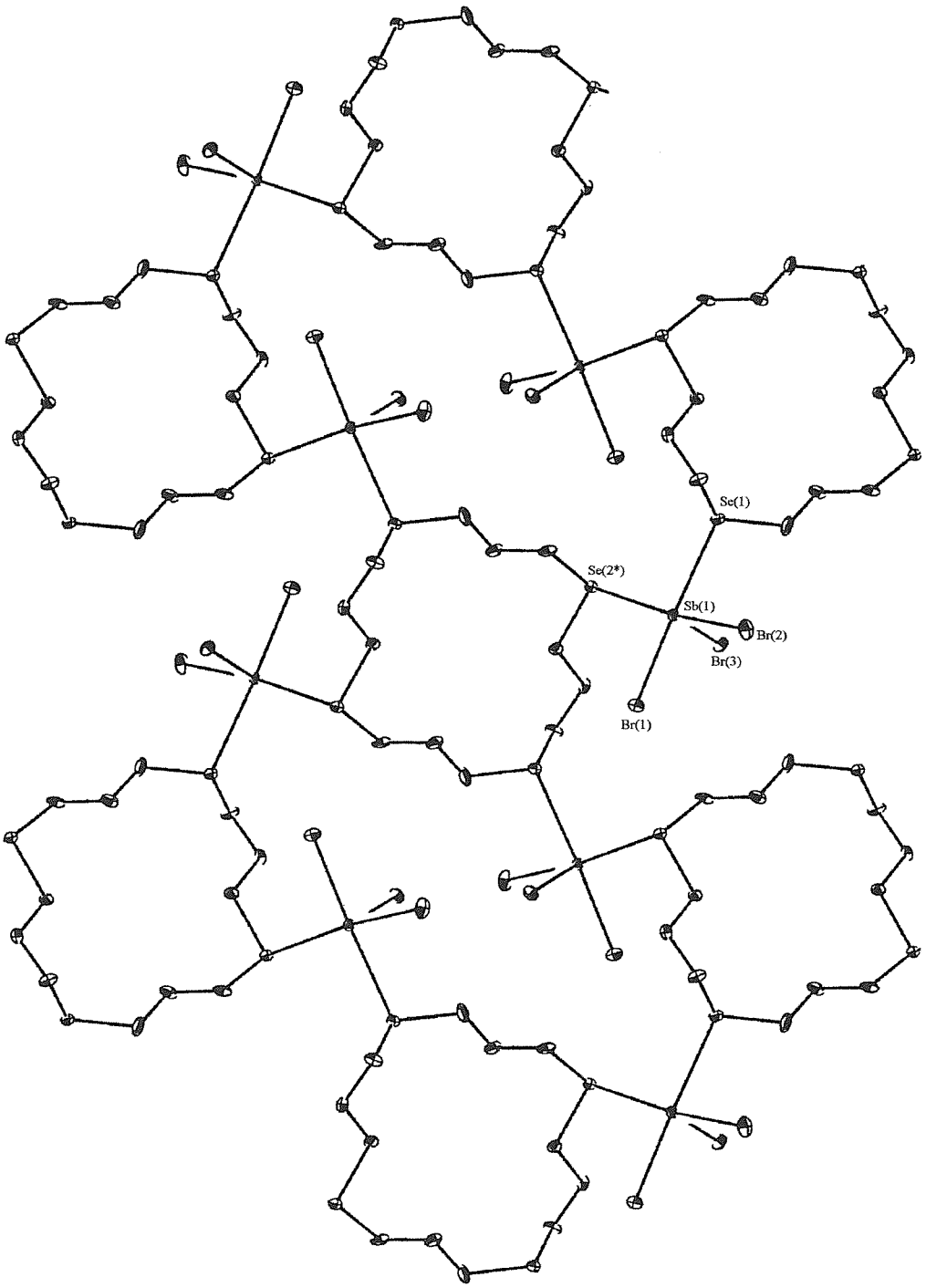

Figure 6.22 – View of a portion of the infinite 2-dimensional structure adopted by $[(SbBr_3)_2([16]aneSe_4)]$. Ellipsoids are drawn at the 40 % probability level.

Table 6.10 – Selected bond lengths (Å) for $[(SbBr_3)_2([16]aneSe_4)]$

Sb(1)	Br(1)	2.687(1)	Sb(1)	Br(2)	2.537(1)
Sb(1)	Br(3)	2.601(1)	Sb(1)	Se(1)	2.989(1)
Sb(1)	Se(2*)	3.193(1)	Se(1)	C(1)	1.97(1)
Se(1)	C(6*)	1.95(1)	Se(2)	C(3)	1.95(1)
Se(2)	C(4)	1.97(1)	C(1)	C(2)	1.53(1)
C(2)	C(3)	1.51(2)	C(4)	C(5)	1.52(2)
C(5)	C(6)	1.50(2)			

Table 6.11 – Selected bond angles (degrees) for $[(SbBr_3)_2([16]aneSe_4)]$

Br(1)	Sb(1)	Br(2)	90.67(4)	Br(1)	Sb(1)	Br(3)	92.43(4)
Br(1)	Sb(1)	Se(1)	171.51(4)	Br(1)	Sb(1)	Se(2*)	93.94(4)
Br(2)	Sb(1)	Br(3)	93.67(4)	Br(2)	Sb(1)	Se(1)	81.31(4)
Br(2)	Sb(1)	Se(2*)	84.02(40	Br(3)	Sb(1)	Se(1)	90.83(4)
Br(3)	Sb(1)	Se(2*)	173.24(5)	Se(1)	Sb(1)	Se(2*)	82.55(3)
Sb(1)	Se(1)	C(1)	97.6(3)	Sb(1)	Se(1)	C(6)	104.3(4)
C(1)	Se(1)	C(6)	99.4(5)	Sb(1*)	Se(2)	C(3)	99.2(3)
Sb(1*)	Se(2)	C(4)	97.2(3)				

It is noteworthy that while this complex is the first macrocyclic selenoether complex involving antimony, there is also a structurally characterised bismuth species which involves exocyclic $[16]aneSe_4$, i.e. $[BiBr_3([16]aneSe_4)]$ discussed in Chapter 5. In this case the macrocycles are bonded (and therefore bridge) *via* mutually *trans* selenium donors to Bi centres (Figure 6.22). Therefore, for $[16]aneSe_4$ we have observed structures for both bismuth(III) and antimony(III) that differ in various structural ways but share the preference to adopt the rare exocyclic conformation. The only other species $[Cu_n([16]ane)_n]^{n+}$ was reported by Pinto and co-workers.[44] Another point of comparison is that the Sb-Se interactions in $[(SbBr_3)_2([16]aneSe_4)]$ are shorter than those in $[SbCl_3\{MeSe(CH_2)_3SeMe\}]$[43] (Figure 6.16) although this may be due to the lower coordination number at Sb in the former. A main feature of this new compound is the occurrence of weak, secondary Sb-Se interactions on the

opposite face to the three halides which leads to the Se atoms occupying mutually *cis* coordination sites.

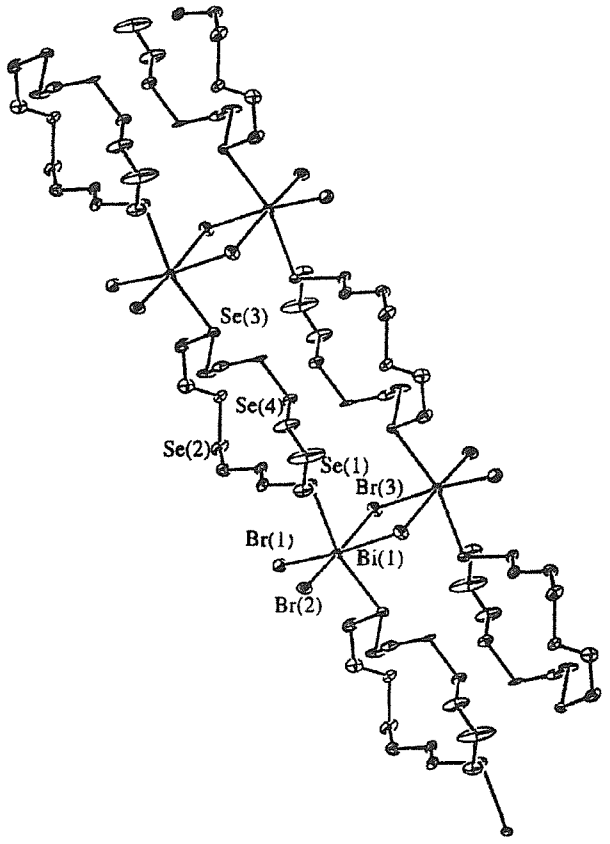

Figure 6.23 – View of the structure of the 1-dimensional ladder adopted by [$BiBr_3$([16]aneSe_4)] from Chapter 5 (for comparison)

Subsequent work in Southampton has generated a structure formed from the reaction of $SbBr_3$ with the thioether macrocycle [14]aneS_4.[45] The structure observed for [($SbBr_3$)$_2$([14]aneS_4)] also involves the macrocycles adopting an exocyclic conformation in their bonding to antimony(III) (Figure 6.24). The diagram shows Sb_2Br_6 units linked to S-donor atoms from four independent macrocycles.

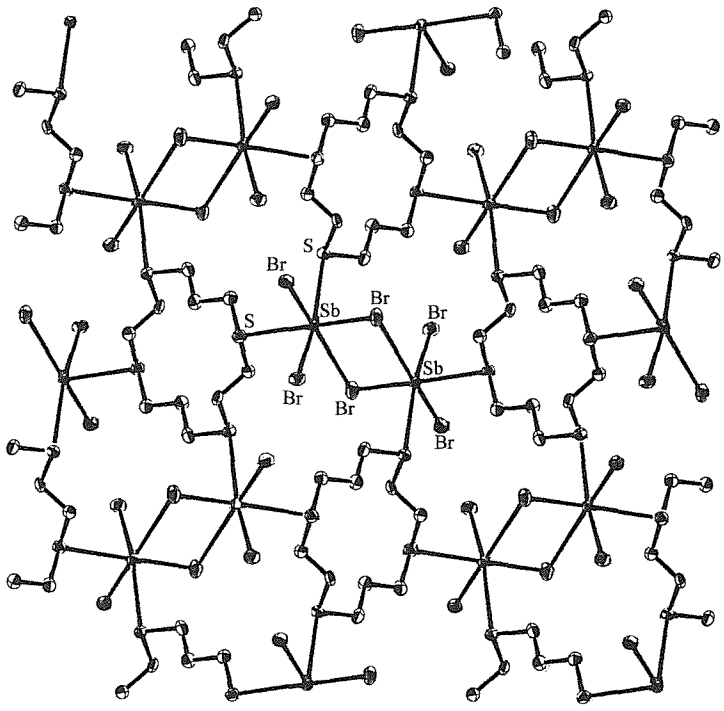

Figure 6.24 – View of the structure of $[(SbBr_3)_2([14]aneS_4)]$ showing the thiacrown adopting exocyclic conformation taken from ref. 45

A noteworthy point after viewing the first set of structurally characterised acyclic Group 16 ligand complexes and the first macrocylcic selenoether complex is that all the motifs repeat infinitely along one or two dimensions, with no dimers or capped species observed, as previously witnessed for Group 16 complexes of antimony(III). As briefly mentioned further work is being carried out in this area investigating the structures obtained for Group 16 ligands of different denticities to the ones discussed in this chapter.

6.3 CONCLUSIONS

This work represents the first investigation of antimony(III) halide complexes of acyclic Group 16 donor ligands including sulfur, selenium and tellurium and macrocyclic selenoethers

By the very nature of these antimony(III) species, their characterisation is restricted to analytical data, IR spectroscopy and single crystal X-ray diffraction studies. While the stoichiometry of the products is not in question, the structural motifs described here represent those species which yielded suitable quality crystals. Other motifs may be obtainable under different conditions. At present we can only discuss those structures which we have identified, but there is clearly the caveat that the discussion may need modification in light of further results. The large variety of structural motifs for these Group 16 ligand complexes means that it is not possible to formulate any structures on the basis of the analytical data or IR spectroscopy. The X-ray crystal structures obtained for these species have shown unexpected structural motifs in stark contrast to previous examples involving acyclic or macrocylic ligand complexes.[23,26,27,28,31,32] For the thioether ligand, $MeC(CH_2SMe)_3$, infinite one-dimensional arrays where observed for the complexes with $SbCl_3$ and SbI_3. Antimony(III) was 5-coordinate in the chloride species with each $SbCl_3$ unit linked to the next by a μ^2-bridging ligand, whereas in $[SbI_3\{MeC(CH_2SMe)_3\}]$ we observe a Sb_2I_6 bioctahedral unit with each antimony(III) having a donor set of two terminal I, two bridging I and two monodentate S-donors. The Sb_2X_6 units have been identified in other antimony(III) halide complexes.[23] The complex formed between $SbBr_3$ and $MeC(CH_2SeMe)_3$ has also been found to form a one-dimensional structural array with the antimony(III) centre 6-coordinate. However, there is no Sb_2X_6 unit and unlike $[SbCl_3\{MeC(CH_2SMe)_3\}]$ each antimony(III) has a donor set which includes one monodentate and one bidentate selenoether.

The structure adopted by the [16]aneSe_4 complex of $SbBr_3$ is a two-dimensional array which displays the macrocycle in an exocyclic conformation

bonding to four independent $SbBr_3$ units *via* the four Se donors within the ring. This is in stark contrast to the structures determined for antimony(III) halogeno complexes involving crown ethers and crown thioethers (apart from $[(SbBr_3)_2([14]aneS_4])$ which reflect the dominance of the pyramidal SbX_3 unit with weak Sb-O or Sb-S interactions replacing the secondary Sb-X interactions in the parent halides generally leading to capping of the antimony(III) in a half-sandwich fashion.

6.4 EXPERIMENTAL

6.4.1 Ligand and Complex Synthesis

The antimony(III) chloride, bromide and iodide were purchased from Aldrich chemicals. Solvents were dried and distilled prior to use. The ligands $MeC(CH_2EMe)_3$ (E = S, Se or Te), [8]aneSe_2, [16]aneSe_4 and [24]aneSe_6 were all produced by literature methods.[46-49]

a). Synthesis of $[SbCl_3\{MeC(CH_2SMe)_3\}]$

An ice cold solution of the compound $SbCl_3$ (0.2 g, 0.88 mmol) in MeCN (10 cm^3) was treated, dropwise, with $MeC(CH_2SMe)_3$ (0.18 g, 0.88 mmol) under an inert atmosphere of N_2. The solvent was slowly removed *in vacuo* to give a white microcrystalline solid (yield 0.23 g, 60 %). Required for $[C_8H_{18}Cl_3S_3Sb]$: C = 22.2, H = 4.2 %; found: C = 22.0, H = 4.3 %. IR spectrum (Nujol mull, CsI plates): 327, 290 cm^{-1}.

b). Synthesis of $[SbBr_3\{MeC(CH_2SMe)_3\}]$

Method as for $[SbCl_3\{MeC(CH_2SMe)_3\}]$ but using $SbBr_3$ (0.2 g, 0.55 mmol) and $MeC(CH_2SMe)_3$ (0.12 g, 0.55 mmol) to give a pale yellow solid (yield 0.13 g, 40 %). Required for $[C_8H_{18}Br_3S_3Sb]$: C = 16.8, H = 3.5 %; found: C = 16.5, H = 3.0 %.

c). Synthesis of $[SbI_3\{MeC(CH_2SMe)_3\}]$

Method as for $[SbCl_3\{MeC(CH_2SMe)_3\}]$ but using SbI_3 (0.2 g, 0.40 mmol) and $MeC(CH_2SMe)_3$ (0.1 g, 0.40 mmol) to give a yellow/orange solid (yield 0.15 g, 52 %). Required for $[C_8H_{18}I_3S_3Sb]$: C = 13.5, H = 2.5 %; found: C = 13.2, H = 2.6 %.

d). Synthesis of $[SbCl_3\{MeC(CH_2SeMe)_3\}]$

Method as for $[SbCl_3\{MeC(CH_2SMe)_3\}]$ but using $SbCl_3$ (0.2 g, 0.88 mmol) and $MeC(CH_2SeMe)_3$ (0.31 g, 0.88 mmol) to give a cream solid (yield 0.31 g, 60 %).

Required for $[C_8H_{18}Cl_3SbSe_3]$: C = 16.6, H = 3.1 %; found: C = 16.8, H = 2.9 %. IR spectrum (Nujol mull, CsI plates): 290, 252 cm^{-1}.

e). Synthesis of $[SbBr_3\{MeC(CH_2SeMe)_3\}]$

Method as for $[SbCl_3\{MeC(CH_2SMe)_3\}]$ but using $SbBr_3$ (0.2 g, 0.55 mmol) and $MeC(CH_2SeMe)_3$ (0.19 g, 0.55 mmol) to give a yellow solid (yield 0.19 g, 49 %). Required for $[C_8H_{18}Br_3SbSe_3]$: C = 13.5, H = 2.5 %; found: C = 13.0, H = 2.3 %.

f). Synthesis of $[SbI_3\{MeC(CH_2SeMe)_3\}]$

Method as for $[SbCl_3\{MeC(CH_2SMe)_3\}]$ but using SbI_3 (0.2 g, 0.40 mmol) and $MeC(CH_2SeMe)_3$ (0.14 g, 0.40 mmol) to give an orange solid (yield 0.20 g, 59 %). Required for $[C_8H_{18}I_3SbSe_3]$: C = 11.3, H = 2.1 %; found: C = 10.8, H = 1.8 %.

g). Synthesis of $[SbCl_3\{MeC(CH_2TeMe)_3\}]$

Method as for $[SbCl_3\{MeC(CH_2SMe)_3\}]$ but using $SbCl_3$ (0.2 g, 0.88 mmol) and $MeC(CH_2TeMe)_3$ (0.44 g, 0.88 mmol) to give an orange/brown solid (yield 0.35 g, 55 %). Required for $[C_8H_{18}Cl_3SbTe_3]$: C = 13.2, H = 2.5 %; found: C = 12.5, H = 2.0 %. IR spectrum (Nujol mull, CsI plates): 302, 280 cm^{-1}.

h). Synthesis of $[SbBr_3\{MeC(CH_2TeMe)_3\}]$

Method as for $[SbCl_3\{MeC(CH_2SMe)_3\}]$ but using $SbBr_3$ (0.2 g, 0.55 mmol) and $MeC(CH_2TeMe)_3$ (0.27 g, 0.55 mmol) to give a yellow solid (yield 0.25 g, 53 %). Required for $[C_8H_{18}Br_3SbTe_3]$: C = 11.2, H = 2.1 %; found: C = 10.6, H = 2.0 %.

i). Synthesis of $[SbI_3\{MeC(CH_2TeMe)_3\}]$

Method as for $[SbCl_3\{MeC(CH_2SMe)_3\}]$ but using SbI_3 (0.2 g, 0.40 mmol) and $MeC(CH_2TeMe)_3$ (0.2 g, 0.40 mmol) to give an orange/brown solid (yield 0.24

g, 61 %). Required for [$C_8H_{18}I_3SbTe_3$]: C = 9.6, H = 1.8 %; found: C = 8.3, H = 1.0 %.

j). Synthesis of [$SbCl_3$([8]aneSe_2)]

Method as for [$SbCl_3${$MeC(CH_2SMe)_3$}] but using $SbCl_3$ (0.2 g, 0.88 mmol) and [8]aneSe_2 (0.21 g, 0.88 mmol) to give a yellow solid (yield 0.29 g, 70 %). Required for [$C_6H_{12}Cl_3SbSe_2$]: C = 15.3, H = 2.6 %; found: C = 15.0, H = 2.2 %. IR spectrum (Nujol mull, CsI plates): 349, 280 cm^{-1}.

k). Synthesis of [$SbBr_3$([8]aneSe_2)]

Method as for [$SbCl_3${$MeC(CH_2SMe)_3$}] but using $SbBr_3$ (0.2 g, 0.55 mmol) and [8]aneSe_2 (0.13 g, 0.55 mmol) to give an orange-red solid (yield 0.21 g, 63 %). Required for [$C_6H_{12}Br_3SbSe_3$]: C = 11.9, H = 2.0 %; found: C = 11.6, H = 2.2 %.

l). Synthesis of [SbI_3([8]aneSe_2)]

Method as for [$SbCl_3${$MeC(CH_2SMe)_3$}] but using SbI_3 (0.2 g, 0.40 mmol) and [8]aneSe_2 (0.1 g, 0.40 mmol) to give a red solid (yield 0.20 g, 66 %). Required for [$C_6H_{12}I_3SbSe_3$]: C = 9.7, H = 1.6 %; found: C = 9.4, H = 1.6 %.

m). Synthesis of [($SbCl_3$)$_2$([16]aneSe_4)]

Method as for [$SbCl_3${$MeC(CH_2SMe)_3$}] but using $SbCl_3$ (0.2 g, 0.88 mmol) and [16]aneSe_4 (0.43 g, 0.88 mmol) to give a white solid (yield 0.22 g, 35 %) (based on isolation of 2:1 ratio of $SbCl_3$:ligand after initial mixture of 1:1). Required for [$C_{12}H_{24}Cl_6Sb_2Se_4$]: C = 15.3, H = 2.6 %; found: C = 15.6, H = 3.0 %. IR spectrum (Nujol mull, CsI plates): 304, 291 cm^{-1}.

n). Synthesis of [($SbBr_3$)$_2$([16]aneSe_4)]

Method as for [$SbCl_3${$MeC(CH_2SMe)_3$}] but using $SbBr_3$ (0.2 g, 0.55 mmol) and [16]aneSe_4 (0.27 g, 0.55 mmol) to give a bright yellow solid (yield 0.20 g, 30 %). Required for [$C_{12}H_{24}Br_6Sb_2Se_4$]: C = 11.9, H = 2.0 %; found: C = 11.7, H = 2.1 %.

o). Synthesis of $[(SbI_3)_2([16]aneSe_4)]$

Method as for $[SbCl_3\{MeC(CH_2SMe)_3\}]$ but using SbI_3 (0.2 g, 0.40 mmol) and [16]aneSe$_4$ (0.2 g, 0.40 mmol) to give an orange solid (yield 0.14 g, 23 %). Required for $[C_{12}H_{24}I_6Sb_2Se_4]$: C = 9.7, H = 1.6 %; found: C = 9.3, H = 1.5 %.

p). Synthesis of $[SbCl_3([24]aneSe_6)]$

Method as for $[SbCl_3\{MeC(CH_2SMe)_3\}]$ but using $SbCl_3$ (0.2 g, 0.88 mmol) and [24]aneSe$_6$ (0.64 g, 0.88 mmol) to give a white solid (yield 0.49 g, 58 %). Required for $[C_{18}H_{32}Cl_3SbSe_6]$: C = 22.6, H = 3.4 %; found: C = 22.4, H = 3.4 %. IR spectrum (Nujol mull, CsI plates): 353, 336 cm^{-1}.

q). Synthesis of $[SbBr_3([24]aneSe_6)]$

Method as for $[SbCl_3\{MeC(CH_2SMe)_3\}]$ but using $SbBr_3$ (0.2 g, 0.55 mmol) and [24]aneSe$_6$ (0.4 g, 0.55 mmol) to give a bright yellow solid (yield 0.24 g, 40 %). Required for $[C_{18}H_{32}Br_3SbSe_6]$: C = 19.9, H = 3.0 %; found: C = 19.5, H = 2.9 %.

r). Synthesis of $[SbI_3([24]aneSe_6)]$

Method as for $[SbCl_3\{MeC(CH_2SMe)_3\}]$ but using SbI_3 (0.2 g, 0.40 mmol) and [24]aneSe$_6$ (0.3 g, 0.40 mmol) to give an orange solid (yield 0.27 g, 54 %). Required for $[C_{18}H_{32}I_3SbSe_6]$: C = 17.6, H = 2.6 %; found: C = 17.5, H = 2.5 %.

6.4.2 X-ray Crystallography

$[SbCl_3\{MeC(CH_2SMe)_3\}]$ and $[SbI_3\{MeC(CH_2SMe)_3\}]$

Details of the crystallographic data collection and refinement parameters are given in Table 6.1. The crystals were grown by slow evaporation from a solution of each complex in MeCN. The selected crystals were coated with mineral oil and placed in a stream of N_2 gas at 150 K. Data collection used a Rigaku AFC7S four-circle diffractometer and graphite-monochromated Mo-Kα X-radiation (λ = 0.71073 Å). The structure of $[SbCl_3\{MeC(CH_2SMe)_3\}]$ was

solved by direct methods[50] whereas the structure of $[SbI_3\{MeC(CH_2SMe)_3\}]$ was solved by heavy-atom Patterson methods.[51] In both cases the structure was developed by iterative cycles of full-matrix least-squares refinement and Fourier difference syntheses.[53] All fully occupied non-H atoms were refined anisotropically.

$[SbBr_3\{MeC(CH_2SeMe)_3\}]$ and $[(SbBr_3)_2([16]aneSe_4)]$

Details of the crystallographic data collection and refinement parameters are given in Table 5.4. Crystals of $[SbBr_3\{MeC(CH_2SeMe)_3\}]$ and $[(SbBr_3)_2([16]aneSe_4)]$ were obtained by slow evaporation from solutions of the appropriate complexes in MeCN. For $[(SbBr_3)_2([16]aneSe_4)]$ data collection used a Rigaku AFC7S four-circle diffractometer but for $[SbBr_3\{MeC(CH_2SeMe)_3\}]$ an Enraf-Nonius Kappa-CCD diffractometer was used and graphite-monochromated Mo-Kα X-radiation (λ = 0.71073 Å) at 150 K. No significant crystal decay or movement was observed. The AFC7S data were corrected for absorption using ψ-scans. However, for $[(SbBr_3)_2([16]aneSe_4)]$ ψ-scans did not provide a satisfactory correction and with the model at isotropic convergence the data were corrected for absorption using DIFABS.[52] The structures were solved by heavy atom methods[51] and developed by iterative cycles of full-matrix least-squares refinement and Fourier difference syntheses.[53] All fully occupied non-H atoms were refined anisotropically.

6.5 REFERENCES

1. E.G. Hope and W. Levason, *Coord. Chem. Rev.*, 1993, **122**, 109.
2. S.E. Dann, A.R.J. Genge, W. Levason and G. Reid, *J. Chem. Soc., Dalton Trans.*, 1996, 4471.
3. S.E. Dann, A.R.J. Genge, W. Levason and G. Reid, *J. Chem. Soc., Dalton Trans.*, 1997, 2207.
4. A.R.J. Genge, W. Levason and G. Reid, *J. Chem. Soc., Dalton Trans.*, 1997, 4549.
5. A.R.J. Genge, W. Levason and G. Reid, *J. Chem. Soc., Chem. Commun.*, 1998, 2159.
6. A.J. Barton, A.R.J. Genge, W. Levason and G. Reid, *J. Chem. Soc., Dalton Trans.*, 2000, 859.
7. A.J. Barton, A.R.J. Genge, W. Levason and G. Reid, *J. Chem. Soc., Dalton Trans.*, 2000, 2163.
8. C.J. Carmalt, W. Clegg, M.R.J. Elsegood, *Inorg. Chem.*, 1996, **35**, 3709.
9. C.J. Carmalt., A.H. Cowley, A. Decken and N.C. Norman, *J. Organomet. Chem.*, 1995, **496**, 59.
10. V. Spridonov and A.G. Gershikov, *J. Mol. Struct. (Theochem.)*, 1986, **140**, 173.
11. A. Lipka, *Acta Cryst.*, 1979, **B35**, 3020.
12. S.C. Nyburg, G.A. Ozin and J.T. Szymanski, *Acta Cryst.*, 1971, **B27**, 2298.
13. D.W. Cushen and R. Hulme, *J. Chem. Soc.*, 1964, 4162.
14. D.W. Cushen and R. Hulme, *J. Chem. Soc.*, 1962, 2218.
15. H. von Benda, *Z. Krist.*, 1980, **151**, 271.
16. J. Trotter and T. Zorbel, *Z. Krist.*, 1966, **123**, 67.
17. S. Pohl and W. Saak, *Z. Krist.*, 1984, **169**, 177.
18. R. Hulme and J.S. Scruton, *J. Chem. Soc., A*, 1968, 2448.
19. A. Lipka and H. Wunderlich, *Z. Natursforsch., Teil B*, 1980, **35**, 1548.
20. R.R. Holmes and E.F. Bertant, *J. Am. Chem. Soc.*, 1958, **80**, 2980.

21. J.C. Summers and H.H. Sisler, *Inorg. Chem.*, 1970, **9**, 862.
22. W. Clegg, M.R.J. Elsegood, V. Graham, *J.Chem. Soc., Dalton Trans.*, 1993, 997.
23. W. Clegg, M.R.J. Elsegood, V. Graham, N.C. Norman, N.L. Pickett and K. Tavakkoli, *J. Chem. Soc., Dalton Trans.*, 1994, 1743.
24. G.A. Fisher and N.C. Norman, *Adv. Inorg. Chem.*, in the press.
25. N.C. Norman, *Phosphorus Sulfur*, in the press.
26. E. Hough, D.G. Nicholson and A.K. Vasudevan, *J. Chem. Soc., Dalton Trans.*, 1987, 427.
27. N.W. Alcock, M. Ravindran and G.R. Willey, *Acta Cryst.*, 1993, **B49**, 507.
28. N.W. Alcock, M. Ravindran, S.M. Roe and G.R. Willey, *Inorg., Chim. Acta*, 1990, **167**, 115.
29. N.W. Alcock, M. Ravindran and G.R. Willey, *J. Chem. Soc., Chem. Commun.*, 1989, 1063.
30. M.G.B. Drew, D.G. Nicholson, I. Sylte and A.K. Vasudevan, *Inorg. Chim. Acta*, 1990, **171**, 11.
31. M. Schafer, J. Pebler and K. Dehnicke, *Z. Anorg. Allg. Chem.*, 1992, **611**, 149.
32. G.R. Willey, D.R. Aris and W. Errington, *Inorg. Chim. Acta*, 2000, **300**, 1004.
33. A.J. Blake, D. Fenske, W.-S. Li, V. Lippolis and M. Schröder, *J. Chem. Soc., Dalton Trans.*, 1998, 3961.
34. G.R. Willey, M.T. Lakin, M. Ravindran and N.W. Alcock, *J. Chem. Soc., Chem. Commun.*, 1991, 271.
35. S.Pohl, D. Hasse and M. Peters, *Z. Anarg. Allg. Chem.*, 1993, **619**, 727.
36. M.G.B. Drew, J.M. Kisenyi and G.R. Willey, *J. Chem. Soc., Dalton Trans.*, 1982, 1729.
37. M. Schmidt, R. Bender and C. Burschka, *Z. Anorg. Allg. Chem.*, 1979, **454**, 160.

38. J.M. Kisenyi, G.R. Willey and M.G.B. Drew, *J. Chem. Soc., Dalton Trans.*, 1985, 1073.

39. M.G.B. Drew, J.M. Kisenyi, G.R. Willey and S.O. Wandiga, *J. Chem. Soc., Dalton Trans.*, 1984, 1717.

40. G.R. Willey, M.T. Lakin and N.W. Alcock, *J. Chem. Soc., Dalton Trans.*, 1992, 591.

41. G.R. Willey, M.T. Lakin and N.W. Alcock, *J. Chem. Soc., Dalton Trans.*, 1992, 1339.

42. J. Trotter, *Z. Kristallogr.*, 1965, **122**, 230.

43. A.J. Barton, N.J. Hill, W. Levason, B. Patel and G. Reid, *J. Chem. Soc., Chem. Commun.*, Submitted, 2000.

44. R.J. Batchelor, F.W.B. Einstein, I.D. Gay, J.-H. Gu and B.M. Pinto, *J. Organomet. Chem.*, 1991, **411**, 147.

45. N.J. Hill, University of Southampton, Unpublished results.

46. R.Ali,, S.J. Higgins and W. Levason, *Inorg. Chim. Acta*, 1984, **84**, 65.

47. D.J. Gulliver, E.G. Hope, W. Levason, S.G. Murray, D.M. Potter and G.L. Marshall, *J. Chem. Soc., Perkin Trans. II*, 1985, 429.

48. R.J. Batchelor, F.W.B. Einstein, I.D. Gay, J.H. Gu, B.D. Johnston and B.M. Pinto, *J. Am. Chem. Soc.*, 1989, **111**, 6582.

49. E.G. Hope, T. Kemmitt and W. Levason, *Organometallics*, 1987, **6**, 206.

50. SHELXS 86, G.M. Sheldrick, *Acta Crystallogr., Sect. A*, 1990, **46**, 467.

51. PATTY, The DIRDIF program System, P.T. Beurskens, G. Admiraal, G. Beurskens, W.P. Bosman, S. Garcia-Granda, R.O. Gould, J.M.M. Smits and C. Smykalla, Technical Report of the Crystallography Laboratory, University of Nijmegen, 1993.

52. R.H. Blessing, *Acta Crystallogr., Sect. A*, 1995, **51**, 33; *J. Appl. Crystallogr.*, 1997, **30**, 421.

53. TEXSAN, Crystal Structure Analysis Package, Molecular Structure Corporation, Houston, TX, 1995.

APPENDIX

All procedures involving air sensitive materials were performed under an inert atmosphere of N_2 or argon using standard Schlenk techniques. All solvents were degassed prior to use by bubbling N_2 through them.

Infra-red spectra were measured as CsI discs, Nujol mulls or solutions in CH_2Cl_2 using a Perkin-Elmer 1600 FTIR spectrometer.

Mass spectra were obtained by fast atom bombardment (FAB) using 3-NOBA (3-nitrobenzyl alcohol) as a matrix on a VG Analytical 70-250-SE Normal Geometry Double Focusing Mass Spectrometer, or by positive ion electrospray mass spectrometry in MeCN solutions (0.1 μm) on a Hewlett Packard Series 1050 mass spectrometer.

Multinuclear NMR were recorded on a Bruker AM 360 spectrometer as solutions containing 5 % of the deuterated solvent as lock in 10mm outside diameter tubes. $^{13}C\{^1H\}$ NMR spectra were recorded at 90.4 MHz and referenced to Me_4Si; $^{3}1P\{^1H\}$ NMR spectra were recorded at 145.8 MHz and referenced to 85 % H_3PO_4; $^{77}Se\{^1H\}$ NMR spectra were recorded at 68.68 MHz and referenced to Me_2Se; ^{95}Mo spectra were recorded at 23.48 MHz and referenced to aq. Na_2MoO_4; $^{125}Te\{^1H\}$ NMR spectra were recorded at 113.58 MHz and referenced to Me_2Te. ^1H and $^{13}C\{^1H\}$ (ligands) were recorded on a Bruker AM 300 spectrometer operating at 300.13 MHz and 75.47 MHz respectively in 5mm tubes and referenced to Me_4Si.

Microanalyses were performed at Strathclyde University (Glasgow) or by Prof. W. Levason at Southampton University.